
The Peccei–Quinn Supermultiplet and its Cosmological Implications

Peter Graf



München 2013

The Peccei–Quinn Supermultiplet and its Cosmological Implications

Peter Graf

Dissertation
an der Fakultät für Physik
der Ludwig–Maximilians–Universität
München

vorgelegt von
Peter Graf
aus Oberviechtach

München, den 04. März 2013

This thesis is based on the author's work partly published in [1–3] conducted at the Max–Planck–Institut für Physik (Werner–Heisenberg–Institut), München from January 2010 until February 2013 under the supervision of Dr. Frank Daniel Steffen.

Erstgutachter: PD Dr. habil. Georg Raffelt
Zweitgutachter: Prof. Dr. Gerhard Buchalla
Tag der mündlichen Prüfung: 18. April 2013

Zusammenfassung

Das starke CP Problem kann durch den Peccei–Quinn (PQ) Mechanismus gelöst werden, welcher das Axion einführt. In supersymmetrischen (SUSY) Axionmodellen ist die Saxionmasse typischerweise von der Ordnung der Gravitinomasse. Zusammen mit dem Axino können die PQ-Teilchen erhebliche kosmologische Folgen haben.

Wir konzentrieren uns auf hadronische Axionmodelle. In diesen Modellen koppeln die PQ-Teilchen nur an zusätzliche schwere (S)Quarks, während alle anderen Teilchen keine PQ-Ladung tragen. Wir berechnen die thermischen Produktionsraten der PQ-Teilchen durch Streuung an Quarks, Gluonen, Squark und Gluinos im heißen Plasma des frühen Universums. Dabei verwenden wir systematische Methoden der Feldtheorie, um ein eichinvariantes, endliches Ergebnis in führender Ordnung in der starken Kopplung zu erhalten. Wir berechnen den thermisch produzierten Yield und die Entkopplungstemperatur von Axionen, Saxionen und Axinos.

Wir aktualisieren den Vergleich von thermischen und nicht-thermischen Saxionenergiedichten. Dann betrachten wir hauptsächlich Zerfälle des Saxions in Axionen, welche dann zusätzliche Strahlung bilden. Wir erneuern entsprechende Schranken, auferlegt durch aktuelle Untersuchungen der primordialen ^4He -Menge und durch präzise kosmologische Messungen. Wir zeigen, dass der Trend für zusätzliche Strahlung in diesen Studien durch Saxionzerfälle in Axionen erklärt werden kann.

Zwei Szenarien werden im Detail untersucht. Beide Szenarien erklären die kalte dunkle Materie (CDM) und zusätzliche Strahlung in Übereinstimmung mit bestehenden Schranken. Die hohe Reheatingtemperatur nach Inflation in beiden Szenarien ermöglicht Baryogenese durch thermische Leptogenese.

(i) Gravitino CDM: Axionen aus dem Zerfall von thermischen Saxionen bilden zusätzliche Strahlung bereits vor der Nukleosynthese und Zerfälle eines aus kosmologischen Gründen schweren Axinos (TeV-Skala) produzieren Entropie.

(ii) Axion CDM: Leichte Axinos (eV-Skala) werden bedingt durch Schranken an heiße dunkle Materie. Gravitinos zerfallen spät in Axionen und Axinos, die zusammen mit Strahlung aus früheren Saxionzerfällen existieren können.

Der Planck-Satellit wird die zusätzliche Strahlung in beiden Szenarien genau vermessen. Weitere Tests dieser Szenarien sind durch die Suche nach Axionen durch ADMX und nach SUSY-Teilchen am Large Hadron Collider gegeben.

Abstract

The strong CP problem can be solved by the Peccei–Quinn (PQ) mechanism, which introduces the axion. In supersymmetric (SUSY) axion models, the saxion mass is typically of order of the gravitino mass. Together with the axino, the PQ particles and their decay products can then have potentially severe cosmological effects.

We focus on hadronic axion models. In these models, the PQ particles couple to additional heavy (s)quarks, whereas all other particles do not carry PQ charge. We calculate the thermal production rate of axions, saxions, and axinos via scatterings of quarks, gluons, squarks, and gluinos in a hot primordial plasma. Systematic field theoretical methods are applied to obtain a gauge-invariant, finite result consistent to leading order in the strong gauge coupling. We compute the thermally produced yield and the decoupling temperature for axions, saxions, and axinos.

We update the comparison of the energy density of thermal and misalignment saxions. Then, we mainly focus on the case where saxions decay into axions, which provide extra radiation. We update associated limits imposed by recent studies of the primordial ^4He abundance and by precision cosmology. We show that the trend towards extra radiation seen in those studies can be explained by late decays of thermal saxions into axions.

Two cosmological scenarios are analyzed in detail. Both scenarios consistently explain cold dark matter (CDM) and extra radiation in agreement with existing limits. Moreover, the high reheating temperature after inflation possible in these scenarios allows for baryogenesis through thermal leptogenesis.

(i) Gravitino CDM: Axions from decays of thermal saxions provide extra radiation already prior to big bang nucleosynthesis (BBN) and decays of axinos with a cosmologically required TeV-scale mass can produce extra entropy.

(ii) Axion CDM: A light eV-scale axino is required by hot dark matter constraints. Weak-scale gravitinos decay into axions and axinos. These decays lead to late extra radiation after BBN which can coexist with the early contributions from saxion decays.

Results of the Planck satellite will probe extra radiation for both scenarios. Further experimental prospects are the searches for axions at the axion CDM experiment ADMX and for supersymmetric particles at the Large Hadron Collider.

Contents

1	Introduction	1
2	SUSY and the PQ Supermultiplet	5
2.1	The Strong CP Problem and Axions	5
2.2	Supersymmetry	8
2.2.1	SUSY Algebra	9
2.2.2	Chiral Superfields	10
2.2.3	Vector Superfields	12
2.2.4	Supersymmetric Interactions	13
2.2.5	SUSY Breaking	16
2.2.6	Local SUSY and the Gravitino	17
2.3	The PQ Supermultiplet	18
2.4	The Hadronic Axion Model	19
2.4.1	Interaction Vertices obtained from Loops	21
2.4.2	The Effective Lagrangian	24
2.4.3	Axion - Saxion Interaction from the Kinetic Term	24
2.5	Properties of the PQ Particles	25
3	Thermal Production of the PQ Particles	29
3.1	Saxions	29
3.1.1	Hard Part	31
3.1.2	Soft Part	37
3.2	Axions	40
3.3	Axinos	41
3.4	Yields and Decoupling Temperatures	42

3.4.1	Introductory Cosmology	42
3.4.2	Thermally Produced Yields	46
3.4.3	Estimating the Decoupling Temperatures	49
3.5	Inflation and the Reheating Temperature	50
4	Cosmological Implications of the Saxion	55
4.1	Saxions from Misalignment	56
4.2	Early Decay and Entropy	61
4.3	Decay during BBN	61
4.4	Late Decay	63
5	Extra Radiation	65
5.1	Parameterizing Additional Radiation	65
5.2	Hints from CMB and LSS	68
5.3	Hints from BBN	73
5.3.1	Primordial Nucleosynthesis	73
5.3.2	Observations	75
5.3.3	Computation with <code>ParthENoPE</code> and Likelihood Analysis	77
5.3.4	Extra Radiation at BBN	80
5.4	Relic Axion Density	81
6	Saxion Decays with Gravitino CDM	87
6.1	Numerical Treatment	88
6.1.1	Extra Radiation and CDM for $x = 1$	93
6.1.2	Extra Radiation and CDM for $x < 1$	96
6.2	Limits from Collider Searches	99
6.3	Analytic Approximation	100
7	Saxion Decays with Axion CDM	103
7.1	Extra Radiation from Decaying Gravitinos	104
7.2	Numerical Treatment	105
7.2.1	Extra Radiation for $x = 1$	108
7.2.2	Extra Radiation for $x < 1$	109
7.3	Limits from Colliders and from Cosmology	112

8	Summary and Conclusion	115
A	Notations and Conventions	119
A.1	Pauli and Dirac Matrices	119
A.2	Weyl Spinors	120
A.3	Dirac and Majorana Spinors	121
A.4	Grassmann Variables	122
B	Derivation of the Effective PQ Lagrangian	123
C	Feynman Rules	129
C.1	External Lines and Propagators	129
C.2	SUSY QCD Vertices	131
C.3	PQ Vertices	132
D	Hard Production Rate	136
D.1	Calculation of FBF Processes	137
D.2	Calculation of FFB Processes	141
E	Phase Space Distribution of Saxions	142
	Bibliography	144

Chapter 1

Introduction

Modern day astrophysics and cosmology are based on two “standard models”, which show considerable success in explaining many observations and measurements. Nevertheless, both have their limitations. The first of these models, the standard model (SM) of particle physics [4–11], summarizes our current knowledge of sub-atomic physics and is tested to very high precision [12]. Recently, the last missing piece, the Higgs particle [13–18], may have been found [19, 20]. Despite its great success, the SM fails to explain some major features of cosmology, for example dark matter and dark energy.

The other one of these two models is often called the standard model of cosmology, although it is not as uniquely defined as the SM and it is not a fundamental model. The most prominent form, the lambda cold dark matter (Λ CDM) model, describes many cosmological observations [21–23], but also here, e.g., the cold dark matter (CDM) is introduced without a real microscopic model. Thus, one needs to specify or expand both models in order to arrive at a consistent description of cosmology. This connection of physics at the smallest observable scales to the one at the largest known scales provides a unique opportunity for both fields to learn from each other. We try to contribute to such a more complete picture with this thesis.

We focus on two expansions of the SM, the Peccei–Quinn (PQ) mechanism [24, 25], or more precisely, hadronic axion models [26, 27], and supersymmetry (SUSY) [28–33]. Both draw their original motivation solely from particle physics. They can, however, help to solve some of the open questions in cosmology.

The PQ mechanism was introduced to solve the strong CP problem, thus the question why CP is not badly violated in the strong interaction. As a result, a new light boson appears, the axion [34, 35]. Although it has not been found yet and is constrained from laboratory, astrophysics, and cosmology searches [12, 36], an axion condensate resulting from the misalignment mechanism [37–42] remains one of the most prominent dark matter candidates. But also thermal axions can have interesting cosmological implications.

The concept of SUSY links fermions and bosons and was introduced to combine internal symmetries and the Poincaré group in a non-trivial manner. Furthermore, SUSY provides a solution of the hierarchy problem. To avoid terms that would otherwise lead to rapid proton decays, one usually introduces R -parity in SUSY models. This results in the stability of the lightest supersymmetric particle (LSP). But this means that such a LSP can be an ideal candidate for dark matter [43, 44], and in fact a lot of effort is put into searching for such particles.

The combination of these two concepts leads to a supersymmetric version of the PQ mechanism, and, therefore, also to a SUSY partner of the axion, the axino. This new fermion can contribute significantly to the energy density of the early Universe and can even form dark matter [45–55].

The particle that we lay our main focus on in this work is the saxion. It is a scalar that is in principle also present in PQ models without SUSY, but then its mass is typically very large [56]. A SUSY version of the PQ model introduces a flat direction in the saxion potential and thereby makes the saxion massless in unbroken SUSY [57]. Once SUSY gets broken, the saxion acquires a mass and it becomes unstable. Its decay products can then have a significant influence on the early Universe [58–66]. In fact, only in combination with SUSY the mass of the saxion can be in the range where its presence in the Universe can leave observable traces.

One of these observables is the amount of extra radiation, usually expressed as the effective number of additional light neutrino species ΔN_{eff} . This number can for instance be inferred via measuring the abundance of the primordial light elements and comparing it to the predictions of big bang nucleosynthesis (BBN). Another possibility is the analysis of the cosmic microwave background (CMB) and the large scale structures (LSS), which also lead to informations on ΔN_{eff} . Interestingly, precision cosmology [23, 67–71] and recent studies of the primordial ^4He abundance [72, 73] show a trend towards a radiation content that exceeds the predictions of the SM. In fact, the Planck satellite mission is expected to release their measurements soon, so we will get a precise answer to the question of extra radiation in the near future.

Various explanations for $\Delta N_{\text{eff}} \sim 1$ have been explored in the literature invoking, e.g., light sterile neutrinos [74, 75], other light species [76, 77], neutrino asymmetries [78, 79], or decays of heavy particles [47, 56, 64, 80–90]. We focus on explanations involving the PQ multiplet. Saxions can decay into axions, which then are a form of additional radiation and can contribute significantly to ΔN_{eff} [47, 64, 80, 89–92]. Saxions are produced in the early Universe either thermally [58, 91, 92] or via misalignment [61, 64, 91–93]. In order to be prepared for the precision of the Planck data, we need an unambiguous and precise value of the saxion production rate. We focus on thermal saxions in a hadronic SUSY axion model here. The results are then used to provide detailed results of ΔN_{eff} , including other cosmological and laboratory limits, such as dark matter overproduction, entropy releasing decays, or masses of SUSY particles.

This thesis is organized as follows:

In Chap. 2 we briefly review the strong CP problem and the solution proposed by Peccei and Quinn. Thereby, the axion is introduced. The next section is devoted to an introduction of global SUSY, basic facts about SUSY breaking, and a short description of local SUSY. After a review of the hadronic axion we then combine these two concepts to arrive at a SUSY hadronic axion model, introducing the saxion and the axino. In this chapter and with some details in the Appendix, we carefully compute the interactions of the axion and saxion and thereby clarify the connection of parameters of the effective interaction terms with the fundamental PQ fields. The last section of this chapter summarizes some properties of the PQ particles.

These properties are used in Chap. 3 to calculate one of the main results of this thesis. These are the thermal production rates of saxions, axions, and also an update for the one of axinos, all of them in a hot primordial SUSY plasma. We use thermal field theoretical tools to systematically account for potential infrared divergences and provide gauge-invariant, finite results to leading order in the strong coupling constant. With the help of these production rates, we also provide the thermal yield and the decoupling temperature for the respective particles. These calculations are done assuming instantaneous reheating. A connection to more realistic models of reheating by a decaying inflaton is shown in the last section.

Chapter 4 begins with the update of another important source for saxions, the misalignment mechanism. Next, we focus on cosmological consequences of the PQ particles, in particular on the saxion and its decay products. We give a general overview over possible implications of the saxion and update limits shown previously in the literature [64].

In Chap. 5 we then introduce our main observable, the amount of extra radiation ΔN_{eff} measured in the early Universe. After reporting hints from CMB + LSS observations done in the literature, we show how ΔN_{eff} can be obtained from measurements of the primordial abundance of light elements. We provide an update of the theoretical results using the recent value of the neutron lifetime. These results are used to constrain the saxion parameter space with both CMB + LSS and BBN results. Finally, the relic abundance of axions possibly present today is shown.

Up to this point the presented calculations of ΔN_{eff} relied on the sudden-decay approximation. Moreover, other cosmological limits from, e.g., the gravitino, were not included. In Chap. 6 we go beyond sudden-decay and provide a scenario in which the gravitino is the LSP and forms the CDM, a heavy axino releases some entropy in its decay and axions from decaying thermal saxions provide ΔN_{eff} . All of these components are included in a set of Boltzmann equations to arrive at exact numerical results. These results are then confronted with cosmological as well as collider limits and used to constrain the saxions parameter space. Regions of high reheating temperature are shown, where baryogenesis through thermal leptogenesis is viable.

The second scenario shown in Chap. 7 features an axion condensate as the main component of dark matter, a light axino LSP, and the decay of thermal saxions and gravitinos both release extra radiation. Again we perform a full numerical analysis and provide limits from colliders and cosmology.

Chapter 8 contains a summary and concluding remarks.

Appendix A summarizes the notation and conventions used in our work. The following Appendix B presents the details of the calculation of the effective low-energy interaction Lagrangian of the PQ particles in Chap. 2. In Appendix C we show the Feynman rules necessary for our calculations. In Appendix D we show some details of the calculation of the hard thermal production rate of saxions in a hot primordial plasma. The last Appendix E gives arguments for the near thermal spectrum of thermally produced saxions.

Chapter 2

SUSY and the PQ Supermultiplet

We start with a description of the two main building blocks of our scenario, the Peccei–Quinn (PQ) mechanism and supersymmetry (SUSY). In the first section, we introduce the strong CP problem and its most compelling solution, the PQ mechanism. This solution introduces a new scalar particle, the axion.

Section 2.2 then briefly describes the concept of SUSY. We utilize the framework of the minimal supersymmetric extension to the standard model (MSSM). The combination of both yields a new supermultiplet in addition to the particles of the MSSM. This PQ supermultiplet contains not only the axion, but also another scalar, the saxion and a Majorana fermion, the axino. In order to define the low energy interactions of these particles, we need to further specify a certain model. We focus on hadronic axion models and calculate in detail the effective interaction vertices. Finally, we sum up some of the properties of the particles in the PQ multiplet.

2.1 The Strong CP Problem and Axions

The theory describing the interactions of quarks and gluons is Quantum Chromodynamics (QCD) [8–11]. Despite its great phenomenological success, one deficit, the strong CP problem, first discovered in the seventies, is still an issue. Our description of the history of the strong CP problem follows [94].

The origin of the strong CP problem is related to the $U(1)_A$ problem as explained in the following. At the classical level, the QCD Lagrangian possesses an $U(n_f^0)_V \times U(n_f^0)_A$ symmetry when one neglects the masses of n_f^0 quark flavors. Here the indices V and A stand for vector and axial-vector symmetries. If the up- and down-quarks are considered massless, one would expect the QCD Lagrangian to be symmetric under $U(2)_V \times U(2)_A$ under this approximation. Indeed, the vector symmetries are realized approximately in nature as can be seen by the approximately conserved quantities isospin and baryon number.

The axial symmetries, however, are spontaneously broken by quark condensates. So, instead of conserved quantities, one searches for four Nambu–Goldstone bosons associated with this spontaneous symmetry breaking (SSB). These bosons should be massless in the limit of massless quarks and can be identified as the pions.

Pushing this argument further, for $n_f^0 = 3$, one expects to find nine approximately massless and mass-degenerate mesons (see, e.g., Ref. [95]). But since one finds experimentally that $m_{\eta'} \gg m_\pi$ [12], there are not enough light bosons in the spectrum. Further investigation of the mass spectrum suggests that the theory has one $U(1)_A$ symmetry too much. In Ref. [96] this was called the $U(1)_A$ problem.

This question was solved by 't Hooft [97, 98], who showed that the QCD vacuum is more complex than the one of an abelian gauge theory, so that this $U(1)_A$ symmetry is not a true symmetry of nature. Let us briefly illustrate this finding. The axial current J_5^μ of QCD has a chiral Adler–Bell–Jackiw anomaly [99, 100]. This anomaly is given by a triangle loop of quarks connected to two gluons. The anomaly makes the divergence of J_5^μ different from zero and an $U(1)_A$ transformation affects the action. It turns out, however, that the resulting term in the action

$$\int d^4x \partial_\mu J_5^\mu \propto \frac{g_s^2}{32\pi^2} \int d^4x G^{b\mu\nu} \tilde{G}_{\mu\nu}^b \quad (2.1)$$

is actually a pure surface integral because $G^{b\mu\nu} \tilde{G}_{\mu\nu}^b$ can be written as a total derivative. Here g_s is the strong gauge coupling constant, $G^{b\mu\nu}$ is the gluon field strength tensor, $\tilde{G}_{\mu\nu}^b = 1/2\epsilon_{\mu\nu\rho\sigma} G^{b\rho\sigma}$ its dual, and b is a gluon color index. Thus naively one would expect that this term vanishes and the $U(1)_A$ symmetry is restored again. However, as shown by 't Hooft, the right boundary condition for the gluon field A^μ to use at spatial infinity is $A^\mu = 0$ or a gauge transformation thereof. This results in a nonzero contribution to the action from the above term and consequently the $U(1)_A$ problem is solved. In fact, the large mass of the η' meson can be understood as a result of this Adler–Bell–Jackiw anomaly. Another consequence is the very rich vacuum structure of QCD. The true vacuum is a superposition of different vacua defined by the winding number n and is given by

$$|\theta\rangle = \sum_n e^{-in\theta} |n\rangle, \quad (2.2)$$

with

$$n = \frac{1}{32\pi^2} \int d^4x G^{b\mu\nu} \tilde{G}_{\mu\nu}^b. \quad (2.3)$$

Note that each of these n -vacua cannot be the true one, since they are not individually invariant under all gauge transformations. In fact, one can define homotopy classes of gauge transformations according to the respective n . See also Ref. [101] for a detailed discussion. When calculating amplitudes for the transition from one vacuum state to another, one gets a nonzero contribution to the action that in turn

can be written as an additional effective term in the Lagrangian closely related to the winding number, the θ -vacuum term, given by

$$\mathcal{L}_\theta = \theta \frac{g_s^2}{32\pi^2} G^{b\mu\nu} \tilde{G}_{\mu\nu}^b. \quad (2.4)$$

This term violates C and CP symmetries for any values of $\theta \neq n\pi$ for $n \in \mathbb{Z}$. An observational consequence is a non-vanishing electric dipole moment of the neutron [102, 103]. However, all searches for such a dipole have been negative so far. This results in a current upper limit $|\theta| \lesssim 10^{-10}$ [104].

Although a vanishing θ can be seen as a natural observation within QCD alone, the combination of QCD with the electroweak theory gives rise to additional problems. Since the origin of the θ -term is closely related to the chiral anomaly, chiral rotations also affect the value of θ [103]. A rotation by an angle α changes the vacuum $|\theta\rangle \rightarrow |\theta + \alpha\rangle$. In the electroweak theory, the masses of quarks are given by a matrix M that is in general complex. To arrive at a physical basis, one must perform precisely such a rotation with the above angle given by $\text{Arg det } M$, the argument of the determinant of the quark mass matrix. Thus, the effective coefficient in (2.4) changes to

$$\bar{\theta} = \theta + \text{Arg det } M. \quad (2.5)$$

Now the same experimental limit requires $|\bar{\theta}| \lesssim 10^{-10}$ and one has no natural reason why these two unrelated quantities should cancel with such precision. This fine-tuning problem is called the strong CP problem.

An elegant solution to this naturalness problem has been proposed by Peccei and Quinn [24, 25], see also Refs. [41, 42, 94, 95, 101, 105] for reviews and lectures about the PQ mechanism. They realized that the presence of an additional global chiral $U(1)$ symmetry, called the Peccei–Quinn symmetry $U(1)_{\text{PQ}}$, solves the strong CP problem dynamically. This symmetry is broken spontaneously at a scale f_{PQ} and the resulting pseudo–Nambu–Goldstone boson is the axion a [34, 35]. This new particle couples to the gluon field strength tensor as

$$\mathcal{L}_{\text{PQ}} = \frac{g_s^2}{32\pi^2} \frac{a}{f_{\text{PQ}}} G^{b\mu\nu} \tilde{G}_{\mu\nu}^b, \quad (2.6)$$

since the $U(1)_{\text{PQ}}$ is color anomalous. The axion potential is formed by instantons. It has a minimum at $\langle a/f_{\text{PQ}} \rangle = -\bar{\theta}$ and, therefore, the QCD Lagrangian together with the axion conserves CP , as required by the Vafa–Witten theorem [106]. In this way, the strong CP problem is solved without any fine-tuning, since the vacuum value of the axion field is such that CP is always conserved, independent of $\bar{\theta}$. The potential leads to a mass term for the axion. In first approximation considering only contributions from the up- and down-quark, it is given by [107]

$$m_a \simeq 6 \text{ meV} \left(\frac{10^9 \text{ GeV}}{f_{\text{PQ}}} \right). \quad (2.7)$$

Note that the axion mass is due to instanton effects that are only effective at temperatures below Λ_{QCD} . Therefore, also the axion mass “turns on” only at energies below Λ_{QCD} .

In the original form, the PQ model had its symmetry breaking scale similar to the electroweak scale, $f_{\text{PQ}} \sim E_{\text{EW}}$, since it assumed the axion to be the phase of two Higgs doublets. Such an axion was ruled out rather soon, because its couplings would be sizable [108]. This experimental limit is overcome if one rises the value of f_{PQ} . But before we discuss actual models of these “invisible” axions, we introduce the second building block of our scenarios, namely the concept of SUSY.

2.2 Supersymmetry

From all the possible extensions of the SM, the concept of supersymmetry [28–33] is one of the most popular ones. In fact, SUSY has some very appealing features common to most versions of this theory.

Although the Higgs mechanism is believed to be the right description of electroweak symmetry breaking and the generation of masses for quarks, charged leptons, and the massive gauge bosons, it suffers from a serious fine-tuning problem. The question of the ultraviolet (UV) stability of the vacuum expectation value (VEV) of the Higgs with respect to the scale until which the electroweak theory is valid, often taken to be the Planck scale, is called the hierarchy problem [109–112]. Since the Higgs mechanism is now possibly verified experimentally [19, 20], this question becomes very important. SUSY offers a very elegant solution [113–118], since it is a symmetry linking bosonic and fermionic degrees of freedom. For a nice pedagogical introduction of SUSY along this argumentation, see for example [119].

From the model-building point of view, SUSY allows to extend the Poincaré group beyond the limitations of the Coleman–Mandula theorem [120].

For cosmology, SUSY provides a promising candidate for dark matter [43, 44], since the stability of the proton typically requires R -parity conservation and, therefore, the lightest SUSY particle is stable. In addition, the unification of the gauge couplings is achieved more easily in SUSY than in the SM.

The crucial new ingredient of SUSY compared to the SM is the introduction of fermionic symmetry generators, i.e., symmetry operations that change the spin of a particle. Let us now describe the related algebra in more detail.¹

¹We give only a brief introduction to SUSY in the following sections. The main references we use in our review are Refs. [119, 121], where the reader can also find many more references and reviews.

2.2.1 SUSY Algebra

The Coleman–Mandula theorem [120] restricts the symmetries of an interacting quantum field theory to be a direct product of any internal symmetry with the Poincaré group. The only possible way to circumvent this theorem is to rely on fermionic generators Q that change the spin of the state they act on by $1/2$. Schematically, this means they change a fermion into a boson and vice versa:

$$Q|\text{fermion}\rangle = |\text{boson}\rangle, \quad Q|\text{boson}\rangle = |\text{fermion}\rangle. \quad (2.8)$$

To be more precise, the theorem of Ref. [122] requires these fermionic generators Q_A and their Hermitian conjugates $\bar{Q}_{\dot{A}}$ to obey the following anticommutation relations²

$$\{Q_A, Q_B\} = \{\bar{Q}_{\dot{A}}, \bar{Q}_{\dot{B}}\} = 0, \quad (2.9a)$$

$$\{Q_A, \bar{Q}_{\dot{B}}\} = 2\sigma_{A\dot{B}}^\mu P_\mu, \quad (2.9b)$$

$$[Q_A, P^\mu] = [\bar{Q}_{\dot{A}}, P^\mu] = 0, \quad (2.9c)$$

$$[Q_A, M^{\mu\nu}] = i\sigma_A^{\mu\nu B} Q_B, \quad (2.9d)$$

$$[\bar{Q}_{\dot{A}}, M^{\mu\nu}] = i\bar{\sigma}^{\mu\nu \dot{B}}_{\dot{A}} \bar{Q}_{\dot{B}}, \quad (2.9e)$$

where P^μ denotes the generator of spacetime translations and $M^{\mu\nu}$ the generator of Lorentz transformations. The indices $A, \dot{A} = 1, 2$ are spinor indices, since Q is a fermionic object. Our notation mainly follows Ref. [121] and we summarize the most important conventions and identities in Appendix A.

In addition to these fermionic generators, we also formally extend the coordinates of spacetime to include the fermionic coordinates θ^A and $\bar{\theta}^{\dot{A}}$. These coordinates anticommute as well and are, therefore, Grassmann numbers with the relations

$$\{\theta^A, \theta^B\} = \{\theta^A, \bar{\theta}^{\dot{B}}\} = \{\bar{\theta}^{\dot{A}}, \bar{\theta}^{\dot{B}}\} = 0. \quad (2.10)$$

The combination of these with the normal spacetime coordinates x^μ is called superspace and all fields defined in this extended space are called superfields. The Taylor expansion of such a general superfield has only a finite number of terms, since any product of three or more θ vanishes. The surviving terms read

$$\begin{aligned} \mathcal{F}(x, \theta, \bar{\theta}) = & f(x) + \sqrt{2}\theta\xi(x) + \sqrt{2}\bar{\theta}\bar{\chi}(x) + \theta\theta M(x) + \bar{\theta}\bar{\theta}N(x) + \theta\sigma^\mu\bar{\theta}A_\mu(x) \\ & + \theta\theta\bar{\theta}\bar{\lambda}(x) + \bar{\theta}\bar{\theta}\theta\chi(x) + \frac{1}{2}\theta\theta\bar{\theta}\bar{\theta}D(x). \end{aligned} \quad (2.11)$$

Here f, M, N and D are complex scalar fields, A_μ is a four-component vector field, and ξ, χ, λ and ζ are two-component Weyl fermion fields, where the bar denotes also Hermitian conjugation.

²Here we confine ourselves to one fermionic generator Q , so we consider $N = 1$ SUSY. We do not consider extended SUSY or central charges.

2.2.2 Chiral Superfields

We now want to introduce the simplest objects that obey all SUSY transformation laws, hence the smallest number of degrees of freedom compatible with the above commutators. In light of (2.8), we know that we need both a fermionic component and a bosonic one. Each irreducible set of fields related by Q is called supermultiplet. In fact, with the help of (2.9), one can show that the number of bosonic and fermionic degrees of freedom have to match in each supermultiplet.

For covariance in superspace, we need the definition of a SUSY invariant derivative \mathcal{D} , thus a derivative with respect to the superspace coordinates that commutes with the generators Q . It can be shown that they are given by [121]

$$\mathcal{D}_A = \frac{\partial}{\partial \theta^A} - i \sigma_{A\dot{B}}^\mu \bar{\theta}^{\dot{B}} \frac{\partial}{\partial x^\mu}, \quad (2.12a)$$

$$\mathcal{D}^A = -\frac{\partial}{\partial \theta_A} + i \bar{\theta}_{\dot{B}} \bar{\sigma}^{\mu\dot{B}A} \frac{\partial}{\partial x^\mu}, \quad (2.12b)$$

$$\bar{\mathcal{D}}^{\dot{A}} = \frac{\partial}{\partial \bar{\theta}_{\dot{A}}} - i \bar{\sigma}^{\mu\dot{A}B} \theta_B \frac{\partial}{\partial x^\mu}, \quad (2.12c)$$

$$\bar{\mathcal{D}}_{\dot{A}} = -\frac{\partial}{\partial \bar{\theta}^{\dot{A}}} + i \theta^B \sigma_{B\dot{A}}^\mu \frac{\partial}{\partial x^\mu}. \quad (2.12d)$$

Note that here and in the following we omit the details of SUSY transformations and present only the results of such calculations. For a detailed treatment, the reader is referred to the literature.

Applying these derivatives to a general superfield and requiring

$$\bar{\mathcal{D}}_{\dot{A}} \Phi(x, \theta, \bar{\theta}) = 0, \quad (2.13)$$

left chiral superfield are defined. As the name suggests, when executing the above differentiation, the result contains only left chiral Weyl superfields. Similarly, right chiral superfields are defined by the equation

$$\mathcal{D}_A \Phi^\dagger(x, \theta, \bar{\theta}) = 0. \quad (2.14)$$

It is convenient to define

$$y^\mu = x^\mu - i \theta \sigma^\mu \bar{\theta}, \quad (2.15a)$$

$$\bar{y}^\mu = x^\mu + i \theta \sigma^\mu \bar{\theta}, \quad (2.15b)$$

and rewrite the left and right chiral superfields as functions of these coordinates. From the explicit form of the derivatives, it follows

$$\bar{\mathcal{D}}_{\dot{A}} \theta = \bar{\mathcal{D}}_{\dot{A}} y = 0, \quad (2.16a)$$

$$\mathcal{D}_A \bar{\theta} = \mathcal{D}_A \bar{y} = 0. \quad (2.16b)$$

So we see that a left chiral superfield is given by

$$\Phi(y, \theta) = \phi(y) + \sqrt{2}\theta\xi(y) + \theta\theta F(y), \quad (2.17)$$

and a right chiral one by

$$\Phi(\bar{y}, \bar{\theta}) = \phi^*(\bar{y}) + \sqrt{2}\bar{\theta}\bar{\xi}(y) + \bar{\theta}\bar{\theta}F^*(\bar{y}), \quad (2.18)$$

where the star denotes complex conjugation. Expanding in $(x^\mu, \theta, \bar{\theta})$, we find for the left chiral superfield

$$\begin{aligned} \Phi(x, \theta, \bar{\theta}) = & \phi(x) + \sqrt{2}\theta\xi(x) - i\theta\sigma^\mu\bar{\theta}\partial_\mu\phi(x) + \frac{i}{\sqrt{2}}\theta\theta\partial_\mu\xi(x)\sigma^\mu\bar{\theta} \\ & - \frac{1}{4}\theta\theta\bar{\theta}\bar{\theta}\partial^\mu\partial_\mu\phi(x) + \theta\theta F(x), \end{aligned} \quad (2.19)$$

and a similar expression for the right chiral superfield.

We see that (2.19) contains two complex scalar fields, ϕ and F and one two-component left handed Weyl spinor ξ , so four real bosonic and four real fermionic degrees of freedom.

Note that although F is part of the superfield, it has no kinetic term, as we will see later. It is still necessary, however, since it ensures that this superfield is indeed supersymmetric. In fact, on-shell, the SUSY algebra would close without the F -term, but not off-shell. This means, without the F -term, SUSY would only hold at the classical level, but not quantum mechanically. This can also be seen from the fact that the numbers of degrees of freedom for the above superfield without the F -term match on-shell (two bosonic and two fermionic ones), whereas off-shell the fermion is a complex two-component object. From this perspective, one can view the F -terms as being auxiliary, since they are a sort of “book-keeping devices” to ensure SUSY conservation. As we will see, they can be eliminated from the Lagrangian via their equations of motions.

This concludes the introduction of the first class of superfields. When one applies the above supersymmetrization to the fields in the SM one finds that all matter fields present in the SM are represented by chiral superfields. We adopt the notation that superpartners of SM fields are written with a tilde. So each quark q_i of a certain chirality and charge is in one supermultiplet with its scalar superpartner, the squark \tilde{q}_i . The same is true for the lepton supermultiplet, containing the charged leptons l_i and the sleptons \tilde{l}_i as well as the neutrinos ν_i and the sneutrinos $\tilde{\nu}_i$. All of these particles are present in the usual three families. Moreover, for each chirality of the SM particles, there is a separate sparticle. In the case of the Higgs boson, there is one additional complication. The details of electroweak symmetry breaking in SUSY require the existence of two Higgs doublets, $H_u^{+/-}$ and $H_d^{0/-}$, that couple to the up-type and down-type quarks, respectively. Consequently, before electroweak symmetry breaking, there are two types of Higgsinos \tilde{H} in these multiplets.

The gauge bosons and their superpartners, the gauginos, however, are of a different type and cannot be described by chiral superfields. They require vector superfields.

2.2.3 Vector Superfields

Vector superfields are defined such that they contain the vector field A_μ already visible in (2.11). It turns out that the relation

$$V(x, \theta, \bar{\theta}) = V^\dagger(x, \theta, \bar{\theta}) \quad (2.20)$$

gives the desired result. As for the chiral field, this constraint reduces the degrees of freedom and we arrive at

$$\begin{aligned} V(x, \theta, \bar{\theta}) = & C(x) + \sqrt{2}\theta\xi(x) + \sqrt{2}\bar{\theta}\bar{\xi}(x) + \theta\theta M(x) + \bar{\theta}\bar{\theta}M^\dagger(x) + \theta\sigma^\mu\bar{\theta}A_\mu(x) \\ & + \theta\theta\bar{\theta}\bar{\lambda}(x) + \bar{\theta}\bar{\theta}\theta\lambda(x) + \frac{1}{2}\theta\theta\bar{\theta}\bar{\theta}D(x). \end{aligned} \quad (2.21)$$

Note that C and D are now real scalar fields, M is still complex, A_μ is a real vector field and we are left with only two complex Weyl spinors, ξ and λ .

In contrast to the case of chiral fields, we cannot identify these fields with the gauge bosons present in the SM and their superpartners yet, because (2.21) contains unphysical degrees of freedom that can be removed by a “supergauge” transformation. This gauge transformation, however, is not one of the usual gauge transformations of the SM, rather it involves adding chiral superfields to V . Consider the transformation

$$V \rightarrow V + i(\Lambda^* - \Lambda) \quad (2.22)$$

where $\Lambda = \phi + \sqrt{2}\theta\psi + \theta\theta F$ is the chiral superfield that acts as a gauge transformation parameter. The resulting transformations of the components of (2.21) read

$$C \rightarrow C + (\phi + \phi^*), \quad (2.23a)$$

$$\xi \rightarrow \xi + \psi, \quad (2.23b)$$

$$M \rightarrow M + F, \quad (2.23c)$$

$$A_\mu \rightarrow A_\mu + i\partial_\mu(\phi - \phi^*), \quad (2.23d)$$

$$\lambda \rightarrow \lambda, \quad (2.23e)$$

$$D \rightarrow D. \quad (2.23f)$$

Since in the end we want to identify A_μ with the gauge fields of the SM, we can see from (2.23d) that the “supergauge” transformation (2.22) already includes ordinary U(1) gauge transformation as a special case. Note that the transformation parameter of such ordinary transformations is given by $2\text{Im}(\phi)$, so we have enough free parameters left to eliminate the fields C , ξ , and M from (2.21). Such a supergauge transformation is known as the Wess–Zumino gauge [123] and the resulting vector field reads

$$V_{\text{WZ}}(x, \theta, \bar{\theta}) = \theta\sigma^\mu\bar{\theta}A_\mu(x) + \theta\theta\bar{\theta}\bar{\lambda}(x) + \bar{\theta}\bar{\theta}\theta\lambda(x) + \frac{1}{2}\theta\theta\bar{\theta}\bar{\theta}D(x). \quad (2.24)$$

The D -terms are also auxiliary, similar to the F -terms discussed earlier. Note that also in this case all fermion fields are written as two-component fields. Some identities relating this notation to the more common one using four-component spinors are given in Appendix A.

For non-abelian gauge groups, the vector field has the same form as (2.24), the details of the gauge interaction are, however, more involved as mentioned in the next section.

2.2.4 Supersymmetric Interactions

Let us now describe the interaction of these two types of superfields. As in the SM, there are basically two types of interaction terms, Yukawa and gauge interactions. We first describe the former type. We begin by noting that a product of left (right) chiral superfields is invariant under SUSY transformations and is again a left (right) chiral superfield.

The product of a left and a right chiral superfield, however, is a vector superfield, since

$$(\Phi_i^\dagger \Phi_j)^\dagger = \Phi_i^\dagger \Phi_j. \quad (2.25)$$

By construction, all superfields are invariant under SUSY transformations. But since these fields live in superspace, we cannot use them directly to describe physics in our four-dimensional spacetime. We must look for SUSY invariant components of these combinations of superfields, hence components that are either invariant under SUSY transformations or transform only by a total derivative. The latter is enough, because a total derivative does not contribute to the action. Although there are no invariant components, it turns out that the F -terms or, more general, the terms proportional to $\theta\theta$ or $\bar{\theta}\bar{\theta}$ of a chiral superfield, transform just by a total derivative. For the vector superfields, one finds that the D -terms, hence the terms proportional to $\theta\theta\bar{\theta}\bar{\theta}$ also transform by a total derivative. Thus, we can write a SUSY invariant Lagrangian as

$$\mathcal{L} = \left[\mathcal{K}(\Phi_i^\dagger \Phi_j) \right]_{\theta\theta\bar{\theta}\bar{\theta}} + \left[\mathcal{W}(\Phi_i) \right]_{\theta\theta} + \left[\mathcal{W}^\dagger(\Phi_i^\dagger) \right]_{\bar{\theta}\bar{\theta}}, \quad (2.26)$$

where \mathcal{W} is called the superpotential, which is a holomorphic function of the superfields Φ_i , the real function \mathcal{K} is the Kähler potential and $[\dots]_X$ indicates to take only the terms proportional to X .

As a side mark, the last notation is often written as $[\dots]_{F/D}$ to indicate the F - or D -term contribution, respectively. Moreover, one can define integrals over the fermionic superspace coordinates. The Grassmann nature of θ and $\bar{\theta}$ then turns some of these integrals into projectors, allowing one to write, e.g., $[\dots]_{\theta\theta}$ as $\int d^2\theta \dots$. The necessary formulas are given in Appendix A.

Coming back to (2.26), the Kähler potential is responsible for the form of the kinetic terms of this theory. In all of this work we deal only with canonical kinetic terms, which are obtained by setting

$$\mathcal{K}(\Phi_i^\dagger \Phi_j) = \sum_i \Phi_i^\dagger \Phi_i. \quad (2.27)$$

The superpotential \mathcal{W} , on the other hand, includes all the Yukawa interaction of our theory, as we will show now. Since \mathcal{W} is holomorphic, it can only contain Φ and not Φ^\dagger . Moreover, products of more than three superfields lead to non-renormalizable interactions, which we do not want to include here. This leaves us with

$$\mathcal{W} = \frac{1}{2} M^{ij} \Phi_i \Phi_j + \frac{1}{6} y^{ijk} \Phi_i \Phi_j \Phi_k, \quad (2.28)$$

where we have also omitted a potential term linear in Φ , since such a term is only allowed for gauge singlets. This choice of \mathcal{K} and \mathcal{W} is called the Wess–Zumino model [33, 124].

Plugging the explicit forms of the Kähler potential and the superpotential for a chiral field given by (2.19) into (2.26), one arrives at

$$\begin{aligned} \mathcal{L}_{\text{WZ}} = & \partial^\mu \phi^{*i} \partial_\mu \phi_i + \frac{i}{2} \bar{\psi}^i \sigma^\mu (\partial_\mu \psi_i) - \frac{i}{2} (\partial_\mu \bar{\psi}^i) \sigma^\mu \psi_i + F^{*i} F_i \\ & + \left(M^{ij} \phi_i F_j + \frac{y^{ijk}}{2} \phi_i \phi_j F_k - \frac{M^{ij}}{2} \psi_i \psi_j - \frac{y^{ijk}}{2} \phi_i \psi_j \psi_k + \text{h.c.} \right), \end{aligned} \quad (2.29)$$

where h.c. denotes Hermitian conjugation. As already highlighted before, we see that there are no kinetic terms for the F fields. Therefore, they can be eliminated via their equations of motion

$$0 = F_i^\dagger + M^{ij} \phi_j + \frac{y^{ijk}}{2} \phi_j \phi_k, \quad (2.30)$$

and we cast the Lagrangian in the useful form

$$\mathcal{L}_{\text{WZ}} = \partial^\mu \phi^{*i} \partial_\mu \phi_i + \frac{i}{2} \bar{\psi}^i \sigma^\mu (\partial_\mu \psi_i) - \frac{i}{2} (\partial_\mu \bar{\psi}^i) \sigma^\mu \psi_i - \frac{1}{2} (\mathcal{W}^{ij} \psi_i \psi_j + \text{h.c.}) - \mathcal{W}^i \bar{\mathcal{W}}_i, \quad (2.31)$$

with the abbreviations

$$\mathcal{W}^i = \frac{\partial \mathcal{W}}{\partial \phi_i}, \quad (2.32a)$$

$$\mathcal{W}^{ij} = \frac{\partial^2 \mathcal{W}}{\partial \phi_i \partial \phi_j}, \quad (2.32b)$$

and their respective Hermitian conjugates. After integrating out the fermionic superspace coordinates, we can view \mathcal{W} as a holomorphic function of the scalar fields ϕ_i treated as complex variables.

To sum up, the above discussion shows that all Yukawa interactions and the scalar potential of a SUSY theory are given by one function, the superpotential \mathcal{W} . Using (2.29), one can then deduce the interaction terms of each field. The gauge interactions, however, are not covered by the above consideration and must be treated separately, as shown in the following.

Although we have already calculated a compact expression for the vector superfield that does not contain any unphysical degrees of freedom in (2.24), it is not as straightforward as for chiral superfields to arrive at supersymmetric and gauge-invariant components for the four-dimensional Lagrangian. A detailed discussion is beyond the scope of this introduction, we merely present the resulting equations that are necessary for our purposes.

It can be shown that the term

$$\left[\Phi_i^\dagger \left(e^{2g_b V^b T^b} \right)^{ij} \Phi_j \right]_{\theta\theta\bar{\theta}\bar{\theta}} \quad (2.33)$$

provides gauge-invariant interaction terms corresponding to the gauge group with coupling strength g_b and generators T^b . This holds for abelian as well as for non-abelian gauge groups. Details about the derivation of the above term can be found in the literature, e.g., Ref. [121].

The terms

$$W_A = -\frac{1}{4} \bar{\mathcal{D}} \bar{\mathcal{D}} \mathcal{D}_A V_{\text{WZ}}(y, \theta, \bar{\theta}) \quad (2.34)$$

and

$$\bar{W}_{\dot{A}} = -\frac{1}{4} \mathcal{D} \mathcal{D} \bar{\mathcal{D}}_{\dot{A}} V_{\text{WZ}}(\bar{y}, \theta, \bar{\theta}) \quad (2.35)$$

yield left and right chiral superfields, which, in the combination

$$\frac{1}{4} \left[W^A W_A \right]_{\theta\theta} + \frac{1}{4} \left[\bar{W}_{\dot{A}} \bar{W}^{\dot{A}} \right]_{\bar{\theta}\bar{\theta}}, \quad (2.36)$$

form gauge-invariant and supersymmetric kinetic terms for gauge bosons and their superpartners, the gauginos. Here W_A should not be confused with the superpotential $\mathcal{W}(\phi)$. The former is a chiral superfield, whereas the latter is a complex function of scalar fields. Details about the calculation of W_A and $\bar{W}_{\dot{A}}$ can be found in Appendix B, where we calculate these two superfields in detail. The $\theta\theta$ component of (B.25) and the $\bar{\theta}\bar{\theta}$ component of (B.27) give the desired kinetic terms. Note that (B.25) and (B.27) are written without covariant derivatives. By making the replacement

$$\partial_\mu \rightarrow D_\mu^{bd}, \quad (2.37)$$

where $D_\mu^{bd} = \partial_\mu \delta^{bd} - g_b f^{bcd} A_\mu^c$ for the generic gauge group also used above, one arrives at

$$\mathcal{L}_{\text{gauge}}^{\text{kin}} = -\frac{1}{4} F^{b\mu\nu} F_{\mu\nu}^b + i \lambda^b \sigma^\mu D_\mu^{bd} \bar{\lambda}^d. \quad (2.38)$$

Here λ^b denotes the Weyl spinor of the gaugino of the respective gauge group and we have performed a partial integration to simplify its kinetic term. The D -terms as well as interactions with chiral fields have been dropped and can be found in the literature, e.g., in Ref. [121].

In this form we can now identify the gauge bosons of the abelian SM gauge group, $U(1)_{\text{em}}$. The photon γ is described by its field strength tensor $F^{\mu\nu}$, the photino $\tilde{\gamma}$ by the Weyl spinor λ and $f^{bcd} \rightarrow 1$ in the definition of the covariant derivative.

In the case of $SU(3)_c$, the gluon g^b is represented by its field strength tensor $G^{b\mu\nu}$, the superpartner is the gluino \tilde{g}^b and f^{bcd} are the structure constants of $SU(3)_c$. The weak interactions can be obtained in a similar manner. However, since we do not need them in the following, they are not stated explicitly.

We showed both types of interactions that are present in the SM, Yukawa and gauge interactions, also in a supersymmetrized version. When one attempts to construct a SUSY version of the SM with minimal field content, one realizes that there are possible terms in the superpotential that are allowed by SUSY and gauge symmetry, but that violate baryon number B or total lepton number L . Such terms would yield interaction vertices that lead to rapid proton decay. This is in conflict with experiment and, therefore, one introduces a new discrete symmetry called R -parity [125] defined as

$$R_p = (-1)^{3(B-L)+2S}, \quad (2.39)$$

where S denotes the spin of a particle. From this definition, one finds that for all particles of the SM, $R_p = 1$, whereas for all their superpartners, called sparticles, $R_p = -1$. The imposed R -parity conservation at each vertex then forbids terms leading to fast proton decays. Moreover, the LSP is stable due to R -parity conservation, since at each vertex the number of sparticles has to be even. This will be of great importance when we discuss the effects of SUSY in the early Universe.

2.2.5 SUSY Breaking

In all of the above discussion, SUSY was considered as an exact symmetry of nature. But if this were true, we would have seen some superpartners of the SM particles, since all particles in one supermultiplet are mass-degenerate because the square of the momentum operator P^2 commutes with the generators of SUSY, Q and \bar{Q} . Thus, SUSY has to be broken.

In general, there are two ways to break a symmetry, explicitly by the inclusion of non-symmetric terms or spontaneously by a ground state that does not respect the symmetry. The latter is clearly theoretically more appealing, but for phenomenological purposes the details of the SUSY breaking mechanism are often not relevant. Thus, one introduces terms in the Lagrangian that parametrize the effects of a spontaneous breaking of SUSY. These terms should be soft, meaning they should have mass dimension less than four. In this way one avoids the introduction of terms

that spoil the solution of the hierarchy problem given by unbroken SUSY. The most general set of soft SUSY breaking terms that are gauge-invariant are [126]

$$\mathcal{L}_{\text{soft}} = -\phi_i^* m_{ij}^2 \phi_j + \left(\frac{1}{6} A_{ijk} \phi_i \phi_j \phi_k - \frac{1}{2} B_{ij} \phi_i \phi_j + C_i \phi_i + \text{h.c.} \right) - \frac{1}{2} (M \lambda^a \lambda^a + \text{h.c.}), \quad (2.40)$$

where ϕ_i denotes the scalar part of a superfield Φ_i and λ^a is a gaugino field. The parameters A_{ijk} and B_{ij} are tensors of trilinear and bilinear scalar interaction terms, respectively, C_i is a constant for a linear scalar term, and m_{ij}^2 and M are mass parameters for scalar and gaugino mass terms.

The constants of (2.40) are typically inferred from an explicit model of SUSY breaking. Since we do not go into details of SUSY breaking, we consider all soft breaking parameters and the resulting sparticle masses as free parameters unless stated otherwise.

Note that although we have just parametrized the resulting effective terms of a spontaneously broken SUSY in (2.40), there is, as for every spontaneously broken symmetry, also here a Goldstone particle present in the mass spectrum. Since the Noether current associated with SUSY transformations is fermionic, here this Goldstone particle is a fermion, the goldstino [127]. If there are no terms that break SUSY explicitly, the goldstino is massless. This particle is especially of importance, when one looks at generalizations of SUSY to include also local SUSY transformations.

2.2.6 Local SUSY and the Gravitino

So far, we have treated the SUSY generators Q as global symmetry generators, thus coordinate independent. If we make them local (so we “gauge” them), invariance under such SUSY transformation requires the introduction of new fields that are the gauge fields of the local SUSY transformations in the same way as one gets the photon field as the gauge boson of the local $U(1)_{\text{em}}$. Again, because the Noether current associated with SUSY transformations is fermionic, local SUSY actually introduces gauge fermions.³

By looking at (2.9b), one can see that the requirement of local SUSY implies an invariance under local coordinate transformations. This is the principle of General Relativity, thus local SUSY is also called supergravity [129–135]. It turns out that the gauge fermion mentioned above is the superpartner of the graviton and is called the gravitino \tilde{G} . It is a spin-3/2 particle with mass $m_{\tilde{G}}$. For unbroken SUSY, $m_{\tilde{G}} = 0$. In analogy to the bosonic gauge fields of the SM, here a spontaneous breaking of SUSY makes the gravitino massive by “eating” the goldstino. This mechanism is called the super-Higgs mechanism [136]. We do not go into detail of this mechanism but simply treat $m_{\tilde{G}}$ as a free parameter.

³We give only a very brief introduction to local SUSY and supergravity following Ref. [121]. For a textbook version of a more detailed treatment, see for example Ref. [128].

The interactions of the gravitino are all suppressed by $1/M_{\text{Pl}}$, with the reduced Planck mass $M_{\text{Pl}} = (8\pi G_N)^{-1/2} \simeq 2.4 \times 10^{18} \text{ GeV}$ [12] and Newton's constant G_N . We skip all the details of the derivation of the interaction Lagrangian and refer the reader to the literature. In fact, the only interaction we need here is the coupling of gravitinos to a chiral supermultiplet. The relevant Lagrangian reads in four-component notation [121]

$$\mathcal{L}_{\tilde{G}} \supset -\frac{1}{\sqrt{2}M_{\text{Pl}}} (\mathcal{G}_j^i \bar{\Psi}_\mu \mathcal{D} \phi^{*i} \gamma^\mu \psi_{jL} + \text{h.c.}), \quad (2.41)$$

where Ψ_μ is the gravitino spinor, γ^μ is the Dirac gamma matrix, $\mathcal{D} = \gamma^\nu \mathcal{D}_\nu$ is the general covariant derivative, so the sum of the gauge covariant derivative D^{bd} defined after (2.37) and the affine connection term of General Relativity. Note that in the case of a flat spacetime and if the chiral superfield is a gauge singlet, $\mathcal{D} = \partial$. The scalar part of the chiral superfield is denoted by ϕ and the fermionic one by ψ . The prefactor includes the Kähler metric \mathcal{G}_j^i given by the derivative of the Kähler function \mathcal{G} and reads

$$\mathcal{G}_j^i = \frac{\partial^2 \mathcal{G}}{\partial \phi_i \partial \phi^{*j}} = \frac{\partial^2}{\partial \phi_i \partial \phi^{*j}} M_{\text{Pl}}^2 \left[\mathcal{K} \left(\frac{\phi_i}{M_{\text{Pl}}}, \frac{\phi^{*j}}{M_{\text{Pl}}} \right) - \ln \frac{|\mathcal{W}(\phi_i)|^2}{M_{\text{Pl}}^6} \right]. \quad (2.42)$$

In order to get canonical kinetic terms, we use (2.27) and then $\mathcal{G}_j^i = -\delta_j^i$. Other interactions of the gravitino can be found in the literature.

This concludes our introduction to SUSY and we now combine these results with the PQ mechanism.

2.3 The PQ Supermultiplet

The axion is a gauge singlet, so in a SUSY theory it is part of a chiral supermultiplet, given in the general form by (2.19). Its superpartner is a Weyl fermion, the axino \tilde{a} . Since the axion is a real scalar field, there is another scalar degree of freedom called the saxion σ . The combined PQ supermultiplet⁴ then reads

$$\begin{aligned} A(x, \theta, \bar{\theta}) = & \frac{\sigma(x) + ia(x)}{\sqrt{2}} + \sqrt{2}\theta\tilde{a}(x) - i\theta\sigma^\mu\bar{\theta}\partial_\mu \frac{\sigma(x) + ia(x)}{\sqrt{2}} + \frac{i}{\sqrt{2}}\theta\theta\partial_\mu\tilde{a}(x)\sigma^\mu\bar{\theta} \\ & - \frac{1}{4}\theta\theta\bar{\theta}\bar{\theta}\partial^\mu\partial_\mu \frac{\sigma(x) + ia(x)}{\sqrt{2}} + \theta\theta F_A(x), \end{aligned} \quad (2.43)$$

or, in the more compact form as functions of y ,

$$A(y, \theta) = \frac{\sigma(y) + ia(y)}{\sqrt{2}} + \sqrt{2}\theta\tilde{a}(y) + \theta\theta F_A(y). \quad (2.44)$$

⁴From a historic perspective, the name PQ supermultiplet may arguably be misleading, since Peccei and Quinn did not immediately realize the presence of the axion as a result of their mechanism [34, 35]. Nevertheless, we stick to the name PQ multiplet/particles in our work.

Note that although the saxion was not mentioned in Sect. 2.1, it is not a superpartner in the sense of R -parity, since it has $R_p = 1$. The reason why the saxion is normally not considered in PQ theories without SUSY is its mass, which is large in the absence of SUSY.

2.4 The Hadronic Axion Model

The interactions of the PQ particles with the other fields of the SM or the MSSM are all non-renormalizable, as can be seen from (2.6) for the case of the axion. Thus, there has to be an underlying renormalizable theory with the interaction terms of the PQ particles as a low energy limit. Here we focus on a specific group of models, the hadronic or KSVZ axion model [26, 27]. The other group is the DSFZ models [137, 138]. We first describe the original version of the KSVZ model, which is an extension of the SM, and then we present a SUSY version of the hadronic axion model.

In the original implementation, this model consists of a hypothetical $SU(3)_c$ triplet, $SU(2)_L$ singlet heavy Dirac quark field ψ_Q and a gauge singlet complex scalar ϕ . The Lagrangian reads [27]

$$\mathcal{L}_{\text{KSVZ}} = i\bar{\psi}_Q \not{D} \psi_Q + \partial^\mu \phi^* \partial_\mu \phi + h (\phi \bar{\psi}_{Q_R} \psi_{Q_L} + \phi^* \bar{\psi}_{Q_L} \psi_{Q_R}) + V(\phi, \phi^*), \quad (2.45)$$

where h is a Yukawa coupling taken to be sufficiently small to allow for perturbative calculations, D is the covariant derivative that provides kinetic terms for the heavy quarks and a coupling to gluons, and V is the scalar potential given by

$$V(\phi, \phi^*) = m^2 \phi^* \phi - \lambda (\phi^* \phi)^2 \quad (2.46)$$

with $\lambda > 0$. The above Lagrangian is invariant under the global $U(1)_{\text{PQ}}$ transformations

$$\psi_{Q_R} \rightarrow e^{i\alpha/2} \psi_{Q_R}, \quad (2.47a)$$

$$\psi_{Q_L} \rightarrow e^{-i\alpha/2} \psi_{Q_L}, \quad (2.47b)$$

$$\phi \rightarrow e^{i\alpha} \phi. \quad (2.47c)$$

The heavy quarks carry a PQ charge of $-1/2$ and ϕ carries a PQ charge of 1. The potential has a minimum at

$$|\langle \phi \rangle| = \phi_0 = \pm \frac{m}{\sqrt{2\lambda}}, \quad (2.48)$$

which leads to a spontaneous breaking of the $U(1)_{\text{PQ}}$. In order to arrive at canonically normalized kinetic terms, the scalar field is parametrized as

$$\phi(x) = \sigma(x) \exp \left[i \frac{a(x)}{\sqrt{2}\phi_0} \right]. \quad (2.49)$$

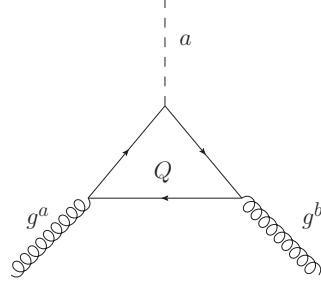


Figure 2.1: *Triangle loop of KSVZ quarks coupling to one axion and two gluons. Note that there is a second diagram with opposite direction of the arrows.*

We see that σ rolls towards its VEV ϕ_0 whereas a stays massless. This means that a is the pseudo–Nambu–Goldstone boson of the broken PQ symmetry, so we can identify it as the axion. The radial field σ on the other hand has a mass $\sqrt{2}m$ and is called the saxion.

In the low energy limit of the broken symmetry, we can expand the exponential in the Yukawa interaction. The zeroth-order term provides an effective mass term for the heavy quarks, $m_Q = h\phi_0$. The first-order term results in an interaction of the heavy quarks with the phase of ϕ , hence with the axion. This coupling is proportional to the Dirac matrix γ^5 , since the axion is a pseudoscalar. The heavy quarks couple to gluons just as the SM quarks, so we can construct a triangle loop with Q fields coupling to one axion and two gluons. This loop is shown in Fig. 2.1. There is also a box diagram where an axion couples to a box of heavy quarks which, in turn, couple to three external gluons.

Since the mass of the quarks is taken to be large we can integrate them out in these loops and we are left with the following effective term in the Lagrangian

$$\mathcal{L}^{\text{int}} = \frac{g_s^2 h \phi_0}{32\pi^2 \sqrt{2} m_Q \phi_0} a G^{b\mu\nu} \tilde{G}_{\mu\nu}^b. \quad (2.50)$$

Comparing this to (2.6), we see that by defining

$$f_{\text{PQ}} = \sqrt{2} \phi_0 \quad (2.51)$$

we recover the original effective interaction term of the axion. So we see that this model provides us with the expected form of the axion interaction term and no other light degree of freedom, since these KSVZ quarks turn out to be typically too heavy to be excited in the scenarios we consider.

Note that one could also perform an axion-dependent chiral rotation of the quark fields

$$\psi_{Q_{L/R}} \rightarrow \exp\left(\pm i \frac{a}{\sqrt{2}\phi_0}\right) \psi_{Q_{L/R}} \quad (2.52)$$

to arrive at physical mass terms for the KSVZ quarks. This rotation introduces the shift $\bar{\theta} \rightarrow \bar{\theta} + a$ and thereby also results in the above \mathcal{L}^{int} for the axion.

If one constructs a hadronic axion model with $N_Q > 1$ heavy quark field, for each of them one repeats the above calculation and we are left with N_Q additional terms in the Lagrangian, each of the form of (2.50). The definition of the PQ breaking scale then changes to

$$f_{\text{PQ}} = \frac{\sqrt{2}\phi_0}{N_Q}. \quad (2.53)$$

The number N_Q is often called the domain wall number N_Q , e.g., in Ref. [42], since for $N_Q > 1$ one has more than one CP conserving vacuum and, therefore, domain walls form after the breaking of the PQ symmetry. These domain walls can have severe cosmological consequences [139], so we set $N_Q = 1$ in our work.

In the following, we construct a SUSY version of this hadronic axion model.

2.4.1 Interaction Vertices obtained from Loops

We have seen that the supersymmetric Yukawa interactions are given by the superpotential. In the case of the hadronic axion model, this potential is often chosen to be [140]

$$\mathcal{W}_{\text{KSVZ}} = \kappa R \left(\Phi_1 \Phi_2 - \frac{v_{\text{PQ}}^2}{2} \right) + h \Phi_1 \bar{Q}_1 Q_2, \quad (2.54)$$

where the PQ charges of Φ_1 , Φ_2 , Q_i , and the gauge-singlet superfield R are 1, -1, -1/2, and 0, respectively. The parameter v_{PQ} has the dimension of mass. In contrast to the original model in Ref. [140], but in line with most of the later literature (e.g., Refs. [62, 64, 92, 141]), we have just one R field. The invariance of (2.54) under PQ transformations is manifest. The superpotential (2.54) has an additional R -symmetry with charges 0 and 2 for Q_i and R , respectively. The R -symmetry is a continuous version of the R -parity introduced earlier. R -symmetries can be used in model building to motivate certain choices of terms, but since we do not need it in the following, we point the interested reader to the literature, e.g., see Ref. [119].

The scalar potential resulting from the first term of the above superpotential reads

$$V = \left| \phi_1 \phi_2 - \frac{v_{\text{PQ}}^2}{2} \right|^2 + |\phi_R \phi_1|^2 + |\phi_R \phi_2|^2, \quad (2.55)$$

where ϕ_i denotes the scalar component of the respective superfield. The minimum of this potential is at $\langle \phi_1 \phi_2 \rangle = v_{\text{PQ}}^2/2$ and $\langle \phi_R \rangle = 0$. Note that we cannot deduce the value of the VEV of each PQ scalar field from (2.55), so for illustrative purposes we assume that $\langle \phi_1 \rangle \simeq \langle \phi_2 \rangle \simeq v_{\text{PQ}}/\sqrt{2}$.

This choice can be motivated as follows. The above description with the superpotential (2.54) does not include SUSY breaking effects. The inclusion of soft SUSY

breaking terms provides a VEV for ϕ_R and also fixes the ratio $\langle\phi_1\rangle/\langle\phi_2\rangle$. This breaking of SUSY defines the saxion and axino masses. Since we do not elaborate on the details of SUSY breaking here and treat both the saxion and axino mass as free parameters, we can assume that the soft breaking terms are such that the ratio $\langle\phi_1\rangle/\langle\phi_2\rangle \simeq 1$ without loss of generality of our scenario, see also Ref. [53].

One naively would expect that the masses of the fields contained in R , Φ_1 , and Φ_2 are all of order of the only scale in the superpotential, namely v_{PQ} . It can be shown, however, that for unbroken SUSY the mass spectrum of this setup contains one massless scalar, the saxion, one massless pseudoscalar, the axion, and a massless fermion, the axino. All other degrees of freedom have masses $\mathcal{O}(v_{\text{PQ}})$ [56]. This mass spectrum is a result of the imposed PQ symmetry. In fact, without SUSY, the PQ symmetry guarantees a massless scalar as a result of the spontaneous breaking of $U(1)_{\text{PQ}}$. This symmetry is called real, since it involves transformations like

$$\phi \rightarrow e^{i\alpha}\phi,$$

where $\alpha \in \mathbb{R}$. In SUSY theories, the superpotential has to be holomorphic, as we have seen, because otherwise the resulting Lagrangian is not supersymmetric. Thus, the real $U(1)_{\text{PQ}}$ gets promoted to a complex $U(1)_{\text{PQ}}^C$ when imposed on a superpotential [57]. By complex, we mean it generates transformations like

$$\phi \rightarrow e^{i\Lambda}\phi,$$

where now $\Lambda = \alpha + i\beta \in \mathbb{C}$. This leads to a flat direction in the scalar potential visible as $\langle\phi_1\phi_2\rangle = v_{\text{PQ}}^2/2$ in (2.55). Moreover, one also gets a massless scalar perpendicular to the axion, the aforementioned saxion. For brevity, we drop the superscript C of $U(1)_{\text{PQ}}^C$ in the following.

Thus, one can expand the PQ scalar fields ϕ_i with PQ charges q_i near their VEVs v_i as

$$\phi_i = v_i \exp \left[\frac{q_i(\sigma + ia)}{\sqrt{2}v_{\text{PQ}}} \right]. \quad (2.56)$$

This formula is also valid if there are more than two PQ supermultiplets. We adopt the convention that the smallest PQ charge is set to one, because this assures that a shift by 2π of the axion field brings all PQ scalars back to their original values as required by the PQ symmetry. For small fields, so for $a/v_{\text{PQ}} \ll 1$, one can always make the above parameterization. The connection between q_i , v_i , and v_{PQ} for more than two PQ fields will be discussed later. Note that most supersymmetric hadronic axion models have more than one PQ field. A notable exception is described in Ref. [92].

Let us now turn to the second term in (2.54). The resulting scalar potential has no new effects on the mass spectrum, since it minimizes for $\langle\phi_{Q_1}\rangle = \langle\phi_{Q_2}\rangle = 0$. Nevertheless, it defines the interaction of one PQ field with the heavy KSVZ quarks

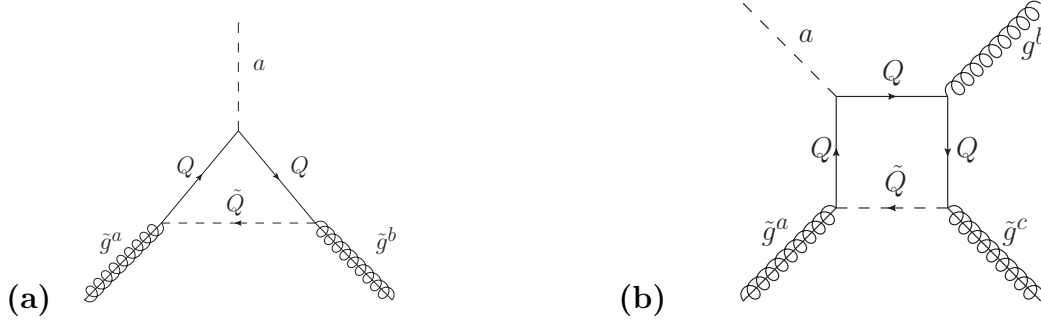


Figure 2.2: Examples of triangle and box loops of KSVZ quarks coupling to one axion, two gluinos and, in the case of the box, one gluon in SUSY hadronic axion models.

and squarks similar to the non-SUSY case. Again, we can expand the exponential in (2.56) and get a mass term for the heavy KSVZ (s)quarks, $m_{Q,\tilde{Q}} = hv_1$ and triangle diagrams like the one shown in Fig. 2.1 and its supersymmetrized version, shown in Fig. 2.2(a). After integrating out the loops, we get for the triangle diagram with one axion and two gluons,

$$\mathcal{L}^{\text{int}} = \frac{g_s^2 h v_1}{32\pi^2 \sqrt{2} m_Q v_{\text{PQ}}} a G^{b\mu\nu} \tilde{G}_{\mu\nu}^b. \quad (2.57)$$

This expression is the same as in the non-SUSY case if one changes the notation accordingly. This is expected, since a supersymmetric hadronic axion model should of course also be able to solve the strong CP problem.

Also in the SUSY case there are box diagrams, one example is shown in Fig. 2.2(b). In fact, there are six box diagrams according to the six possible permutations of the external particles. Note, however, that the sum of the box diagrams with an external axion is suppressed by additional powers of v_{PQ} relative to the triangle diagrams. This means that there is no effective low energy axion-gluon-gluino-gluino vertex.

These loop diagrams can also be constructed with the saxion instead of the axion. The coupling of the saxion does not contain a factor of γ^5 , since it is not a pseudoscalar. Here the box diagrams are not suppressed by more powers of v_{PQ} , thus indeed there is a saxion-gluon-gluino-gluino vertex. To fix the relation of f_{PQ} and v_{PQ} we need to compare the result of these loops to the terms resulting from the effective SUSY Lagrangian.

2.4.2 The Effective Lagrangian

Here we derive the explicit effective low energy interaction terms of the PQ supermultiplet with squarks, gluons, and gluinos. The starting point is the Lagrangian

$$\mathcal{L}_{\text{PQ}}^{\text{int}} = -\frac{\sqrt{2}\alpha_s}{8\pi f_{\text{PQ}}} \int d^2\theta A W^b W^b + \text{h.c.} \quad (2.58)$$

with the PQ supermultiplet A introduced above and $\alpha_s = g_s^2/4\pi$. The calculation of this integral is presented in detail in Appendix B. The result reads

$$\begin{aligned} \mathcal{L}_{\text{PQ}}^{\text{int}} = \frac{\alpha_s}{8\pi f_{\text{PQ}}} & \left[\sigma \left(G^{b\mu\nu} G_{\mu\nu}^b - 2D^b D^b - 2i\tilde{g}_M^b \gamma^\mu D_\mu^{bd} \tilde{g}_M^d \right) \right. \\ & + a \left(G^{b\mu\nu} \tilde{G}_{\mu\nu}^b + 2\tilde{g}_M^b \gamma^\mu \gamma^5 D_\mu^{bd} \tilde{g}_M^d \right) \\ & \left. - i\tilde{a}_M \frac{[\gamma^\mu, \gamma^\nu]}{2} \gamma^5 \tilde{g}_M^b G_{\mu\nu}^b + 2\tilde{a}_M D^b \tilde{g}_M^b \right], \end{aligned} \quad (2.59)$$

where $D^b = -g_s \sum_{\tilde{q}} \tilde{q}_i^* T_{ij}^b \tilde{q}_j$ is the color-gauge auxiliary field with a sum over all squark fields, T_{ij}^b is the $\text{SU}(3)_c$ generator in the fundamental representation, and the subscript M denotes four-component Majorana fermions.

For comparisons with similar $\mathcal{L}_{\text{PQ}}^{\text{int}}$ expressions given in Refs. [51, 54], we remark that the second term in the brackets in the second line of (2.59) can be written as $D_\mu^{bd} (\tilde{g}_M^b \gamma^\mu \gamma^5 \tilde{g}_M^d)$. However, our result for the saxion-gluino interaction term differs from the corresponding terms in [51] and [54] by factors of -2 and -1 , respectively. Moreover, our findings for the axino interactions differ by a factor of -1 from the ones in [51, 54]. This may result partially from metric conventions: If we translate (2.59) into the corresponding expression valid for $g_{\mu\nu} = g^{\mu\nu} = \text{diag}(-1, +1, +1, +1)$ using Appendix A of Ref. [142], the sign of our result for the axino-gluino-gluon interaction term will change, whereas all other terms in (2.59) will not be affected.

When comparing the expression for the axion gluon interaction term in the effective Lagrangian (2.59) with the result from the integrated loop (2.57), we see that the two scales are related by

$$f_{\text{PQ}} = \sqrt{2} v_{\text{PQ}}. \quad (2.60)$$

Note that in the low energy limit of the PQ hadronic model, these two scales cannot be distinguished. In the following, we present the connection of these scales to the parameters of the fundamental PQ fields, namely to the PQ charges and the VEVs.

2.4.3 Axion - Saxion Interaction from the Kinetic Term

The kinetic terms of the PQ fields in this hadronic axion model are given in their canonical form. The inclusion of the expansion of the scalar PQ fields (2.56)

yields [47]

$$\mathcal{L}_{\text{PQ}}^{\text{kin}} = \sum_{i=1}^N \partial^\mu \phi_i \partial_\mu \phi_i^* \simeq \left(1 + \frac{\sqrt{2}x}{v_{\text{PQ}}} \sigma\right) \left(\frac{1}{2} \partial^\mu a \partial_\mu a + \frac{1}{2} \partial^\mu \sigma \partial_\mu \sigma\right) + \dots \quad (2.61)$$

where

$$x = \sum_i \frac{q_i^3 v_i^2}{v_{\text{PQ}}^2}. \quad (2.62)$$

In order to arrive at canonically normalized kinetic terms for axions and saxions in (2.61), one defines

$$v_{\text{PQ}} = \sqrt{\sum_i q_i^2 v_i^2}. \quad (2.63)$$

This shows the connection of the PQ scale to the parameters of the fundamental PQ fields. Note that (2.61) gives an interaction term of saxions with axions that is not present in (2.59). This interaction depends on x and, therefore, on the details of the underlying PQ model. For example, in the model presented above with the superpotential given by (2.54), $x = (v_1^2 - v_2^2)/v_{\text{PQ}}^2$. This illustrates that $x \ll 1$ is possible if $v_1 \simeq v_2 \simeq v_{\text{PQ}}/\sqrt{2}$ [47, 64, 143]. On the other hand, in a KSVZ axion model with just one PQ scalar (with $v = v_{\text{PQ}}$ and $q = 1$) [92], one finds $x = 1$. There are other interaction terms resulting from the kinetic terms in (2.61) that we omitted because they involve the axino or are of higher order in $1/v_{\text{PQ}}$.

In order to arrive at a consistent definition of the two scales, v_{PQ} , inferred from canonically normalized kinetic terms, and f_{PQ} , defined by the prefactor of the effective interaction in (2.59), one has to derive both values from the fundamental PQ fields as done here.

Note that an alternative convention with $\langle \phi_i \rangle = \tilde{v}_i/\sqrt{2}$ and $f_{\text{PQ}} = \sqrt{\sum_i \tilde{v}_i^2 q_i^2}$ can be found in the literature [56]. Then, $\phi_i = (\tilde{v}_i/\sqrt{2}) \exp[q_i(\sigma + ia)/f_{\text{PQ}}]$. Indeed, with this convention, one arrives directly at an agreement of (2.57) with the corresponding term in (2.59). However, we prefer to work explicitly with both f_{PQ} and v_{PQ} also to allow for a direct comparison with literature that uses the parameterization given in (2.56) or a directly related one; see e.g. Refs. [62, 92] or [64, 80, 141] in which their f_{PQ} or F_a agree with our v_{PQ} .

Having derived the Lagrangian for all relevant interactions, we now list the important properties for our cosmological studies.

2.5 Properties of the PQ Particles

All interactions of the PQ particles are suppressed by $1/f_{\text{PQ}}$. Numerous laboratory, astrophysical and cosmological limits imply [12, 36]

$$f_{\text{PQ}} \gtrsim 6 \times 10^8 \text{ GeV}, \quad (2.64)$$

which translates into an upper limit on the axion mass via (2.7), yielding

$$m_a \lesssim 10 \text{ meV}. \quad (2.65)$$

As we have already seen above, SUSY provides a flat direction in the scalar potential for the saxion and a massless eigenstate of the fermion mass matrix, so in unbroken SUSY the saxion and the axino are also massless.

When SUSY gets broken, the flat direction of the saxion in the scalar potential get lifted and the saxion acquires a mass m_σ . The exact values of the saxion mass, however, depends on the model of SUSY breaking. In gravity-mediated SUSY breaking, one expects m_σ to be of order of the gravitino mass [58, 62, 92]. Here we do not look at a specific model but treat m_σ as a free parameter.

The axino mass $m_{\tilde{a}}$ is also model dependent [47, 144–147] and we treat it as a free parameter, too.

The Feynman rules governing the interactions of axions, saxions, and axinos can be obtained from the Lagrangian pieces (2.59) and (2.61). Results are given in Appendix C. Here we list some important decay widths of saxions and axinos. The saxion decay width into axions reads⁵

$$\Gamma_{\sigma \rightarrow aa} = \frac{x^2 m_\sigma^3}{64\pi v_{\text{PQ}}^2} = \frac{x^2 m_\sigma^3}{32\pi f_{\text{PQ}}^2}, \quad (2.66)$$

and the width for the saxion decay into gluons,

$$\Gamma_{\sigma \rightarrow gg} = \frac{\alpha_s^2 m_\sigma^3}{16\pi^3 f_{\text{PQ}}^2}. \quad (2.67)$$

For KSVZ (s)quarks that carry a non-zero electrical charge $e_Q e$ with $e = \sqrt{4\pi\alpha}$ and the fine-structure constant α , the saxion can decay into photons via KSVZ quark loops. After integrating out those loops, we find the associated width

$$\Gamma_{\sigma \rightarrow \gamma\gamma} = \frac{9e_Q^4 \alpha^2 m_\sigma^3}{64\pi^3 f_{\text{PQ}}^2}. \quad (2.68)$$

Other decay modes depend on the mass hierarchy. In settings with $m_\sigma > 2m_{\tilde{g}}$, the saxion can also decay into gluinos with mass $m_{\tilde{g}}$. The resulting decay width is given by

$$\Gamma_{\sigma \rightarrow \tilde{g}\tilde{g}} = \frac{\alpha_s^2 m_\sigma m_{\tilde{g}}^2}{4\pi^3 f_{\text{PQ}}^2} \left(1 - \frac{4m_{\tilde{g}}^2}{m_\sigma^2}\right)^{3/2}. \quad (2.69)$$

If $x \gtrsim 0.2$, the saxion decay into axions governs the saxion lifetime τ_σ . Indeed, in the region $m_\sigma \gtrsim 10 \text{ GeV}$ in which the competing decay $\sigma \rightarrow gg$ is relevant, such x

⁵Our result (2.66) agrees with the ones of Refs. [62, 92], where $x = 1$ and $f_{\text{PQ}} \equiv v_{\text{PQ}}$, and of Refs. [64, 80, 141], where $F_a \equiv v_{\text{PQ}}$.

values imply the branching ratio $\text{BR}(\sigma \rightarrow aa) \gtrsim 0.9$. For m_σ below the threshold to form hadrons, where $\sigma \rightarrow \gamma\gamma$ is the competing decay, the decay into axions governs τ_σ for even smaller values of x , e.g., for $e_Q = 1$ and $x = 0.02$, we still find the branching ratio $\text{BR}(\sigma \rightarrow aa) \gtrsim 0.9$. The decay into gluinos is never dominant.

If $m_{\tilde{a}} > m_{\tilde{g}}$, the dominant axino decay channel from (2.59) is the decay into a gluon and a gluino with the associated decay width

$$\Gamma_{\tilde{a} \rightarrow g\tilde{g}} = \frac{\alpha_s^2 m_{\tilde{a}}^3}{16\pi^3 f_{\text{PQ}}^2} \left(1 - \frac{m_{\tilde{g}}^2}{m_{\tilde{a}}^2}\right)^3. \quad (2.70)$$

There are other decay channels possible depending on the mass hierarchy, but for our purposes this is the only decay width we need.

For the gravitino, we just need the details of its decay width into axinos and axions. To get this term, we plug (2.44) into (2.41), apply (2.27) and find for the interaction Lagrangian in four-component notation

$$\mathcal{L}_{\tilde{G}\tilde{a}a} = \frac{1}{2} \left(\partial_\mu \sigma \bar{\Psi}_{M\nu} \gamma^\mu \gamma^\nu \tilde{a}_M + i \partial_\mu a \bar{\Psi}_{M\nu} \gamma^\mu \gamma^\nu \gamma^5 \tilde{a}_M \right). \quad (2.71)$$

The resulting Feynman rules are given in Appendix C. In order to calculate the squared matrix element of the gravitino decay width into axinos and axions, we need the polarization tensor of a gravitino with momentum P [148]

$$\Pi_{\mu\nu}(P) = -(\not{P} + m_{\tilde{G}}) \left(\eta_{\mu\nu} - \frac{P_\mu P_\nu}{m_{\tilde{G}}^2} \right) - \frac{1}{3} \left(\gamma^\mu + \frac{P_\mu}{m_{\tilde{G}}} \right) (\not{P} - m_{\tilde{G}}) \left(\gamma^\nu + \frac{P_\nu}{m_{\tilde{G}}} \right). \quad (2.72)$$

With this tensor and for mass hierarchies with $m_{\tilde{G}} > m_{\tilde{a}}$, we arrive at the decay width

$$\Gamma_{\tilde{G} \rightarrow \tilde{a}a} = \frac{(m_{\tilde{G}} - m_{\tilde{a}})^5 (m_{\tilde{G}} + m_{\tilde{a}})^3}{192\pi m_{\tilde{G}}^5 M_{\text{Pl}}^2}, \quad (2.73)$$

which in the case of $m_{\tilde{G}} \gg m_{\tilde{a}}$ reduces to [48, 149]

$$\Gamma_{\tilde{G} \rightarrow \tilde{a}a} \simeq \frac{m_{\tilde{G}}^3}{192\pi M_{\text{Pl}}^2}. \quad (2.74)$$

In the next chapter, we use the Feynman rules obtained from (2.59) to calculate the axion and saxion production rate in the early Universe and provide also an update of the production rate of the axino.

Chapter 3

Thermal Production of the PQ Particles

In this chapter we calculate the thermal production rate, the yield, and the decoupling temperatures of the PQ particles using the interactions derived above.

In the first Sects. 3.1 and 3.2, we compute the thermal production rate of saxions and axions in the primordial quark-gluon-squark-gluino plasma (QGSGP). In our calculation we apply hard thermal loop (HTL) resummation [150] and the Braaten–Yuan prescription [151] to systematically account for screening effects in the QGSGP. This method was introduced on the example of axion production in a hot Quantum Electrodynamics (QED) plasma [151]; see also Ref. [148]. Moreover, it has been applied to calculate the thermal production of gravitinos [148, 152–154] and axinos [50] in SUSY settings and of axions in a non-SUSY quark-gluon plasma (QGP) [1, 155]. This method allows us to reach a gauge invariant result consistent to leading order in g_s .

It has been realized in Ref. [51] that there is an axino-squark-squark-gluino vertex given by the last term in (2.59) that has not been included in the calculation of the thermal axino production rate in Ref. [50]. In Sect. 3.3, we provide an update to this calculation by including that vertex.

After a brief review of basic cosmology in Sect. 3.4, we compute the thermally produced yield and the decoupling temperature for each of these particles.

Regarding the relation of the reheating temperature with the inflaton decay width, we provide a numerical calculation including the decay of the inflaton in Sect. 3.5.

3.1 Saxions

Let us start with the calculation of the thermal production rate of saxions in the early Universe. Assuming that inflation governs the earliest moments of the Universe, any

initial saxion population has been diluted away by the exponential expansion during the slow-roll phase. After the completion of the reheating phase that leads to the reheating temperature T_R , thermal production of saxions becomes efficient. In fact, we focus on cosmological settings where radiation governs the energy density of the Universe as long as this production mechanism is efficient (i.e., for T down to at least $T \sim 0.01 T_R$). The details of the connection between T_R and the inflaton decay are discussed in Sect. 3.5. While inflation models can point to T_R well above 10^{10} GeV [156–158], we consider the case $T_R < f_{PQ}$ such that no PQ symmetry restoration takes place after inflation. Moreover, $T_R < m_{Q,\tilde{Q}}$ is assumed so that integrating out the heavy (s)quark loops is always possible. Scenarios with radiation-dominated periods in which T exceeds $m_{Q,\tilde{Q}}$ are described in Ref. [53].

The calculation of the thermal production of saxions with energy $E \gtrsim T$ follows closely [1], where thermal axion production in a SM QGP is considered. Since all saxion interactions are suppressed by $1/f_{PQ}$, inelastic $2 \rightarrow 2$ processes dominate the production rate. The saxion thermal production rate is given by [157]

$$E \frac{dW_\sigma}{d^3p} = \frac{1}{2(2\pi)^3} \int \frac{d\Omega_p}{4\pi} \int \left[\prod_{j=1}^3 \frac{d^3p_j}{(2\pi)^3 2E_j} \right] (2\pi)^4 \delta^4(P_1 + P_2 - P_3 - P) \times \left\{ \sum f_1(E_1) f_2(E_2) [1 \pm f_3(E_3)] [1 + f_\sigma(E)] |M_{1+2 \rightarrow 3+\sigma}|^2 - \sum f_3(E_3) f_\sigma(E) [1 \pm f_1(E_1)] [1 \pm f_2(E_2)] |M_{3+\sigma \rightarrow 1+2}|^2 \right\}, \quad (3.1)$$

where the matrix elements M are weighed by the phase space densities $f_i(E_i)$ of the respective particles, the \pm accounts for Bose enhancement/Pauli blocking depending on whether the final state is a boson or a fermion. The sum runs over all relevant $2 \rightarrow 2$ processes. The energy and four-momentum of external particles are given by E_i and P_i , where no subscript denotes the saxion. The integration over the direction of the saxion momentum is performed in the first integral. The matrix elements are summed over initial and final spins and are multiplied by the appropriate multiplicities and statistical factors.

The MSSM particles of the QGSGP are interacting much stronger with one another than with the saxion for high T_R , so we consider them to be in thermal equilibrium. In the rest frame of the plasma, their phase space densities are accordingly given by equilibrium Fermi–Dirac distributions f_F and Bose–Einstein distributions f_B ,

$$f_F(E_i) = \frac{1}{e^{E_i/T} + 1}, \quad (3.2a)$$

$$f_B(E_i) = \frac{1}{e^{E_i/T} - 1}. \quad (3.2b)$$

Using the assumption of inflation diluting all initial saxions, we can neglect the saxion disappearance reactions described by the last line of (3.1), since they are

proportional to the saxion phase space distribution $f_\sigma(E)$, which is negligibly small when the saxion is far away from thermal equilibrium. This allows us to also set $1 \pm f_\sigma(E) \approx 1$ in (3.1). We then arrive at

$$E \frac{dW_\sigma}{d^3p} \simeq \frac{1}{2(2\pi)^3} \int \frac{d\Omega_p}{4\pi} \int \left[\prod_{j=1}^3 \frac{d^3p_j}{(2\pi)^3 2E_j} \right] (2\pi)^4 \delta^4(P_1 + P_2 - P_3 - P) \quad (3.3)$$

$$\times \sum f_1(E_1) f_2(E_2) [1 \pm f_3(E_3)] |M_{1+2 \rightarrow 3+\sigma}|^2.$$

Note that this negligence of the backreaction is no longer a valid approximation if the saxion comes close to thermal equilibrium. We denote the temperature at which the saxion abundance calculated by (3.3) reaches the equilibrium value as the saxion decoupling temperature T_D^σ .

The evaluation of the matrix elements in (3.3) using zero-temperature Feynman rules leads to terms $\propto 1/t$, where t is one of the Mandelstam variables given by

$$s = (P_1 + P_2)^2, \quad (3.4a)$$

$$t = (P_1 - P_3)^2, \quad (3.4b)$$

$$u = (P_2 - P_3)^2. \quad (3.4c)$$

Such terms $\propto 1/t$ arise if a massless gluon is exchanged in the t- or u-channel and are potentially infrared (IR) divergent. The ad hoc introduction of a finite gluon mass cures this divergences. However, this procedure breaks gauge-invariance.

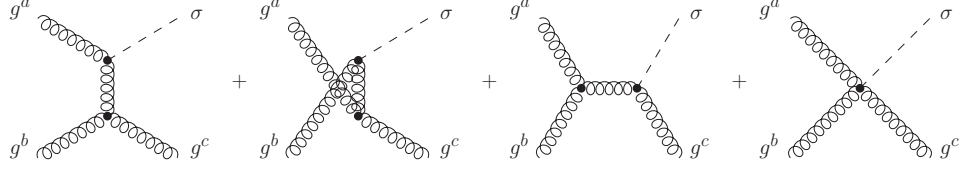
Here we use a different approach. In fact, screening effects of the plasma provide a way to treat the setting properly. In Refs. [150, 151] a systematic method is introduced to account for such screening effects in a gauge-invariant way. Following Ref. [151], we introduce a momentum scale k_{cut} such that $g_s T \ll k_{\text{cut}} \ll T$ in the weak coupling limit $g_s \ll 1$. This separates soft gluons with momentum transfer of order $g_s T$ from hard gluons with momentum transfer of order T . By summing the respective soft and hard contributions, the finite rate for thermal production of saxions with $E \gtrsim T$ is obtained in leading order in g_s and independent of k_{cut} ,

$$E \frac{dW_\sigma}{d^3p} = E \frac{dW_\sigma}{d^3p} \Big|_{\text{hard}} + E \frac{dW_\sigma}{d^3p} \Big|_{\text{soft}}. \quad (3.5)$$

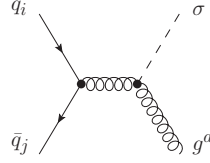
3.1.1 Hard Part

In the calculation of the matrix element in (3.3) we take into account the couplings given in (2.59). All other possible couplings of the saxion are model-dependent, as the coupling to leptons and fermions, which do not occur at tree-level in hadronic axion models. Also a coupling to Higgs bosons is not present in hadronic models. Couplings to photons generate Primakoff processes such as $e^- \gamma \rightarrow e^- \sigma$, but they

Process A $g^a + g^b \rightarrow g^c + \sigma$

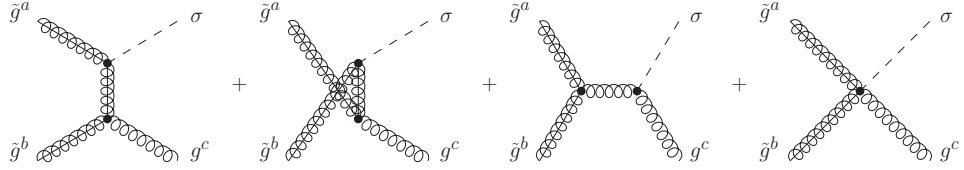


Process B $q_i + \bar{q}_j \rightarrow g^a + \sigma$



Process C $q_i + g^a \rightarrow q_j + \sigma$ (Crossing of B)

Process D $\tilde{g}^a + \tilde{g}^b \rightarrow g^c + \sigma$



Process E $\tilde{g}^a + g^b \rightarrow \tilde{g}^c + \sigma$ (Crossing of D)

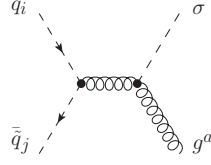
Figure 3.1: *First part of the $2 \rightarrow 2$ processes for saxon production in a SUSY QCD plasma. The charge conjugated of process C with antiquarks $\bar{q}_{i,j}$ replacing $q_{i,j}$ is included in terms of multiplicities in our calculation of the thermal production rate.*

depend on the electric charge of the heavy quarks $e_Q e$ and are usually far less efficient in the early Universe [159] and, therefore, are also neglected.

The Feynman diagrams of the processes obtained from (2.59) are shown in Figs. 3.1 and 3.2. Additional processes exist but can be accounted for by multiplying the squared matrix elements of the shown processes with appropriate multiplicity factors.¹ Note that there is no diagram corresponding to the $\sigma D^b D^b$ term in (2.59), because such a process is suppressed by an additional factor of α_s relative to the other diagrams depicted. The necessary Feynman rules for the calculation of these

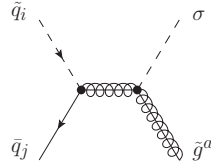
¹Note that $2 \rightarrow 2$ processes, which involve the saxon-(s)axion interaction (2.61), such as $g^a + g^b \rightarrow \sigma + a$, are suppressed by an additional factor of $1/f_{\text{PQ}}^2$ in the respective squared matrix element and thus negligible.

Process F $\tilde{q}_i + \tilde{\bar{q}}_j \rightarrow g^a + \sigma$



Process G $\tilde{q}_i + g^a \rightarrow \tilde{q}_j + \sigma$ (Crossing of F)

Process H $\tilde{q}_i + \bar{q}_j \rightarrow \tilde{g}^a + \sigma$



Process I $\tilde{g}^a + q_i \rightarrow \tilde{q}_j + \sigma$ (Crossing of H)

Process J $\tilde{g}^a + \tilde{q}_i \rightarrow q_j + \sigma$ (Crossing of H)

Figure 3.2: Second part of the $2 \rightarrow 2$ processes for saxion production in a SUSY QCD plasma. Additional charge conjugated processes are included in terms of multiplicities in our calculation of the thermal production rate: Process G with antisquarks $\tilde{\bar{q}}_{i,j}$ replacing $\tilde{q}_{i,j}$, process H with antisquarks/quarks $\tilde{\bar{q}}_i/\bar{q}_j$ replacing \tilde{q}_i/\tilde{q}_j , and processes I and J with \bar{q}_i and $\tilde{\bar{q}}_j$ replacing q_i and \tilde{q}_j , respectively.

diagrams can be found in Appendix C. In fact, we can use zero-temperature Feynman rules here, because in the hard part of the production rate calculated in this section we use k_{cut} as an IR cut-off.

We show the results for the squared matrix elements in Table 3.1 where we use the Mandelstam variables (3.4). Sums over initial and final spins have been performed. Working in the limit, $T \gg m_i$, the masses m_i of all MSSM particles have been neglected. For quarks and squarks, the contribution of a single chirality is given. The obtained squared matrix elements can be calculated conveniently, e.g., with the help of **FeynArts** [160] and **FormCalc** [161]. The possibly divergent $1/t$ terms can now be seen explicitly in the squared matrix elements of processes A, C, E, and G.

These results need to be weighted with the appropriate multiplicities and statistical factors. For processes A, D, and E the $\text{SU}(3)_c$ color sum yields

$$\sum_i |f^{abc}|^2 = N_c(N_c^2 - 1) = 24.$$

Table 3.1: *Squared matrix elements for saxion production in two-body processes involving MSSM quarks and squarks of a single chirality, gluons, and gluinos in the high-temperature limit, $T \gg m_i$, with the $SU(3)_c$ color matrices f^{abc} and T_{ji}^a . Sums over initial and final state spins have been performed. The class is given by the MSSM particles of the respective process being a boson (B) or a fermion (F).*

Label i	Class	Process i	$ M_i ^2 / \left(\frac{g_s^6}{128\pi^4 f_{\text{PQ}}^2} \right)$
A	BBB	$g^a + g^b \rightarrow g^c + \sigma$	$-4 \frac{(s^2 + st + t^2)^2}{st(s+t)} f^{abc} ^2$
B	FFB	$q_i + \bar{q}_j \rightarrow g^a + \sigma$	$\left(\frac{2t^2}{s} + 2t + s \right) T_{ji}^a ^2$
C	FBF	$q_i + g^a \rightarrow q_j + \sigma$	$\left(-\frac{2s^2}{t} - 2s - t \right) T_{ji}^a ^2$
D	FFB	$\tilde{g}^a + \tilde{g}^b \rightarrow g^c + \sigma$	$2 \left(\frac{2t^2}{s} + 2t + s \right) f^{abc} ^2$
E	FBF	$\tilde{g}^a + g^b \rightarrow \tilde{g}^c + \sigma$	$2 \left(-\frac{2s^2}{t} - 2s - t \right) f^{abc} ^2$
F	BBB	$\tilde{q}_i + \tilde{q}_j \rightarrow g^a + \sigma$	$-2 \left(\frac{t^2}{s} + t \right) T_{ji}^a ^2$
G	BBB	$\tilde{q}_i + g^a \rightarrow \tilde{q}_j + \sigma$	$-2 \left(\frac{s^2}{t} + s \right) T_{ji}^a ^2$
H	FBF	$\tilde{q}_i + \bar{q}_j \rightarrow \tilde{g}^a + \sigma$	$(s+t) T_{ji}^a ^2$
I	FFB	$\tilde{g}^a + q_i \rightarrow \tilde{q}_j + \sigma$	$s T_{ji}^a ^2$
J	FBF	$\tilde{g}^a + \tilde{q}_i \rightarrow q_j + \sigma$	$-t T_{ji}^a ^2$

For processes A and D there is an additional factor of 1/2, because there are identical particles in the initial state. For the processes B, C, F, G, H, I, and J the color sum yields

$$\sum_i |T_{ji}^a|^2 = \frac{N_c^2 - 1}{2} = 4,$$

and all those processes are multiplied by the number of quark flavors $n_f = 6$ and the inclusion of both chiralities eventually results in a factor of two. The processes C, G, H, I, and J are also possible with anti(s)quarks and, therefore, they need to be multiplied by another factor of two.

The Mandelstam invariants (3.4) are defined such that $s + t + u = \sum m_i^2$, which is zero in the high energy limit $T \gg m_i$. Thus, one can write $s + 2t = t - u$, which is odd under the exchange of P_1 and P_2 . Thus, the integral over such a term will be zero if the rest of the integrand and the measure is even under this exchange. Therefore, there is no contribution from $s + 2t$ in $|M_B|^2$ and $|M_D|^2$. Moreover, we replace s by $-2t$ in $|M_H|^2$ and $|M_I|^2$. In $|M_A|^2$ we make the following replacement

$$-\frac{(s^2 + st + t^2)^2}{st(s+t)} = -t - 2s - \frac{s^2}{t} + \frac{s^2}{s+t} - \frac{t^2}{s} \rightarrow -t - 2s - \frac{2s^2}{t} - \frac{t^2}{s}.$$

These manipulations allow us to write all squared matrix elements in terms of

$$|M_1|^2 = -t - 2s - \frac{2s^2}{t}, \quad (3.6a)$$

$$|M_2|^2 = t, \quad (3.6b)$$

$$|M_3|^2 = \frac{t^2}{s}. \quad (3.6c)$$

We also introduce the shorthanded notation

$$f_{\text{BBB}} = f_{\text{B}}(E_1)f_{\text{B}}(E_2)[1 + f_{\text{B}}(E_3)], \quad (3.7a)$$

$$f_{\text{FFB}} = f_{\text{F}}(E_1)f_{\text{F}}(E_2)[1 + f_{\text{B}}(E_3)], \quad (3.7b)$$

$$f_{\text{FBF}} = f_{\text{F}}(E_1)f_{\text{B}}(E_2)[1 - f_{\text{F}}(E_3)], \quad (3.7c)$$

to group the squared matrix elements according to their class shown in Table 3.1. The result reads

$$|M_{\text{BBB}}|^2 = \frac{g_s^6(N_c^2 - 1)(N_c + n_f)}{64\pi^4 f_{\text{PQ}}^2} (|M_1|^2 - |M_3|^2), \quad (3.8a)$$

$$|M_{\text{FFB}}|^2 = \frac{g_s^6(N_c^2 - 1)}{64\pi^4 f_{\text{PQ}}^2} [(N_c + n_f)|M_3|^2 - 2n_f|M_2|^2], \quad (3.8b)$$

$$|M_{\text{FBF}}|^2 = \frac{g_s^6(N_c^2 - 1)}{64\pi^4 f_{\text{PQ}}^2} [(N_c + n_f)|M_1|^2 - 2n_f|M_2|^2]. \quad (3.8c)$$

This allows us to rewrite the hard part of the production rate (3.3) as follows

$$\begin{aligned} E \frac{dW_\sigma}{d^3p} \Big|_{\text{hard}} &= \frac{1}{2(2\pi)^3} \int \frac{d\Omega_p}{4\pi} \int \left[\prod_{j=1}^3 \frac{d^3p_j}{(2\pi)^3 2E_j} \right] (2\pi)^4 \delta^4(P_1 + P_2 - P_3 - P) \\ &\times \{ f_{\text{BBB}} |M_{\text{BBB}}|^2 + f_{\text{FFB}} |M_{\text{FFB}}|^2 + f_{\text{FBF}} |M_{\text{FBF}}|^2 \} \Theta(|p_1 - p_3| - k_{\text{cut}}). \end{aligned} \quad (3.9)$$

Only $|M_1|^2$ contains a potentially divergent $1/t$ term and there we need k_{cut} as an IR cut-off. The integrated results have a logarithmic dependence on k_{cut} that can be extracted analytically. The two integrals including $|M_1|^2$ are of the class BBB and FBF. Details of their calculation can be found in Appendix C in Ref. [155]. After separating the analytic part, we are left with

$$\begin{aligned} E \frac{dW_\sigma}{d^3p} \Big|_{\text{hard}} &= E \frac{g_s^6(N_c^2 - 1)(N_c + n_f)}{512\pi^7 f_{\text{PQ}}^2} \\ &\left\{ \frac{f_{\text{B}}(E)T^3}{32\pi} \left[\ln \left(\frac{T^2}{k_{\text{cut}}^2} \right) + \frac{17}{3} - 2\gamma + \frac{2\zeta'(2)}{\zeta(2)} + \frac{2}{3} \ln(2) \right] \right. \\ &\quad \left. + \left(I_{\text{BBB}}^{(1)} + I_{\text{FBF}}^{(1)} - I_{\text{BBB}}^{(3)} + I_{\text{FFB}}^{(3)} \right) - 2 \frac{n_f(I_{\text{FBF}}^{(2)} + I_{\text{FFB}}^{(2)})}{N_c + n_f} \right\}, \end{aligned} \quad (3.10)$$

with Euler's constant γ , Riemann's zeta function $\zeta(z)$, and the remaining integrals defined as

$$I_X^{(i)} = \frac{1}{2E} \int \frac{d\Omega_p}{4\pi} \int \left[\prod_{j=1}^3 \frac{d^3 p_j}{(2\pi)^3 2E_j} \right] (2\pi)^4 \delta^4(P_1 + P_2 - P_3 - P) f_X |M_i|^2 \Theta(|p_1 - p_3| - k_{\text{cut}}), \quad (3.11)$$

where in the case of $|M_1|^2$ we only take the terms that cannot be integrated analytically, see Appendix C in Ref. [155] for details. Integrals over $|M_2|^2$ and $|M_3|^2$ give finite results, so we can set $k_{\text{cut}} = 0$ from the beginning of the integration. The integration over $|M_3|^2$ is also shown in detail in Appendix C in Ref. [155]. The remaining integration over $|M_2|^2$ is presented in detail in our Appendix D. The result reads

$$\begin{aligned} I_{\text{BBB(FBF)}}^{(1)} &= \frac{1}{32\pi^3 E^2} \int_0^\infty dE_3 \int_0^{E+E_3} dE_1 \ln \left(\frac{|E_1 - E_3|}{E_3} \right) \\ &\quad \times \left\{ -\Theta(E_1 - E_3) \frac{d}{dE_1} [f_{\text{BBB(FBF)}} E_2^2 (E_1^2 + E_3^2)] \right. \\ &\quad + \Theta(E_3 - E_1) \frac{d}{dE_1} [f_{\text{BBB(FBF)}} E^2 (E_1^2 + E_3^2)] \\ &\quad \left. + \Theta(E - E_1) \frac{d}{dE_1} [f_{\text{BBB(FBF)}} (E_1^2 E_2^2 - E_3^2 E^2)] \right\}, \quad (3.12a) \end{aligned}$$

$$\begin{aligned} I_{\text{FBF(FFB)}}^{(2)} &= \frac{1}{96\pi^3 E^2} \int_0^\infty dE_3 \int_0^{E+E_3} dE_2 f_{\text{FBF(FFB)}} \\ &\quad \times \left\{ \Theta(E - E_3) [E_3^2 (E_3 - 3E_1) - \Theta(E_2 - E)(E_2 - E)^3] \right. \\ &\quad + \Theta(E_3 - E) [(E - 3E_2) E^2 + \Theta(E - E_2)(E_2 - E)^3] \\ &\quad + [\Theta(E_3 - E_2)\Theta(E - E_3) - \Theta(E_3 - E)\Theta(E_2 - E_3)] \\ &\quad \left. \times [(E_2 - E_3)^2 (E_2 + 2E_3) - 3(E_2^2 - E_3^2)E] \right\}, \quad (3.12b) \end{aligned}$$

$$\begin{aligned} I_{\text{BBB(FFB)}}^{(3)} &= \frac{1}{32\pi^3 E^2} \int_0^\infty dE_3 \int_0^{E+E_3} dE_2 f_{\text{BBB(FFB)}} \\ &\quad \times \left\{ \Theta(E - E_3) \frac{E_1^2 E_3^2}{E_3 + E} + \Theta(E_3 - E) \frac{E^2 E_2^2}{E_3 + E} \right. \\ &\quad + [\Theta(E_3 - E)\Theta(E_2 - E_3) - \Theta(E - E_3)\Theta(E_3 - E_2)] \\ &\quad \left. \times (E_2 - E_3) [E_2(E_3 - E) - E_3(E_3 + E)] \right\}. \quad (3.12c) \end{aligned}$$

This concludes our calculation of the hard part. In (3.10) we see explicitly the dependence on k_{cut} . In the next section, we calculate the soft part, which allows us to cancel this dependence in the summed final result.

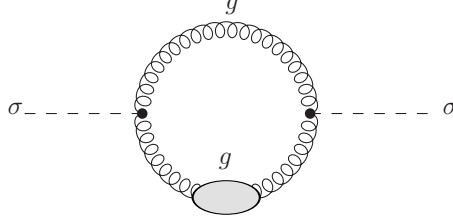


Figure 3.3: *The saxion self energy used to compute the leading contribution to the thermal production rate of hard saxions. The blob indicates the HTL-resummed gluon propagator.*

3.1.2 Soft Part

For calculating the soft part, we employ the finite temperature version of the optical theorem [162]. It relates the imaginary part of the saxion self energy Π_σ shown in Fig. 3.3 to the rate of approaching a thermal equilibrium,

$$E \frac{dW_\sigma}{d^3p} \Big|_{\text{soft}} = -\frac{f_B(E)}{(2\pi)^3} \text{Im} \Pi_\sigma(E + i\epsilon, \vec{p})|_{k < k_{\text{cut}}}. \quad (3.13)$$

Note that only terms with a potential $1/t$ divergence need to be divided into hard and soft parts. This is included in our calculation, since in the computation of the hard part we set $k_{\text{cut}} = 0$ for all terms that do not diverge and then use zero-temperature Feynman rules. Also (3.13) is used only for $k < k_{\text{cut}}$ and, therefore, it only applies if $k_{\text{cut}} > 0$.

Thus, all diagrams that need to be calculated with the help of (3.13) have a soft gluon in the t- or u-channel. Loop corrections to the propagators of these gluons with four-momentum K are of the form $g_s^2 T^2 / K^2$ times the tree-level amplitude, where the momentum running in the loop is hard. If K is also hard, these loop corrections are suppressed and, therefore, part of usual perturbation theory. If K is soft, however, the propagators of these gluons receive loop contributions that are not suppressed by g_s^2 as in zero-temperature field theory, but are of the same order in the coupling constant. This leads to an infinite series of loop diagrams that need to be resummed in order to arrive at a result that is consistent to leading order in the coupling constant [150].

In the Feynman diagram for the axion self energy shown in Fig. 3.3, the blob denotes the HTL-resummed gluon propagator which is given by [163, 164]

$$i\Delta^{\mu\nu}(K) = i(A^{\mu\nu}\Delta_T + B^{\mu\nu}\Delta_L + \xi C^{\mu\nu}), \quad (3.14)$$

with

$$A^{\mu\nu} = -g^{\mu\nu} - \frac{1}{k^2} [K^2 v^\mu v^\nu - K \cdot v (K^\mu v^\nu + K^\nu v^\mu) + K^\mu K^\nu], \quad (3.15a)$$

$$B^{\mu\nu} = v^\mu v^\nu - \frac{K \cdot v}{K^2} (K^\mu v^\nu + K^\nu v^\mu) + \left(\frac{K \cdot v}{K^2} \right) K^\mu K^\nu, \quad (3.15b)$$

$$C^{\mu\nu} = \frac{K^\mu K^\nu}{(K^2)^2}. \quad (3.15c)$$

In the above expressions, v denotes the velocity of the thermal bath and ξ is a gauge fixing parameter. The transverse (T) and longitudinal (L) propagators in (3.14) are given by [164]

$$\Delta_T(k_0, k) = \frac{1}{k_0^2 - k^2 - \Pi_T(k_0, k)}, \quad (3.16a)$$

$$\Delta_L(k_0, k) = \frac{1}{k^2 - \Pi_L(k_0, k)}, \quad (3.16b)$$

which have the spectral representation

$$\Delta_{T/L}(k_0, k) = \int_{-\infty}^{\infty} d\omega \frac{1}{k_0 - \omega} \rho_{T/L}(\omega, k). \quad (3.17)$$

For $|\omega| < k$, the spectral densities $\rho_{T/L}$ are given by

$$\rho_T(\omega, k) = \frac{3}{4m_g} \frac{x}{(1-x^2) \{A_T(x)^2 + [z + B_T(x)]^2\}}, \quad (3.18a)$$

$$\rho_L(\omega, k) = \frac{3}{4m_g} \frac{2x}{A_L(x)^2 + [z + B_L(x)]^2}, \quad (3.18b)$$

with $x = \omega/k$, $z = k^2/m_g^2$, and

$$\begin{aligned} A_T(x) &= \frac{3}{4}\pi x, & B_T &= \frac{3}{4} \left(2 \frac{x^2}{1-x^2} + \ln \frac{1+x}{1-x} \right), \\ A_L(x) &= \frac{3}{2}\pi x, & B_L &= \frac{3}{2} \left(2 - x \ln \frac{1+x}{1-x} \right), \end{aligned}$$

where

$$m_g^2 = \frac{g_s^2 T^2}{6} (N_c + n_f) \quad (3.19)$$

denotes the thermal gluon mass in the MSSM for N_c colors and n_f quark flavors [150].

Applying the Feynman rules given in Appendix C together with the resummed propagator above, we get for the saxion self-energy diagram shown in Fig. 3.3

$$i\Pi_\sigma(E, \vec{p}) = -(N_c^2 - 1) \frac{g_s^4}{32\pi^3 f_{PQ}^2} \int \frac{d^4 K}{(2\pi)^4} \frac{1}{(P-K)^2} (D_T \Delta_T + D_L \Delta_L), \quad (3.20)$$

with

$$D_T = -\frac{1}{k^2} \left(K^4 [3k^2 + (P \cdot v)^2 - 2v^2 K \cdot P - (K \cdot v)^2] \right. \\ \left. + K^2 \{ 2K \cdot P [(K \cdot v)^2 - K \cdot v P \cdot v - 3k^2] + v^2 (K \cdot P)^2 + k^2 P^2 \} \right. \\ \left. + 2k^2 (K \cdot P)^2 + v^2 K^6 \right), \quad (3.21)$$

and

$$D_L = v^2 [K^2 - (K \cdot P)^2] + (P \cdot v - K \cdot v) [K^2 (K \cdot v + P \cdot v) - 2K \cdot P K \cdot v]. \quad (3.22)$$

Note that the result is independent of ξ and, therefore, manifestly gauge-invariant. Equations (3.31) and (3.32) in Ref. [155] give the corresponding expressions of the axion self energy in a SM QGP. In fact, the evaluation of the transverse and longitudinal propagators shown after (3.32) in Ref. [155] can be used in our case as well, since the phase-space densities of the involved particles are identical. Thus, we use the simplifications given above (3.38) in this reference, repeated here for convenience

$$v^2 = 1, \quad (3.23a)$$

$$K \cdot v = \omega, \quad (3.23b)$$

$$P \cdot v = E, \quad (3.23c)$$

$$K \cdot P = E\omega - \vec{p} \cdot \vec{k}. \quad (3.23d)$$

Plugging these results into (3.21) and (3.22), we arrive at

$$D_T = -\frac{1}{4k^2} (k^2 - \omega^2)^2 (4E^2 - 4E\omega + k^2 + \omega^2), \quad (3.24)$$

and

$$D_L = \frac{1}{4} (k^2 - \omega^2) (-4E^2 + 4E\omega + k^2 - \omega^2). \quad (3.25)$$

These results are identical to the axion case, thus to (3.38) and (3.39) in Ref. [155]. Consequently, for the soft part we find the same result as in the case of a thermal axion in a SM QED plasma [151] or a QCD plasma [1, 155], except for the thermal gluon mass (3.19). It reads

$$E \frac{dW_\sigma}{d^3p} \Big|_{\text{soft}} = E f_B(E) \frac{3m_g^2 g_s^4 (N_c^2 - 1) T}{8192 \pi^8 f_{\text{PQ}}^2} \left[\ln \left(\frac{k_{\text{cut}}^2}{m_g^2} \right) - 1.379 \right]. \quad (3.26)$$

More details on the calculation of (3.26) can be found in Refs. [148, 151, 154, 155].

The final result for the integrated thermal production rate of saxions in the QGSGP is then given by the sum of (3.10) and (3.26). The remaining integrals have to be performed numerically and we arrive at [2]

$$W_\sigma = \int d^3p \frac{dW_\sigma}{d^3p} = \frac{9\zeta(3) g_s^6 T^6}{256 \pi^7 f_{\text{PQ}}^2} \left[\ln \left(\frac{T^2}{m_g^2} \right) + 0.4305 \right]. \quad (3.27)$$

We evaluate (3.27) for $g_s = g_s(T) = \sqrt{4\pi\alpha_s}$ with the strong gauge coupling evaluated according to its one-loop running in the MSSM [12]

$$\alpha_s(T) = \frac{\alpha_s(m_Z)}{1 + \frac{\alpha_s(m_Z)}{2\pi} \left(\frac{11}{3}N_c - \frac{4}{3}n_f \right) \ln \left(\frac{T}{m_Z} \right)}, \quad (3.28)$$

where $\alpha_s(m_Z) = 0.1176$ is given at the Z -boson mass $m_Z = 91.1876$ GeV and for $N_c = 3$ colors and $n_f = 6$ quark flavors with mass $m_i < T$. The unphysical negative values in Eq. (3.27) encountered for lower temperatures are a result of the extrapolation of $g_s \ll 1$ to $g_s \approx 1$. Since the applied methods [150,151] require $g_s \ll 1$, the result is most reliable in the perturbative regime where $T \gg 10^6$ GeV. This is a well-known limitation of this technique (cf. [1,50]) that calls for generalizations of the gauge-invariant methods introduced in Refs. [150,151] modified to extend the applicability beyond the weak coupling limit. However, as we will see in the chapters presenting the cosmological effects, this limitation is of no great concern for us.

This concludes the calculation of the thermal production rate of saxions.

3.2 Axions

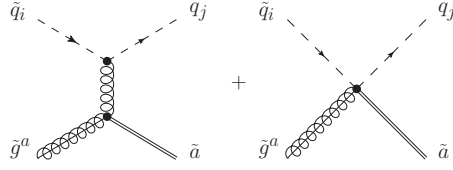
The calculation of thermal axion production in the primordial SUSY QCD plasma proceeds analogously to the saxion calculation presented in the previous section.² After substituting the saxion σ by the axion a , the Feynman diagrams can be read directly from Figs. 3.1, 3.2, and 3.3 with one modification: there is no axion-gluon-gluino-gluino vertex as already pointed out in Sect. 2.4.1 and thus no quartic interaction such as the one that contributes to processes D and E in the saxion case.

Although the Feynman rules for the axion interactions derived from (2.59) differ from the ones describing saxion interactions, we obtain squared matrix elements for the axion production processes in the high-temperature limit, $T \gg m_i$, that agree with the ones for the corresponding saxion production processes given in Table 3.1. Moreover, we find that both the soft and the hard contributions to the thermal production rate of hard axions agree with (3.26) and (3.10), respectively. Our result for the thermal axion production rate $E dW_a/d^3p$ thus agrees with the one for the thermal saxion production rate obtained above. This implies an agreement of the associated integrated thermal production rates and of the thermally produced yields of axions and saxions prior to decay, which is calculated below.

Before proceeding, let us stress that we can neglect production processes like $\pi\pi \rightarrow \pi a$ in the primordial hot hadronic gas [165,166] because of the f_{PQ} limit (2.64). Moreover, also here Primakoff processes such as $e^-\gamma \rightarrow e^-a$ are not taken into account since they are usually far less efficient in the early Universe [159].

²A first attempt to calculate the thermal axion production in a QGSGP has been done in Ref. [155], but there the axion-gluino-gluino vertex has been overlooked.

Process H $\tilde{q}_i + \tilde{g}^a \rightarrow \tilde{q}_j + \tilde{a}$



Process J $\tilde{q}_i + \tilde{\bar{q}}_j \rightarrow \tilde{g}^a + \tilde{a}$ (Crossing of H)

Figure 3.4: The $2 \rightarrow 2$ processes of axino production affected by the inclusion of the additional vertex. Process H is also possible with antisquarks, replacing $\tilde{q}_{i,j}$ by $\tilde{\bar{q}}_{i,j}$.

3.3 Axinos

As in the case of the saxion and the axion, also the axino matrix elements show potential IR divergent terms when using naive perturbation theory. To arrive at a gauge-invariant result consistent to leading order in the strong gauge coupling, the thermal production rate of axinos has been calculated in Ref. [50] using the same field-theoretical methods presented here. In this reference, only the first term in the last line of (2.59) was used to generate Feynman rules for the axino coupling. The omission of the axino-squark-squark-gluino vertex given by the last term in the last line of (2.59) has been realized in Ref. [51]. In this section, we include this interaction to present an update of the results of Ref. [50], see also Appendix A of [3].

The corresponding Feynman rule of the axino-squark-squark-gluino vertex can be found in Appendix C. We divide the axino production rate into a hard and a soft part. The inclusion of this vertex in the calculation of the hard part introduces one more diagram to each of the processes $\tilde{q}_i + \tilde{g}^a \rightarrow \tilde{q}_j + \tilde{a}$ and $\tilde{q}_i + \tilde{\bar{q}}_j \rightarrow \tilde{g}^a + \tilde{a}$ labeled H and J in [50]. The complete set of diagrams for process H is shown in Fig. 3.4. Process J is a crossing of H.

The values for the squared matrix elements $|M_i|^2$ of the respective processes for one chirality and with sums over initial and final spins evaluated read

$$|M_H|^2 / \frac{g_s^6}{128\pi^4 f_{PQ}^2} = -2 \left(t + 2s + 2\frac{s^2}{t} \right) |T_{ji}^a|^2, \quad (3.29a)$$

$$|M_J|^2 / \frac{g_s^6}{128\pi^4 f_{PQ}^2} = 2 \left(s + 2t + 2\frac{t^2}{s} \right) |T_{ji}^a|^2. \quad (3.29b)$$

The other processes listed in Table 1 in [50] are not affected. After weighting the matrix elements with the respective multiplicities and statistical factors we arrive

at

$$|M_{\text{BBF}}|^2 = \frac{g_s^6(N_c^2 - 1)}{64\pi^4 f_{\text{PQ}}^2} \left[(N_c + n_f) \left(s + 2t + \frac{2t^2}{s} \right) + 2n_f s \right], \quad (3.30a)$$

$$|M_{\text{BFB}}|^2 = \frac{g_s^6(N_c^2 - 1)}{32\pi^4 f_{\text{PQ}}^2} \left[(N_c + n_f) \left(-t - 2s - \frac{2s^2}{t} \right) - 2n_f t \right], \quad (3.30b)$$

with the same notation and definition as in the previous sections. Similar arguments as the ones presented before Eq. (3.6a) allow us to simplify these expressions to

$$|M_{\text{BBF}}|^2 \rightarrow \frac{g_s^6(N_c^2 - 1)}{32\pi^4 f_{\text{PQ}}^2} [(N_c + n_f) |M_3|^2 - 2n_f |M_2|^2], \quad (3.31a)$$

$$|M_{\text{BFB}}|^2 = \frac{g_s^6(N_c^2 - 1)}{32\pi^4 f_{\text{PQ}}^2} [(N_c + n_f) |M_1|^2 - 2n_f |M_2|^2]. \quad (3.31b)$$

Equations (3.7), (3.8), (3.12), (3.13), and (E.1) of Ref. [50] change accordingly, when one includes the additional axino interaction term.

The calculation of the phase space integrals and the soft part are not affected by this additional vertex. Thus, we arrive at the following expression for the axino collision term

$$W_{\tilde{a}}(T) = \frac{(N_c^2 - 1)}{f_{\text{PQ}}^2} \frac{3\zeta(3)g_s^6 T^6}{4096\pi^7} \left[\ln \left(\frac{1.647T^2}{m_g^2} \right) (N_c + n_f) + 0.5781n_f \right]. \quad (3.32)$$

The effect of the inclusion of the axino-squark-squark-gluino term changes the numerical prefactor of the last term in square brackets from 0.4336 in (E.2) of Ref. [50] to 0.5781 in (3.32). The qualitative statements and the plots of [50] are only mildly affected by this correction.

Now that we have discussed the production rates for saxions, axions, and axinos in a hot QGSGP, we apply these results to the early Universe.

3.4 Yields and Decoupling Temperatures

In this section, we first calculate the thermally produced yields of each PQ particle and then present an estimate for the decoupling temperature, below which the respective particle does not reach thermal equilibrium in the early Universe. But before we proceed we first want to review some basic Cosmology.

3.4.1 Introductory Cosmology

Here we provide a short overview over the standard hot big bang model. For a detailed introduction in textbook form, see for example Ref. [157], which we follow in this introduction.

Observations indicate that the observable Universe is expanding and that it is homogeneous and isotropic at scales larger than $\mathcal{O}(100)$ Mpc. The metric describing such a Universe is the maximally symmetric Robertson–Walker metric

$$ds^2 = dt^2 - R^2(t) \left(\frac{dr^2}{1 - kr^2} + r^2 d\theta^2 + r^2 \sin \theta d\phi^2 \right), \quad (3.33)$$

where the coordinates (r, θ, ϕ) are called comoving coordinates, because any observer initially at rest within this frame remains at rest. The time t is the time measured by such a comoving observer and is called proper time. The parameter k in (3.33) describes the spatial curvature and – after appropriate rescaling of r – equals -1, 0, and 1 for negative, zero and positive curvature, respectively. The expansion of the Universe is parametrized by the scale factor $R(t)$, which has units of length. The physical distance between two points at a given t is then given by the comoving distance times $R(t)$.

The evolution of the scale factor is governed by the energy content of the Universe. This connection is given by the Einstein equation

$$R_{\mu\nu} - \mathcal{R}g_{\mu\nu} = 8\pi G_N T_{\mu\nu} + \Lambda g_{\mu\nu}, \quad (3.34)$$

where $R_{\mu\nu}$ is the Ricci tensor, \mathcal{R} the Ricci scalar, $T_{\mu\nu}$ the energy-momentum tensor, and Λ describes a possible cosmological constant. Homogeneity and isotropy require $T_{\mu\nu}$ to be diagonal and its spatial components to be equal. The simplest realization is a perfect relativistic fluid with energy density ρ and pressure p , for which

$$T_{\mu\nu} = \text{diag}(-\rho, p, p, p). \quad (3.35)$$

One then gets the evolution of $R(t)$ by the equation of state $p = w\rho$ of the stress energy of the Universe. For the case that w is independent of time, one finds $\rho \propto R^{-3(1+w)}$. The most important examples include pressureless matter ($w = 0$), radiation ($w = 1/3$), and vacuum energy ($w = -1$). If the Universe is dominated by one of these components, the time evolution of R can be inferred with the help of the 0-0 component of (3.34), the Friedmann equation

$$\frac{\dot{R}^2}{R^2} + \frac{k}{R^2} = \frac{8\pi G_N}{3} \rho, \quad (3.36)$$

where the dot denotes derivation with respect to t . The expansion rate of the Universe is described by the Hubble parameter

$$H \equiv \frac{\dot{R}}{R}. \quad (3.37)$$

The present day value of the Hubble expansion rate is called the Hubble constant denoted by H_0 .

It is useful to define the energy density parameter

$$\Omega \equiv \frac{\rho}{\rho_c}, \quad (3.38)$$

where

$$\rho_c = \frac{3H^2}{8\pi G_N} \quad (3.39)$$

is the critical energy density. With the help of (3.36) one can see that $\Omega = 1$ corresponds to a flat Universe.

Measurements indicate that the total energy density parameter of our Universe is close to one [12], so we set $k = 0$ for all our calculations. One then finds that if the energy density of the Universe is dominated by a relativistic fluid with equation of state $p = w\rho$, the time evolution of the scale factor is given by $R \propto t^{2/3(1+w)}$.

To link these cosmological parameters to microscopic physics, one needs to include thermodynamics in our considerations. The energy density, number density, and pressure of a particle species i with phase space distribution $f_i(\vec{p})$ and internal degrees of freedom g_i are given by

$$\rho_i = \frac{g_i}{(2\pi)^3} \int E(\vec{p}) f_i(\vec{p}) d^3p, \quad (3.40a)$$

$$n_i = \frac{g_i}{(2\pi)^3} \int f_i(\vec{p}) d^3p, \quad (3.40b)$$

$$p_i = \frac{g_i}{(2\pi)^3} \int \frac{|\vec{p}|^2}{3E} f_i(\vec{p}) d^3p. \quad (3.40c)$$

If one assumes kinetic equilibrium, that means the phase space distributions are the Fermi–Dirac or Bose–Einstein distributions, the energy density, the number density, and the pressure of a particle species in the relativistic limit ($T \gg m$) with vanishing chemical potential ($T \gg \mu$) read

$$\rho_i = \begin{cases} 1 \\ 7/8 \end{cases} \frac{\pi^2}{30} g_i T_i^4, \quad (3.41a)$$

$$n_i = \begin{cases} 1 \\ 3/4 \end{cases} \frac{\zeta(3)}{\pi^2} g_i T_i^3, \quad (3.41b)$$

$$p_i = \frac{\rho_i}{3}, \quad (3.41c)$$

where the upper (lower) value of the prefactor accounts for bosons (fermions). The total energy density of a radiation dominated Universe is given by

$$\rho_{\text{rad}} = \frac{\pi^2}{30} g_* T^4, \quad (3.42)$$

where g_* counts all effectively massless degrees of freedom at a given temperature and accounts for the different statistics of fermions and bosons. It is given by

$$g_* = \sum_{i=\text{bosons}} g_i \left(\frac{T_i}{T} \right)^4 + \frac{7}{8} \sum_{i=\text{fermions}} g_i \left(\frac{T_i}{T} \right)^4, \quad (3.43)$$

where T denotes the temperature of the photon background and we take the possibility into account that the particles may have a thermal distribution, but with a different temperature T_i than that of the photons. The value of g_* changes with temperature and depends on the particle physics model. For example, if all particles in the MSSM and the PQ supermultiplet can be considered massless, $g_* = 232.5$.

As long as local thermal equilibrium holds, which is a good approximation for the early Universe, the entropy per comoving volume $S = R^3(p + \rho)/T$ is conserved. Since the energy density and pressure of a relativistic species is exponentially larger than that of a non-relativistic one, the entropy density s is given by

$$s = \frac{2\pi^2}{45} g_{*S} T^3, \quad (3.44)$$

where

$$g_{*S} = \sum_{i=\text{bosons}} g_i \left(\frac{T_i}{T} \right)^3 + \frac{7}{8} \sum_{i=\text{fermions}} g_i \left(\frac{T_i}{T} \right)^3, \quad (3.45)$$

again counts only relativistic degrees of freedom. For most of the early Universe, (3.43) and (3.45) are the same. Only after neutrino decoupling at $T \sim 1 \text{ MeV}$, a difference arises in standard cosmology. The decoupled neutrino does not receive the entropy released by the subsequent e^+e^- annihilation and, therefore, today $g_* = 3.36$ and $g_{*S} = 3.91$. Note that the entropy density given by (3.44) includes only those degrees of freedom that are or have been in thermal contact with the photons. Any species that is decoupled from the plasma has its own entropy that is conserved separately. Such decoupled species do, therefore, not contribute to (3.45) but only to (3.43).

The relation between time and temperature depends on the composition of the Universe at that time. In a flat Universe dominated by radiation, one can give the relation in closed form as

$$H = \sqrt{\frac{4\pi^3}{45} g_*} \frac{T^2}{m_{\text{Pl}}} = \frac{1}{2t}, \quad (3.46)$$

where $m_{\text{Pl}} \simeq 1.22 \times 10^{19} \text{ GeV}$ [12] is the Planck mass.

The evolution of each species is governed by the Boltzmann equation

$$\frac{dn_i}{dt} + 3Hn_i = W_i, \quad (3.47)$$

where the right hand side is the collision term, an example of which is given by Eq. (3.27). Further details about standard cosmology can be found in the literature.

3.4.2 Thermally Produced Yields

Let us start with the thermally produced (TP) saxion yield $Y_\sigma^{\text{TP}} = n_\sigma/s$, where n_σ is the corresponding saxion number density and s the entropy density. With the results obtained in Sect 3.2, we know beforehand that this yield prior to decay agrees with the thermally produced axion yield $Y_a^{\text{TP}} = n_a/s$. While the calculation and results are indeed valid for both saxion and axion, we focus on the saxion case.

At temperatures well below the saxion decoupling temperature T_D^σ , the evolution of n_σ with cosmic time t is governed by the Boltzmann equation

$$\frac{dn_\sigma}{dt} + 3Hn_\sigma = W_\sigma, \quad (3.48)$$

where W_σ is given by (3.27). Assuming conservation of entropy per comoving volume element, (3.48) can be written as $dY_\sigma^{\text{TP}}/dt = W_\sigma/s$. Since thermal saxion production is efficient only in the hot radiation dominated epoch with temperatures well above the one of matter-radiation equality, $T_{\text{mat=rad}}$, we can change variables from cosmic time t to temperature T accordingly. With an initial temperature T_R at which all initial saxions are diluted away by inflation (so $Y_\sigma^{\text{TP}}(T_R) \simeq 0$), the relic saxion yield prior to decay is³

$$\begin{aligned} Y_\sigma^{\text{TP}} &\approx Y_\sigma^{\text{TP}}(T_{\text{low}}) = \int_{T_{\text{low}}}^{T_R} dT \frac{W_\sigma(T)}{Ts(T)H(T)} \\ &= 1.33 \times 10^{-3} g_s^6 \ln\left(\frac{1.01}{g_s}\right) \left(\frac{10^{11} \text{ GeV}}{f_{\text{PQ}}}\right)^2 \left(\frac{T_R}{10^8 \text{ GeV}}\right), \end{aligned} \quad (3.49)$$

with a fiducial temperature T_{low} well below T_R and well above T_σ , which we use to denote the temperature of the primordial plasma at $t = \tau_\sigma$: $T_\sigma \ll T_{\text{low}} \ll T_R$.

In the case of the axion, $T_{\text{low}} = T_{\text{mat=rad}}$ can be used since its lifetime exceeds the time of matter-radiation equality significantly. Note that the resulting saxion/axion yield is insensitive to the exact choice of T_{low} for $T_{\text{low}} < 0.01 T_R$ since additional contributions from thermal production at $T < 0.01 T_R$ are found to be negligible.

Figure 3.5 shows the saxion yield (3.49) for $f_{\text{PQ}} = 10^{10}$, 10^{11} , and 10^{12} GeV as red dotted, blue dashed, and black solid lines, respectively.

Note that (3.49) is only valid for $T_R \ll T_D^\sigma$, because otherwise saxion disappearance processes neglected in (3.3) become important. For $T_R \gtrsim T_D^\sigma$ saxions are in thermal equilibrium in the early Universe and decouple as thermal relics. Since for the parameter regions considered in this work, $m_\sigma \ll T_D^\sigma$, they decouple as relativistic

³Note that the particle content of the MSSM plus the PQ supermultiplet allows for non-standard Cosmologies, where a massive particle comes to dominate the energy density at temperatures above $T_{\text{mat=rad}}$. The computation of $Y_\sigma^{\text{TP}}(T_{\text{low}})$ is, however, not affected, since such a domination typically happens at temperatures $T \ll 0.01 T_R$, see Chaps. 6 and 7 for details.

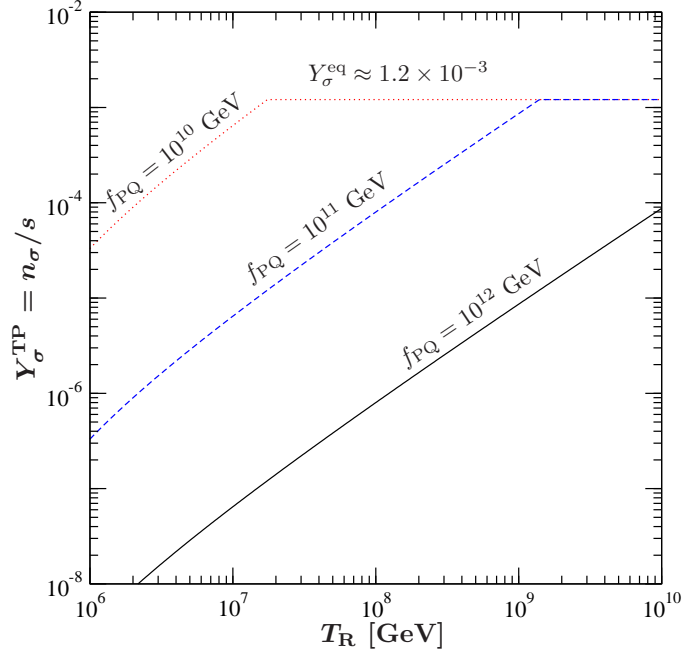


Figure 3.5: The relic saxion yield prior to decay originating from thermal processes in the primordial plasma for cosmological scenarios characterized by different T_R values covering the range from 10^6 to 10^{10} GeV. The red dotted, blue dashed, and black solid lines are obtained for $f_{PQ} = 10^{10}$, 10^{11} , and 10^{12} GeV. The relic axion yield $Y_a^{\text{eq/TP}}$ from thermal processes agrees with $Y_\sigma^{\text{eq/TP}}$ and can thus be read from this figure as well.

species and their yield depends on the internal degrees of freedom g of the saxion. The saxion is a real scalar, so $g = 1$ and we arrive at

$$Y_\sigma^{\text{eq}} = \frac{n_\sigma^{\text{eq}}}{s} = \frac{45\zeta(3)}{2\pi^4 g_{*S}} \approx 1.2 \times 10^{-3}, \quad (3.50)$$

where $g_{*S} = 228.75$. The yield from thermal production cannot exceed the equilibrium yield, so (3.50) represents an upper limit on (3.49) visible in Fig. 3.5. For values of T_R where (3.49) exceeds (3.50), saxion disappearance reactions described by the last term in (3.1) would have to be included. Their inclusion would lead to almost the same T_R dependence as shown in Fig. 3.5, but with a smooth approach of Y_σ^{TP} to the equilibrium value at T_R values for which $Y_\sigma^{\text{eq}} \simeq Y_\sigma^{\text{TP}}$.

For axions, $m_a \ll T_D^a$ is always satisfied so that they will be hot thermal relics with $Y_a^{\text{eq}} = Y_\sigma^{\text{eq}}$ as given in (3.50) if $T_R \gtrsim T_D^a$. In fact, the relic axion yield $Y_a^{\text{eq/TP}}$ from thermal processes agrees fully with $Y_\sigma^{\text{eq/TP}}$ described above and can be read from Fig. 3.5 as well.

The thermally produced axino yield is calculated in the same way as (3.49). The

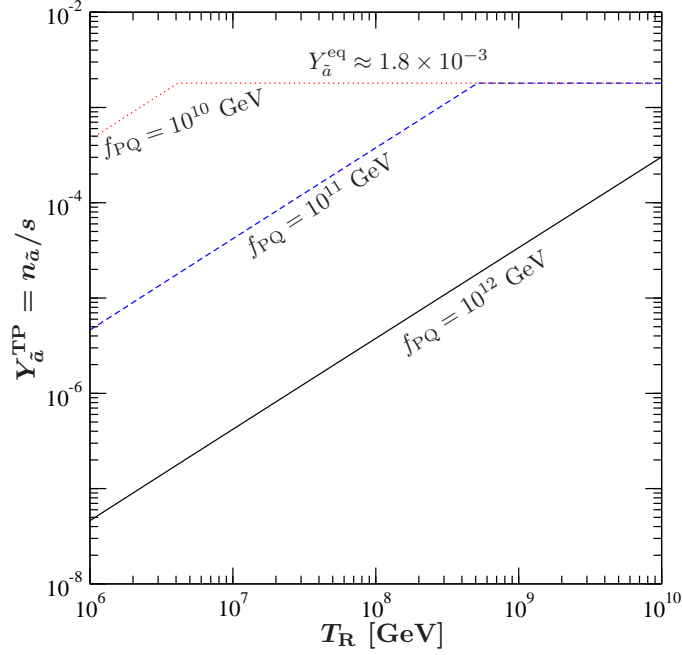


Figure 3.6: The relic axino yield prior to decay originating from thermal processes in the primordial plasma for cosmological scenarios characterized by different T_R values covering the range from 10^6 to 10^{10} GeV. The red dotted, blue dashed, and black solid lines are obtained for $f_{\text{PQ}} = 10^{10}$, 10^{11} , and 10^{12} GeV.

result reads

$$Y_{\tilde{a}}^{\text{TP}}(T) \approx \int_{T_{\text{low}}}^{T_R} dT \frac{W_{\tilde{a}}(T)}{Ts(T)H(T)} = 2.0 \times 10^{-3} g_s^6 \ln\left(\frac{1.271}{g_s}\right) \left(\frac{10^{11} \text{ GeV}}{f_{\text{PQ}}}\right)^2 \left(\frac{T_R}{10^8 \text{ GeV}}\right). \quad (3.51)$$

We see that the inclusion of the axino-squark-squark-gluino vertex changes the constant under the logarithm compared to (E.3) in [50] in accordance with our comments after Eq. (3.32). The axino yield is shown in Fig. 3.6 for $f_{\text{PQ}} = 10^{10}$, 10^{11} , and 10^{12} GeV as red dotted, blue dashed, and black solid lines, respectively. We again use (3.28) to account for the renormalization group evolution of the strong gauge coupling.

In analogy to the saxion case, also (3.51) is only valid for T_R smaller than the axino decoupling temperature $T_{\text{D}}^{\tilde{a}}$. The axino is a fermion with two internal degrees of freedom, hence the equilibrium yield is

$$Y_{\tilde{a}}^{\text{eq}} \approx 1.8 \times 10^{-3}. \quad (3.52)$$

This yield is an upper limit for (3.51) and similar arguments as after (3.50) apply here.

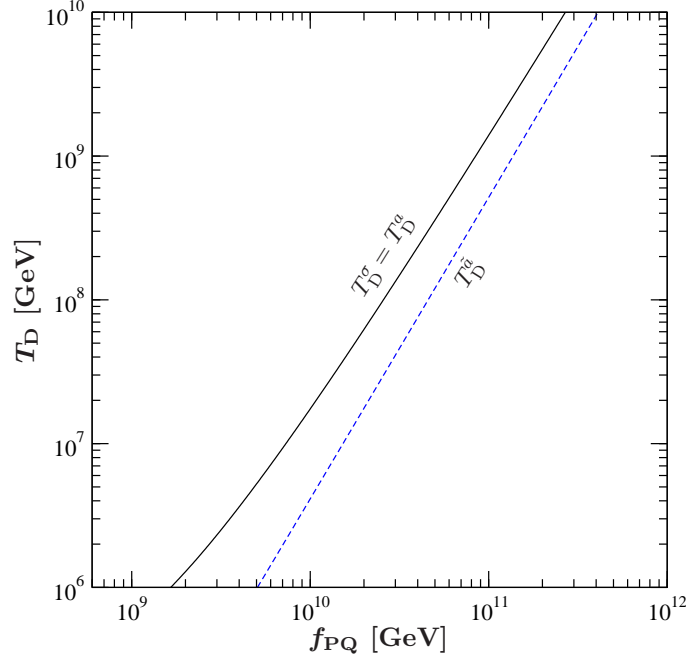


Figure 3.7: The decoupling temperature of the saxion T_D^σ depicted as the black solid line and the decoupling temperature of the axino $T_D^{\tilde{a}}$ as the blue dashed line. The decoupling temperature of the axion $T_D^a = T_D^\sigma$.

3.4.3 Estimating the Decoupling Temperatures

Let us now turn to the decoupling temperatures of each of the PQ particles. Considering Fig. 3.5, one can see that the kinks indicate critical T_R values. For scenarios with T_R higher than the value indicated by the kink for a given f_{PQ} , saxions have been in thermal equilibrium in the early Universe and have decoupled as thermal relics, whereas for T_R lower than this critical value, saxions never reached equilibrium. Thus, we estimate the decoupling temperature of the saxion T_D^σ by the position of the kinks. Considering Fig. 3.6, the axino decoupling temperature $T_D^{\tilde{a}}$ is estimated in an analogue way.

Figure 3.7 shows T_D^σ and $T_D^{\tilde{a}}$ as a function of f_{PQ} . We find that our numerical results are well described by

$$T_D^\sigma \approx 1.4 \times 10^9 \text{ GeV} \left(\frac{f_{PQ}}{10^{11} \text{ GeV}} \right)^2, \quad (3.53)$$

and

$$T_D^{\tilde{a}} \approx 5.2 \times 10^8 \text{ GeV} \left(\frac{f_{PQ}}{10^{11} \text{ GeV}} \right)^2. \quad (3.54)$$

The estimate for T_D^σ is similar to the one in Ref. [45]. Such an agreement was expected and is used to provide estimates of the thermally produced saxion yield

Y_σ^{TP} in Refs. [48, 62, 64, 92]. Another recent study applies the thermally produced axino yield $Y_{\tilde{a}}^{\text{TP}}$ [50] to estimate $Y_\sigma^{\text{TP}} \simeq (2/3) Y_{\tilde{a}}^{\text{TP}}$ [141].⁴ With our results illustrated in Figs. 3.5 and 3.6 above, one can now see explicitly the similarity between Y_σ^{TP} and $Y_{\tilde{a}}^{\text{TP}}$.

In light of Sect. 3.2, it is clear that Eq. (3.53) describes the axion decoupling temperature in the considered SUSY settings as well. Accordingly, it is also shown by the black solid line in Fig. 3.7. When comparing (3.53) with the axion decoupling temperature in non-SUSY scenarios, given in Eq. (15) of Ref. [1], we find only small differences. In fact, for a fixed $g_s \ll 1$, the additional diagrams in the SUSY case (which lead to a different thermal gluon mass m_g also) increase the collision term for thermal axion production W_a only by at most 30% with respect to Eq. (12) of Ref. [1] obtained for the non-SUSY case. Note also that $Y_a^{\text{eq/TP}}$ is normalized to an entropy density that is more than two times larger in the SUSY case than in the non-SUSY case due to the additional sparticles, which can all be considered to be relativistic at very high temperatures such as the axion decoupling temperature.

3.5 Inflation and the Reheating Temperature

In the above calculations of the thermal production rate we did not take the reheating phase into account, but took T_R as the initial temperature of the radiation dominated epoch. A more complete treatment of the reheating phase will allow us to compare our thermal production rates to other production mechanisms of saxions.

Inflation is a period of exponential expansion of the Universe.⁵ In most inflation models, this is achieved by a scalar field ϕ called inflaton that slowly rolls down a potential, so that the Universe is dominated by the potential energy of this field. Inflation ends if the kinetic energy dominates over the potential one, which occurs when the inflaton oscillates around the bottom of its potential. These coherent oscillations behave as non-relativistic matter.

After the end of inflation, the Universe is dominated by the energy density of ϕ , with most energy in the zero-momentum mode. In order to arrive at the presumably hot stage of the early Universe, the inflaton has to decay into interacting relativistic particles, which we collectively term as radiation here. This process is called reheating. We do not go into details of inflation, especially we do not assume a specific model of inflation. All we need is a massive inflaton with decay width into radiation Γ_ϕ .

⁴Note that f_{PQ} in [62, 92] and F_a in [64, 141] correspond to our $v_{\text{PQ}} = f_{\text{PQ}}/\sqrt{2}$ and thereby differ by $1/\sqrt{2}$ from our f_{PQ} . With these differences in the definitions of the PQ scale, we find that the Y_σ^{TP} estimates in Refs. [62, 64, 92, 141] exceed the result (3.49) of our calculation by about a factor of two for fixed f_{PQ} and T_R .

⁵The concept of inflation was introduced in Refs. [167, 168] and the idea of slow-roll in Refs. [169–171]. There are many reviews and books about inflation, we mainly use [157].

We focus on thermally produced saxions first. Similar calculations for thermal gravitino production has been performed in Refs. [153, 172, 173]. The time evolution of the saxion number density is given by (3.48) with the collision term in (3.27). The temperature on the right hand side (rhs) of (3.27) is the temperature of the background radiation that is assumed to be in thermal equilibrium, since it interacts strongly at this high temperatures. In other words, we assume that the thermalization time scale of the radiation background is much smaller than the decay time scale of the inflaton. Temperature and energy density are related by (3.42). The evolution of the energy densities of the inflaton ρ_ϕ and of radiation ρ_{rad} is governed by the Boltzmann equations

$$\frac{dn_\sigma}{dt} + 3Hn_\sigma = \frac{9\zeta(3)g_s^6}{256\pi^7 f_{\text{PQ}}^2} \left[\ln \left(\frac{2}{3g_s^2} \right) + 0.4305 \right] \left(\frac{30\rho_{\text{rad}}}{\pi^2 g_*} \right)^{3/2}, \quad (3.55a)$$

$$\frac{d\rho_\phi}{dt} + 3H\rho_\phi = -\Gamma_\phi \rho_\phi, \quad (3.55b)$$

$$\frac{d\rho_{\text{rad}}}{dt} + 4H\rho_{\text{rad}} = \Gamma_\phi \rho_\phi. \quad (3.55c)$$

Note that the first equation describes the evolution of a number density, hence the factor of 3 in front of the second term on the left hand side (lhs) accounts for dilution due to the expansion of the Universe. The last two equations describe energy densities, where in the case of relativistic particles the redshift is manifested by the factor of 4 on the lhs of (3.55c).

The time evolution of the scale factor is given by the Friedmann equation (3.36), which in our case reads

$$H^2 = \frac{8\pi}{3m_{\text{Pl}}^2} (\rho_\phi + \rho_{\text{rad}}), \quad (3.56)$$

where we have neglected the small contribution of the saxion to the total energy density.

The relation of T_{R} to the properties of the inflaton is given by Γ_ϕ . T_{R} is taken as the temperature below which the Universe expands as a radiation dominated Universe. When the inflaton decays, all energy is transferred into radiation, where we ignore the small amount that goes into saxions. Then, T_{R} is given by

$$\Gamma_\phi = \xi H(T_{\text{R}}), \quad (3.57)$$

where we have introduced a factor ξ to later connect our analytic results obtained in the previous section to the numerical result. The value of ξ used to define T_{R} varies between 1 and 3 in the literature. The above equation can be rewritten as

$$T_{\text{R}}^\xi = \frac{1}{\sqrt{\xi}} \left(\frac{45}{4\pi^3 g_*} \right)^{1/4} \sqrt{\Gamma_\phi m_{\text{Pl}}}. \quad (3.58)$$

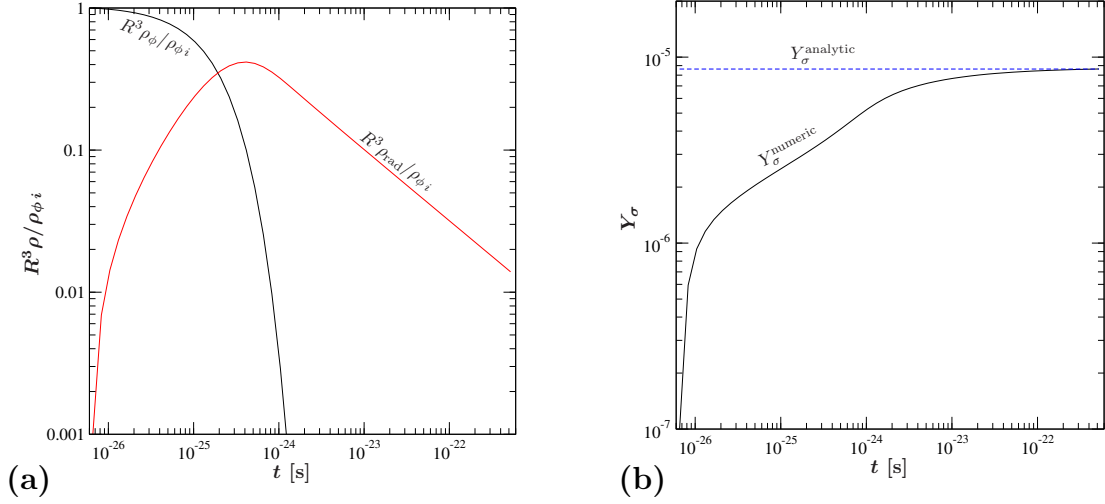


Figure 3.8: **(a):** Time evolution of the energy per comoving volume $R^3 \rho$ of the inflaton (black) and radiation (red) normalized to the initial energy per comoving volume of the inflaton $R_0^3 \rho_{\phi 0}$. Here $R_0 = 1 \text{ GeV}^{-1}$ and $\xi = 1.8$.

(b): Time evolution of the saxion yield from the numerical integration of (3.55) and (3.56) labeled $Y_{\sigma}^{\text{numeric}}$ in black compared to the analytic result of (3.49) with $T_R = 10^9 \text{ GeV}$ labeled $Y_{\sigma}^{\text{analytic}}$ in blue for $\xi = 1.8$.

In Fig. 3.8 we show the results of the numerical integration of (3.55) and (3.56). Figure 3.8(a) shows the evolution of the energy per comoving volume $R^3 \rho$ of the inflaton in black and of radiation in red, both of them normalized to the initial energy per comoving volume of the inflaton. The initial value of the scale factor $R_0 = 1 \text{ GeV}^{-1}$ and $\xi = 1.8$. We choose $\Gamma_{\phi} = 3.7 \text{ GeV}$ such that we get $T_R^{\xi} \simeq 10^9 \text{ GeV}$ for $\xi = 1.8$, because eventually we want to compare the numerical result for Y_{σ} with our analytical result for the exemplary point $T_R^{\xi} = 10^9 \text{ GeV}$. Since the initial amount of radiation is diluted away by the exponential expansion, the decay of the inflaton results in a step rise of the energy in the form of radiation. After the transition from matter to radiation dominated era, the energy per comoving volume in radiation decreases as R^{-1} . Figure 3.8(b) shows the corresponding saxion yield obtained by integrating (3.55) and (3.56) labeled as $Y_{\sigma}^{\text{numeric}}$ in black. The blue dashed line depicts the analytic result $Y_{\sigma}^{\text{TP}}(T_{\text{low}})$ from (3.49) obtained with $\xi = 1.8$ and $T_R = 10^9 \text{ GeV}$. Thus, to account for a reheating process happening in a finite time, we must use $\xi = 1.8$ to get an agreement of the analytic approximation with the numerical result.

The numerical result for the saxion yield with an alternative definition of T_R with different ξ can be described with our analytical approximation after substituting T_R with $\sqrt{\xi/1.8} T_R^{\xi}$ in (3.49). Note that the value of ξ that describes our analytic

solution best depends slightly on T_R^ξ . It reads $\xi = 1.7$ (1.9) for $T_R^\xi = 10^{11}$ (10^7) GeV. In the similar calculation for thermal gravitino production done in Ref. [153], the same value of $\xi = 1.8$ was obtained. The reason is the dependence of both the saxion and gravitino collision term on T^6 and, therefore, on $\rho_{\text{rad}}^{3/2}$. Thus, also for thermally produced axinos we get $\xi = 1.8$, since the axino collision term also depends on T^6 . In light of Sect. 3.2, the above calculation is valid for the axion as well. Now we have a proper relation between the inflaton and thermal production of PQ particles. Having calculated the respective thermal yields and decoupling temperatures of the PQ particles, we are now ready to explore possible cosmological consequences of the saxion, the axion, and the axino.

Chapter 4

Possible Cosmological Implications of the Saxion

Cosmological implications of the PQ particles have been studied extensively in the literature. Some of the references can be found in our Introduction. For a recent review including also the PQ particles, see, e.g., Ref. [174], and further references therein. In this chapter, we focus on the saxion and present an overview over possible implications. But first we need to introduce another production mechanism in addition to the thermal production.

In Sect. 4.1, we present an updated estimate of the energy density of saxions from this second production mechanism, namely coherent oscillations of the saxion field in the early Universe [61, 62, 64, 90–93]. Our update includes the combination with the reheating model in Sect. 3.5 and the use of the scales v_{PQ} and f_{PQ} presented in Sect. 2.4. The oscillations provide a population of cold saxions. We also compare the yield of the two saxion populations and show regions where one of them dominates.

The next three sections summarize cosmological implications of these saxions depending on the saxion lifetime. Our presentation follows [64], but we provide updates of the corresponding limits. For $\tau_\sigma \lesssim 1$ s, the saxion decay happens before BBN. Depending on the decay products, these decays can produce entropy and/or additional radiation. We present only a short overview here in Sect. 4.2, since this is the main topic of the following three chapters.

For $1 \text{ s} \lesssim \tau_\sigma \lesssim 10^{12} \text{ s}$, the saxions decay during or in the aftermath of BBN. Possible implications for the observed abundance of light elements include photo- and hadro-dissociation of nuclei. We show corresponding limits in Sect. 4.3. In this and the next section, we use the approximate envelopes given in [64] for the limits.

For $\tau_\sigma \gtrsim 10^{12} \text{ s}$, the decay of the saxion can affect the CMB, the diffuse X- and γ -ray background radiation and the ionization history of the Universe. We illustrate these limits in Sect. 4.4.

4.1 Saxions from Misalignment

As explained in Chap. 2, the supersymmetric extension of the PQ mechanism introduces a flat direction in the scalar potential also for the saxion. This flat direction gets lifted by SUSY breaking effects, which results in a non-zero mass for the saxion. Before SUSY breaking, the initial value of the saxion field is arbitrary and not necessarily at its true minimum value σ_{\min} , which is only effective after SUSY breaking. Thus, the saxion field rolls towards σ_{\min} when SUSY is broken and the field is not hindered by too much friction. Then, it performs coherent oscillations around σ_{\min} .

Note the close similarity of this mechanism with the misalignment mechanism of the axion [37–42]. In the axion case, however, the potential is flat because of the (real or complex) PQ symmetry, so also without SUSY. The lifting of the flat direction arises through instanton effects, thus the oscillations start typically much later than in the case of the saxion. Moreover, the initial value of the axion field can vary in the interval $(-\pi, \pi]$, because the axion is the phase of one of the complex fundamental PQ fields. Because the PQ symmetry breaking can take place at energies well above T_R , the initial value of the axion field can be fixed already before reheating. Therefore, its value can be the same for the whole observable Universe. In fact, as already stated earlier, we assume that the PQ symmetry is broken before inflation and is not restored afterwards.

In the case of the saxion, the value of the true minimum depends on the exact choice of the superpotential and the details of SUSY breaking. With our \mathcal{W} given in (2.54) and the discussion following Eq. (2.54), we find $v_1 = v_{\text{PQ}}/\sqrt{2}$. The equation of motion for the saxion field can be obtained by considering the kinetic term of the saxion in the Lagrangian (2.61) (neglecting the three-saxion coupling for the moment) and from the harmonic potential in (2.55), which yield¹

$$\mathcal{L}_\sigma^{\text{osc}} = \frac{1}{2} \partial^\mu \sigma \partial_\mu \sigma - \frac{1}{2} m_\sigma^2 (\sigma - \sigma_{\min})^2 + \dots \quad (4.1)$$

where the ellipsis denote possible terms of higher order or thermal corrections not included in (2.55).² Note that the exact value of the minimum is not important for the resulting saxion density in this setup, because it can be removed from the Lagrangian via a redefinition of the saxion field. The equation of motion for an expanding Universe reads after such a redefinition

$$\ddot{\sigma} + 3H\dot{\sigma} + m_\sigma^2 \sigma = 0, \quad (4.2)$$

where we neglected the gradient part, because it is suppressed by $1/R^2$.

We want to combine the evolution of the saxion field with inflation, so we use (3.55b), (3.55c), (3.56), and (4.2) to form a closed set of differential equations. We assume

¹For the generic case of such scalar field oscillations, see, e.g., Ref. [157].

²Thermal effects are studied, e.g., in Refs. [141, 175], the results are, however, strongly model-dependent and therefore we do not consider them here.

that the saxion does not dominate the energy density at this early stage and, therefore, we can neglect the saxion energy density in (3.56). The saxion energy density from these oscillations behaves like matter and such an early domination would alter the cosmological history completely by significantly delaying the radiation dominated epoch.

In Sect. 3.5 we showed that the integration of (3.55) and (3.56) results in a thermal saxion population. Its yield that can be calculated by (3.49) when one uses (3.57) with $\xi = 1.8$ to link Γ_ϕ and T_R . Here we use the same relations, so that we can provide a meaningful comparison of the thermal and the misalignment saxion yield.

As a reference point, we take $T_R = 10^9 \text{ GeV}$, thus also $\Gamma_\phi = 3.7 \text{ GeV}$. The initial displacement relative to the true minimum of the saxion field σ_i is taken as a free parameter and in principle can vary between 0 and m_{Pl} .

Note that if the saxion field is initially at the origin, the saxion has unsuppressed interactions with the particles in the thermal bath [62]. The reason is that for very small v_1 , the KSVZ (s)quarks are light and the PQ interactions are not suppressed, as explained in Chap. 2. In this case, the saxion receives an additional thermal mass term not shown in (4.2) that delays the beginning of the saxion oscillations considerably. It has been shown that for reasonable values of the thermal mass, T_R is then constrained to be very small [62]. Since we want to focus on scenarios with a high reheating temperature, we do not consider the case where the saxion is originally at the origin.

If the initial position of the saxion field is sufficiently far away from the origin, the saxion oscillations obey (4.2). For $H \gg m_\sigma$, the oscillations are overdamped and the saxion field remains at its initial position. At a later time, when $H \approx m_\sigma$, the oscillations start. The system behaves as a damped harmonic oscillator with the $3H$ term providing Hubble friction.

The ratio of the energy density in these oscillations over s is given by the potential energy of the initial misalignment over s (see also [62])

$$\frac{\rho_\sigma^{\text{osc}}}{s} \simeq \frac{\frac{1}{2}m_\sigma^2\sigma_i^2}{\frac{2\pi^2}{45}g_*sT_c^3}, \quad (4.3)$$

where T_c denotes the temperature when the saxions start to oscillate. This temperature can be obtained by

$$m_\sigma = \zeta H(T_c), \quad (4.4)$$

where the parameter $\zeta = \mathcal{O}(1)$ will be determined by the comparison to the numerical result below. This equation can be recast as

$$T_c^\zeta = \frac{1}{\sqrt{\zeta}} \left(\frac{45}{4\pi^3 g_*} \right)^{1/4} \sqrt{m_\sigma m_{\text{Pl}}}, \quad (4.5)$$

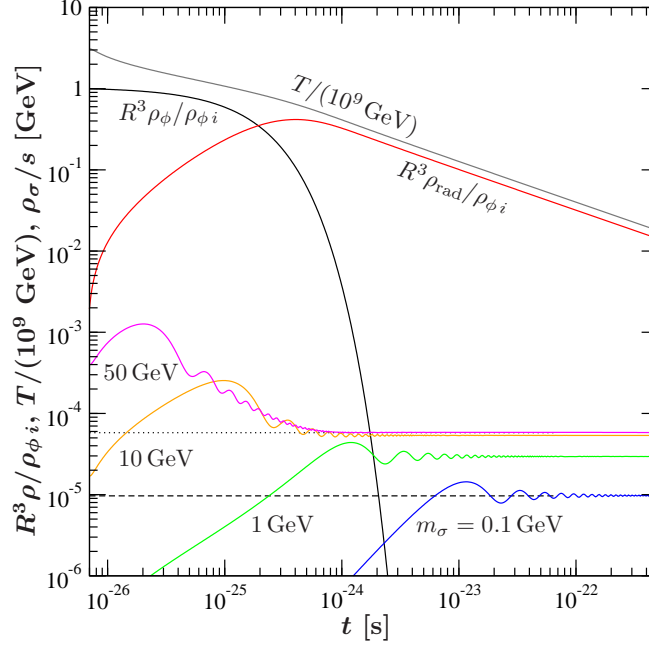


Figure 4.1: Time evolution of the inflaton, radiation, temperature, and saxion field obtained by integrating (3.55b), (3.55c), (3.56), and (4.2). The black solid line depicts the energy per comoving volume of the inflaton, the red line the one of radiation, both normalized to the corresponding initial value of the inflaton. Here $R_i = 1 \text{ GeV}^{-1}$ and $\Gamma_\phi = 3.7 \text{ GeV}$, which gives $T_R = 10^9 \text{ GeV}$. The gray line shows the temperature divided by 10^9 GeV . The blue, green, orange, and magenta lines show the energy density over entropy density of oscillating saxion fields for $\sigma_i = 10^{12} \text{ GeV}$ and $m_\sigma = 0.1, 1, 10, \text{ and } 50 \text{ GeV}$, respectively. The dashed line is the analytic approximation of the final amount for $m_\sigma = 0.1 \text{ GeV}$, the dotted one approximates the final amount for $m_\sigma = 10 \text{ and } 50 \text{ GeV}$. Both approximations are drawn for $\zeta = 1.6$.

and plugged into (4.3). The result reads

$$\frac{\rho_\sigma^{\text{osc}}}{s} \simeq 9.7 \times 10^{-6} \text{ GeV} \left(\frac{m_\sigma}{0.1 \text{ GeV}} \right)^{1/2} \left(\frac{\sigma_i}{10^{12} \text{ GeV}} \right)^2 \left(\frac{\zeta}{1.6} \right)^{3/2}. \quad (4.6)$$

For $T_c < T_R$, the saxion field starts to oscillate after the end of inflation. With no major release of entropy until today, (4.6) stays constant.

For $T_c > T_R$, the oscillations of the saxion field start already before the decay of the inflaton and the saxion energy density gets diluted by the inflaton decay. The energy density of saxions at $T = T_R$ is then given by (see also [62])

$$\frac{\rho_\sigma^{\text{osc}}}{s} \simeq \frac{\frac{1}{2} m_\sigma^2 \sigma_i^2}{\frac{2\pi^2}{45} g_{*S} T_R^3} \left[\frac{R(T_c)}{R(T_R)} \right]^{3/2}. \quad (4.7)$$

If one makes the reasonable assumption that g_{*S} is constant during this period and

one uses (4.5), one obtains

$$\frac{\rho_{\sigma}^{\text{osc}}}{s} \simeq 5.9 \times 10^{-5} \text{ GeV} \left(\frac{T_R}{10^9 \text{ GeV}} \right) \left(\frac{\sigma_i}{10^{12} \text{ GeV}} \right)^2 \left(\frac{\zeta}{1.6} \right)^2. \quad (4.8)$$

In Fig. 4.1 we show the results of the integration of (3.55b), (3.55c), (3.56), and (4.2) as a function of time t . The solid black line depicts the energy per comoving volume $R^3 \rho_{\phi}$ of the inflaton, the red line the one of radiation, both normalized to the initial value of the energy density of the inflaton. The initial value of the scale factor $R(t_i) = 1 \text{ GeV}^{-1}$ and $\Gamma_{\phi} = 3.7 \text{ GeV}$. The gray line shows the temperature normalized to 10^9 GeV . The blue, green, orange, and magenta lines show the energy density over entropy density resulting from oscillating saxions for $\sigma_i = 10^{12} \text{ GeV}$ and $m_{\sigma} = 0.1, 1, 10$, and 50 GeV , respectively. The dashed black line illustrates the approximation (4.6) used to describe the resulting energy density over entropy density of saxion oscillations for $m_{\sigma} = 0.1 \text{ GeV}$, where we set $\zeta = 1.6$ to arrive at the shown agreement. For $m_{\sigma} = 10$ and 50 GeV , $T_c > T_R$, and we use (4.8) to approximate the resulting saxion energy density, as shown by the black dotted line. To reach agreement with the numerical result for $m_{\sigma} = 10$ and 50 GeV , we again find $\zeta = 1.6$. Note that in contrast to (4.6), the result (4.8) does not depend on the saxion mass, as clearly confirmed by the numerical result in the figure. Similar results have been reported in the literature, see, e.g., Refs. [62, 64], but there the value of ζ was not specified and usually set equal to one.

The initial value of the saxion field has a strong influence on the resulting energy density from saxion oscillations, see (4.6) and (4.8). Here we treated σ_i as a free parameter, as it is not determined by the PQ superfield in our case. In the literature it is often assumed that $\sigma_i \sim v_{\text{PQ}}$. In fact, Ref. [64] provides a model that arrives at $\sigma_i \sim |\Phi| \sim F_a$ because of saxion-inflaton couplings resulting from supergravity. We do not go into the details of this model. Let us just note that with our notation and the superpotential (2.54), this would mean $\sigma_i \sim v_{\text{PQ}}/\sqrt{2} = f_{\text{PQ}}/2$. To compare the energy density from saxion oscillations with the thermal density, we write both in terms of f_{PQ} . Thus, our results yield a factor of four less energy density from oscillations and, as already pointed out in footnote 4 the previous chapter, a factor of two less thermal energy density.

In Fig. 4.2, we show the energy density over entropy density from thermal saxion production in red and from saxion oscillations in blue, both as a function of m_{σ} , for $\sigma_i = f_{\text{PQ}}/2$ and $\zeta = 1.6$. The contours are drawn solid, dashed, and dotted for $T_R = 10^{11}$, 10^9 , and 10^7 GeV , respectively. The PQ scale $f_{\text{PQ}} = 10^{10}$, 10^{12} , and 10^{14} GeV in Figs. 4.2(a), (b), and (c), respectively. Note a similar figure in Ref. [64].

As one can see, for $f_{\text{PQ}} \lesssim 10^{12} \text{ GeV}$, $m_{\sigma} \gtrsim 1 \text{ GeV}$ and high T_R , thermal production is more effective than the misalignment mechanism. This finding allows us to neglect saxions from oscillations in the Chaps. 5 - 7.

In the remainder of this chapter, however, we take both saxion populations into account when analyzing possible cosmological results of the saxions.

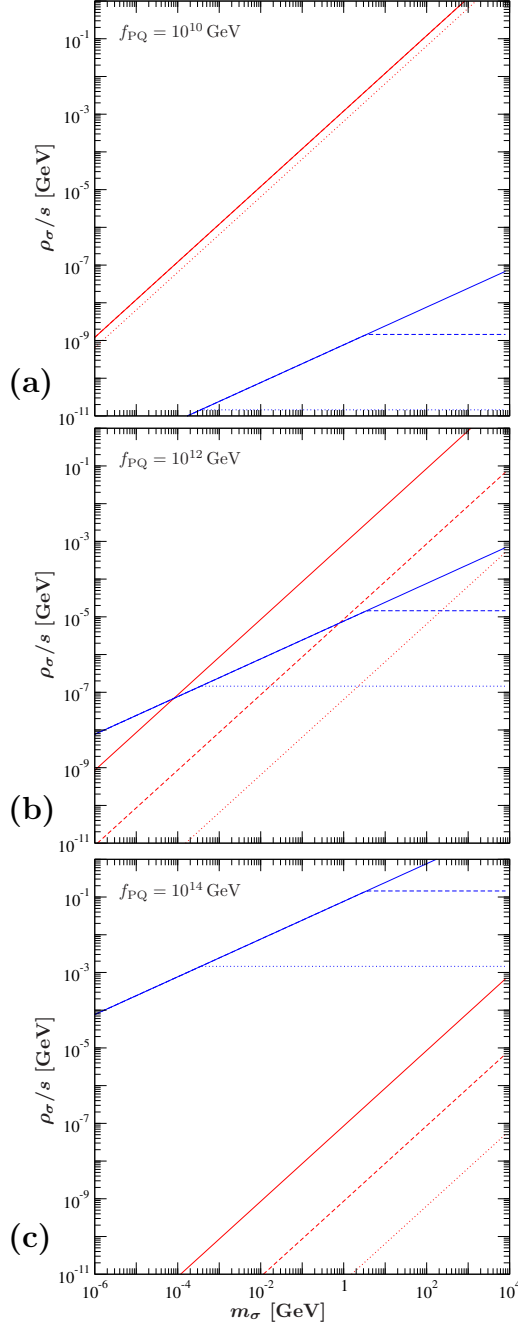


Figure 4.2: **(a):** Energy density of saxions over entropy density ρ_σ/s from thermal processes in red and from misalignment in blue as a function of the saxon mass m_σ . Lines are drawn solid, dashed, and dotted for $T_R = 10^{11}$, 10^9 , and 10^7 GeV, respectively. Here $f_{\text{PQ}} = 10^{10}$ GeV, $\zeta = 1.6$, and $\sigma_i = f_{\text{PQ}}/2$.

(b): Same as (a), but for $f_{\text{PQ}} = 10^{12}$ GeV.

(c): Same as (a), but for $f_{\text{PQ}} = 10^{14}$ GeV.

4.2 Early Decay and Entropy

Apart from the initial abundance, the other crucial parameter for saxions in cosmology is its lifetime. In case of thermal saxions, both of them are related via m_σ , f_{PQ} , whereas the initial amount of the oscillations is in principle free. For definiteness and in light of the discussion above, we set $\sigma_i = \langle \phi_1 \rangle = f_{\text{PQ}}/2$ in the following.

If the saxion lifetime $\tau_\sigma \lesssim 1$ s, the decay happens before BBN. Therefore, it can influence BBN only indirectly via additional radiation or entropy production. The former is most important if the saxion decays mainly into axions, hence $x \simeq 1$, whereas the latter is most efficient for $x \ll 1$.

The release of extra radiation by decaying saxions has been considered previously in Refs. [47, 64, 89–92, 176]. The application of our new result for the thermal production yield and updated cosmological constraints is discussed in detail in the following three chapters.

For $x \ll 1$, the saxion decays mainly into particles that interact with the thermal bath and, therefore, the decay releases entropy. This has been considered in Refs. [58, 59, 61, 62, 65, 66]. The generic case of a decaying thermal particle considered in Ref. [65] poses an upper limit on the entropy release of thermal saxions. The reason for this limit is basically that thermal production and decay of the saxion are governed by the same interaction term and, therefore, by the same suppression scale f_{PQ} . For some interesting parameter regions, the amount of released entropy is calculated in Chaps. 6 and 7. These chapters also contain a combination of the release of extra radiation and entropy by decaying thermal saxions. If one includes saxions from oscillations, the entropy release can be quite large, see, e.g., Ref. [65].

4.3 Decay during BBN

If $\tau_\sigma \gtrsim 10^{-2}$ s, the decay products of saxions may affect BBN [173, 177–183]. In the following, we rely on Ref. [64]. A very early decay can disturb neutrino freeze-out. For $\tau_\sigma \lesssim 10^2$ s, injected pions can change proton-neutron interconversion reactions, which results in too much ^4He . Later decays may inject energetic photons or hadrons that reprocess light nuclei. For smaller energies of the injected particles the constraints are substantially weaker. The energy of the particles is equal to half of the saxion mass, thus for $m_\sigma \lesssim 4.5$ MeV, which corresponds to twice the threshold of photo-dissociation of D, the constraints disappear altogether.

In Figs. 4.3 and 4.4 we illustrate in red the limits imposed by BBN for thermal and non-thermal saxions. We use the envelopes given in Ref. [64], which themselves are derived from Ref. [173]. In Fig. 4.3 we set $f_{\text{PQ}} = 10^{10}$ GeV and in (a) we set $x = 0$, in (b), $x = 1$. In Fig. 4.4 we use $f_{\text{PQ}} = 10^{12}$ GeV, again for both values of x . Note that in Fig. 4.3(b) there are no limits from BBN in contrast to Fig. 4.4(b). This

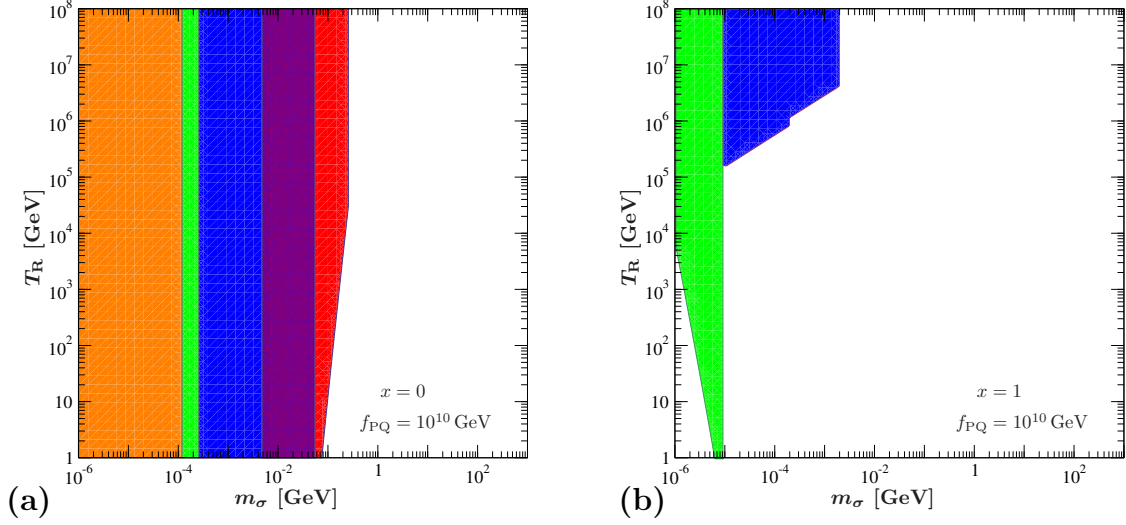


Figure 4.3: **(a):** Disfavored regions of T_R due to saxion decays inferred from BBN (red), CMB blackbody spectrum (blue), reionization (green), and diffuse X- and γ -ray spectrum (orange) as a function of m_σ for $f_{\text{PQ}} = 10^{10}$ GeV and $x = 0$. In the violet region, BBN and CMB constraints overlap. Colored regions are disfavored. Limits taken from Ref. [64].

(b): Same as (a), but for $x = 1$.

is because in Fig. 4.3(b) the saxions with the right lifetime have a mass below the threshold for photo- or hadro-dissociation due to the smaller value of f_{PQ} . In this case, however, the results of BBN can still be affected by extra radiation, which will be analyzed in detail in the following chapters.

There are similar plots in Ref. [64]. Although the overall results are comparable, there are differences for various reasons. As mentioned in the previous chapters, the definition of f_{PQ} is different and, therefore, also the result for the thermal yield. Also the saxion decay width into gluons differs from our result. Moreover, we use a different value for the initial amplitude of the saxion field. Remaining differences of the BBN limits are due to an inclusion of more limits in the plots in Ref. [64] than stated in the envelopes, e.g, for $10^{-2} \text{ s} \lesssim \tau_\sigma \lesssim 1 \text{ s}$. In total, our analysis has some conceptual improvements over the one in Ref. [64] like the new result for the thermal yield and the relation between v_{PQ} and f_{PQ} , but in light of the uncertainties in the envelopes, we refrain from a more detailed comparison.

As one can see, the limits from BBN can be quite restrictive, especially for large T_R . In light of these limitations, in the following chapters we focus on saxion decays happening prior to BBN.

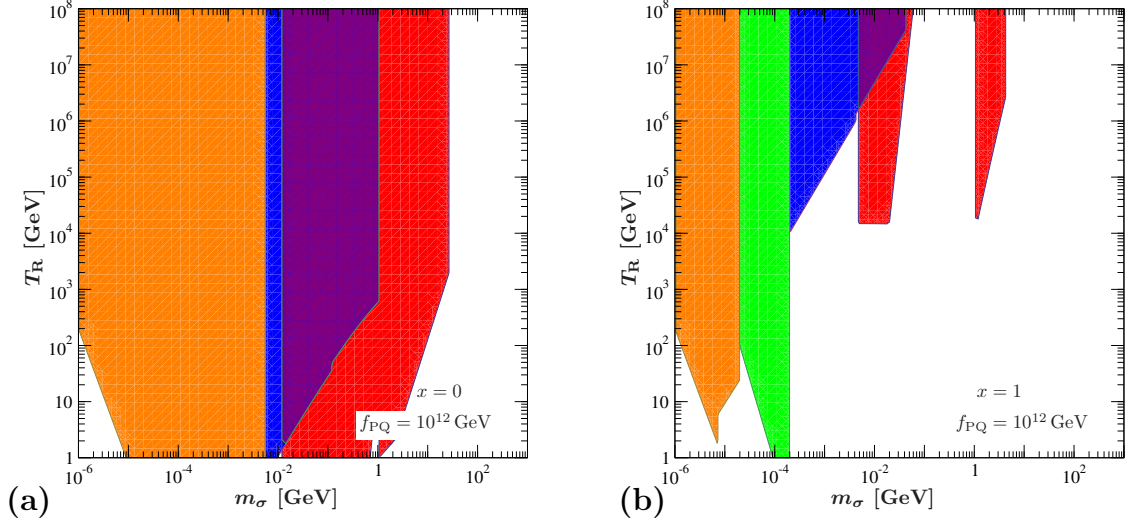


Figure 4.4: **(a):** Disfavored regions of T_R due to saxion decays inferred from BBN (red), CMB blackbody spectrum (blue), reionization (green), and diffuse X- and γ -ray spectrum (orange) as a function of m_σ for $f_{PQ} = 10^{12}$ GeV and $x = 0$. In the violet region, BBN and CMB constraints overlap. Colored regions are disfavored. Limits taken from Ref. [64].

(b): Same as (a), but for $x = 1$.

4.4 Late Decay

Longer saxion lifetimes are typically only possible if $m_\sigma \ll 1$ GeV, thus the saxion decays only into photons and, depending on x , into axions.

Photons from such photon number-violating processes can disturb the blackbody spectrum of CMB, if the decay happens prior to recombination. Photon number-violating processes become inefficient after 10^6 s, thus for $10^6 \text{ s} \lesssim \tau_\sigma \lesssim 10^{13} \text{ s}$ [62, 64], photons from saxion decays distort the CMB spectrum.

Photons from saxions that decay later than $\sim 10^{13}$ s may either contribute to the diffuse X- or γ -ray background or alter the reionization history [60, 62–64].

In Figs. 4.3 and 4.4 we illustrate the bound coming from such long-lived saxions, using again the envelopes given in Ref. [64]. For the bounds from reionization, we use also the original work Ref. [184]. Bounds from the CMB blackbody spectrum are drawn blue, limits from reionization in green, and from the diffuse X- and γ -ray background in orange. Values of f_{PQ} and x are as above. Note that there are no bounds from reionization in Fig. 4.4(a), since the photons coming from saxions with the right lifetime are too energetic to be efficiently absorbed by the intergalactic medium and therefore the Universe appears transparent for them. They show up as

diffuse X- or γ -rays today [63].

Saxions with an even longer lifetime contribute to today's dark matter density. This poses no relevant constraint on the saxion parameters, because such saxions need to be very light and, therefore, their contribution to the CDM density is very small.

In this chapter, we have presented the second important saxion production mechanism, saxions from oscillations and presented some cosmological limits. In summary, these limits severely restrict saxions with $\tau_\sigma \gtrsim 1$ s and they are likely to be incompatible with high T_R scenarios. Thus, in the following chapters we focus on the phenomenologically and cosmologically interesting parameter region with $m_\sigma \gtrsim 0.1$ GeV, high T_R , and $x > 0$. The main observable is then the amount of extra radiation.

Chapter 5

Extra Radiation

In this chapter we present the cosmological observable that is of most importance for the considered hadronic axion models, the amount of extra radiation ΔN_{eff} in the early Universe. First, in Sect. 5.1, we give the definition of ΔN_{eff} and the relation to saxion parameters in the case that all extra radiation is provided by axions from the decay of thermal saxions.

Then, in Sect. 5.2, we explain how the presence of additional radiation influences the spectrum of the CMB. We present hints given in the literature for extra radiation obtained from measurements of the CMB and LSS. Taking these hints seriously, we provide saxion parameters that can explain these hints and also show limits on the saxion parameter space from precision cosmology.

Section 5.3 focuses on BBN, which is also influenced by the presence of extra radiation. After a short overview over the mechanism of BBN, we present the observational situation in some detail. We show our calculation done with the public computer code `ParthENoPE` and provide a likelihood analysis that results in hints for additional radiation also at this early stage of the Universe. An explanation in the hadronic axion model is given together with limits on the saxion parameter space.

In the last Sect. 5.4, we provide the relic axion densities possibly present today in the form of the three axion populations: axions from thermal processes, non-thermal axions from saxion decay, and axions from the misalignment mechanism.

5.1 Parameterizing Additional Radiation

The total amount of radiation in the Universe at the onset of BBN can be parametrized by

$$\rho_{\text{rad}}^{\text{tot}} = \left[1 + \frac{7}{8} N_{\text{eff}} \left(\frac{T_\nu}{T} \right)^4 \right] \rho_\gamma, \quad (5.1)$$

where ρ_γ is the energy density of photons with temperature T , the temperature of neutrinos is given by T_ν and the effective number of light thermally excited neutrinos is given by N_{eff} . With the particle content of the SM and in a standard cosmology one expects this parameter to be equal to three for instantaneous decoupling, corresponding to the three neutrino species. It is, however, possible that there are other new light degrees of freedom that contribute to the radiation energy density. In fact, one uses (5.1) to parametrize this new contribution in the form of additional neutrino species expressed by ΔN_{eff} . Thus, at $T \gtrsim 1$ MeV (before neutrino decoupling and e^+e^- annihilation), $N_{\text{eff}} = 3 + \Delta N_{\text{eff}}$ and $T_\nu = T$. Note that these relations change to $T_\nu = (4/11)^{1/3}T$ after neutrino decoupling and to $N_{\text{eff}} = 3.046 + \Delta N_{\text{eff}}$ [185] because of residual neutrino heating by e^+e^- annihilation.

In particular, we are interested in the case that the extra radiation is provided by axions coming from decaying thermal saxions. We call the temperature at $t = \tau_\sigma$ the saxion decay temperature T_σ . At a photon temperature $T < T_\sigma$, the energy density of these relativistic non-thermally produced (NTP) axions from saxion decays $\rho_a^{\text{NTP}}(T)$ yields

$$\Delta N_{\text{eff}}(T) = \frac{120}{7\pi^2 T_\nu^4} \rho_a^{\text{NTP}}(T) = \frac{8}{7} \left(\frac{11}{4} \right)^{4/3} \frac{\rho_a^{\text{NTP}}}{\rho_\gamma}. \quad (5.2)$$

Working in the sudden-decay approximation, all thermally produced saxions are considered to decay instantaneously at $t = \tau_\sigma$. A treatment that goes beyond sudden-decay is postponed to Chaps. 6 and 7. The following considerations serve as a guideline towards the more detailed numerical calculations shown there. If the saxions are non-relativistic when decaying dominantly into two axions, the initial axion momentum is $p_a(T_\sigma) = m_\sigma/2$ and

$$\rho_a^{\text{NTP}}(T) = \frac{m_\sigma}{2} \left[\frac{g_{*S}(T)}{g_{*S}(T_\sigma)} \right]^{1/3} \frac{T}{T_\sigma} Y_a^{\text{NTP}}(T) = \left[\frac{g_{*S}(T)}{g_{*S}(T_\sigma)} \right]^{4/3} \left(\frac{T}{T_\sigma} \right)^4 \rho_\sigma^{\text{eq/TP}}(T_\sigma), \quad (5.3)$$

with $\rho_\sigma^{\text{eq/TP}}(T_\sigma) = m_\sigma Y_\sigma^{\text{eq/TP}}(T_\sigma)$ and $Y_a^{\text{NTP}} = 2Y_\sigma^{\text{eq/TP}}$.

As argued at the end of Chap. 2, for $x \gtrsim 0.2$, the saxion decays dominantly into axions. In particular, the decay into photons and gluinos is subdominant. Thus, we can approximate $\tau_\sigma \simeq 1/(\Gamma_{\sigma \rightarrow aa} + \Gamma_{\sigma \rightarrow gg})$ given by (2.66) and (2.67). With the time-temperature relation in the radiation dominated epoch given by (3.46), we obtain

$$T_\sigma \simeq 10.6 \text{ MeV} \left(x^2 + \frac{2\alpha_s^2}{\pi^2} \right)^{1/2} \left(\frac{m_\sigma}{1 \text{ GeV}} \right)^{3/2} \left(\frac{10^{10} \text{ GeV}}{f_{\text{PQ}}} \right) \left[\frac{10.75}{g_*(T_\sigma)} \right]^{1/4}. \quad (5.4)$$

In the following analysis in this chapter we use $x \simeq 1$ and, therefore, we also neglect

the $2\alpha_s^2/\pi^2$ term in the decay temperature. Then we arrive at

$$\begin{aligned} \Delta N_{\text{eff}}(T) &\simeq \frac{0.95}{x} \left(\frac{100 \text{ GeV}}{m_\sigma} \right)^{1/2} \left(\frac{f_{\text{PQ}}}{10^{11} \text{ GeV}} \right) \left(\frac{Y_\sigma^{\text{eq/TP}}}{10^{-3}} \right) \\ &\times \left(\frac{T}{T_\nu} \right)^4 \left[\frac{g_{*S}(T)}{10.75} \right]^{4/3} \frac{g_*(\tau_\sigma)^{1/4}}{g_{*S}(\tau_\sigma)^{1/3}}. \end{aligned} \quad (5.5)$$

Focusing on saxions from thermal processes, the maximum ΔN_{eff} emerges for scenarios with T_R above the decoupling temperature (3.53) so that the thermal relic yield (3.50) applies and,

$$\begin{aligned} \Delta N_{\text{eff}}(T) &\simeq \frac{1.14}{x} \left(\frac{100 \text{ GeV}}{m_\sigma} \right)^{1/2} \left(\frac{f_{\text{PQ}}}{10^{11} \text{ GeV}} \right) \\ &\times \left(\frac{T}{T_\nu} \right)^4 \left[\frac{g_{*S}(T)}{10.75} \right]^{4/3} \frac{g_*(\tau_\sigma)^{1/4}}{g_{*S}(\tau_\sigma)^{1/3}}. \end{aligned} \quad (5.6)$$

For $T_R < T_D^\sigma$ on the other hand, the yield (3.49) leads to:

$$\begin{aligned} \Delta N_{\text{eff}}(T) &\simeq \frac{1.26 g_s^6 \ln \left(\frac{1.01}{g_s} \right)}{x} \left(\frac{100 \text{ GeV}}{m_\sigma} \right)^{1/2} \left(\frac{10^{11} \text{ GeV}}{f_{\text{PQ}}} \right) \\ &\times \left(\frac{T_R}{10^8 \text{ GeV}} \right) \left(\frac{T}{T_\nu} \right)^4 \left[\frac{g_{*S}(T)}{10.75} \right]^{4/3} \frac{g_*(\tau_\sigma)^{1/4}}{g_{*S}(\tau_\sigma)^{1/3}}. \end{aligned} \quad (5.7)$$

Note that (5.3) only applies if the saxions are non-relativistic when they decay. This is the case if their average momentum at T_σ satisfies

$$\langle p(T_\sigma) \rangle = \langle p(T_D^\sigma) \rangle \left[\frac{g_{*S}(T_\sigma)}{g_{*S}(T_D^\sigma)} \right]^{1/3} \frac{T_\sigma}{T_D^\sigma} \ll m_\sigma. \quad (5.8)$$

Provided that $m_\sigma \ll T_D^\sigma$, those saxions decouple as a relativistic species at a very high temperature (3.53) with a thermal spectrum, $\langle p(T_D^\sigma) \rangle = 2.701 T_D^\sigma$ and $g_{*S}(T_D^\sigma) \simeq 232.5$. We can express (5.8) in terms of the following m_σ -dependent lower limit on the PQ scale

$$\frac{f_{\text{PQ}}}{x} \gg 8.4 \times 10^7 \text{ GeV} \left(\frac{m_\sigma}{1 \text{ GeV}} \right)^{1/2} \frac{g_{*S}(T_\sigma)^{1/3}}{g_*(T_\sigma)^{1/4}}. \quad (5.9)$$

Almost the same limit applies to thermally produced saxions as well since their production is efficient only at high temperatures not far below T_R and leads basically to a thermal spectrum, i.e., (5.8) applies after substituting T_D^σ by T_R and $g_{*S}(T_D^\sigma)$ by $g_{*S}(T_R) \simeq 228.75$. The question of the spectrum of thermally produced saxions is addressed in Appendix E.

Note that the saxions decay while being decoupled from the primordial plasma if $T_\sigma \ll T_D^\sigma$ or equivalently

$$\frac{f_{\text{PQ}}}{x^{1/3}} \gg 7.1 \times 10^7 \text{ GeV} \left(\frac{m_\sigma}{100 \text{ GeV}} \right)^{1/2} \left[\frac{232.5}{g_*(T_\sigma)} \right]^{1/12}. \quad (5.10)$$

If this condition is satisfied, the axions emitted in those decays will not be thermalized, but free-streaming. Thus, the temperature T_{nr} at which the non-thermally produced axions become non-relativistic, defined via $p_a(T_{\text{nr}}) = m_a$, reads

$$T_{\text{nr}} = 0.15 x \text{ eV} \left(\frac{m_\sigma}{10 \text{ TeV}} \right)^{1/2} \left(\frac{10^9 \text{ GeV}}{f_{\text{PQ}}} \right)^2 \left[\frac{3.91}{g_{*S}(T_{\text{nr}})} \right]^{1/3} \frac{g_{*S}(T_\sigma)^{1/3}}{g_*(T_\sigma)^{1/4}}. \quad (5.11)$$

This shows that the emitted axions are expected to be still relativistic at the last scattering surface and even well thereafter for $m_\sigma \lesssim 10 \text{ TeV}$ and $x = \mathcal{O}(1)$. Thereby they can contribute to ΔN_{eff} even at late times where studies of the CMB and LSS allow us to probe the amount of radiation.

Let us now investigate possible observational hints towards the existence of extra radiation.

5.2 Hints from CMB and LSS

Perhaps the biggest source of data for cosmologists are the anisotropies in the CMB [186, 187]. The spectrum of the microwave radiation is well described by a blackbody function with a temperature of $T = 2.7255 \pm 0.0006$ [12]. Apart from this overall smoothness, the CMB contains anisotropies at the level of 10^{-5} [23, 188]. They are commonly expressed by an expansion in spherical harmonics Y_{lm} as

$$T(\theta, \phi) = \sum_{lm} a_{lm} Y_{lm}(\theta, \phi), \quad (5.12)$$

where θ and ϕ are the two angular coordinates on the CMB sky. Since there is no preferred axis, the anisotropies are independent of m . Therefore, one performs a sum over m and uses $l(l+1)C_l$, where $C_l = \langle |a_{lm}|^2 \rangle$, to express the anisotropies. We present here a short overview over the physics behind these anisotropies following closely [12] and refer the reader to the literature for more details, see for example [12] and references therein. We divide the l -range into three parts.

The first part is defined by $l \lesssim 100$. The horizon scale at last scattering corresponds roughly to $l \simeq 100$. This means that anisotropies larger than this horizon, which correspond to smaller l , have not evolved much until now. Therefore, their shape reflects directly the perturbations in the gravitational potential. Photons falling into gravitational wells gain energy, they lose energy when they climb out of a

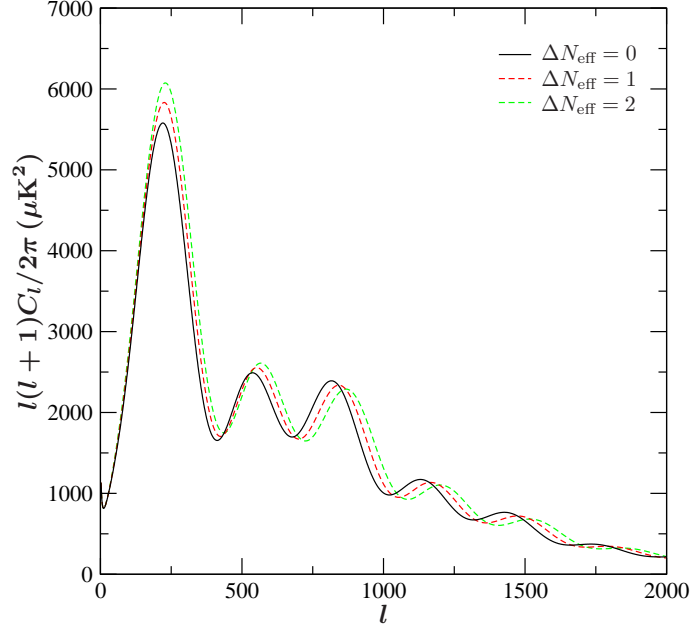


Figure 5.1: *Illustration of the CMB anisotropy power spectrum of a Λ CDM model for $\Delta N_{\text{eff}} = 0, 1$, and 2 in black, red, and green, respectively. All other cosmological parameters are set to their standard value. Spectrum obtained with CAMB [191].*

well. This is called the Sachs–Wolfe (SW) effect [189]. For $l \lesssim 10$, photons traveling through a gravitational well (hill) gain (lose) some amount of net energy, because the dominance of the late Universe by dark energy causes a smoothing of gravitational anisotropies. This is usually referred to as the (late) integrated Sachs–Wolfe (ISW) effect. Since extra radiation has practically no effect in the low multipole region, we do not go into further detail here.

The second part contains the prominent acoustic peaks for $100 \lesssim l \lesssim 1000$. The underlying physics is as follows. Before the Universe becomes neutral, its components form a tightly coupled photon-baryon fluid. Perturbations in the gravitational potential drive oscillations in this fluid, with photon pressure as the main restoring force and baryons giving some inertia. These oscillations produce time-variations in the temperature. At the time of recombination, the photons decouple from the baryons and propagate freely towards us. The first peak corresponds to oscillations that underwent one quarter of a period, reaching maximal compression. The following peaks correspond to oscillations that started earlier and performed more oscillations. Each gravitational perturbation seeds oscillations as soon as it enters the horizon.

The last part is the damping tail at $l \gtrsim 1000$. Here the amplitude of the peaks resulting from the oscillations described above are damped because recombination does not happen instantaneously. This process is called Silk damping [190].

In Fig. 5.1 we show the result of a calculation done with the computer code **CAMB** [191]. This code computes the CMB power spectrum depended on various input parameters, among them is ΔN_{eff} . We set $\Delta N_{\text{eff}} = 0, 1$, and 2 and arrive at the black, red, and green curve, respectively. All other parameters are set to their best fit values given, e.g., in Ref. [12]. One can clearly see the acoustic peaks and the damping tail. Note, however, that these spectra are for illustration purposes only, since **CAMB** is optimized only for $\Delta N_{\text{eff}} = \mathcal{O}(0.1)$. Exact quantitative results for larger ΔN_{eff} are later taken from elsewhere.

The effects from increasing the amount of radiation is two-fold. First, its energy density delays the matter-radiation equality. Second, its anisotropic stress contributes to the total energy density. We describe only the results of the first effect here, since the latter involves the inclusion of LSS data.

Like the late ISW effect, the early ISW effect describes the change in photon energy due to gravitational redshift when a photon travels through a time-evolving gravitational perturbation. The early ISW effect is relevant after matter-radiation equality, because at earlier times the gravitational perturbations are caused by the photons themselves. The end of the early ISW is at last scattering, since afterwards the photons can stream freely, except for late-time effects that are not important here. After matter-radiation equality, residual radiation causes the gravitational potentials to decay and, therefore, the first acoustic peak is less pronounced. A later matter-radiation equality causes the potential to be less affected by the early ISW effect. This influences the height of the first peak relative to the third one [192]. It should be noted that the amount of radiation inferred in this way is degenerate with the amount of matter. One needs to include other cosmological observables to break this degeneracy. At larger l , more radiation also leads to a change in the angular position of the peaks [193].

The degeneracy of parameters describing the radiation and matter content mentioned above is, in fact, not the only one. To arrive at unambiguous results, one has to combine the CMB analysis with LSS measurements. This has been done in the literature and indeed hints towards the existence of extra radiation have been found in various studies [23, 67–70]. For example, the Wilkinson Microwave Anisotropy Probe (WMAP) collaboration finds a 68% credible interval of $N_{\text{eff}} = 4.34^{+0.86}_{-0.88}$ [23] when combining their 7-year data with measurements of the baryonic acoustic oscillation (BAO) scale and today's Hubble constant H_0 .¹ Another precision cosmology study arrives at a 95% credible interval of $N_{\text{eff}} = 4.78^{+1.86}_{-1.75}$ [69] when combining CMB data with data from the Sloan Digital Sky Survey data-release 7 halo power spectrum (HPS) and the Hubble Space Telescope (HST). Based on this combined CMB + HPS + HST data set, we use the mean $\Delta N_{\text{eff}} = 1.73$ and the 95% confidence level (CL) upper limit $\Delta N_{\text{eff}} = 3.59$ to explore implications for the considered SUSY

¹Note that there is a very recent result of WMAP, including the 9-year data [71]. The first version found a 68% credible interval of $N_{\text{eff}} = 3.26 \pm 0.35$ and after correcting an error due to baryonic acoustic oscillations, the value changed to $N_{\text{eff}} = 3.84 \pm 0.40$.

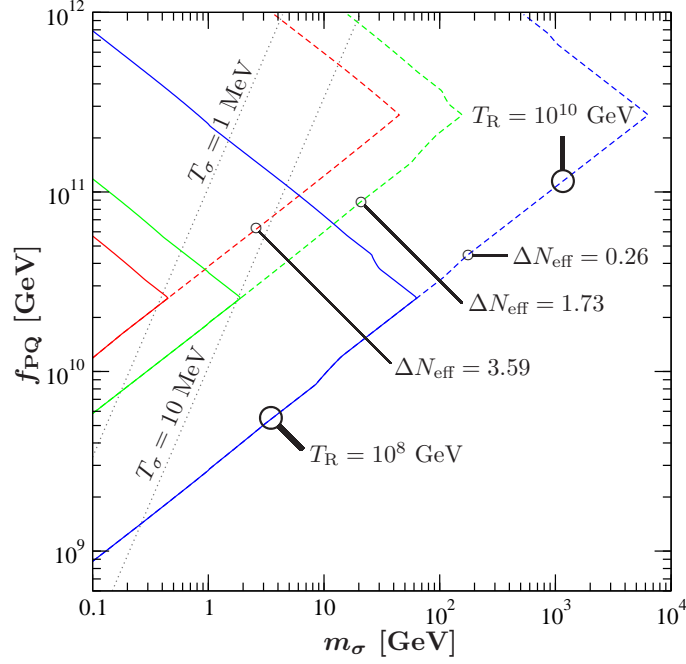


Figure 5.2: Contours of ΔN_{eff} at $T \ll 1$ MeV provided by non-thermally produced axions from decays of thermal saxions for $x = 1$ and $T_R = 10^8$ GeV (solid) and 10^{10} GeV (dashed). The red curve shows the 2σ limit $\Delta N_{\text{eff}} = 3.59$ and the green curve the mean $\Delta N_{\text{eff}} = 1.73$ based on the CMB + HPS + HST result [69] quoted in the main text. The blue curve indicates $\Delta N_{\text{eff}} = 0.26$, which is the expected 68% CL sensitivity of the Planck satellite mission [194, 195]. The dotted lines show $T_\sigma = 1$ and 10 MeV.

axion models.

Evaluating $\Delta N_{\text{eff}}(T)$ from (5.6) and (5.7) for $x = 1$ and at $T \ll 1$ MeV,² we obtain the ΔN_{eff} contours for $T_R = 10^8$ (10^{10}) GeV as shown by the solid (dashed) lines in Fig. 5.2.

The red lines indicate the upper limit $\Delta N_{\text{eff}} = 3.59$ with the m_σ - f_{PQ} parameter regions to their left disfavored at the 2σ level by the CMB + HPS + HST data set. The green lines show the corresponding mean $\Delta N_{\text{eff}} = 1.73$ and the blue lines $\Delta N_{\text{eff}} = 0.26$. The latter is the expected 68% CL accuracy of the Planck satellite mission [194, 195]. To guide the eye, we show the $T_\sigma = 1$ and 10 MeV contours as dotted lines. As explained in Chap. 4, additional restrictive constraints are expected in the region with $T_\sigma \leq 1$ MeV.

The saxions considered here are all of thermal origin. Saxion from the misalignment

²Note that our theoretical results for $\Delta N_{\text{eff}}(T)$ at $T \sim 1$ MeV and at $T \ll 1$ MeV agree. The T dependence in (5.6) and (5.7) results from the factor $(T/T_\nu)^4 [g_{*S}(T)/10.75]^{4/3}$. This factor equals one for $T \sim 1$ MeV, where $T_\nu = T$ and $g_{*S}(T) = 10.75$, and for $T \ll 1$ MeV, where $T_\nu = (4/11)^{1/3}T$ and $g_{*S}(T) = 3.91$.

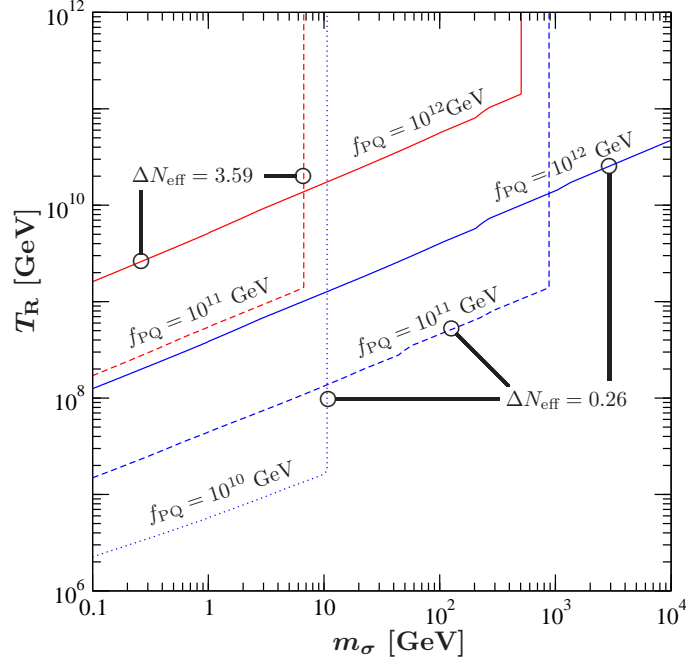


Figure 5.3: Contours of ΔN_{eff} at $T \ll 1$ MeV provided by non-thermally produced axions from decays of thermal saxions for $x = 1$ and $f_{\text{PQ}} = 10^{12}$ GeV (solid), 10^{11} GeV (dashed), and 10^{10} GeV (dotted). The red lines show the 2σ CMB + HPS + HST constraint $\Delta N_{\text{eff}} < 3.59$, which imposes upper limits on the reheating temperature T_{R} . For $f_{\text{PQ}} = 10^{10}$ GeV, this T_{R} limit appears at smaller m_{σ} outside of the considered range. The blue contours indicate the expected Planck sensitivity of $\Delta N_{\text{eff}} = 0.26$.

mechanism can contribute to ΔN_{eff} too. Then the amount of extra radiation depends on the initial misalignment of the saxion field. However, for the considered values of m_{σ} and f_{PQ} , the contribution of this non-thermal source is negligible if $\sigma_i = \langle \phi_1 \rangle = f_{\text{PQ}}/2$, as can be seen in Fig. 4.2.

The limits shown in Fig. 5.2 in the m_{σ} - f_{PQ} plane for fixed T_{R} values can be translated into upper limits on the reheating temperature T_{R} . In Fig. 5.3 the red lines show the upper limits on T_{R} imposed by the 2σ CMB + HPS + HST constraint $\Delta N_{\text{eff}} < 3.59$ as a function of m_{σ} for $x = 1$ and $f_{\text{PQ}} = 10^{12}$ GeV (solid) and 10^{11} GeV (dashed).

The expected Planck sensitivity $\Delta N_{\text{eff}} = 0.26$ [194,195] is indicated by the blue solid, dashed, and dotted lines for $f_{\text{PQ}} = 10^{12}$, 10^{11} , and 10^{10} GeV, respectively. Note that the upper limit does not show up for the latter f_{PQ} value in the considered m_{σ} range. The T_{R} dependence of the contours is described by (5.7) and disappears for cosmological scenarios with $T_{\text{R}} \gtrsim T_{\text{D}}^{\sigma}$ where (5.6) applies. Here we should stress that the shown upper limits on T_{R} rely on non-thermally produced axions from decays of thermal saxions providing the only significant contribution to ΔN_{eff} at $T \ll 1$ MeV. In scenarios with additional sizable contributions (e.g., from late gravitino NLSP decays into an axino LSP and the axion), the considered extra radiation constraint

will impose more restrictive T_R limits as will be shown in Chap. 7.

Note that in the presented parameter regions, additional constraints from other particles are possible depending on the mass spectrum and other parameters of the SUSY model possibly realized in nature. Especially the masses of the axino and gravitino are important, since their thermal production can be very efficient in high T_R scenarios as the one explored in Fig. 5.3. The influence of these particles will be explored in detail in the next two chapters.

Let us compare our results shown in Fig. 5.3 with existing results. For example, the yellow curve in Fig. 5(a) of Ref. [64] presents an upper T_R limit imposed by $\Delta N_{\text{eff}} \leq 1$ that disfavors basically $T_R > 10^6$ GeV for $f_{\text{PQ}} = 10^{10}$ GeV and the whole m_σ range considered above. With the assumed initial saxion field displacement of $\sigma_i \sim v_{\text{PQ}}$, that existing limit is governed also by thermal saxions that decay into axions. However, we find that it is overly restrictive due to the omission of the factor $[g_{*S}(T_\sigma)/g_{*S}(T)]^{4/3}$ in Eq. (24) of Ref. [64].³ Thereby, our ΔN_{eff} expression (5.5) shows different dependences on $g_{*S}(T)$ and $g_{*S}(T_\sigma)$. Remaining differences are due to the result from our explicit calculation of the thermal saxion production rate and the different definitions of the PQ scale addressed already in footnote 5 in Sect. 2.5 and footnote 4 in Sect. 3.4 above. One can see Fig. 5.3 as the completion of Figs. 4.3(b) and 4.4(b) to include also the limits from CMB + LSS on ΔN_{eff} . As a result, we find that a large part of the $(m_\sigma, f_{\text{PQ}}, T_R)$ region previously thought to be excluded is actually not restricted by the amount of additional radiation from late decays of thermal saxions.

5.3 Hints from BBN

The axions from decaying thermal saxions are present at times well before the Universe cooled down to $T = 1$ MeV for a large region of the parameter space, as can be seen from Fig. 5.2 above. So these axions provide extra radiation also for another important and well understood process in the early Universe, the formation of the light elements. Let us review the basic concept of BBN here, for details, see for example Refs. [12, 197–200].

5.3.1 Primordial Nucleosynthesis

The abundance of light elements is determined by the interplay between the expansion rate of the Universe, the weak rates controlling the neutron-proton interconversion, and the nuclear reaction network producing the light elements. At $T \gg 1$ MeV,

³A similar comment can be found in Ref. [196] that refers to the same finding. We thank J. Hasenkamp for clarification.

the weak reactions

$$n + e^+ \leftrightarrow p + \bar{\nu}_e, \quad (5.13a)$$

$$n + \nu_e \leftrightarrow p + e^-, \quad (5.13b)$$

$$n \leftrightarrow p + e^- + \bar{\nu}_e, \quad (5.13c)$$

hold protons and neutrons in equilibrium. At about $T \sim 0.7$ MeV, corresponding to $t \simeq 1$ s, these reactions freeze out and the ratio of the number densities of neutrons and protons reaches approximately

$$\frac{n_n}{n_p} \simeq e^{-Q/T} \sim \frac{1}{6}, \quad (5.14)$$

where $Q = 1.293$ MeV [12] is the mass difference between protons and neutrons. After decoupling, the free neutrons start to decay via (5.13c) with the lifetime $\tau_n = 880.1 \pm 1.1$ s [12].⁴ These decays continue until the free neutrons are bound in stable nuclei. The only such stable nucleus available is D, because the formation of all heavier ones involve D as an initial or intermediate state. Deuterium, however, has a binding energy of $E_B = 2.2$ MeV, so it can easily be dissociated by energetic photons. In fact, the high number of photons per baryon ($\eta \equiv n_b/n_\gamma \simeq 6.2 \times 10^{-10}$ [12]) prevents the formation of sizable amounts of D until $T \lesssim 0.1$ MeV. At this time, the number of photons in the high energy tail of their phase space distribution with $E \gtrsim E_B$ drops below the number of baryons. With the existence of sufficiently sizable amounts of D in the plasma, other nuclei such as ^3H and He and Li isotopes can form. This critical period is, therefore, called the deuterium bottleneck.

Theoretical predictions for the abundances of these nuclei in Fig. 5.4. This figure is taken from Ref. [201]. It shows abundances of protons and neutrons as the black solid and dotted lines, respectively, as a function of time t on the top horizontal axis and temperature T on the bottom axis. The abundance of various other nuclei are shown normalized to the H abundance, as labeled. The main stages of BBN described above are indicated in the figure; from left to right: ν -decoupling, freeze-out of proton-neutron interconversion together with e^+e^- annihilation, the deuterium bottleneck, and freeze-out of all other nuclear reactions. The final ^4He abundance is usually expressed by the primordial helium mass fraction

$$Y_p \equiv \frac{4n_{^4\text{He}}}{n_p + n_n} \simeq \frac{2(n_n/n_p)}{1 + (n_n/n_p)}, \quad (5.15)$$

where we assumed that all neutrons end up in ^4He . Then, an estimate based on the arguments given above yields $Y_p \sim 0.25$.

After the nuclear reactions come to a stop for $t \gtrsim 10^3$ s, basically all neutrons that have not decayed end up in ^4He . On the other hand, the amount of free

⁴We comment on the influence of the exact value of τ_n in the last section of this chapter.

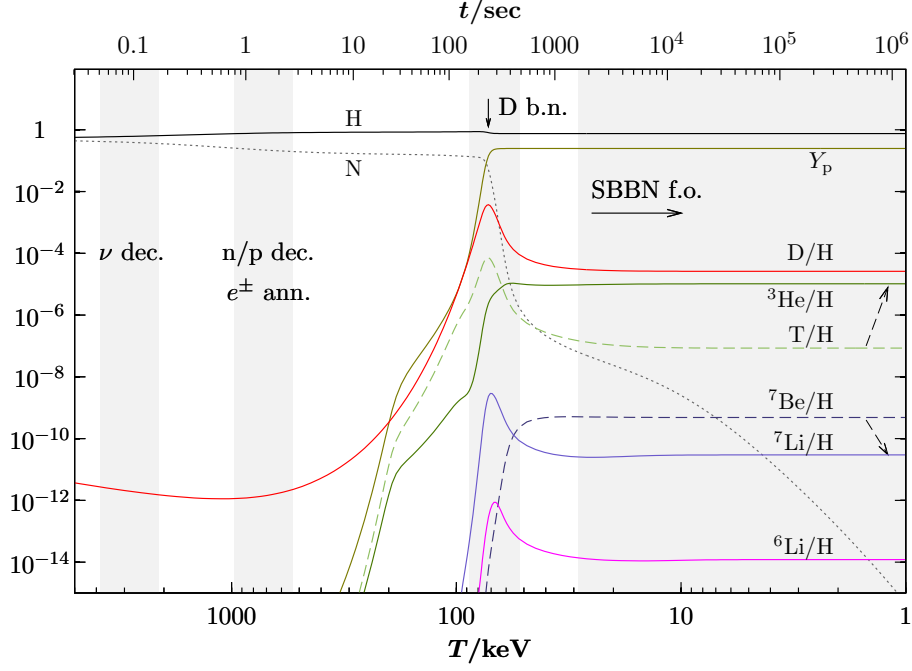


Figure 5.4: *Abundance of light nuclei during BBN as a function of time t on the top horizontal axis and the associated temperature at the bottom axis. The abundance of H (or p) and n are depicted as the black solid and dotted line, respectively. All other nuclei are shown with their abundance normalized to the one of H by the color lines as labeled. Plot taken from [201].*

neutrons that decay depends for a given τ_n on the time between the freeze-out of the weak interactions (5.13) and the deuterium bottleneck. Note that these two points are defined via a certain critical temperature, not a certain time. So the neutron abundance depends via (3.46) on the expansion rate of the Universe during that interval. Therefore, by comparing the resulting Y_p with observations, we can infer informations about g_* during that epoch. In particular, we link Y_p to ΔN_{eff} in the next sections.

5.3.2 Observations

The amount of primordial ^4He is inferred from measuring the helium to hydrogen emission line ratio in clouds of ionized hydrogen, called HII regions. These regions have a very low amount of nuclei heavier than He, called metal in astrophysics. This is important, since ^4He is produced in nuclear fusion in stars and, therefore, not all measured ^4He is of primordial origin. Stars produce other heavier nuclei also. Thus, one expects some correlation between the amount of ^4He and the metallicity of a source. The extrapolation to zero metallicity then allows one to deduce Y_p .

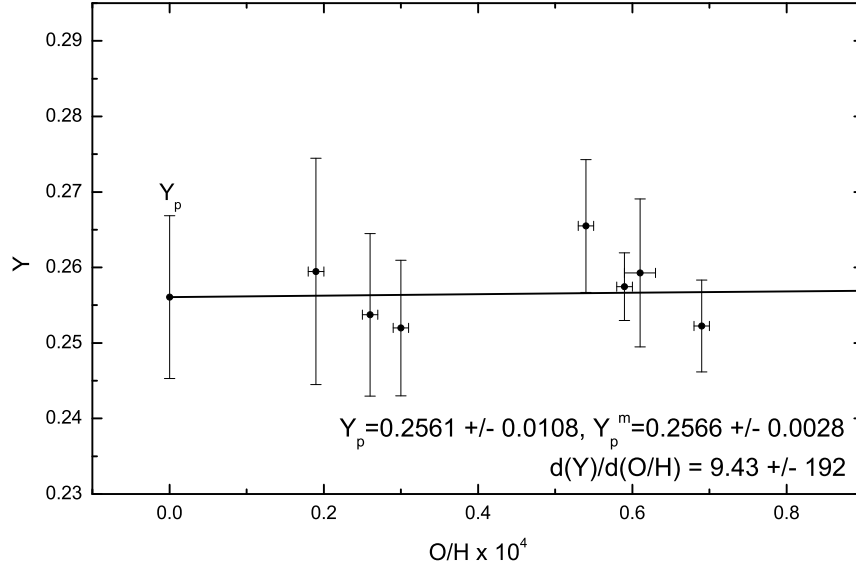


Figure 5.5: Mass fraction of ${}^4\text{He}$ plotted versus the ratio of oxygen over hydrogen O/H of the seven targets of Ref. [202] with 1σ error bars. The resulting primordial Y_p and the slope $d(Y)/d(\text{O}/\text{H})$ of a linear regression to zero metallicity are given. Y_p^m is the mean of the data points without regression. Plot taken from [72].

Unfortunately, measurements of the ${}^4\text{He}$ abundance suffer from large systematic uncertainties, summarized, e.g., in Ref. [72]. Let us mention them briefly here. The observed sources are extragalactic, so photons scatter on dust between the source and the observer. The amount of scattering depends on the wavelength, thus it affects the line spectrum. Moreover, stellar spectra are hard to disentangle from the emission spectrum of the HII region, and the region itself influences the emission lines by absorbing some of the photons. The emission lines are both due to recombination and collisional excitation, but only the former is relevant for the determination of Y_p .

In Fig. 5.5, we show an example for the deduced Y_p from sources mentioned in Ref. [202] computed by Aver *et al.* [72]. The data points indicate the measured amount of ${}^4\text{He}$ dependent on the respective metallicity. The metallicity is expressed by the ratio of oxygen over hydrogen, O/H . As given in the figure, the average of these data points is $Y_p^m = 0.2566 \pm 0.0028$, with a 68% credible interval. Regression to zero O/H yields

$$Y_p^{\text{Av}} = 0.2561 \pm 0.0108. \quad (5.16)$$

On the one hand, this shows that the picture of primordial nucleosynthesis presented above is quite accurate, since this value is different from zero and within the expectation of standard BBN. As we see in the next section, however, this value of

Y_p implies a hint towards the existence of extra radiation.

On the other hand, as given in the figure, the slope $d(Y)/d(O/H)$ of the extrapolation to zero O/H is positive as expected, but compatible with zero. Given this and the large systematic uncertainties, care has to be taken when interpreting this result. Let us take this result at face value and investigate consequences for the considered hadronic axion model in the following.⁵

For comparison, we quote another study here. Izotov and Thuan [73] find

$$Y_p^{\text{IT}} = 0.2565 \pm 0.001(\text{stat.}) \pm 0.005(\text{syst.}), \quad (5.17)$$

with statistical and systematical errors referring also to the 68% interval.

Note that theoretical calculations of Y_p depend mainly on ΔN_{eff} , but also on the baryon density $\omega_b \equiv \Omega_b h^2$. In principle, the baryon density can be measured very accurately in the CMB [23], but given the large time difference between BBN and CMB formation, there could be a difference between ω_b at BBN and during CMB formation. To get an independent measurement of ω_b , one includes measurements of primordial D, since its amount depends strongly on ω_b , but not as much on ΔN_{eff} as Y_p .

Measurements of primordial D are eased by the fact that there are no known astrophysical sources of D [205]. Thus, each measured amount of D provides a lower limit on the primordial value. Nevertheless, systematics are still an issue, see, e.g., Ref. [206]. To get reliable measurements, one looks for high-redshift, hydrogen rich clouds absorbing light of quasars. The analysis of six high-quality DI absorption lines in QSO Q0913+072 done by Petini *et al.* [206] yields for the primordial ratio

$$\log[D/H]_p = -4.56 \pm 0.04. \quad (5.18)$$

We adopt this value for our analysis.

5.3.3 Computation with PArthENoPE and Likelihood Analysis

We perform theoretical calculations of the primordial abundance of the light elements with the publicly available code PArthENoPE [207]. We use $0 \leq \Delta N_{\text{eff}} \leq 4$ and $0.01 \leq \omega_b \leq 0.03$, both with a flat prior. All input parameters are summarized in Table 5.1. The resulting prediction for Y_p is shown in Fig. 5.6(a), the result for $[D/H]_p$ in Fig. 5.6(b), both as a function of ω_b and ΔN_{eff} . From these plots, one can see that Y_p depends strongly on ΔN_{eff} , whereas the dependence on ω_b is weaker, as already indicated above. For $[D/H]_p$, it is the other way round.

⁵There are two subsequent papers by the same group, Refs. [203, 204], which arrive at slightly different values for Y_p . In Ref. [203] a Markov Chain Monte Carlo method is introduced, which is applied to a larger dataset in Ref. [204]. Since none of these analyses yields a statistically significant deviation of ΔN_{eff} from zero, for the purpose of this work we stick to the values also used in Ref. [2].

Table 5.1: *Parameters used in the PARthENoPE computation. We use flat priors when we give a range, otherwise we use a fixed value.*

Parameter	Symbol	Prior range/value
Number of additional neutrinos	ΔN_{eff}	$0 \rightarrow 4$
Baryon density	ω_b	$0.01 \rightarrow 0.03$
Neutron lifetime	τ_n	880.1 s
Neutrino degeneracy parameter	ξ	0

Note that there is an additional parameter that can influence BBN, the neutrino degeneracy parameter $\xi_x = \mu_{\nu_x}/T_{\nu_x}$ for the neutrino species x , where μ_{ν_x} is the chemical potential of ν_x . A non-zero degeneracy contributes to the amount of extra radiation [208]

$$\Delta N_{\text{eff } \nu_i} = \frac{15}{7} \left[2 \left(\frac{\xi_i}{\pi} \right)^2 + \left(\frac{\xi_i}{\pi} \right)^4 \right]. \quad (5.19)$$

It should be noted that in principle in the above equation ξ_i should be replaced by the total lepton degeneracy of generation i . But the contributions of the charged leptons of the second and third generations are subdominant, since $T \ll m_{\mu, \tau}$. Also the contribution of electrons is negligible, because charge neutrality of the Universe ensures that the lepton asymmetry is close to the baryon asymmetry and, therefore, very small [208]. Thus, the degeneracy in any neutrino species (e , μ , or τ) increases the amount of extra radiation independent of the respective sign. As in the case of extra relativistic species, this speeds up the expansion of the Universe and, therefore, leads to a ${}^4\text{He}$ overproduction.

Moreover, a degeneracy of the electron neutrino has an additional effect: it changes the neutron to proton ratio at freeze-out of the weak interactions as

$$\frac{n_n}{n_p} \simeq e^{-Q/T - \xi_e}. \quad (5.20)$$

In the interesting region of a small, non-zero degeneracy of ν_e , it is (5.20) that influences BBN the most. In fact, the effect of $\xi_e > 0$ is opposite to an increase in ΔN_{eff} , so it could eradicate limits from Y_p as presented here, see, e.g., Refs. [75, 78]. However, the recent discovery of a non-zero value of the neutrino mixing angle θ_{13} was used in Ref. [209] to constrain the influence of degenerate neutrinos to

$$\Delta N_{\text{eff } \nu_e} \lesssim 0.1 \quad (5.21)$$

at the preferred value of θ_{13} and only for a normal hierarchy of neutrinos, it is even smaller for an inverted hierarchy. Note that this limit relies on a zero (or very small) initial neutrino asymmetry. It is expected that sphaleron processes equilibrate the

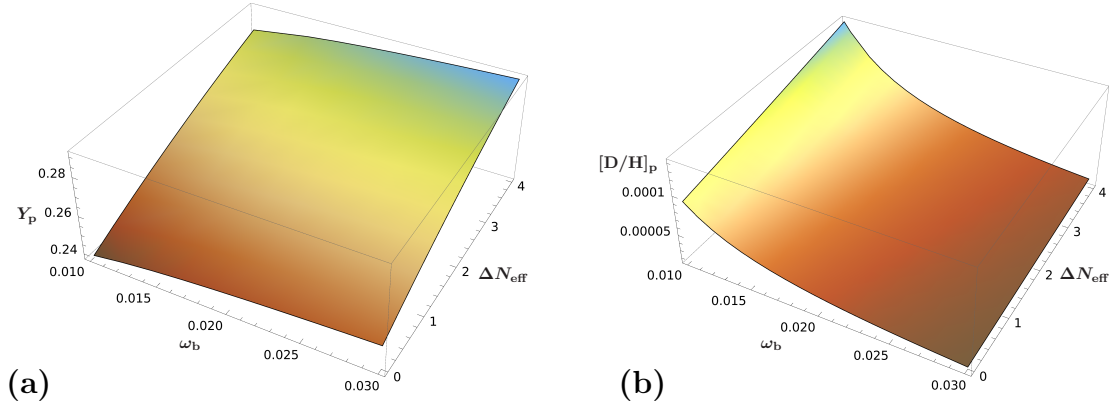


Figure 5.6: Resulting Y_p in (a) and $[D/H]_p$ in (b) of a simulation with PArthENoPE using the input parameters given in Table 5.1.

lepton and baryon asymmetry so that all neutrino asymmetries are of order 10^{-9} or smaller [78]. Nevertheless, since sphalerons have not been observed yet, the existence of such a primordial asymmetry is not excluded. However, no simple mechanism is known that generates such an asymmetry.

As we will see later, also the hints from BBN point towards $\Delta N_{\text{eff}} = \mathcal{O}(1)$ in addition to the hints from CMB + LSS studies, so an explanation of these hints cannot rely only on degenerate neutrinos. In light of the small contribution of degenerate neutrinos, we set $\xi = 0$ in our PArthENoPE calculations.

Now let us compare these theoretical results for Y_p and $[D/H]_p$ with the observations shown in the previous section. We employ a maximum likelihood analysis, where we use the following likelihood functions

$$L_{4\text{He}} = \begin{cases} \exp \left[-\frac{1}{2} \frac{(Y_p - 0.2561)^2}{0.0108^2} \right] & \text{for [72],} \\ \exp \left[-\frac{1}{2} \frac{(Y_p - 0.2565)^2}{0.0051^2} \right] & \text{for [73],} \end{cases} \quad (5.22)$$

$$L_D = \exp \left[-\frac{1}{2} \frac{(\log[D/H]_p + 4.56)^2}{0.04^2} \right], \quad (5.23)$$

where we have assumed a Gaussian shape of the likelihood and we neglect the small theoretical errors of the calculation with PArthENoPE itself. Note the two different functions for ^4He reflecting the two measurements mentioned above. To get the maximum likelihood point, we calculate the combined likelihood function, which is the product of the respective ^4He likelihood in (5.22) and the D likelihood (5.23). This is justified, since the parameters ω_b and ΔN_{eff} can be taken as independent. The resulting combined likelihood is plotted in Fig. 5.7(a) for Y_p^{Av} and in Fig. 5.7(b) for Y_p^{IT} .

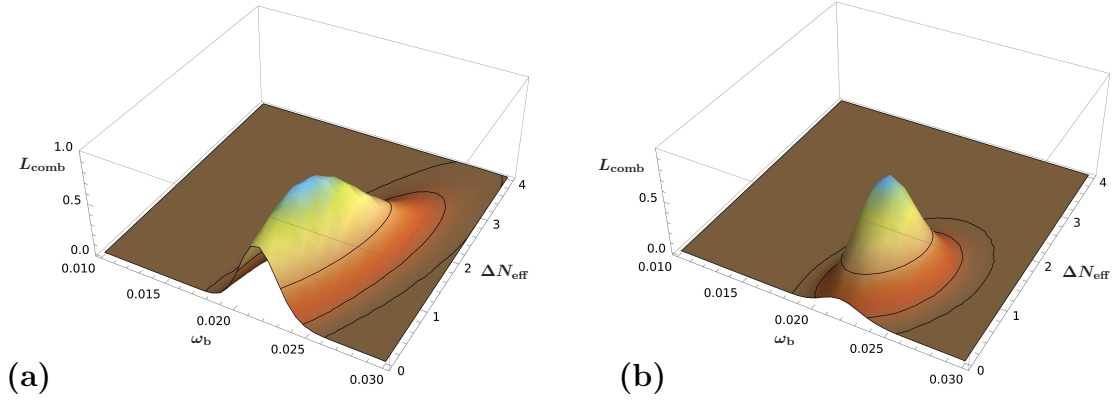


Figure 5.7: Combined likelihood L_{comb} as a function of ω_b and ΔN_{eff} given the observations of D by Petini et al. [206] and of ${}^4\text{He}$ (a) by Aver et al. [72], and (b) by Izotov and Thuan [73], respectively. The individual likelihood functions are given by (5.22) and (5.23). The horizontal lines illustrate the 68%, 95%, and 99.7% confidence interval, respectively.

Our main interest is the amount of extra radiation, so we marginalize over ω_b . Our resulting best fit value $\omega_b \simeq 0.0228$ is within the 1σ error of the WMAP analysis [23]. The posterior maximum and the minimal 99.7% credible interval imposed by BBN based on the two ${}^4\text{He}$ datasets are shown in Table 5.2. Note that both 99.7% credible interval include zero and the prior $\Delta N_{\text{eff}} \geq 0$ leads to an asymmetric interval.⁶

For comparison, in Table 5.2, we also include the mean and the 95% CL upper limit on ΔN_{eff} as obtained in the precision cosmology study of Ref. [69], mentioned in Sect. 5.2.

We see that both CMB + LSS studies and BBN analyses give hints towards the existence of extra radiation. Again, all ΔN_{eff} posterior maxima are compatible with zero, but let us take these hints at face value and investigate whether these hints can be explained in SUSY hadronic axion models.

5.3.4 Extra Radiation at BBN

Let us now apply these BBN constraints to the case of extra radiation from saxion decays into axions. We evaluate $\Delta N_{\text{eff}}(T)$ from (5.6) and (5.7) for $x = 1$ and at $T \sim 1$ MeV, i.e., at the onset of BBN and above the temperature at which neutrinos

⁶Note that the PDG-recommended value for the free neutron lifetime has changed recently from $\tau_n = 885.7 \pm 0.8$ s [210] to $\tau_n = 880.1 \pm 1.1$ s [12]. If we use $\tau_n = 885.7$ s in **ParthENoPE**, we can reproduce the posterior maxima and the minimal 95% credible intervals given in the first two lines of Table III in Ref. [74]. In comparison, those posterior maxima are about 10% below the values obtained with $\tau_n = 880.1$ s given in our Table 5.2.

Table 5.2: Constraints on ΔN_{eff} from BBN and precision cosmology. Based on the indicated data sets, the first two lines give the posterior maximum (p.m.) and the minimal 99.7% credible interval imposed by BBN using the prior $\Delta N_{\text{eff}} \geq 0$ and after marginalization over ω_b . The third line quotes the mean and the 95% CL upper limit on ΔN_{eff} as obtained in the precision cosmology study of Ref. [69] based on CMB data, the Sloan Digital Sky Survey data-release 7 halo power spectrum (HPS), and data from the Hubble Space Telescope (HST) mentioned in Sect. 5.2.

Data	p.m./mean	Upper limit
$Y_{\text{p}}^{\text{IT}} [73] + [\text{D}/\text{H}]_{\text{p}} [206]$	0.76	$< 1.97 (3\sigma)$
$Y_{\text{p}}^{\text{Av}} [72] + [\text{D}/\text{H}]_{\text{p}} [206]$	0.77	$< 3.53 (3\sigma)$
CMB + HPS + HST [69]	1.73	$< 3.59 (2\sigma)$

decouple. Figure 5.8 shows the resulting ΔN_{eff} contours in the m_{σ} – f_{PQ} parameter plane as solid (dashed) lines for $T_{\text{R}} = 10^8$ (10^{10}) GeV. The light green (dark green) curves show – as labeled – the posterior maximum $(\Delta N_{\text{eff}})_{\text{Av(IT)}}^{\text{p.m.}} = 0.77$ (0.76). These lines lie almost on top of each other. The orange (red) lines the upper limit $(\Delta N_{\text{eff}})_{\text{Av(IT)}}^{3\sigma} = 3.53$ (1.97), which disfavors the considered region to its left by more than 3σ . The dotted lines indicate $T_{\sigma} = 1$ and 10 MeV. The parameter region with $T_{\sigma} < 1$ MeV is not considered since our BBN constraints on ΔN_{eff} do not apply to later decays.⁷ Moreover, as described in Chap. 4, again additional cosmological constraints can occur for $T_{\sigma} < 1$ MeV, i.e., towards smaller m_{σ} .

For $T_{\sigma} > 1$ MeV, one sees that the BBN constraints on ΔN_{eff} can disfavor significant regions of the m_{σ} – f_{PQ} parameter plane in high T_{R} scenarios. The shown posterior maxima contours illustrate that non-thermally produced axions from decays of thermal saxions can explain the existence of extra radiation, $\Delta N_{\text{eff}} \sim 1$, in agreement with the hints from BBN studies. For $T_{\text{R}} > T_{\text{D}}^{\sigma}$, the shape of the ΔN_{eff} contours is described by (5.6) from decays of thermal relic saxions. The kink of the ΔN_{eff} contours indicate the respective f_{PQ} value at which $T_{\text{R}} = T_{\text{D}}^{\sigma}$. For larger f_{PQ} , $T_{\text{R}} < T_{\text{D}}^{\sigma}$ and (5.7) applies, which is reflected by the T_{R} dependence of ΔN_{eff} provided by axions from decays of thermally produced saxions.

5.4 Relic Axion Density

We find it instructive to compare the density parameters of three different axion populations that can be present today in the considered SUSY axion mod-

⁷The calculations of **ParthENoPE** start at $T = 10$ MeV with the given ΔN_{eff} values as input already at that temperature. The ΔN_{eff} limits derived above are thus strictly applicable for $T_{\sigma} \geq 10$ MeV only.

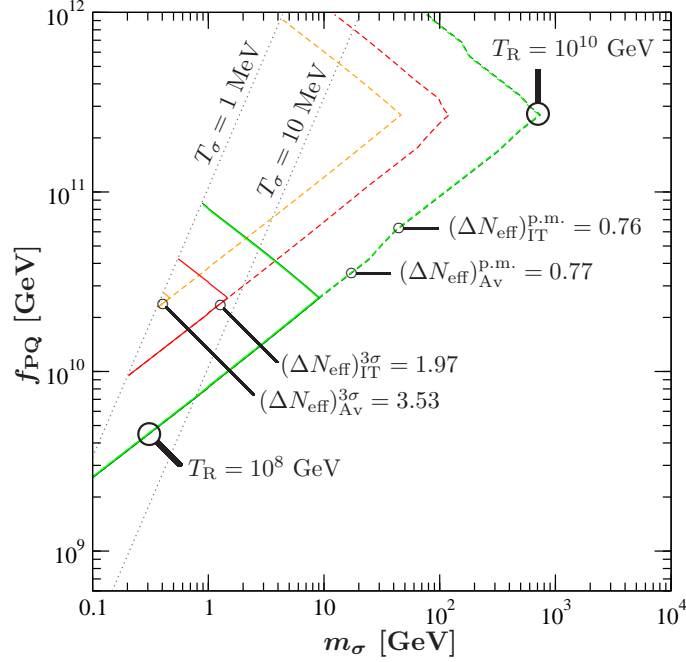


Figure 5.8: Contours of ΔN_{eff} at $T \sim 1$ MeV provided by non-thermally produced axions from decays of thermal saxions for $x = 1$, $T_\sigma > 1$ MeV, and $T_R = 10^8$ GeV (solid) and 10^{10} GeV (dashed). The BBN results given in Table 5.2 are illustrated by the light green (dark green) curves, which indicate the posterior maximum $(\Delta N_{\text{eff}})_{\text{Av(IT)}}^{\text{p.m.}} = 0.77$ (0.76) and the upper 3σ limit is depicted by the orange (red) contour, where $(\Delta N_{\text{eff}})_{\text{Av(IT)}}^{3\sigma} = 3.53$ (1.97) that disfavors the region to its left. The dotted lines show $T_\sigma = 1$ and 10 MeV.

els: (i) $\Omega_a^{\text{eq/TP}} h^2$ of thermal relic/thermally produced axions, (ii) $\Omega_a^{\text{NTP}} h^2$ of non-thermally produced axions from decays of thermal saxions, and (iii) $\Omega_a^{\text{MIS}} h^2$ of the axion condensate from the misalignment mechanism. The latter originates from coherent oscillations of the axion field after it acquires a mass due to instanton effects at $T \lesssim 1$ GeV. This is the axion population that can actually provide the cold dark matter in our Universe. For details on this misalignment mechanism, we refer to [40–42] and references therein. Here we quote the density parameter,

$$\Omega_a^{\text{MIS}} h^2 \sim 0.15 \xi f(\theta_i^2) \theta_i^2 \left(\frac{f_{\text{PQ}}}{10^{12} \text{ GeV}} \right)^{7/6}, \quad (5.24)$$

which is governed by the initial misalignment angle θ_i of the axion field. In the above equation, $\xi = \mathcal{O}(1)$ parametrizes theoretical uncertainties related, e.g., to details of the quark–hadron transition and of the T dependence of m_a . Moreover, $f(\theta_i^2)$ is the anharmonicity factor which satisfies $f(\theta_i^2) \rightarrow 1$ for small $\theta_i^2 \rightarrow 0$ and becomes sizable towards large $\theta_i^2 \rightarrow \pi^2$ [211–213]. This expression for Ω_a^{MIS} applies to non-SUSY and SUSY settings. In the considered case in which the PQ symmetry

breaks before inflation and is not restored thereafter, $T_R < f_{\text{PQ}}$, a single θ_i value enters (5.24). The axion condensate cannot be thermalized by processes such as those considered in Chap. 3 and the respective back reactions since those processes proceed at negligible rates at $T \lesssim 1$ GeV for f_{PQ} respecting (2.64).⁸ Accordingly, $\Omega_a^{\text{MIS}} h^2$ can coexist with $\Omega_a^{\text{eq/TP}} h^2$ and $\Omega_a^{\text{NTP}} h^2$, which we calculate in the following.

Saxions that are thermal relics have a thermal spectrum, because decoupling and redshift do not change the shape of their spectrum and they have a thermal spectrum when they are in equilibrium. For saxions that are thermally produced, we provide arguments for a thermal spectrum Appendix E.

Thus, also thermally produced axions have basically a thermal spectrum and, therefore, one can describe the associated density parameter approximately by

$$\Omega_a^{\text{eq/TP}} h^2 \simeq \sqrt{\langle p_{a,0}^{\text{th}} \rangle^2 + m_a^2} Y_a^{\text{eq/TP}} s(T_0) h^2 / \rho_c, \quad (5.25)$$

where $\rho_c/[s(T_0)h^2] = 3.6$ eV and $Y_a^{\text{eq/TP}} = Y_\sigma^{\text{eq/TP}}$ as described in Sect. 3.2. With the present CMB temperature of $T_0 = 0.235$ meV and an axion temperature today of $T_{a,0} = [g_{*S}(T_0)/228.75]^{1/3} T_0 \simeq 0.06$ meV, the average momentum of thermal axions today is given by $\langle p_{a,0}^{\text{th}} \rangle = 2.701 T_{a,0}$. When comparing this momentum with the axion mass m_a , one finds that this axion population is still relativistic today for $f_{\text{PQ}} \gtrsim 10^{11}$ GeV. At and before the CMB decoupling epoch, $T \gtrsim 1$ eV, axions from thermal processes were relativistic for f_{PQ} in the full allowed range (2.64). In the considered SUSY settings, they contribute at most

$$\Delta N_{\text{eff}}(T) = \frac{4}{7} \left(\frac{T_a}{T_\nu} \right)^4 = \frac{4}{7} \left[\frac{g_{*S}(T)}{228.75} \right]^{4/3} \left(\frac{T}{T_\nu} \right)^4, \quad (5.26)$$

i.e., $\Delta N_{\text{eff}}(T) \leq 0.0097$ for 10 MeV $\gtrsim T \gtrsim 1$ eV, which is far below the Planck sensitivity and easily accommodated by the ΔN_{eff} limits discussed above.

The density parameter of non-thermal axions emitted in late decays of saxions from thermal processes reads

$$\Omega_a^{\text{NTP}} h^2 = 2 \sqrt{(p_{a,0}^{\text{NTP}})^2 + m_a^2} Y_\sigma^{\text{eq/TP}} s(T_0) h^2 / \rho_c, \quad (5.27)$$

with the present momentum of these axions given by

$$p_{a,0}^{\text{NTP}} = \frac{m_\sigma}{2} \left[\frac{g_{*S}(T_0)}{g_{*S}(T_\sigma)} \right]^{1/3} \frac{T_0}{T_\sigma}, \quad (5.28)$$

⁸Recent studies explore the possibility that cold dark matter axions form a Bose–Einstein condensate [214, 215]. It is argued in these studies that the necessary condition of thermal equilibrium can be established via gravitational axion self-interactions when T reaches approximately 500 eV $(f_{\text{PQ}}/10^{12} \text{ GeV})^{1/2}$. This finding relies on the presence of a condensed regime at late times in which the transition rate between momentum states is large compared to their spread in energy. Our study can neither reaffirm nor contradict this finding since our investigations are based on the usual Boltzmann equation and thus restricted to the particle kinetic regime in which the opposite hierarchy holds.

when applying the sudden-decay approximation. Thus, $\Omega_a^{\text{NTP}} h^2$ will depend on m_σ if these axions are still relativistic today, i.e., when $T_0 \gtrsim T_{\text{nr}}$ given by (5.11) above. As extensively discussed in the previous sections, this non-thermal axion population can provide a significant contribution to ΔN_{eff} prior to BBN and thereafter. In fact, one can use (5.2) to relate $\Omega_a^{\text{NTP}} h^2$ to this ΔN_{eff} :

$$\Omega_a^{\text{NTP}} h^2 = \left\{ 1.1 \times 10^{-11} \left(\frac{10^9 \text{ GeV}}{f_{\text{PQ}}} \right)^2 \left(\frac{Y_\sigma^{\text{eq/TP}}}{10^{-3}} \right)^2 + 3.2 \times 10^{-11} \left(\frac{T_\nu}{T} \right)^8 \left[\frac{10.75}{g_{*S}(T)} \right]^{8/3} \Delta N_{\text{eff}}^2(T) \right\}^{1/2}, \quad (5.29)$$

where the m_σ dependence is now absorbed into $\Delta N_{\text{eff}}(T)$. Thus, the discussed ΔN_{eff} constraints translate directly into upper limits on $\Omega_a^{\text{NTP}} h^2$. For $T \lesssim 1$ MeV and f_{PQ} such that the first term on the rhs of (5.29) is negligible, those limits are described by $\Omega_a^{\text{NTP}} h^2 = 5.7 \times 10^{-6} \Delta N_{\text{eff}}$. This applies to thermal axions as well if they are still relativistic today.

Figure 5.9 shows $\Omega_a^{\text{NTP}} h^2$ contours that correspond to ΔN_{eff} values of 3.59 (solid), 1.73 (dashed), and 0.26 (dash-dotted) in blue. As in Fig. 5.2, these values are motivated by the CMB + HPS + HST result [69] quoted in Table 5.2 and the expected 68% CL sensitivity of the Planck satellite mission [194, 195]. Contours of $\Omega_a^{\text{eq/TP}} h^2$ are shown for $T_{\text{R}} = 10^8$ (10^{10}) GeV by the solid (dashed) red lines and for larger $T_{\text{R}} > T_{\text{D}}^a$ by the unlabeled dotted line. On this dotted line at $f_{\text{PQ}} > 10^{11}$ GeV, (5.26) applies so that $\Delta N_{\text{eff}} = 0.0097$ and $\Omega_a^{\text{eq}} h^2 = 5.5 \times 10^{-8}$ reside in thermal relic axions that are still relativistic today. The labeled dotted lines indicate $\Omega_a^{\text{MIS}} h^2$ of the axion condensate from the misalignment mechanism for $\theta_i = 0.01, 0.1$, and 1. For $\theta_i \sim 1$ and $f_{\text{PQ}} \sim 10^{12}$ GeV, this cold axion population can explain the dark matter density $\Omega_{\text{CDM}} h^2 \simeq 0.1$ [12] displayed by the gray bar.

Considering the 2σ limit $\Delta N_{\text{eff}} < 3.59$ in Fig. 5.9, one sees that it constrains $\Omega_a^{\text{NTP}} h^2$ to values that stay below the photon density $\Omega_\gamma h^2 \simeq 2.5 \times 10^{-5}$ [12]. Remarkably, Planck results are expected to probe even much smaller Ω_a^{NTP} . The testable values can be as small as an order of magnitude below Ω_γ if axions emitted in decays of thermal saxions are the only significant contribution to ΔN_{eff} . In contrast and similarly to the non-SUSY case [1], it will remain to be extremely challenging to probe the axion population from thermal processes with its small contribution of $\Delta N_{\text{eff}} \lesssim 0.01$.

Note that m_σ changes along the $\Omega_a^{\text{NTP}} h^2$ curves in Fig. 5.9 for fixed T_{R} and x since we indicate results for fixed values of ΔN_{eff} . Indeed, additional BBN constraints can disfavor parts of the shown contours when $T_\sigma < 1$ MeV. For $T_\sigma > 1$ MeV, BBN constraints on ΔN_{eff} – such as the ones considered in Fig. 5.8 – can also be displayed in terms of $\Omega_a^{\text{NTP}} h^2$. On the logarithmic scale considered in Fig. 5.9, they are similar to the shown ones.

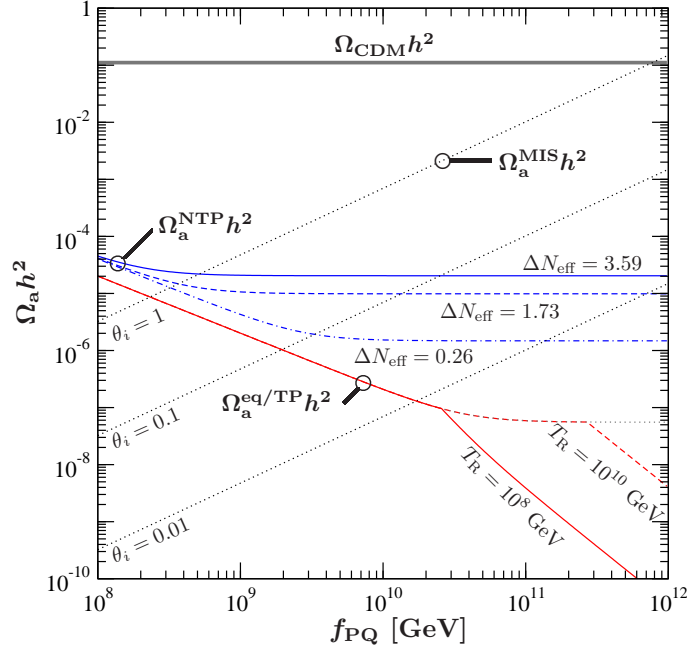


Figure 5.9: The density parameters of the axion condensate from the misalignment mechanism $\Omega_a^{MIS} h^2$ for $\theta_i = 0.01, 0.1$, and 1 (dotted lines), of non-thermally produced axions from decays of thermal saxions $\Omega_a^{NTP} h^2$ for $\Delta N_{eff} = 3.59$ (solid), 1.73 (dashed), and 0.26 (dash-dotted) in blue, and of thermal relic/thermally produced axions $\Omega_a^{eq/TP} h^2$ for $T_R = 10^8$ (solid) and 10^{10} GeV (dashed) in red. The dotted line connected to the latter indicates $\Omega_a^{eq} h^2$ for larger T_R with $T_R > T_D^a$. The dark matter density parameter $\Omega_{CDM} h^2 \simeq 0.1$ [12] is indicated by the horizontal gray bar. As in Fig. 5.2, we consider ΔN_{eff} at $T \ll 1$ GeV and show values based on the CMB + HPS + HST result [69] quoted in Table 5.2 and the expected 68% CL sensitivity of the Planck satellite mission [194, 195].

Taking into account the relation between f_{PQ} and m_a , the analog of a Lee–Weinberg curve is given by $\Omega_a h^2 \geq \Omega_a^{MIS} h^2 + \Omega_a^{NTP} h^2 + \Omega_a^{eq/TP} h^2$ and can be inferred from Fig. 5.9. Depending on the initial displacement of the saxion field from the vacuum and on the mass spectrum, there can be additional contributions to the axion density parameter, e.g., from decays of the saxion condensate into axions. In such cases, sizable additional contributions also to ΔN_{eff} are possible, which will affect the $\Omega_a^{NTP} h^2$ contours in Fig. 5.9.

One can consider Fig. 5.9 as a SUSY generalization of Fig. 4 in Ref. [1], which allows one to infer the axion analog of the Lee–Weinberg curve in non-SUSY scenarios.⁹ Whereas $\Omega_a^{eq/TP} h^2$ can govern the axion density for small θ_i and/or small f_{PQ} in non-SUSY scenarios [1], we find $\Omega_a^{NTP} h^2 \gtrsim 2 \Omega_a^{eq/TP} h^2$ in the considered SUSY scenarios.

⁹A figure similar to Fig. 4 in Ref. [1] is given in Ref. [155], where a fixed relation between f_{PQ} and T_R was used and the axions were taken to be always non-relativistic today.

This can be seen in Fig. 5.9 and when comparing (5.25) and (5.27). If SUSY and a hadronic axion model are realized in nature, the axion density parameter can thus be governed by non-thermal axions from decays of thermal saxions and/or the axion condensate from the misalignment mechanism. Interestingly, both of these populations may be accessible experimentally: While signals of the axion condensate are expected in direct axion dark matter searches [216], the findings of ΔN_{eff} studies may already be first hints for the existence of non-thermal axions from saxion decays.

Chapter 6

Saxion Decays with Gravitino CDM and Entropy from Axinos

In this and the next chapter we extend the results from the previous one to go beyond the sudden-decay approximation and to include other cosmological limits coming primarily from the gravitino and the next-to-lightest SUSY particle (NLSP). We also investigate $x < 1$ in detail and include entropy production.

In this chapter, we investigate a scenario where the gravitino is the LSP and, therefore, stable. The gravitino then contributes to CDM here. Thus, stringent upper limits on T_R from gravitino overproduction apply [153, 217]. Here axions from the decay of thermal saxions contribute to ΔN_{eff} prior to BBN. The thermal axino has to decay before the freeze-out of the lightest ordinary supersymmetric particle (LOSP)¹ and all its decay products have to thermalize, because otherwise they would produce too much dark matter.

Section 6.1 introduces the framework for our numerical treatment of the particles in this scenario. In particular, we focus on extra radiation and entropy release from saxion decays and entropy from decaying axinos. We present resulting limits on saxion parameters from extra radiation measurements and also from the inferred amount of CDM for both $x = 1$ and $x < 1$.

The amount of extra radiation is not the only way to test our scenario. In fact, it shows some amount of testability at colliders. In Sect. 6.2, we explain possible observable hints at colliders and show limits that current searches present to our scenario.

Section 6.3 provides some analytical approximations of our numerical results.

¹By ordinary we mean particles of the MSSM, so not the axino or the gravitino.

6.1 Numerical Treatment of Extra Radiation and Entropy Release

The numerical treatment of the generic case of the decay of a heavy particle into inert radiation, i.e., radiation that does not interact with the thermal background radiation, has been considered in Ref. [218]. This inert radiation is formed by the axion in our case. The role of the heavy particles is taken by saxions from thermal production. In the following, we bring our results from the previous chapter beyond the sudden-decay approximation. But since the saxion and the axino can also decay into particles that interact with the thermal background, we have to include also these entropy releasing decays – which are neglected in the previous chapter – to arrive at an exact result.

The case of out of equilibrium decays of a generic non-relativistic heavy particle producing entropy is considered in Ref. [219]. We adopt the definition of this reference by referring to electromagnetic entropy as the total entropy of photons and all relativistic particles in thermal equilibrium with photons. Thus, in our case, the role of this heavy particle is played by the axino and, depending on the branching ratio, the saxion. The gravitino is stable here and does not contribute to inert radiation or electromagnetic entropy. Combining both cases allows us to calculate the contribution of axions to ΔN_{eff} and the amount of CDM from gravitinos taking into account for the first time entropy release from both axinos and saxions. The full set of Boltzmann equations governing the time evolution of the energy densities ρ_i of these particles is

$$\dot{\rho}_{\tilde{G}} + 3H\rho_{\tilde{G}} = 0, \quad (6.1a)$$

$$\dot{\rho}_{\tilde{a}} + 3H\rho_{\tilde{a}} = -\Gamma_{\tilde{a}}\rho_{\tilde{a}}, \quad (6.1b)$$

$$\dot{\rho}_{\sigma} + 3H\rho_{\sigma} = -\Gamma_{\sigma}\rho_{\sigma}, \quad (6.1c)$$

$$\dot{\rho}_a + 4H\rho_a = \text{BR}(\sigma \rightarrow aa)\Gamma_{\sigma}\rho_{\sigma}, \quad (6.1d)$$

where the dot indicates derivation with respect to cosmic time t . The change in entropy S is given by

$$S^{1/3}\dot{S} = R^4 \left(\frac{2\pi^2}{45} g_{*S} \right)^{1/3} \{ \Gamma_{\tilde{a}}\rho_{\tilde{a}} + [1 - \text{BR}(\sigma \rightarrow aa)]\Gamma_{\sigma}\rho_{\sigma} \}, \quad (6.2)$$

and the time evolution of the scale factor is given by the Friedmann equation

$$H^2 = \frac{8\pi}{3m_{\text{Pl}}^2} (\rho_{\tilde{G}} + \rho_{\tilde{a}} + \rho_{\sigma} + \rho_a + \rho_{\text{rad}}). \quad (6.3)$$

The energy density of the thermal MSSM radiation background in terms of the entropy is given by

$$\rho_{\text{rad}} = \frac{3}{4} \left(\frac{45}{2\pi^2 g_{*S}} \right)^{1/3} \frac{S^{4/3}}{R^4}. \quad (6.4)$$

Here and in the following g_* and g_{*S} count the relativistic degrees of freedom of the MSSM only, i.e., without the PQ multiplet and the gravitino.² Those particles are added explicitly in the Friedmann equation.

The thermal production of all particles involved is not covered by these equations, since it happens at much higher temperatures than the decays, see Chap. 3 for details. Note that since both the axino and the saxion are unstable, the rhs of (6.1b) and (6.1c) depends on the associated decay width Γ_i . For the gravitino, the rhs is set to zero, since it is stable. The decay of the LOSP provides a possible source of gravitinos that would appear on the rhs of its Boltzmann equation. However, we do not model the LOSP explicitly here, thus we do not consider gravitinos from LOSP decays. As in the case of inflaton decays into radiation covered in Sect. 3.5, the factor of 3 in the second term on the lhs of the first three equations accounts for the dilution due to the expansion of the Universe, whereas the axions are in addition to the dilution also redshifted, hence the factor of 4. The axion is produced by decays of the saxion, so the rhs of Eq. (6.1d) has a positive sign and is proportional to ρ_σ multiplied by the branching ratio of saxion to axion decays $\text{BR}(\sigma \rightarrow aa)$. The other decay products of the saxion are coupling to the plasma and produce electromagnetic entropy, see Eq. (6.2). The axino decay produces only electromagnetic entropy.

Equations (6.1) – (6.3) form a closed set of differential equations that we solve numerically. We begin our computation at $t_i = 1.6 \times 10^{-13}$ s corresponding to $T_i \simeq 10^3$ GeV with $R(t_i) = 1 \text{ GeV}^{-1}$ and end at $t_f = 0.7$ s corresponding to $T_f \simeq 1$ MeV. The initial values of the energy densities are given by

$$\rho_{\tilde{G}}(t_i) = s(T_i) m_{\tilde{G}} Y_{\tilde{G}}^{\text{TP}}, \quad (6.5a)$$

$$\rho_{\tilde{a}}(t_i) = s(T_i) m_{\tilde{a}} Y_{\tilde{a}}^{\text{eq/TP}}, \quad (6.5b)$$

$$\rho_\sigma(t_i) = s(T_i) m_\sigma Y_\sigma^{\text{eq/TP}}, \quad (6.5c)$$

$$\rho_a(t_i) = s(T_i) \langle p_{a,i}^{\text{th}} \rangle Y_a^{\text{eq/TP}}. \quad (6.5d)$$

The average thermal axion momentum is given by $\langle p_{a,i}^{\text{th}} \rangle = 2.701 T_{a,i}$ with $T_{a,i} = [g_{*S}(T_i)/228.75]^{1/3} T_i$. The initial entropy $S(t_i) = s(T_i) R(t_i)^3$. In the case of the gravitino, the full thermal production yield is considered. It reads [152, 153]

$$Y_{\tilde{G}}^{\text{TP}} = \sum_{i=1}^3 y_i g_i^2(T_R) \left(1 + \frac{M_i^2(T_R)}{3m_{\tilde{G}}^2} \right) \ln \left(\frac{k_i}{g_i(T_R)} \right) \left(\frac{T_R}{10^{10} \text{ GeV}} \right), \quad (6.6)$$

where the sum runs over the contributions resulting from the respective gauge groups $U(1)_Y$, $SU(2)_L$, and $SU(3)_c$, respectively. The values of the parameters in (6.6) are given in Table 6.1. In our analysis, we consider universal gaugino masses, $m_{1/2} =$

²Note that (6.4) is only correct if $g_* = g_{*S}$. In fact, such an equality is assumed in Refs. [218–220]. While Eq. (6.2) can easily be generalized, the radiation energy density given in the literature only applies for $g_* = g_{*S}$. Since we deal with decays prior to BBN in this chapter, this poses no problem to us.

Table 6.1: *The gauge coupling g_i , the gaugino mass parameters M_i , and the constants k_i and y_i associated with the gauge groups $U(1)_Y$, $SU(2)_L$, and $SU(3)_c$. From [153].*

Gauge group	Label i	g_i	M_i	k_i	$(y_i/10^{-12})$
$U(1)_Y$	1	g'	M_1	1.266	0.653
$SU(2)_L$	2	g	M_2	1.312	1.604
$SU(3)_c$	3	g_s	M_3	1.271	4.276

$M_i(m_{\text{GUT}})$, at the grand unification scale $m_{\text{GUT}} \simeq 2 \times 10^{16}$ GeV. We do not specify a certain SUSY model. Nevertheless, in the following we use only certain pairs of $m_{1/2}$ and $m_{\tilde{g}}$, keeping in mind that these two values are not truly independent. These are $m_{\tilde{g}} \simeq 1.03, 1.25$, and 1.47 TeV together with $m_{1/2} = 400, 500$, and 600 GeV, respectively, obtained by a generic mSUGRA evolution of the coupling constants and masses done with **SPHENO** [221, 222]. The other parameters are: universal scalar mass $m_0 = 1.7$ TeV, $\text{sign}(\mu) = +1$, trilinear coupling $A_0 = 0$, ratio of the up- and down-type Higgs expectation values $\tan \beta = 10$. Even the lowest of these $m_{\tilde{g}}$ and $m_{1/2}$ values are still allowed by current SUSY searches (see, e.g., Ref. [223]). They are, however, well within reach of current experiments.

For all the range $[t_i, t_f]$, we consider gravitinos, axinos, and saxions to be non-relativistic, whereas axions are relativistic. Although for gravitinos and saxions this might not be true for the whole range, we checked numerically that the details are irrelevant for the resulting extra radiation and entropy release. The reason is as follows. Axinos, saxions, (or their decay products) or the gravitino can only have a tangible influence on early Universe cosmology if they are non-relativistic. If the PQ particles are relativistic before decay, their contribution to $\Delta N_{\text{eff}} \lesssim \mathcal{O}(0.01)$, since they decouple (if they reach thermal equilibrium at all) at high temperatures where $g_{*S} \gtrsim 200$. Moreover, a significant entropy release requires an energy density prior to decay that is comparable to the energy density of the background radiation. If any of these particles becomes non-relativistic, its energy density increases relative to the energy density of radiation. Then their decay products can contribute significantly to ΔN_{eff} or produce significant entropy. In the case of the gravitino, it contributes significantly to CDM because it is non-relativistic and has a sizable mass, although $Y_{\tilde{G}}^{\text{TP}}$ is very small. Thus, by assuming that axinos, saxions and gravitinos are non-relativistic, we underestimate the contributions of these particles to ΔN_{eff} , entropy release or CDM only in the non-interesting parameter region where their respective contribution is unmeasurably small anyway.

Release of electromagnetic entropy leads to dilution of all species not in thermal equilibrium. A suitable measure is the dilution factor Δ defined as the ratio

$$\Delta = \frac{S(t_f)}{S(t_i)}. \quad (6.7)$$

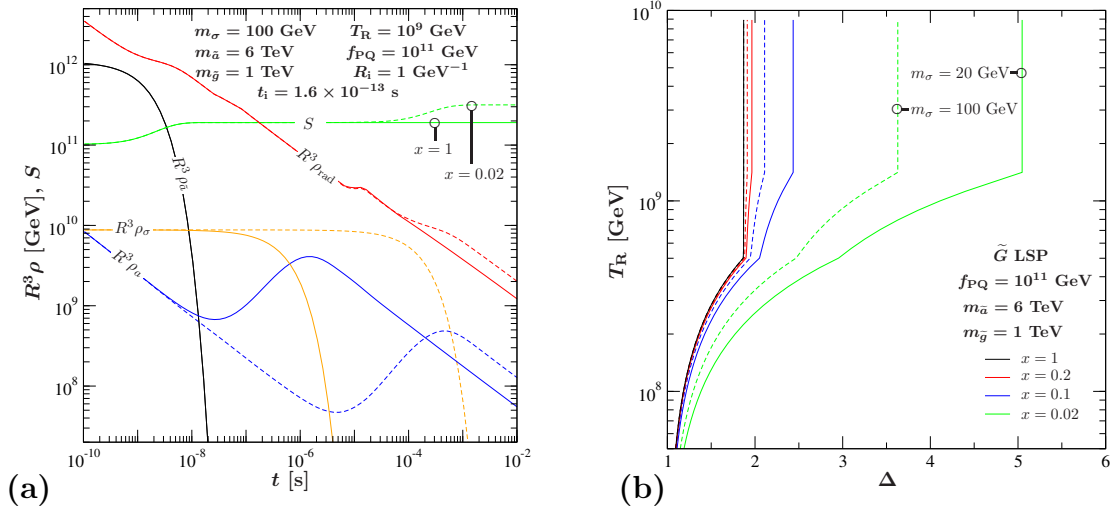


Figure 6.1: **(a):** The evolution of the energy per comoving volume of axinos, saxions, axions, and interacting radiation and the entropy over cosmic time. Here $m_{\tilde{\sigma}} = m_{\tilde{G}} = 100$ GeV, $m_{\tilde{g}} = 1$ TeV, $m_{\tilde{a}} = 6$ TeV, $m_{1/2} = 400$ GeV, $T_R = 10^9$ GeV, and $f_{\text{PQ}} = 10^{11}$ GeV are chosen as input parameters for the Boltzmann equations. The starting value of the scale factor $R_i = 1$ GeV $^{-1}$. The red line shows the energy per comoving volume of interacting radiation, the orange line the one of saxions, the blue depicts the one of axions, and the black line shows the one of axinos. The green line the total entropy. Lines are drawn solid (dashed) for $x = 1$ (0.02). **(b):** The dilution factor defined as $\Delta = S(t_f)/S(t_i)$ on the horizontal axis and the reheating temperature on the vertical one. Here $f_{\text{PQ}} = 10^{11}$ GeV, $m_{\tilde{a}} = 6$ TeV, and $m_{\tilde{g}} = 1$ TeV. The black, red, blue, and green line are drawn for $x = 1, 0.2, 0.1$, and 0.02 , respectively. Contours are solid (dashed) for $m_{\tilde{\sigma}} = 20$ (100) GeV.

In Eq. (6.2) we find the two sources of entropy release, the axino and saxion decay. The dominating axino decay rate is given in (2.5). In addition to the axino contribution, the amount of entropy released depends on the branching ratios of the saxion. The two most important decays are (2.66) and (2.67). Thus, for $x \sim 1$ one gets very little entropy from the saxion decay, whereas for $x \lesssim \mathcal{O}(10^{-2})$ the saxion does indeed produce entropy.

The result of the numerical integration is shown in Fig. 6.1(a) for an exemplary choice of parameters, namely $m_{\tilde{\sigma}} = m_{\tilde{G}} = 100$ GeV, $T_R = 10^9$ GeV, and $f_{\text{PQ}} = 10^{11}$ GeV. For these values of the reheating temperature and the PQ scale, the axino is in thermal equilibrium in the early Universe. If the axino decay would take place after the LOSP freeze-out, essentially all axinos would end up as gravitinos due to R -parity conservation. Combined with $m_{\tilde{\sigma}} \sim m_{\tilde{G}} \gtrsim 1$ GeV this would lead to a dark matter abundance that exceeds the observed amount by many orders of

magnitude [50, 153]. In order to solve this problem, we set $m_{\tilde{a}} = 6$ TeV so that the temperature after the decay of the axino T_{after} (at which $\Gamma_{\tilde{a}} \simeq 3H$) yields: $T_{\text{after}} \simeq 10$ GeV. Then, the approximate rule $T_{\text{D}}^{\text{LOSP}} \simeq m_{\text{LOSP}}/25 \simeq T_{\text{after}}$ allows a realistic LOSP with $m_{\text{LOSP}} \gtrsim 250$ GeV, although such a heavy axino is possibly somewhat contrived from a model building point of view.

Figure 6.1(a) shows the evolution of the energy per comoving volume, $R^3 \rho_i$, of the respective species for $x = 1$ (0.02) depicted by the solid (dashed) lines. In the absence of any decay or entropy release, non-relativistic massive particles show up as horizontal lines, whereas relativistic particles show a decrease of their energy per comoving volume due to redshift of their momentum. The black line is the energy of the axino. Its decay produces entropy, as indicated by the rise in the otherwise horizontal green line showing the total entropy. Moreover, the energy of the background radiation, shown as the red line, decreases slower at the time of axino decay because of the additional entropy. The saxion and the axion energy per comoving volume, shown as the orange and blue line, respectively, are diluted by the axino decay. This effect, however, is not visible in the plot, because the increase of R and the decrease of ρ_i both caused by the entropy release exactly cancel each other when drawing the energy per comoving volume.

The decay of the saxion produces axions for both considered values of x , whereas only for $x = 0.02$ a significant entropy release takes place. This can be seen by the deviation of the dashed entropy and comoving radiation energy contours from the solid ones. Since the axion population from saxion decays represents a form of radiation not in thermal contact with the plasma, it does not change the usual time-temperature relation [218]. The only effect is an increase in the total number of relativistic degrees of freedom, given by the inclusion of the resulting ΔN_{eff} additional neutrinos in the computation of g_* . In particular, the elevated amount of the comoving energy of the background radiation as indicated by the difference between the solid and dashed red line at $t = 10^{-2}$ s is not due to an increased temperature, but stems solely from an increased expansion, so from a larger R . Note that due to these additional relativistic particles, the values of T_i and especially T_f given above Eq. (6.5) are strictly only valid for $\Delta N_{\text{eff}} = 0$. This poses no problem for our calculations, since we can express $\Delta N_{\text{eff}}(t_f)$ and $\rho_{\tilde{G}}(t_f)$ independent of T_f , for the former, see Eq. (5.2).

The other two dips in the red line that are not due to entropy release from axino or saxion decay result from a change in g_* . Note also that the saxion decays much later in the case of small x . In both cases there is extra radiation in the form of axions coming from saxion decays, as can be seen by the steep rise of the blue lines. The gravitino energy per comoving volume is too low to be visible in this scale.

This illustrates the cosmology of this gravitino LSP scenario. There is always an early entropy release by the decay of the axino. The amount of dilution depends on the thermal axino yield, so via Eq. (3.51) it depends on T_{R} . This can be seen by the black curve in Fig. 6.1(b) for the case of $x = 1$, The other parameters are the same

as in Fig. 6.1(a). The kink in this Δ contour indicates the T_R value above which the axino reaches thermal equilibrium in the early Universe. The yield of axinos that have been in thermal equilibrium does not depend on T_R and, therefore, also Δ is independent of T_R for $T_R > T_D^{\tilde{a}}$. For an analytic approximation of the dilution factor, see Eq. (6.15) given below.

For smaller values of x there is also a later entropy release by the decay of the saxion as indicated by the red, blue, and green lines in Fig. 6.1(b) corresponding to $x = 0.2, 0.1$, and 0.02 , respectively. Again the amount depends on the reheating temperature for $T_R < T_D^{\sigma}$. Since $T_D^{\sigma} > T_D^{\tilde{a}}$, the kink due to saxion freeze-out is at higher values of T_R . Moreover, the entropy release depends on the saxion mass, lower mass leading to a later decay and, hence, to more entropy release. This effect is illustrated for $m_{\sigma} = 20$ (100) GeV by the solid (dashed) contours. An analytic approximation is given in Sect. 6.3 below. The entropy from saxion decays dilutes all species not in thermal contact with the plasma at its decay, like the LOSP, the gravitino but also a possible baryon asymmetry. The axino decay cannot dilute, e.g., the LOSP energy density, since it is taken to decay prior to LOSP freeze-out.

6.1.1 Extra Radiation and CDM for $x = 1$

Let us now look at the amount of extra radiation released by saxion decays. As already mentioned in Chap. 5, there are several hints towards the existence of radiation beyond photons and neutrinos. These hints could be an indication towards the existence of axions from saxion decays. We investigate this possibility for three parameter values, $f_{PQ} = 10^{10}, 5 \times 10^{10}$, and 10^{11} GeV. For each of these values, $m_{\tilde{a}}$ is chosen such that the axino decay takes place before LOSP freeze-out. For $m_{\tilde{a}} = 2, 3$, and 6 TeV, the corresponding T_{after} and the estimated limit on m_{LOSP} can be found in Table 6.2.

For each point, we show the amount of extra radiation provided by axions from decays of thermal saxions for $x = 1$ expressed in terms of ΔN_{eff} in Figs. 6.2(a), (b), and 6.3(a) in the $m_{\tilde{G}}-T_R$ parameter plane. The red, blue, and green contours show $\Delta N_{\text{eff}} = 0.78, 0.52$, and 0.26 , respectively. These values are the expected $3, 2$, and 1σ sensitivities of the Planck mission [194, 195]. Note that $\Delta N_{\text{eff}} = 0.78$ almost coincides accidentally with the posterior maxima inferred from our BBN analysis with the results shown in Table 5.2. The T_R dependence of these contours disappears for cosmological scenarios with $T_R > T_D^{\sigma}$. Each contour is drawn solid (dashed) for $m_{\tilde{g}} = 1$ (1.25) TeV. The difference between the solid and dashed ΔN_{eff} contours is due to a dependence of the dilution factor on $m_{\tilde{g}}$. Since a heavier gluino leads to a later decay of the axino, more entropy is released and the ΔN_{eff} value is lower. To reach a given value of ΔN_{eff} , the saxion needs to decay later. This leads to a shift of the ΔN_{eff} contour towards lower values of the saxion mass. Moreover, in Figs. 6.2(b) and 6.3(a) one can see a dip in the ΔN_{eff} contours at T_R values below

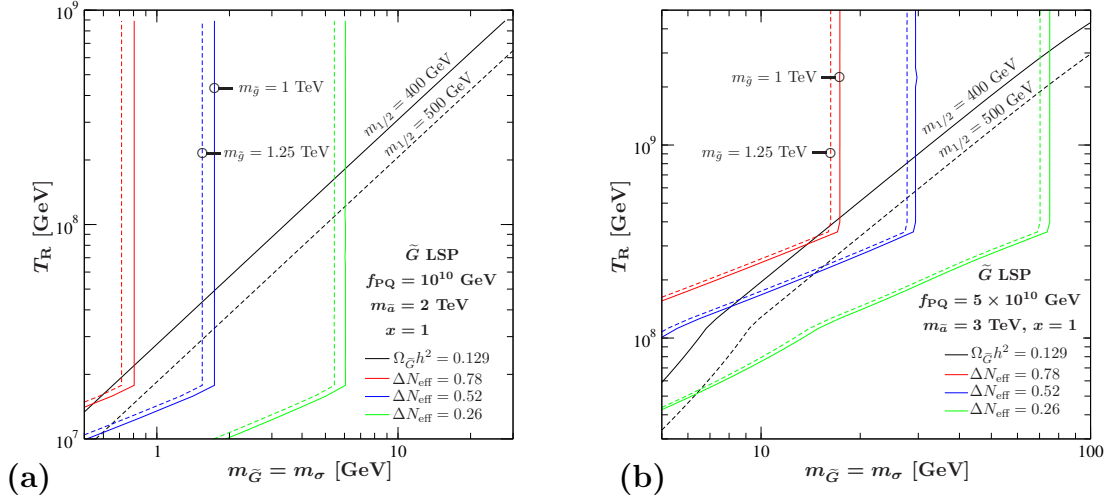


Figure 6.2: **(a):** Contours of ΔN_{eff} provided by axions from decays of thermal saxions and $\Omega_{\tilde{G}} h^2$ in the $m_{\tilde{G}}-T_R$ parameter plane. Here $m_{\sigma} = m_{\tilde{G}}$, $f_{\text{PQ}} = 10^{10}$ GeV, $m_{\tilde{a}} = 2$ TeV, and $x = 1$. The black solid (dashed) line shows the contour $\Omega_{\tilde{G}} h^2 = 0.129$ for $m_{1/2} = 400$ (500) GeV, so the region above this line is excluded by more than 3σ due to gravitino overproduction. The red, blue, and green lines show the $\Delta N_{\text{eff}} = 0.78$, 0.52, and 0.26 contour, respectively. The amount of extra radiation increases to the left of the respective curves. The ΔN_{eff} contours are drawn solid (dashed) for $m_{\tilde{g}} = 1$ (1.25) TeV. **(b):** Same as (a), but with $f_{\text{PQ}} = 5 \times 10^{10}$ GeV and $m_{\tilde{a}} = 3$ TeV.

T_D^σ . This is due to the axino freeze-out, since for T_R values below $T_D^{\tilde{a}}$, the dilution factor depends on T_R as described above.

In the considered gravitino LSP case, thermal gravitino production with the yield given by (6.6) leads to upper bounds on the reheating temperature [153, 217], since the gravitino energy density parameter

$$\Omega_{\tilde{G}} h^2 = m_{\tilde{G}} Y_{\tilde{G}}^{\text{TP}}(T_0) \frac{s(T_0) h^2}{\rho_c} \quad (6.8)$$

cannot exceed the inferred amount of cold dark matter [12]

$$\Omega_{\text{CDM}} h^2 = 0.111(\pm 0.012), \quad (6.9)$$

with errors referring to the 95% confidence level. The black lines in Figs. 6.2(a), (b), and 6.3(a) show the 3σ upper bound from gravitino overproduction, given by the contours $\Omega_{\tilde{G}} h^2 = 0.129$ for $m_{1/2} = 400$ (500) GeV drawn solid (dashed). In all three cases the gravitino is diluted by axino decays, but only in Figs. 6.2(b) and 6.3(a) one can see the kink in the gravitino contour due to the change in the dilution factor caused by axino freeze-out.

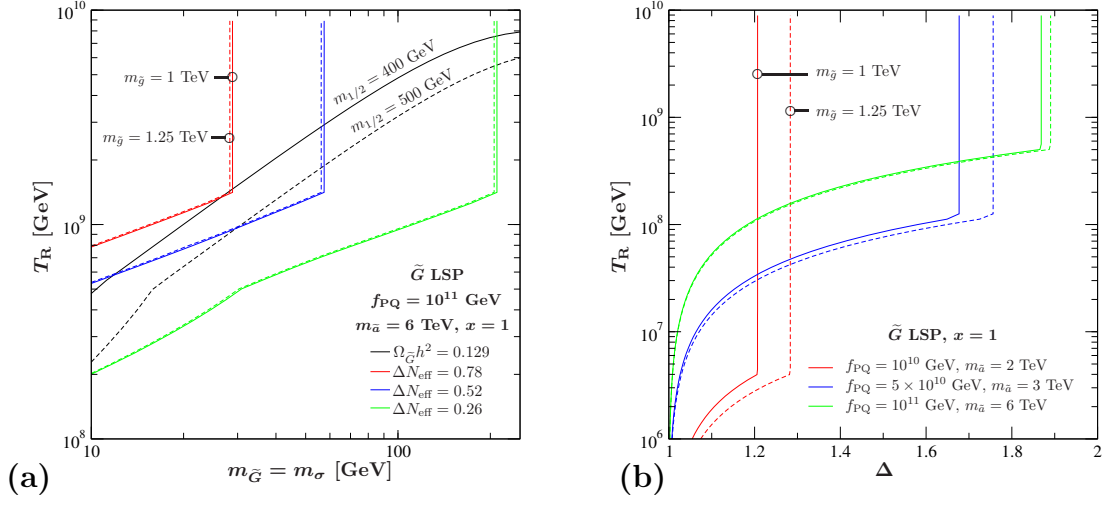


Figure 6.3: **(a):** Same as Fig. 6.2(a), but with $f_{\text{PQ}} = 10^{11}$ GeV and $m_{\tilde{a}} = 6$ TeV. **(b):** The dilution factor defined as $\Delta = S(t_f)/S(t_i)$ on the horizontal axis and the reheating temperature on the vertical one. Here $x = 1$. The red line is drawn for $f_{\text{PQ}} = 10^{10}$ GeV and $m_{\tilde{a}} = 2$ TeV, the blue one for $f_{\text{PQ}} = 5 \times 10^{10}$ GeV and $m_{\tilde{a}} = 3$ TeV, and the green one for $f_{\text{PQ}} = 10^{11}$ GeV and $m_{\tilde{a}} = 6$ TeV. Lines are drawn solid (dashed) for $m_{\tilde{g}} = 1$ (1.25) TeV.

The dilution factor Δ as a function of T_R for $f_{\text{PQ}} = 10^{10}$, 5×10^{10} , and 10^{11} GeV is shown in Fig. 6.3(b) as the red, blue, and green curve, respectively. The axino mass is set as in the previous plots and as shown in Table 6.2. Here $x = 1$ and the solid (dashed) curves are drawn for $m_{\tilde{g}} = 1$ (1.25) TeV. The dependence of Δ on $m_{\tilde{g}}$ explained above is clearly visible. For higher values of $m_{\tilde{a}}$ this dependence is less pronounced, because the difference in the axino decay width decreases, as can be seen from (2.5). Also the dependence of Δ on $T_D^{\tilde{a}}$ explained above is now manifest. Indeed, the kinks in the blue and green contours lead to the ones in the ΔN_{eff} and $\Omega_{\tilde{G}} h^2$ contours in Figs. 6.2(b) and 6.3(a).

As one can see from Figs. 6.2(a), (b), and 6.3(a), axions from saxion decays contribute to the amount of extra radiation. However, for the considered $x = 1$ case, values of $\Delta N_{\text{eff}} \gtrsim 0.78$ are almost completely disfavored by the $\Omega_{\tilde{G}}^{\text{TP}} \leq \Omega_{\text{CDM}}$ constraint if $m_{\tilde{g}} = 1$ TeV and $m_{1/2} = 400$ GeV. In fact, if SUSY searches at the LHC point to minimum $m_{\tilde{g}}$ and $m_{1/2}$ values of respectively 1.25 TeV and 500 GeV, the $\Omega_{\tilde{G}}^{\text{TP}} \leq \Omega_{\text{CDM}}$ constraint will clearly disfavor $\Delta N_{\text{eff}} \gtrsim 0.78$ and the BBN-inferred posterior maxima $\Delta N_{\text{eff}} = 0.76$ and 0.77 given in Table 5.2. Still axions from decays of thermal saxions can then provide a viable explanation of $\Delta N_{\text{eff}} \lesssim 0.52$. This matches the 2σ sensitivity of the Planck satellite mission, which implies that a statistically significant 3σ detection of ΔN_{eff} cannot be expected.

Table 6.2: The temperature T_{after} at which $\Gamma_{\tilde{a}} \simeq 3H$ for different combinations of the PQ scale f_{PQ} , the axino mass $m_{\tilde{a}}$, and the gluino mass $m_{\tilde{g}}$ together with the LOSP mass $m_{\text{LOSP}}^{\text{max}}$ for which $T_D^{\text{LOSP}} \simeq m_{\text{LOSP}}/25 \simeq T_{\text{after}}$.

f_{PQ} [GeV]	$m_{\tilde{a}}$ [TeV]	$m_{\tilde{g}}$ [TeV]	T_{after} [GeV]	$m_{\text{LOSP}}^{\text{max}}$ [GeV]
10^{10}	2	1 (1.25)	13 (9)	325 (225)
5×10^{10}	3	1 (1.25)	6 (5)	150 (135)
10^{11}	6	1 (1.25)	10 (9)	250 (235)

In high-reheating temperature scenarios, thermal leptogenesis with hierarchical heavy Majorana neutrinos [224] can explain the baryon asymmetry of the Universe. Without late-time entropy production, $M_{\text{R1}} \sim T_{\text{R}}$ of at least about 10^9 GeV is then required to generate the observed baryon asymmetry η , where M_{R1} denotes the mass of the lightest among the heavy right-handed Majorana neutrinos. With late-time entropy production, a baryon asymmetry generated prior to the entropy-producing events must have been larger by the associated dilution factor Δ . In the framework of thermal leptogenesis, this can be realized for up to $\Delta \sim 10^4$ with $M_{\text{R1}} \sim T_{\text{R}} \sim 10^{13} \text{ GeV}$, as can be seen in Fig. 7(a) of Ref. [225] and in Fig. 2 of Ref. [226]. In fact, with a dilution factor of Δ , the required minimum temperature for successful leptogenesis has to be larger by that factor:

$$T_{\text{R}} \gtrsim 10^9 \text{ GeV} \quad \rightarrow \quad \frac{1}{\Delta} T_{\text{R}} \gtrsim 10^9 \text{ GeV}. \quad (6.10)$$

To explore the simultaneous viability of successful leptogenesis and an explanation of, e.g., $\Delta N_{\text{eff}} \simeq 0.52$ by axions from decays of thermal saxions, one has to consider the minimum T_{R} value together with the dilution factors shown in Fig. 6.3(b) as described in (6.10). Indeed, if the minimum T_{R} is 10^9 GeV without the entropy producing axino decays, it will become almost twice as large in the scenarios with $f_{\text{PQ}} = 10^{11} \text{ GeV}$. Accordingly, as can be seen in Fig. 6.3(a), experimental insights on $m_{\tilde{g}}$ and $m_{1/2}$ will decide on such a simultaneous viability for $x = 1$. For the lower f_{PQ} values considered in Figs. 6.2(a) and (b), that simultaneous viability is excluded already with $m_{\tilde{g}} \simeq 1 \text{ TeV}$ and $m_{1/2} \simeq 400 \text{ GeV}$.

6.1.2 Extra Radiation and CDM for $x < 1$

All of the above interpretation relied on $x = 1$. If one goes to smaller values of x , one can get considerably more ΔN_{eff} because of the later decay of the saxion and some of the above exclusion statements need to be modified. Note that $x < 1$

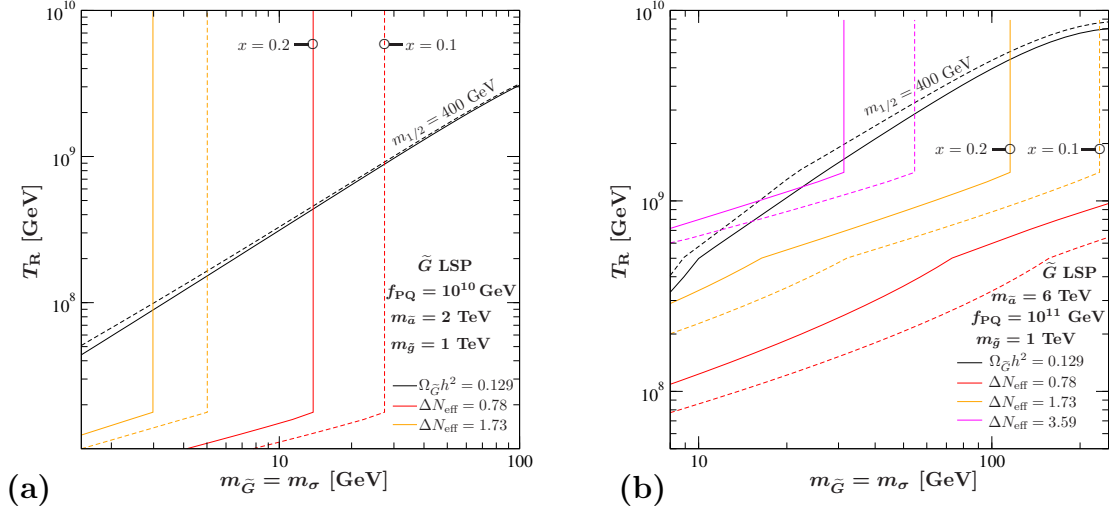


Figure 6.4: **(a):** Contours of ΔN_{eff} provided by axions from decays of thermal saxions and $\Omega_{\tilde{G}} h^2$ in the $m_{\tilde{G}}-T_R$ parameter plane. Here $m_{\sigma} = m_{\tilde{G}}$, $f_{\text{PQ}} = 10^{10}$ GeV, $m_{\tilde{a}} = 2$ TeV, and $m_{\tilde{g}} = 1$ TeV. The black line shows the contour $\Omega_{\tilde{G}} h^2 = 0.129$ for $m_{1/2} = 400$ GeV, so the region above this line is excluded by more than 3σ due to gravitino overproduction. The red and orange line show the $\Delta N_{\text{eff}} = 0.78$ and 1.73 contour, respectively. Curves are solid (dashed) for $x = 0.2$ (0.1).

(b): Same as (a), but with $f_{\text{PQ}} = 10^{11}$ GeV and $m_{\tilde{a}} = 6$ TeV. The magenta line shows the $\Delta N_{\text{eff}} = 3.59$ contour.

also introduces entropy release from saxion decays. This is shown in Fig. 6.4(a) for $f_{\text{PQ}} = 10^{10}$ GeV and $m_{\tilde{a}} = 2$ TeV and in Fig. 6.4(b) for $f_{\text{PQ}} = 10^{11}$ GeV and $m_{\tilde{a}} = 6$ TeV, both in the $m_{\tilde{G}}-T_R$ parameter plane. In each plot the red and orange line show the $\Delta N_{\text{eff}} = 0.78$ and 1.73 contour, respectively. In addition, the magenta line in Fig. 6.4(b) shows the $\Delta N_{\text{eff}} = 3.59$ contour. In both plots, $m_{1/2} = 400$ GeV and $m_{\tilde{g}} = 1$ TeV and the black line shows the $\Omega_{\tilde{G}} h^2 = 0.129$ contour. All lines are drawn solid (dashed) for $x = 0.2$ (0.1). One can see that for smaller x the dilution due to saxion decays is stronger, as the $\Omega_{\tilde{G}} h^2$ contour is pushed towards higher T_R values and the ΔN_{eff} contours towards lower m_{σ} values. In Fig. 6.4(b), the two different sources of entropy release, the axino decay and the saxion decay, leave a tangible imprint on the $\Omega_{\tilde{G}} h^2$ contour. The kink at the lower T_R value is due to axino freeze-out, as in the $x = 1$ case, also visible in the ΔN_{eff} contour. The one at higher T_R is only present if $x < 1$ and is due to saxion freeze-out corresponding to the vanishing of the ΔN_{eff} line. As above, the underlying T_R dependence of Δ can be seen in Fig. 6.1(b).

As already indicated, the resulting amount of extra radiation at a given parameter point is significantly larger than in the $x = 1$ case. Note that the maximum ΔN_{eff} that one can get at a given parameter point is reached for $x \simeq 0.1$. The exact x value depends slightly on the parameter point, because the branching ratio is a function of m_σ . One can see that not only the posterior maximum inferred from BBN analyses, $\Delta N_{\text{eff}} = 0.78$, but also the larger mean value from CMB + LSS, $\Delta N_{\text{eff}} = 1.73$, both shown in Table 5.2, are easily explained by axions from thermal saxions here. It would require a sizable increase in the limits on $m_{\tilde{g}}$ and $m_{1/2}$ to $m_{\tilde{g}} \gtrsim 1.5$ TeV (1.7 TeV) and $m_{1/2} \gtrsim 600$ GeV (700 GeV) to challenge any of these two values by direct SUSY searches.

In contrast to the case $x = 1$, if Planck should find a mean of $\Delta N_{\text{eff}} = 0$, then T_R is constrained from above by 3σ , as indicated by the red line in both plots. On the other hand, if Planck finds a significant amount of extra radiation, say a mean of $\Delta N_{\text{eff}} = 1.73$, then the red lines indicate a 3σ lower limit on the reheating temperature in this scenario. Already for $x = 0.2$, however, the amount of extra radiation exceeds current limits from CMB + LSS analyses for parameter values that would be allowed by the gravitino overproduction limit. So even without the precise measurements from Planck, axions from the decay of thermal saxions can provide stronger T_R limits than the gravitino. For $f_{\text{PQ}} = 10^{11}$ GeV, this is shown by the magenta line in Fig. 6.4(b).

Throughout this analysis we have used $m_{\tilde{G}} = m_\sigma$. This is well motivated because for most models of SUSY breaking, m_σ is of order of $m_{\tilde{G}}$, as already indicated in Sect. 2.5. Let us describe the differences that arise if there is a deviation of $\mathcal{O}(1)$ between these two masses. To do so, we fix the mass scale on the horizontal axis in Figs. 6.2(a), (b), 6.3(a), and 6.4 to be $m_{\tilde{G}}$ and vary m_σ by a factor $\mathcal{O}(1)$.

Let us first look at the case $x = 1$. Increasing (decreasing) m_σ relative to $m_{\tilde{G}}$ moves the ΔN_{eff} contours in Figs. 6.2(a), (b), 6.3(a), and 6.4 to the left (right). For the case of $x = 1$, as depicted in Figs. 6.2(a), (b), and 6.3(a), there is practically no change to the $\Omega_{\tilde{G}}$ contour, since the entropy release from saxion decay is negligible in this case.

For $x < 1$, Δ depends on m_σ as can be seen in Fig. 6.1(b). Therefore, increasing m_σ relative to $m_{\tilde{G}}$ in Fig. 6.4 reduces the dilution due to saxion decays and decreases the dip in the $\Omega_{\tilde{G}}$ contour resulting from saxion freezeout, and vice versa. Moreover, the $\Omega_{\tilde{G}}$ contour moves downwards (upwards) for an increased (decreased) m_σ . Care should be taken when varying m_σ , since for $\tau_\sigma \gtrsim 1$ s additional bounds on m_σ resulting from decays during BBN can become relevant, as explained in Chap. 4. Further details can be inferred with the help of the analytic approximations in the last section of this chapter.

6.2 Limits from Collider Searches

A very intriguing feature of this scenario is the testability through collider searches. In general, new limits from direct SUSY searches at the LHC are expected to increase the lower limits on $m_{\tilde{g}}$ and thereby on $m_{1/2}$. Since the gravitino contour moves towards higher values of $m_{\tilde{G}}$ and the ΔN_{eff} contour towards lower values in the case of stronger SUSY limits, the explanation of the current hints towards extra radiation with axions from decaying thermal saxions may be challenged in the future.

The LOSP plays a particular important role in testing this scenario. The mass of the LOSP puts an upper limit on $m_{\tilde{G}}$, because here the gravitino is assumed to be the LSP. A charged LOSP such as the lightest stau would leave significant signatures at the LHC [227]. The late decay of a charged LOSP has severe cosmological consequences for BBN [228–230]. Its decay can inject hadronic and electromagnetic energy that disturb the network of nuclear reactions. The strongest constraint, however, often comes from the formation of bound states of the charged LOSP and ^4He . These bound states lead to a catalyzed creation of ^6Li and ^9Be that exceeds observations. Thus, there are strong upper limits on the lifetime of the charged LOSP, since it has essentially to decay before bound states develop. For a cosmological history with only small additional entropy release and, therefore, a typical thermal relic LOSP yield, the lifetime is constrained to $\tau_{\text{LOSP}} \lesssim 5 \times 10^3 \text{ s}$ (see Ref. [230] and references therein). For the exemplary case of a stau LOSP with $m_{\tilde{\tau}_1} = 300 \text{ GeV}$, in our case this translates into an upper limit on the gravitino mass, yielding $m_{\tilde{G}} \lesssim 4 \text{ GeV}$. So the discovery of such a charged LOSP would exclude the high T_{R} explanation of additional radiation via saxion decay. Smaller f_{PQ} values are still viable, but then $T_{\text{R}} < 10^8 \text{ GeV}$, as can be seen in Fig. 6.2(a).

Even if the LOSP is neutral, there are constraints from BBN. In this case the injection of energetic hadrons is the dominant limit. For example, in the case of a bino LOSP the SM fermions produced in the decays lead to overproduction of ^4He and D, depending on the LOSP mass. The former is due to changes of the $p \leftrightarrow n$ interconversion, whereas the latter results from hadro-dissociation of ^4He [231], see also [232]. From the observed primordial abundance of ^4He and D one can infer limits on $m_{\tilde{G}} \lesssim 1 \text{ GeV}$ for $m_{\text{LOSP}} \simeq 300 \text{ GeV}$. So again, a high T_{R} scenario is excluded. Although negative results from direct collider searches for a charged LOSP continue to relax these upper bounds on $m_{\tilde{G}}$, a higher LOSP mass requires also a higher axino mass, so that the axino decay can happen before LOSP freezeout, see Table 6.2 for details.

This is different in the case of a sneutrino LOSP. Since the sneutrino decays dominantly into gravitinos and neutrinos, there are very weak limits except that $m_{\text{LOSP}} > m_{\tilde{G}}$ [231], see also Refs. [232, 233]. One will then, however, face the challenge to identify a long-lived sneutrino as the LOSP [233–236], which will be a much more difficult task than, e.g., the identification of a long-lived charged slepton LOSP.

Here the CDM resides mainly in the form of stable gravitinos, which direct and

indirect dark matter detection experiments are not able to see. There seems to be no consensus on whether the signals measured at some of the current direct detection experiments are due to dark matter, so this scenario is not challenged from this side.³

6.3 Analytic Approximation

Here we provide some approximate analytic formulas that illustrate the behavior of the numerical solutions presented above. We start with the dilution factor, where we follow closely Ref. [220]. The equation describing the change in entropy due to the decay of a single heavy particle X reads

$$S^{1/3} \dot{S} = R^4 \left(\frac{2\pi^2}{45} g_{*S} \right)^{1/3} \Gamma_X \rho_X. \quad (6.11)$$

This is the basis of (6.2) in the previous section. Equation (6.11) can be integrated [220] and reads in our notation

$$S^{4/3} = S_i^{4/3} \left\{ 1 + \frac{4}{3} \rho_{X_i} R_i^4 \int_{t_i}^t \left(\frac{2\pi^2}{45} g_{*S} \right)^{1/3} \left[\frac{R(t')}{R_i} \right] e^{-\Gamma_X t'} dt' \right\}. \quad (6.12)$$

where t_i does not necessarily have to be the value we used in our numerical simulation in Sect. 6.1. The main contribution to the total value of the integral comes from the time interval around the decay of X and, therefore, the borders of the integration can be chosen closer to its decay time τ_X . To solve this integral, one needs to know the evolution of the scale factor. This is given by the Friedmann equation and, therefore, depends on the energy content of the Universe. There are two interesting limiting cases for which an approximate solution for the ratio of the entropy before and after the decay can be obtained analytically.

If the decaying particle dominates the energy density of the Universe at the time of its decay, the evolution of the scale factor is the one of a matter dominated Universe, hence $R \propto t^{2/3}$. The approximate solution then is [220]

$$\Delta_{\text{large}} \simeq 1.83 \langle g_{*S} \rangle^{1/4} \frac{m_X Y_X}{(\Gamma_X m_{\text{Pl}})^{1/2}}, \quad (6.13)$$

where $\langle g_{*S} \rangle$ denotes the suitably averaged value of g_{*S} over the integration interval. If g_{*S} is more or less constant during the X decay, one can set $\langle g_{*S} \rangle = g_{*S}(\tau_X)$. As the decaying particle is assumed to dominate the total energy density, $\Delta_{\text{large}} \gg 1$.

³There has been much activity regarding direct and indirect dark matter detection recently. For a more general review, see for example Ref. [237]. A collection of links to experiments and conferences can be found at <http://lpsc.in2p3.fr/mayet/dm.php>.

The other case is characterized by ρ_X being always smaller than the energy density in radiation. The approximation then reads [220]

$$\Delta_{\text{small}} \simeq 1 + 1.61 \left[\frac{\langle g_{*S} \rangle^{1/3}}{g_{*S}(t_i)^{1/12}} \right] \frac{m_X Y_X}{(\Gamma_X m_{\text{Pl}})^{1/2}}. \quad (6.14)$$

Again, one can set $\langle g_{*S} \rangle = g_{*S}(\tau_X)$ if g_{*S} is approximately constant.

Let us now apply these formulas to the case of entropy release from axino decay. Since for all of the parameter points examined in this work, $\rho_{\tilde{a}} < \rho_{\text{rad}}$, and, therefore, the additional entropy $\Delta_{\tilde{a}} = \mathcal{O}(1)$, we use (6.14) to approximate the entropy release from axino decay. We find that our numerical results are well approximated if one sets $g_{*S}(t_i) = g_{*S}(0.01 \tau_{\tilde{a}})$ in (6.14). We substitute the respective quantities for thermal axinos and arrive at

$$\begin{aligned} \Delta_{\tilde{a}} \simeq & 1 + 2.3 \times 10^{-2} \left(\frac{2 \text{ TeV}}{m_{\tilde{a}}} \right)^{1/2} \left(\frac{f_{\text{PQ}}}{10^{10} \text{ GeV}} \right) \\ & \times \left(\frac{Y_{\tilde{a}}^{\text{eq/TP}}}{10^{-3}} \right) \left(\frac{0.1}{\alpha_s} \right) \left[\frac{g_{*S}(\tau_{\tilde{a}})^{1/3}}{g_{*S}(0.01 \tau_{\tilde{a}})^{1/12}} \right] \left(1 - \frac{m_{\tilde{g}}^2}{m_{\tilde{a}}^2} \right)^{-3/2}. \end{aligned} \quad (6.15)$$

For the saxion, matters are a bit more complicated, since the saxion can also decay into inert radiation. The saxion yield relevant for (6.12) is the total thermal yield multiplied by the branching ratio for saxion decays into gluons, gluinos, and photons. If one neglects the branching ratio into photons (2.68) and gluinos (2.69), which are small for the parameter range of interest, the branching ratio into gluons can be obtained from the decay into axions (2.66) and gluons (2.67) and reads

$$\text{BR}(\sigma \rightarrow gg) \simeq \frac{1}{1 + \frac{x^2 \pi^2}{2\alpha_s^2}}. \quad (6.16)$$

Consequently, we use (6.16) in the analytic approximation of the entropy production from saxion decays. Moreover, the entropy release of the saxion depends on x and can be sizable for smaller x . We find that our numerical results are well described by using (6.14) for $x \gtrsim 0.02$ and $\Delta < 10$. The resulting dilution factor reads

$$\begin{aligned} \Delta_{\sigma}^{\text{small}} \simeq & 1 + 1.03 \times 10^{-2} \left(\frac{100 \text{ GeV}}{m_{\sigma}} \right)^{1/2} \left(\frac{f_{\text{PQ}}}{10^{10} \text{ GeV}} \right) \\ & \times \left(\frac{Y_{\sigma}^{\text{eq/TP}}}{10^{-3}} \right) \left[\frac{g_{*S}(\tau_{\sigma})^{1/3}}{g_{*S}(0.01 \tau_{\sigma})^{1/12}} \right] \left[\frac{\alpha_s^2}{(\alpha_s^2 + 0.5 x^2 \pi^2)^{3/2}} \right]. \end{aligned} \quad (6.17)$$

Again, we have used $g_{*S}(t_i) = g_{*S}(0.01 \tau_{\sigma})$ in (6.14). For an analytic treatment of entropy from saxion decay, see also Ref. [65].

If one has the case of two particles decaying and releasing entropy, the final amount of entropy is given by the product of the individual Δ_i .

Let us now turn to the question of inert radiation in the form of axions. In general, the amount of ΔN_{eff} released by the decay of thermal saxions is given by

$$\Delta N_{\text{eff}}^{\sigma \rightarrow aa}(T) = \frac{120}{7\pi^2 T_\nu^4} \left[\frac{g_{*S}(T)}{g_{*S}(T_\sigma)} \right]^{4/3} \left(\frac{T}{T_\sigma} \right)^4 \frac{\text{BR}(\sigma \rightarrow aa) \rho_\sigma^{\text{eq/TP}}}{\Delta}, \quad (6.18)$$

with the temperature at saxion decay given by (5.4). Note that this formula for T_σ relies on the sudden-decay approximation. A realistic treatment results in a reduced ρ_a by $\sim 13\%$, see also [49, 88], since the axions from saxion decays released before τ_σ are more redshifted with respect to the sudden-decay approximation. Thus, we multiply (6.18) by 0.87 and arrive at

$$\begin{aligned} \Delta N_{\text{eff}}^{\sigma \rightarrow aa}(T) \simeq 0.082 \left(\frac{100 \text{ GeV}}{m_\sigma} \right)^{1/2} \left(\frac{f_{\text{PQ}}}{10^{10} \text{ GeV}} \right) \frac{x^2}{(x^2 + 2\alpha_s^2/\pi^2)^{3/2}} \\ \left(\frac{Y_\sigma^{\text{eq/TP}}}{10^{-3}} \right) \frac{1}{\Delta_{\tilde{a}} \Delta_\sigma} \left(\frac{T}{T_\nu} \right)^4 \left[\frac{g_{*S}(T)}{10.75} \right]^{4/3} \frac{g_*(T_\sigma)^{1/4}}{g_{*S}(T_\sigma)^{1/3}}. \end{aligned} \quad (6.19)$$

Now we turn to the gravitino. If the gravitino is the LSP, then the value of its energy density parameter today is given by

$$\Omega_{\tilde{G}}(T_0) h^2 = \frac{\Omega_{\tilde{G}}(T_i) h^2}{\Delta_{\tilde{a}} \Delta_\sigma}, \quad (6.20)$$

where $T_i \gg T_{\tilde{a}}, T_\sigma$.

Chapter 7

Saxion Decays with Axion CDM and Extra Radiation from Gravitinos

This chapter explores the scenario where the axino is the LSP and the gravitino is the NLSP. All other SUSY particles are assumed to be heavier. The CDM is provided by axions from the misalignment mechanism. Decays of both thermal saxions and gravitinos produce extra radiation.

In axino LSP scenarios one often finds restrictive T_R constraints imposed by the dark matter constraint [49–51, 238] and also additional f_{PQ} constraints depending on the properties of the NLSP [227, 238, 239].

The axino - gravitino mass hierarchy used in this chapter was initially introduced to circumvent the limits from gravitino decays injecting energetic particles during BBN. A gravitino NLSP decaying into a light axino with $m_{\tilde{a}} \lesssim \mathcal{O}(1)$ keV allows for high reheating temperatures [48, 149]. The scenario was further analyzed in Ref. [66] for the case of a pure bino neutralino LSP, in Ref. [227, 240] for the case of a stau LSP. Although the former included entropy production from saxion decays, the issue of additional radiation was not addressed.

In Ref. [80] this ΔN_{eff} release by gravitino decay is analyzed. The recent study [82] showed that the amount of ΔN_{eff} released is sizable and provides more stringent upper limits on the reheating temperature. We expand the results of these studies in Sect. 7.1.

In Sect. 7.2, we combine this source of extra radiation with the contribution of axions from decays of thermal saxions to ΔN_{eff} . We include entropy release by the saxion and go beyond the sudden-decay approximation.

Section 7.3 summarizes constraints from collider searches and from current cosmological data and provides an outlook to future observations.

7.1 Extra Radiation from Decaying Gravitinos

The scenario presented in Ref. [48] includes a gravitino NLSP with $m_{\tilde{G}} \approx 100 \text{ GeV}$ and an axino LSP with $m_{\tilde{a}} \lesssim \mathcal{O}(1) \text{ keV}$. A neutralino LSP is taken to decay into axinos and photons and is shown to be cosmologically harmless. This was analyzed for a neutralino that consists mainly of the photino. For the case of a pure bino neutralino, see Ref. [66]. In both cases, the low value of the axino mass allows one to evade overproduction of axino CDM in this scenario.

Here we use an even lighter axino $m_{\tilde{a}} \lesssim 37 \text{ eV}$ to avoid bounds from hot dark matter [227], which are not considered in [48]. Entropy production from saxion decay was briefly addressed in [48], here we provide detailed numerical results later.

The most important point not considered in Ref. [48] is the fact that the decay of the gravitino into axinos and axions produces sizable amounts of extra radiation. This ΔN_{eff} contribution is mentioned in Ref. [80] and the resulting T_{R} limits are analyzed in Ref. [82]. For these axinos and axions from gravitino decay to provide extra radiation, both species need to be relativistic. It is shown in [82] that this is indeed the case for $m_{\tilde{a}} \sim \mathcal{O}(1) \text{ keV}$ and $m_{\tilde{G}} \sim \mathcal{O}(100) \text{ GeV}$. In fact, these axinos are still relativistic today. Due to the small axion mass, the axion is also relativistic. The resulting ΔN_{eff} contribution from gravitino decays is of $\mathcal{O}(1)$ for $m_{\tilde{G}} \sim 100 \text{ GeV}$, $m_{\tilde{a}} \sim 1 \text{ TeV}$, and $T_{\text{R}} \sim 10^{10} \text{ GeV}$.

Let us mention here that although we confirm the findings of [82] regarding the gravitino decay, we show that the saxion can have a sizable influence on T_{R} limits that can be more stringent than the ones from only gravitino decays.

Finally, in our numerical calculation, we go beyond sudden-decay, include the full gravitino production yield (6.6), and include entropy production from saxion decay. The numerical calculation is presented in detail in the next section, but for completeness we give the analytic approximations already here. Thus, in this setup, the temperature at gravitino decay is given by [82]

$$T_{\tilde{G}} = 24 \text{ eV} \left(\frac{m_{\tilde{G}}}{100 \text{ GeV}} \right)^{3/2}, \quad (7.1)$$

which can be obtained with the help of (2.73) in the sudden-decay approximation, if one neglects $m_{\tilde{a}}$. For the gravitino masses considered in our analysis, the gravitino decay happens always after BBN, so when neutrinos are decoupled and $g_{*S} = 3.91$ in standard cosmology. Therefore, the resulting amount of additional radiation is then given by

$$\Delta N_{\text{eff}}^{\tilde{G} \rightarrow \tilde{a}a} \simeq 0.42 \left(\frac{100 \text{ GeV}}{m_{\tilde{G}}} \right)^{1/2} \left(\frac{Y_{\tilde{G}}^{\text{eq/TP}}}{10^{-11}} \right) \frac{1}{\Delta_{\sigma}}. \quad (7.2)$$

As in the case of extra radiation from saxion decays shown in Sect. 6.3, we have multiplied by 0.87 to compensate the use of the sudden-decay approximation in

the analytic formula. Without this correction and for $\Delta_\sigma = 1$ the above estimate reduces to the one given in Ref. [82].

In this chapter the CDM is provided by an axion condensate, thus $f_{\text{PQ}} \simeq 10^{12} \text{ GeV}$. Then, for $x = 0.02$ and $T_{\text{R}} \gtrsim 5 \times 10^{10} \text{ GeV}$, we find parameter regions with $\Delta \gtrsim 10$. There, the entropy release is best described by using the approximation for large entropy release given in (6.13). The resulting approximation reads

$$\Delta_\sigma^{\text{large}} \simeq 19 \left(\frac{100 \text{ GeV}}{m_\sigma} \right)^{1/2} \left(\frac{f_{\text{PQ}}}{10^{12} \text{ GeV}} \right) \left(\frac{Y_\sigma^{\text{eq/TP}}}{10^{-3}} \right) \left(\frac{0.117}{\alpha_s} \right) \left[\frac{g_{*S}(\tau_\sigma)}{10.75} \right]^{1/4}, \quad (7.3)$$

where we set $x = 0$ in Γ_σ and in $\text{BR}(\sigma \rightarrow gg)$. This introduces an error of $< 20\%$ for $x \leq 0.02$.

7.2 Numerical Treatment

As in the previous scenario of Chap. 6, we use a closed set of differential equations to describe the time evolution of the energy densities of the respective particles with entropy injection beyond the sudden-decay approximation. Here the gravitino is unstable and due to R -parity conservation the only decay channel is $\tilde{G} \rightarrow \tilde{a}a$. Since both axions and axinos are non-interacting, relativistic particles that contribute to the amount of additional radiation [82], we treat them as part of the same relativistic energy density, which we call dark radiation ρ_{dr} . Note that axions from the misalignment mechanism are not included in ρ_{dr} , since they behave as cold dark matter rather than radiation. The Boltzmann equations for gravitinos, saxions, and dark radiation read

$$\dot{\rho}_{\tilde{G}} + 3H\rho_{\tilde{G}} = -\Gamma_{\tilde{G}}\rho_{\tilde{G}}, \quad (7.4a)$$

$$\dot{\rho}_\sigma + 3H\rho_\sigma = -\Gamma_\sigma\rho_\sigma, \quad (7.4b)$$

$$\dot{\rho}_{\text{dr}} + 4H\rho_{\text{dr}} = \text{BR}(\sigma \rightarrow aa)\Gamma_\sigma\rho_\sigma + \Gamma_{\tilde{G}}\rho_{\tilde{G}}. \quad (7.4c)$$

In this scenario the only particle whose decay produces entropy is the saxion, so the increase in S is given by

$$S^{1/3}\dot{S} = R^4 \left(\frac{2\pi^2}{45} g_{*S} \right)^{1/3} [1 - \text{BR}(\sigma \rightarrow aa)] \Gamma_\sigma \rho_\sigma. \quad (7.5)$$

The evolution of the scale factor is described by the Friedmann equation in the following form

$$H^2 = \frac{8\pi}{3m_{\text{Pl}}^2} (\rho_{\text{dr}} + \rho_\sigma + \rho_{\tilde{G}} + \rho_{\text{rad}}), \quad (7.6)$$

where ρ_{rad} is given by

$$\rho_{\text{rad}} = \frac{3}{4} \frac{g_*}{g_{*S}} \left(\frac{45}{2\pi^2 g_{*S}} \right)^{1/3} \frac{S^{4/3}}{R^4}. \quad (7.7)$$

Note the different prefactor with respect to (6.4). This change is necessary, because here we deal with decays at times when $g_* \neq g_{*S}$.

A main difference with respect to the gravitino LSP case is that now there are two sources of extra radiation, axions from saxion decays and axions/axinos from gravitino decays, but only one source of entropy release, the saxion.¹ Although both decay rates are suppressed by large scales, since $M_{\text{Pl}} \gg f_{\text{PQ}}$, for $m_\sigma = m_{\tilde{G}}$ the decay of the gravitino happens much later, as can be seen from (2.74). In fact, here the lifetime of the gravitino constrains the common mass scale. We consider $\tau_{\tilde{G}} > 10^3 \text{ s}$, so the decay does not happen during BBN. The corresponding mass limit, $m_{\tilde{G}} < \mathcal{O}(10) \text{ TeV}$, poses no further limitation on our spectrum, if one wants to have observable signatures of SUSY at colliders. The lower limit on $m_{\tilde{G}}$ comes from the non-observation of a significant release of extra radiation after $5.2 \times 10^{10} \text{ s}$ [81], when the smallest observable modes of the CMB reenter the horizon. The corresponding mass limit is $m_{\tilde{G}} > 35 \text{ GeV}$. Since $\tau_\sigma(m_\sigma = 35 \text{ GeV}, x = 0.02) \simeq 0.5 \text{ s}$ for $f_{\text{PQ}} = 10^{12} \text{ GeV}$, we see that the saxion always decays prior to BBN for this mass range, even for small x .

We solve the above differential equations numerically beginning at $t_i = 1.6 \times 10^{-13} \text{ s}$ corresponding to $T_i \simeq 1 \text{ TeV}$ with $R(t_i) = 1 \text{ GeV}^{-1}$, since for the considered parameter range the saxion decays after t_i . The end of the evolution is set at $t_f = 10^{12} \text{ s}$ corresponding to $T_f \simeq 1.1 \text{ eV}$. The Boltzmann equation for axion cold dark matter and their contribution to (7.6) are not included. In fact, including this population explicitly leads to at most an 1-2 % effect in ΔN_{eff} and only in settings with $\tau_{\tilde{G}} \gtrsim 10^{10} \text{ s}$.

$$\rho_{\tilde{G}}(t_i) = s(T_i) m_{\tilde{G}} Y_{\tilde{G}}^{\text{TP}}, \quad (7.8a)$$

$$\rho_\sigma(t_i) = s(T_i) m_\sigma Y_\sigma^{\text{eq/TP}}, \quad (7.8b)$$

$$\rho_{\text{dr}}(t_i) = s(T_i) \langle p_{a,i}^{\text{th}} \rangle Y_a^{\text{eq/TP}}, \quad (7.8c)$$

$$S(t_i) = s(T_i) R(t_i)^3. \quad (7.8d)$$

The initial value of the energy density of dark radiation is clearly only an approximation, as it does not include thermal axinos. Since their contribution to $\Delta N_{\text{eff}} \lesssim 0.017$ [227], this assumption is well justified.

The resulting curves of the numerical integration are shown in Fig. 7.1(a) for the parameter point $m_\sigma = m_{\tilde{G}} = 100 \text{ GeV}$, $T_{\text{R}} = 1.3 \times 10^{10} \text{ GeV}$, $f_{\text{PQ}} = 10^{12} \text{ GeV}$, and $m_{1/2} = 400 \text{ GeV}$. Note that saxion decays into gluinos are kinematically forbidden, because the gravitino is the NLSP here. The evolution of each species is illustrated by the total energy of the respective species per comoving volume, $R^3 \rho_i$. The red curve shows the energy in interacting radiation, the orange one depicts the saxion,

¹Note that in the kinetic terms mentioned in Ref. [47], a saxion-axino-axino vertex is present. The associated decay width of $\sigma \rightarrow \tilde{a}\tilde{a}$ is, however, proportional to $m_{\tilde{a}}^2 m_\sigma$ and, therefore, negligible in our scenario.

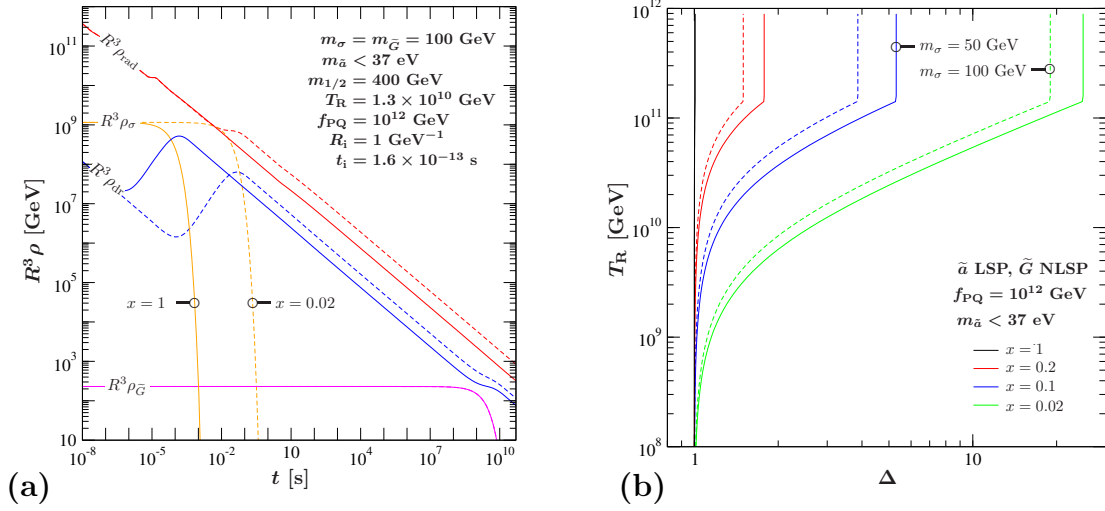


Figure 7.1: **(a):** Evolution of the comoving energy density of saxions, dark radiation, gravitinos, and interacting radiation over cosmic time. Here $m_\sigma = m_{\tilde{G}} = 100$ GeV, $m_{\tilde{a}} < 37$ eV, $m_{1/2} = 400$ GeV, $T_R = 1.3 \times 10^{10}$ GeV, and $f_{\text{PQ}} = 10^{12}$ GeV. The starting value of the scale factor $R_i = 1 \text{ GeV}^{-1}$. The red line shows the comoving energy density of interacting radiation, the orange curves the one of the saxion, the blue line the one of the dark radiation and the magenta one is the gravitino energy density. Lines are drawn solid (dashed) for $x = 1$ (0.02).

(b): The dilution factor $\Delta = S(t_f)/S(t_i)$ versus the reheating temperature T_R . Here $f_{\text{PQ}} = 10^{12}$ GeV, $m_{\tilde{a}} < 37$ eV, and $m_{\tilde{g}} = 1$ TeV. The black, red, blue, and green lines show the contour for $x = 1, 0.2, 0.1$, and 0.02 , respectively. Lines are drawn solid (dashed) for $m_\sigma = 50$ (100) GeV.

the blue one shows the energy of dark radiation and the magenta line shows the gravitino energy per comoving volume. The lines are drawn solid (dashed) for $x = 1$ (0.02).

Although we do not explicitly draw the entropy curve in Fig. 7.1(a), the dilution effect is visible by the difference between the two red curves by the slower decrease of the temperature due to entropy injection. The T_R dependence of the corresponding dilution factor Δ is shown in Fig. 7.1(b). Here we also choose $f_{\text{PQ}} = 10^{12}$ GeV and $m_{\tilde{g}} = 1$ TeV. The black, red, blue, and green curves show Δ for $x = 1, 0.2, 0.1$, and 0.02 , respectively. The lines are drawn solid (dashed) for $m_\sigma = 50$ (100) GeV. The kink in the Δ curves is due to the change in the T_R dependence of the saxion yield at saxion freeze-out as already described in the previous section. Note that the amount of released electromagnetic entropy is much larger than in the previous section because here $f_{\text{PQ}} = 10^{12}$ GeV.

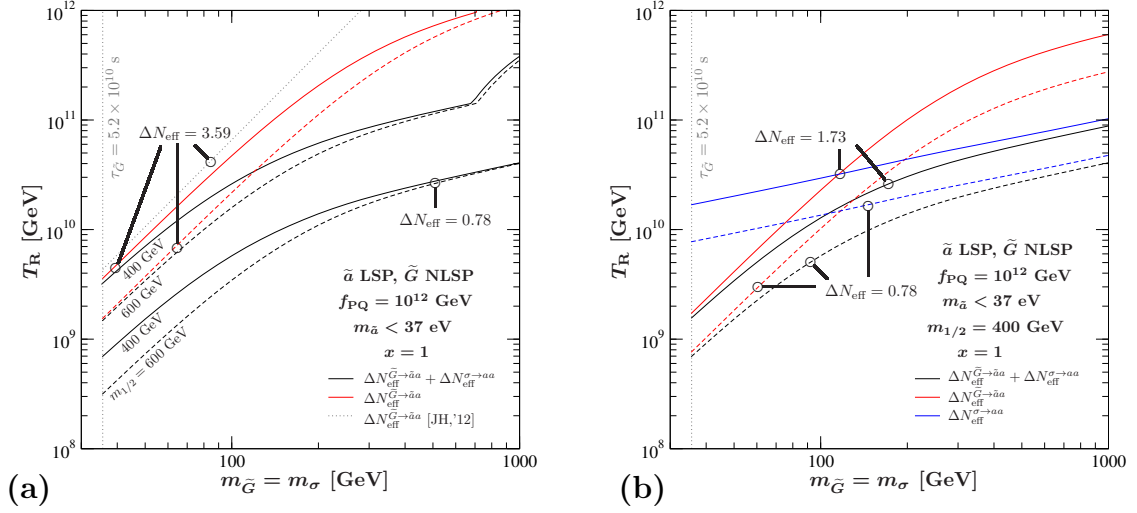


Figure 7.2: **(a):** Contours of ΔN_{eff} provided by decays of thermal saxions and gravitinos in the $m_{\tilde{G}} - T_R$ parameter plane. Here $f_{\text{PQ}} = 10^{12}$ GeV and $x = 1$. The black lines show, as labeled, $\Delta N_{\text{eff}} = 3.59$ and 0.78 , from the sum of ΔN_{eff} released by saxion and gravitino decay. The red lines show the contribution from the gravitino only. The diagonal dotted line is the result from [82] for $m_{\tilde{g}} = 1$ TeV. Contours are drawn solid (dashed) for $m_{1/2} = 400$ (600) GeV. The vertical dotted line shows the lower $m_{\tilde{G}}$ limit from $\tau_{\tilde{G}} \lesssim 5.2 \times 10^{10}$ s.

(b): Contours of ΔN_{eff} provided by decays of thermal saxions and gravitinos. Here $f_{\text{PQ}} = 10^{12}$ GeV, $m_{1/2} = 400$ GeV, and $x = 1$. The solid (dashed) lines show $\Delta N_{\text{eff}} = 1.73$ (0.78). The red (blue) line shows the contribution from the gravitino (saxion) only. The black contour shows the sum of both ΔN_{eff} contributions. The vertical dotted line shows the lower $m_{\tilde{G}}$ limit from $\tau_{\tilde{G}} \lesssim 5.2 \times 10^{10}$ s.

7.2.1 Extra Radiation for $x = 1$

As already described above, in this scenario axions from decaying thermal saxions contribute to ΔN_{eff} prior to BBN. In Fig. 7.1(a), the parameters are chosen such that this contribution is close to the posterior maximum of the BBN analysis performed in Sect. 5.3, i.e. $\Delta N_{\text{eff}}^{\sigma \rightarrow aa} \simeq 0.7$ for $x = 1$. The other contribution is due to the gravitino decay happening much later, as can be seen in the figure. The parameters are such that $\Delta N_{\text{eff}}^{\tilde{G} \rightarrow \tilde{a}a} \simeq 1$, so that the sum of both equals 1.7, the mean of the BBN + LSS study quoted in Table 5.2. Moreover, since here the gravitino can not be dark matter, we have set $f_{\text{PQ}} = 10^{12}$ GeV in order to allow for axion CDM. Figure 7.1(a) illustrates the explanation of two different contributions to ΔN_{eff} released at different times. Interestingly, current BBN and CMB + LSS analyses mentioned in Chap. 5 suggest the existence of such a difference, so these hints possibly indicate the realization of such a scenario in nature.

In Fig. 7.2(a) we show ΔN_{eff} contours in the $m_{\tilde{G}}-T_R$ parameter plane. The lower mass limit, $m_{\tilde{G}} > 35 \text{ GeV}$ from $\tau_{\tilde{G}} < 5.2 \times 10^{10} \text{ s}$, is indicated by the vertical gray dotted line. Here we use $f_{\text{PQ}} = 10^{12} \text{ GeV}$ and $x = 1$. The red line shows the dark radiation contribution from the gravitino decay amounting to $\Delta N_{\text{eff}} = 3.59$. The black lines show the sum of the contributions from gravitino and saxion decays resulting in $\Delta N_{\text{eff}} = 3.59$ and 0.78 , as labeled. The lines are drawn solid (dashed) for $m_{1/2} = 400$ (600) GeV. The diagonal dotted line shows the result of Ref. [82] for $m_{\tilde{g}} = 1 \text{ TeV}$. The difference is due to the inclusion of electroweak processes and spin-3/2 contributions to the thermal gravitino production and the treatment beyond sudden-decay approximation in our calculations. The electroweak contributions increase the initial gravitino yield by $\sim 20 \%$, the spin-3/2 component further enhance the yield towards higher masses, whereas the sudden-decay approximation overestimates the resulting ΔN_{eff} contribution by $\sim 10 \%$.

The $\Delta N_{\text{eff}} = 3.59$ contours in Fig. 7.2(a) show the current upper limit on the total amount of extra radiation present at late times. One can see that for the chosen value of f_{PQ} the contributions from saxion decays are not negligible. In fact, for $m_{\sigma} \gtrsim 100 \text{ GeV}$ they tighten the T_R limit coming from the gravitino by up to almost one order of magnitude. In the sudden-decay approximation, this behavior of the ΔN_{eff} from saxion decay can be seen in Fig. 5.3. As in the previous scenario, this limit will be tested further by the upcoming Planck data. If Planck should find a mean of $\Delta N_{\text{eff}} = 0$, then the contour $\Delta N_{\text{eff}} = 0.78$ shows the expected 3σ upper limit inferred from the measurement. This would restrict T_R even more.

After having discussed the exclusion bounds on T_R from ΔN_{eff} in this scenario, let us now discuss the amount of extra radiation released at different times in greater detail. As mentioned above, the difference between the hints for an early released ΔN_{eff} , as suggested by BBN, and a late one, suggested by CMB + LSS analyses, points towards parameters where $\Delta N_{\text{eff}}^{\sigma \rightarrow aa} = 0.78$ and $\Delta N_{\text{eff}}^{\text{total}} = 1.73$. Such parameter regions are indicated in Fig. 7.2(b), where $f_{\text{PQ}} = 10^{12} \text{ GeV}$ and $m_{1/2} = 400 \text{ GeV}$. Solid (dashed) lines show $\Delta N_{\text{eff}} = 1.73$ (0.78). The red lines show the contribution from gravitino decay, the blue ones the contribution from saxion decay and the black contours show the sum of both. Again, the vertical dotted line is the lower $m_{\tilde{G}}$ limit.

The parameter points where $\Delta N_{\text{eff}}^{\sigma \rightarrow aa} = 0.78$ and $\Delta N_{\text{eff}}^{\text{total}} = 1.73$ are exactly fulfilled are indicated by the intersection of the blue dashed $\Delta N_{\text{eff}} = 0.78$ and the black solid $\Delta N_{\text{eff}} = 1.73$ contour. These points provide a scenario that explains the hints for extra radiation given in Table 5.2.

7.2.2 Extra Radiation for $x < 1$

Let us now turn to the case of $x < 1$. As in the previous chapter, the amount of released extra radiation increases for smaller x , until the maximum is reached at $x \simeq 0.1$, for even smaller x , the resulting ΔN_{eff} decreases again. The amount of

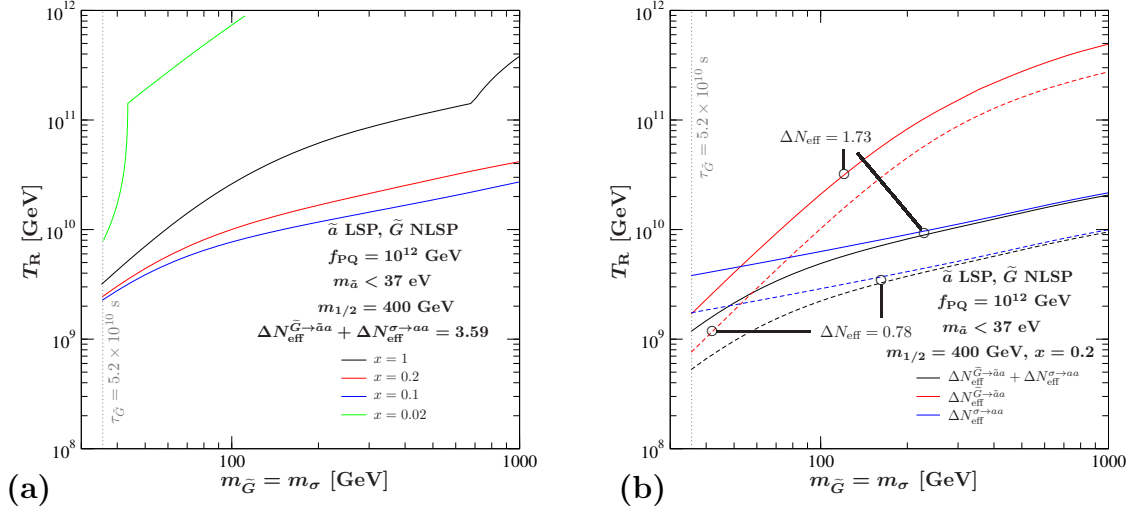


Figure 7.3: **(a):** Contour $\Delta N_{\text{eff}} = 3.59$ resulting from the sum of extra radiation from decays of thermal saxions and gravitinos. Here $f_{\text{PQ}} = 10^{12}$ GeV and $m_{1/2} = 400$ GeV. The black, red, blue, and green lines show the ΔN_{eff} contour for $x = 1, 0.2, 0.1$, and 0.02 , respectively. The vertical dotted line shows the lower $m_{\tilde{G}}$ limit from the requirement $\tau_{\tilde{G}} \lesssim 5.2 \times 10^{10}$ s.

(b): Contours of ΔN_{eff} provided by decays of thermal saxions and gravitinos in the $m_{\tilde{G}}-T_R$ parameter plane. Here $f_{\text{PQ}} = 10^{12}$ GeV, $m_{1/2} = 400$ GeV, and $x = 0.2$. The solid (dashed) lines show, as labeled, $\Delta N_{\text{eff}} = 1.73$ (0.78). The black contour shows the sum of extra radiation released by saxion and gravitino decay. The red (blue) line shows the contribution from the gravitino (saxion) only. The vertical dotted line shows the lower $m_{\tilde{G}}$ limit from the requirement $\tau_{\tilde{G}} \lesssim 5.2 \times 10^{10}$ s.

extra entropy is increasing with decreasing x . These effects can be seen in Fig. 7.3(a), where we show the contours of the sum of extra radiation from gravitino and saxion decays amounting to $\Delta N_{\text{eff}} = 3.59$ in the $m_{\tilde{G}}-T_R$ parameter plane. Here $f_{\text{PQ}} = 10^{12}$ GeV and $m_{1/2} = 400$ GeV. The black, red, blue, and green lines show the ΔN_{eff} value for $x = 1, 0.2, 0.1$, and 0.02 , respectively. The vertical gray dotted line shows the lower limit on $m_{\tilde{G}}$.

The difference between the black and the blue line shows the effect of decreasing x and, therefore, T_R is much stronger constrained from above. Note, however, that even for $x = 0.1$ thermal leptogenesis with $T_R \simeq 10^9$ GeV is still possible for all gravitino masses analyzed here. This will not be excluded easily by increasing limits on $m_{1/2}$ bearing in mind that the effect of an increase of $m_{1/2}$ affects mainly the region with lower $m_{\tilde{G}}$, see Fig. 7.2(a). When analyzing the viability of thermal leptogenesis in the presence of entropy release, a higher reheating temperature is needed, as shown in (6.10), because also the baryon asymmetry gets diluted.

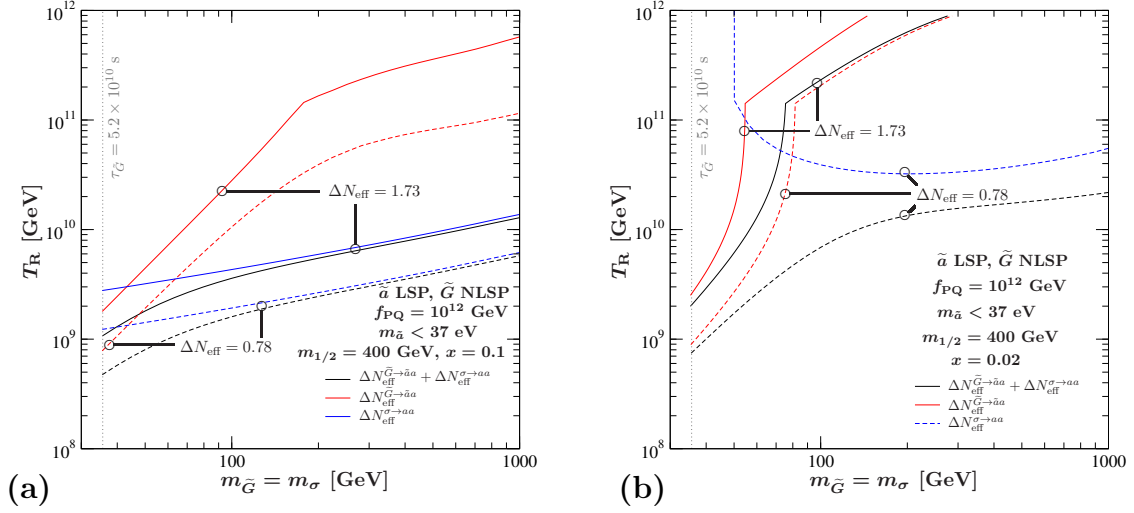


Figure 7.4: **(a)**: Same as Fig. 7.3(b), but for $x = 0.1$.
(b): Same as Fig. 7.3(b), but for $x = 0.02$.

On the other hand, for $x = 0.02$, the limit from too much extra radiation is significantly softened. This is due to the high amount of entropy released by the saxion decay, see Fig. 7.1(b). The maximum of ΔN_{eff} from saxion decay is actually not in the top right corner of the parameter space as it is the case for scenarios with lower entropy release. Instead, the maximum happens to be around $m_{\sigma} \simeq 400$ GeV and for T_R above T_D^{σ} . Therefore, the extra radiation depicted by the green line in Fig. 7.3(a) results mainly from gravitino decays. The kink at $T_R > 10^{11}$ GeV is due to saxion freeze-out, just more pronounced here than in the plots in the previous chapter.

As in the $x = 1$ case, we look at parameter points where $\Delta N_{\text{eff}}^{\sigma \rightarrow a a} = 0.78$ and $\Delta N_{\text{eff}}^{\text{total}} = 1.73$. Those are shown in Figs. 7.3(b), and 7.4(a), (b). In each plot we set $f_{\text{PQ}} = 10^{12}$ GeV and $m_{1/2} = 400$ GeV and show solid (dashed) lines for $\Delta N_{\text{eff}} = 1.73$ (0.78). The value of $x = 0.2, 0.1$, and 0.02 in Figs. 7.3(b), and 7.4(a), (b), respectively. Note that there is no $\Delta N_{\text{eff}}^{\sigma \rightarrow a a} = 1.73$ contour in Fig. 7.4(b) because the above mentioned maximum ΔN_{eff} from saxion decay is smaller than 0.94 for $x = 0.02$. Colors are the same as in Fig. 7.2(b).

The entropy released by saxion decays also dilutes the amount of CDM formed by an axion condensate here. The energy density of these cold axions is given by (5.24). Since θ_i can be as large as π and given the theoretical uncertainties in (5.24), misalignment axions can still provide enough CDM for $f_{\text{PQ}} = 10^{12}$ GeV, even for $\Delta = \mathcal{O}(10)$.

Let us now examine the results of a possible difference between $m_{\tilde{G}}$ and m_{σ} . We consider the mass scale in all our figures fixed to $m_{\tilde{G}}$ and vary m_{σ} . Increasing

(decreasing) m_σ relative to $m_{\tilde{G}}$ moves the $\Delta N_{\text{eff}}^{\sigma \rightarrow aa}$ contours in Figs. 7.2, 7.3 and 7.4 to the left (right). The gray dotted line indicating $\tau_{\tilde{G}} = 5.2 \times 10^{10} \text{ s}$ is not affected. Also the red lines indicating the $\Delta N_{\text{eff}}^{\tilde{G} \rightarrow aa}$ in Figs. 7.2(a) and 7.3(a) do not change. When the total amount of ΔN_{eff} is dominated by saxion contributions, the black lines depicting the sum in Figs. 7.2(a), (b), and 7.3(a) change as the $\Delta N_{\text{eff}}^{\sigma \rightarrow aa}$ contours. If the sum is dominated by contributions from gravitino decay, the lines do not change.

For $x < 1$, the entropy release from saxion decays becomes sizable and, therefore, there is a change in the $\Delta N_{\text{eff}}^{\tilde{G} \rightarrow aa}$ contours depending on m_σ in Figs. 7.3(b) and 7.4(a) and (b). Thus, increasing m_σ gives less released entropy and results in a qualitative change of the $\Delta N_{\text{eff}}^{\tilde{G} \rightarrow aa}$ contours comparable to the change when increasing x , and vice versa. The red, blue, and green curves in in Fig. 7.3(a) change accordingly.

7.3 Limits from Colliders and from Cosmology

After offering explanations for the hints given in Table 5.2, let us comment on the testability of this scenario at colliders. Since the axino and the gravitino are very hard to detect, the strongest limits again come from LOSP searches. As in the previous chapter, $m_{\tilde{G}} < m_{\text{LOSP}}$. Note that since the shown range for $m_{\tilde{G}}$ is larger here, a possible discovery will notably constrain the common mass scale. The limits from the early enough decay of the LOSP depend on f_{PQ} and are in general less restrictive in this scenario. For example, if the LOSP is the lightest stau with $m_{\tilde{\tau}_1} = 300 \text{ GeV}$, there is indeed no limit on $m_{\tilde{G}}$ for $f_{\text{PQ}} < 5 \times 10^{12} \text{ GeV}$ [227]. In fact, this upper limit on f_{PQ} together with the requirement $\Omega_a^{\text{MIS}} \simeq \Omega_{\text{CDM}}$ leading to $f_{\text{PQ}} \gtrsim 10^{12}$ for a natural initial misalignment $\theta_i \simeq 1$ motivates the choice of the PQ scale in this scenario. Interestingly, this range of f_{PQ} is currently being probed by ADMX [216]. A detection of axions there together with a discovery of extra radiation would, therefore, point towards the realization of this scenario rather than the previous one.

The lower limit on $m_{\tilde{G}}$ can improve in the future with more precise measurements of the CMB and LSS. It could even be that future cosmological analyses find hints on the time of the release of extra radiation. Such a release should manifest itself in the perturbation spectrum, so precision cosmology might pin down the lifetime of a heavy particle like the gravitino that produces radiation at times before $5.2 \times 10^{10} \text{ s}$.

The strongest hint for this scenario would, however, be the detection of extra radiation both at BBN and at later times, with a significant difference between the two values. The upcoming results of the Planck mission are expected to have the necessary sensitivity to allow for the detection of a mean $\Delta N_{\text{eff}} \gtrsim 1.6$ with a statistical significance of 3σ at late times. For ΔN_{eff} at BBN, current observations are not sensitive enough. Applying new statistical methods analyzing existing data sets improves the reliability of the results, but does not yield significant evidence for

excess radiation [203, 204]. The availability of new, high quality spectra of He and H emission lines in HII regions, however, would allow for a more precise determination of ΔN_{eff} prior to BBN [204]. Together with all the limits and detection possibilities mentioned above, we can hope for a proof or the exclusion of axions from decaying thermal saxions in the foreseeable future.

Chapter 8

Summary and Conclusion

The axion arises as a consequence of the PQ mechanism, which is still the most elegant solution of the strong CP problem. In a non-SUSY version of axion models, a very important cosmological consequence of the PQ mechanism is an axion condensate that can provide the dark matter. For smaller values of the PQ breaking scale f_{PQ} , thermal axions are hot dark matter and provide lower limits on f_{PQ} [36, 166].

A supersymmetric version of axion models introduces the saxion as a cosmologically interesting particle. In Chap. 2, we have shown how axion and saxion interactions in supersymmetric hadronic axion models arise and provide a low energy effective Lagrangian in Eq. (2.59). We have traced carefully the relation of the low energetic axion parameters to the ones of the fundamental PQ fields.

There are two scales involved: The normalization parameter v_{PQ} of the scalar PQ fields around their VEVs, which is defined in terms of the PQ charges and the VEVs of the fundamental PQ fields via the requirement of canonically normalized kinetic terms. The other parameter f_{PQ} is defined by the usual form of the low-energy effective interaction term of the axion. Both scales are related via loops of heavy quarks. We find the relation $f_{\text{PQ}} = \sqrt{2} v_{\text{PQ}}$, in contrast to numerous existing studies that treat v_{PQ} and f_{PQ} synonymously. This allows, e.g., for a meaningful comparison of the saxion decay rate into axions, involving the former scale, and the decay rate into gluons, involving the latter.

Starting from these low-energy interaction terms, we have calculated the thermal production rate of saxions, axions, and an update for the thermal axino production rate in a hot primordial quark-gluon-squark-gluino plasma in Chap. 3. We have used the HTL resummation technique [150] and the Braaten–Yuan description [151] to arrive at a finite result in a gauge-invariant way consistent to leading order in the strong coupling constant. Following [151], we have divided the production rate of the saxion into a hard part and a soft part. The sum of both yields the collision term (3.27), one of our main results.

The production rate of the axion in a SUSY plasma turns out to be identical to the

one of the saxion, in the limit that all masses can be neglected. In case of the axino, we have included the axino-squark-squark-gluino vertex overlooked in Ref. [50] and arrive at a new collision term. For all three PQ particles, we show the thermal yield and the decoupling temperature.

There is another source of saxions, similar to the case of axions. The saxion potential has a flat direction in the limit of unbroken SUSY. This direction gets lifted by SUSY breaking effects, and a minimum occurs, around which the saxion field oscillates. To provide a meaningful comparison of the resulting energy density with the thermal one, we have linked both calculations to the decay width of the inflaton in Sects. 3.5 and 4.1. For the initial displacement of the saxion field $\sigma_i = f_{\text{PQ}}/2$, $f_{\text{PQ}} \lesssim 10^{12}$ GeV, and $m_\sigma \gtrsim 0.1$ GeV, the energy density from thermal saxions is larger than the one of saxions from the misalignment mechanism. Armed with these results, we have investigated some of the possible cosmological consequences of the PQ particles in the remainder of Chap. 4. We find that saxions with a lifetime $\tau_\sigma > 1$ s are severely restricted and are likely to be incompatible with a high T_{R} scenario, especially when the saxion decays not only into axions. Therefore, we have mainly focused on scenarios with $\tau_\sigma \lesssim 1$ s.

A central cosmological observable is the number of additional light effective neutrino species ΔN_{eff} present at BBN and much later at the formation of the CMB. Axions from decaying thermal saxions can contribute to this amount of extra radiation and, therefore, we could link the parameters of the SUSY hadronic axion model to this observable in Chap. 5. In fact, there are hints in the literature towards the existence of extra radiation at the time of CMB formation, as inferred from CMB + LSS analyses, see e.g., Ref. [69].

In the case of BBN, we have computed ΔN_{eff} values using the publicly available code **ParthENoPE** [207] and recent measurements of the ^4He [72,73] and D [206] abundance together with the recently updated neutron lifetime [12]. We have performed a likelihood analysis to arrive at posterior maxima $\Delta N_{\text{eff}}^{\text{p.m.}} \simeq 0.77$ and upper limits that also point towards the existence of additional radiation, in accordance with results in the literature. Taking these hints at face value, we provide an explanation for $\Delta N_{\text{eff}} > 0$ via axions coming from decaying thermal saxions. In the considered range, $6 \times 10^8 \text{ GeV} \lesssim f_{\text{PQ}} \lesssim 10^{12} \text{ GeV}$, this explanation requires high reheating temperatures $T_{\text{R}} \gtrsim 10^7 \text{ GeV}$ and saxion masses $m_\sigma \gtrsim 1 \text{ GeV}$.

We have also used the inferred upper limits on ΔN_{eff} to constrain significant parts of the parameter space of the considered SUSY axion model. Nevertheless, we find that our limits leave open a considerable parameter region previously thought to be excluded [64]. The results of the Planck mission expected to be released very soon will likely be able to access a significant part of this open parameter range.

If a SUSY hadronic axion model is realized in nature, at least three different axion populations will be present today: thermally produced/thermal relic axions, non-thermally produced axions from decays of thermal saxions, and the axion condensate

from the misalignment mechanism. We have calculated and compared the associated density parameters. The results allow us to infer the axion analog of the Lee–Weinberg curve. For $f_{\text{PQ}} \gtrsim 10^{12}$ GeV and an initial axion misalignment angle of $\theta_i \sim 1$, the axion density parameter is governed by the axion condensate. In that parameter region this population may be accessible in direct axion dark matter searches. For smaller f_{PQ} and smaller θ_i , axions from saxion decays can dominate the axion density parameter. While it will be extremely challenging to probe thermal axions, Planck may confirm ΔN_{eff} signals of this non-thermally produced population in the full allowed f_{PQ} range.

Note that the presented explanation of the hints for $\Delta N_{\text{eff}} > 0$ requires a high T_{R} and can, therefore, be subject to other limitations from, e.g., the gravitino. In order to include this, we performed a detailed numerical analysis including the PQ particles and the gravitino, where we took entropy production by the decay of the axino and the saxion into account. We use $m_{\tilde{G}} = m_{\sigma}$ and present two scenarios, that both explain CDM and extra radiation:

- Gravitino LSP, heavy axino (Chapter 6): Here the gravitino provides the majority of CDM and, therefore, T_{R} is constrained from above due to gravitino overproduction. The axino is heavy in order to decay before LOSP decoupling, which happens at the temperature $T_{\text{D}}^{\text{LOSP}} \simeq m_{\text{LOSP}}/25$. For example, for $f_{\text{PQ}} = 10^{11}$ GeV, we take $m_{\tilde{a}} = 6$ TeV to allow for $m_{\text{LOSP}} \simeq 250$ GeV with $m_{\tilde{g}} = 1$ TeV. Limits from collider searches and BBN require the LOSP to be a sneutrino. For $x = 1$, so when the saxion decays almost completely into axions, we find that $\Delta N_{\text{eff}} = 0.78$ is almost entirely excluded by gravitino overproduction. Nevertheless, $\Delta N_{\text{eff}} = 0.52$, which equals the expected 2σ error of the Planck mission, is still viable. Note that baryogenesis through thermal leptogenesis [224] is possible in this scenario for $f_{\text{PQ}} \sim 10^{11}$ GeV, since $T_{\text{R}} \gtrsim 10^9$ GeV, should such a ΔN_{eff} value be discovered.

For $x < 1$, the amount of ΔN_{eff} released can be significantly larger. Here, even the mean $\Delta N_{\text{eff}} = 1.73$ from the CMB + LSS study in Ref. [69] can be explained by axions from thermal saxions. This is due to the higher amount of entropy released by saxion decays that dilute the gravitino abundance and the later decay of the saxion. Also here thermal leptogenesis is viable, because $T_{\text{R}} \gtrsim 10^9$ GeV can be achieved easily for $f_{\text{PQ}} \sim 10^{11}$ GeV.

- Axino LSP, gravitino NLSP (Chapter 7): Here the axino is light, $m_{\tilde{a}} \lesssim 37$ eV, in order to avoid hot dark matter constraints. A late decaying gravitino produces axions and axinos [82], which contribute to ΔN_{eff} in addition to the axions from saxion decay. In this scenario, the CDM is provided by axions from the misalignment mechanism and, therefore, $f_{\text{PQ}} \simeq 10^{12}$ GeV is required. Remarkably, the ongoing direct axion CDM search by ADMX [216] is sensitive in exactly that f_{PQ} range and may find signals supporting this CDM expla-

nation in the near future. The gravitino has to decay before CMB formation, thus $m_{\tilde{G}} > 35 \text{ GeV}$. The resulting total ΔN_{eff} limits T_{R} from above.

Note that in this scenario additional radiation is released at two very different times: An early release prior to BBN from decaying saxions (along with some entropy) and a late one after BBN by decaying gravitinos. This results in two different values for ΔN_{eff} , one at BBN and a second larger one later. Interestingly, such a difference may be suggested by the hints provided by BBN and CMB + LSS analyses and given in Table 5.2. An explanation of these hints is naturally achieved in our scenario for both $x = 1$ and $x < 1$. In all of these cases, $T_{\text{R}} \gtrsim 10^9 \text{ GeV}$, and thus thermal leptogenesis can be used to explain the baryon asymmetry of the Universe, although the dilution due to entropy from saxion decays can be sizable.

With upcoming new results from the direct axion dark matter search experiment ADMX, the Planck satellite mission, and the LHC, it will be exciting to see further hints for or against the viability of the considered scenarios soon.

Appendix A

Notations and Conventions

Our notation and conventions follow Ref [121], except for a different sign convention of the ϵ tensor. Here we summarize our notation.

We work with natural units, so with

$$\hbar = c = 1. \quad (\text{A.1})$$

The sign convention of the Lorentz metric for a flat spacetime we use is

$$\eta_{\mu\nu} = \eta^{\mu\nu} = \text{diag}(+1, -1, -1, -1), \quad (\text{A.2})$$

where Greek indices $\mu, \nu, \dots = 0, \dots, 3$ denote spacetime indices. The sign of the totally antisymmetric tensor $\epsilon^{\mu\nu\rho\sigma}$ is set to

$$\epsilon^{0123} = +1. \quad (\text{A.3})$$

A.1 Pauli and Dirac Matrices

The Dirac γ matrices form a Clifford algebra and satisfy the anticommutation relation

$$\{\gamma^\mu, \gamma^\nu\} = 2\eta_{\mu\nu}\mathbb{1}. \quad (\text{A.4})$$

For the discussion of SUSY it is convenient to use the Weyl basis to express these γ matrices

$$\gamma^\mu = \begin{pmatrix} 0 & \sigma^\mu \\ \bar{\sigma}^\mu & 0 \end{pmatrix} \quad (\text{A.5})$$

with

$$\begin{aligned} \sigma^0 &= \bar{\sigma}^0 = \begin{pmatrix} 1 & 0 \\ 0 & 1 \end{pmatrix}, & \sigma^1 &= -\bar{\sigma}^1 = \begin{pmatrix} 0 & 1 \\ 1 & 0 \end{pmatrix}, \\ \sigma^2 &= -\bar{\sigma}^2 = \begin{pmatrix} 0 & -i \\ i & 0 \end{pmatrix}, & \sigma^3 &= -\bar{\sigma}^3 = \begin{pmatrix} 1 & 0 \\ 0 & -1 \end{pmatrix}. \end{aligned}$$

This reads in the more compact notation

$$\sigma^\mu = (\mathbb{1}, \sigma^i), \quad (\text{A.6a})$$

$$\bar{\sigma}^\mu = (\mathbb{1}, -\sigma^i). \quad (\text{A.6b})$$

We define the combination

$$\sigma^{\mu\nu} \equiv \frac{i}{4}(\sigma^\mu \bar{\sigma}^\nu - \sigma^\nu \bar{\sigma}^\mu), \quad (\text{A.7a})$$

$$\bar{\sigma}^{\mu\nu} \equiv \frac{i}{4}(\bar{\sigma}^\mu \sigma^\nu - \bar{\sigma}^\nu \sigma^\mu). \quad (\text{A.7b})$$

From this it follows that

$$\gamma^5 = i\gamma^0\gamma^1\gamma^2\gamma^3 = \begin{pmatrix} -\mathbb{1} & 0 \\ 0 & \mathbb{1} \end{pmatrix}. \quad (\text{A.8})$$

A.2 Weyl Spinors

To describe supersymmetry, it is very convenient to write the Lagrangian in two-component Weyl notation. A two-component Weyl spinor ξ_A transforms under Lorentz transformations as

$$\xi'_A = M_A^B \xi_B, \quad (\text{A.9})$$

and a right chiral one $\bar{\xi}_{\dot{A}}$ as

$$\bar{\xi}'_{\dot{A}} = (M^*)_{\dot{A}}^{\dot{B}} \bar{\xi}_{\dot{B}}, \quad (\text{A.10})$$

where M is a two-dimensional matrix representing the Lorentz transformations. The two sets of spinor indices are $A = 1, 2$ and $\dot{A} = 1, 2$. Weyl spinor indices are raised and lowered using the antisymmetric symbol

$$\epsilon^{AB} = \epsilon^{\dot{A}\dot{B}} = \begin{pmatrix} 0 & 1 \\ -1 & 0 \end{pmatrix}, \quad \epsilon_{AB} = \epsilon_{\dot{A}\dot{B}} = \begin{pmatrix} 0 & -1 \\ 1 & 0 \end{pmatrix}.$$

The spinor ξ_A is the Hermitian conjugate of $\bar{\xi}_{\dot{A}}$. Lorentz invariant bilinears can be formed as

$$\xi\chi \equiv \xi^A \chi_A = \chi^A \xi_A = \chi\xi, \quad (\text{A.11a})$$

$$\bar{\xi}\bar{\chi} \equiv \bar{\xi}_{\dot{A}} \bar{\chi}^{\dot{A}} = \bar{\chi}_{\dot{A}} \bar{\xi}^{\dot{A}} = \bar{\chi}\bar{\xi} = (\chi\xi)^\dagger \quad (\text{A.11b})$$

and repeated indices contracted like A_A and $_{\dot{A}}^{\dot{A}}$ are suppressed by convention.

Other important combinations are $\xi\sigma^\mu\bar{\chi} = (\chi\sigma^\mu\bar{\xi})^\dagger$ and $\bar{\chi}\bar{\sigma}^\mu\xi = (\bar{\xi}\bar{\sigma}^\mu\chi)^\dagger$. The σ^μ matrix satisfies

$$\sigma_{A\dot{B}}^\mu = \epsilon_{AC}\epsilon_{\dot{A}\dot{D}}\bar{\sigma}^{\mu\dot{D}C}. \quad (\text{A.12})$$

Further identities we use in calculations in Appendix B are given there and can be found in the literature.

A.3 Dirac and Majorana Spinors

A four-component Dirac spinor Ψ is given in terms of two two-component Weyl spinors ξ and χ as

$$\Psi = \begin{pmatrix} \xi_A \\ \bar{\chi}^{\dot{A}} \end{pmatrix}, \quad (\text{A.13})$$

and

$$\bar{\Psi} = \Psi^\dagger \gamma^0 = (\chi^B \quad \bar{\xi}_{\dot{A}}). \quad (\text{A.14})$$

With the chiral projection operators

$$P_L = \frac{1}{2}(1 - \gamma^5), \quad \text{and} \quad P_R = \frac{1}{2}(1 + \gamma^5)$$

one finds

$$P_L \Psi = \begin{pmatrix} \xi_A \\ 0 \end{pmatrix}, \quad P_R \Psi = \begin{pmatrix} 0 \\ \bar{\chi}^{\dot{A}} \end{pmatrix}.$$

Therefore ξ_A is called a left-chiral Weyl spinor and $\bar{\chi}^{\dot{A}}$ a right-chiral one.

The charge conjugation of a Dirac spinor is defined as

$$\Psi^C = C \bar{\Psi}^T = \begin{pmatrix} \chi_A \\ \bar{\xi}^{\dot{A}} \end{pmatrix}, \quad (\text{A.15})$$

where the charge conjugation matrix $C = i\gamma^2\gamma^0$.

A four spinor λ_M that satisfies the constraint

$$\lambda_M^C = \lambda_M \quad (\text{A.16})$$

is a Majorana four spinor with

$$\lambda_M = \begin{pmatrix} \lambda_A \\ \bar{\lambda}^{\dot{A}} \end{pmatrix}. \quad (\text{A.17})$$

The following identities can be used to convert two-component expressions into four-component ones:

$$\bar{\Psi}_1 \Psi_2 = \chi_1 \xi_2 + \bar{\xi}_1 \bar{\chi}_2, \quad (\text{A.18a})$$

$$\bar{\Psi}_1 \gamma^5 \Psi_2 = -\chi_1 \xi_2 + \bar{\xi}_1 \bar{\chi}_2, \quad (\text{A.18b})$$

$$\bar{\Psi}_1 \gamma^\mu \Psi_2 = \chi_1 \sigma^\mu \bar{\chi}_2 + \bar{\xi}_1 \bar{\sigma}^\mu \xi_2, \quad (\text{A.18c})$$

$$\bar{\Psi}_1 \gamma^\mu \gamma^5 \Psi_2 = \chi_1 \sigma^\mu \bar{\chi}_2 - \bar{\xi}_1 \bar{\sigma}^\mu \xi_2, \quad (\text{A.18d})$$

$$\bar{\Psi}_1 \Sigma^{\mu\nu} \Psi_2 = \chi_1 \sigma^{\mu\nu} \bar{\chi}_2 + \bar{\xi}_1 \bar{\sigma}^{\mu\nu} \xi_2, \quad (\text{A.18e})$$

and

$$\bar{\lambda}_{1M}\lambda_{2M} = \lambda_1\lambda_2 + \bar{\lambda}_1\bar{\lambda}_2, \quad (\text{A.19a})$$

$$\bar{\lambda}_{1M}\gamma^5\lambda_{2M} = -\lambda_1\lambda_2 + \bar{\lambda}_1\bar{\lambda}_2, \quad (\text{A.19b})$$

$$\bar{\lambda}_{1M}\gamma^\mu\lambda_{2M} = \lambda_1\sigma^\mu\bar{\lambda}_2 + \bar{\lambda}_1\bar{\sigma}^\mu\lambda_2, \quad (\text{A.19c})$$

$$\bar{\lambda}_{1M}\gamma^\mu\gamma^5\lambda_{2M} = \lambda_1\sigma^\mu\bar{\lambda}_2 - \bar{\lambda}_1\bar{\sigma}^\mu\lambda_2, \quad (\text{A.19d})$$

$$\bar{\lambda}_{1M}\Sigma^{\mu\nu}\gamma^5\lambda_{2M} = \lambda_1\sigma^{\mu\nu}\lambda_2 - \bar{\lambda}_1\bar{\sigma}^{\mu\nu}\bar{\lambda}_2, \quad (\text{A.19e})$$

where

$$\Sigma^{\mu\nu} = \frac{i}{4}[\gamma^\mu, \gamma^\nu]. \quad (\text{A.20})$$

A.4 Grassmann Variables

Grassmann variables θ also carry Weyl spinor indices $A = 1, 2$, are anticommuting, and satisfy the relation

$$\{\theta^A, \theta^B\} = \{\theta^A, \bar{\theta}^B\} = \{\bar{\theta}^{\dot{A}}, \bar{\theta}^{\dot{B}}\} = 0. \quad (\text{A.21})$$

An important result of this is that products θ^n vanish for $n > 2$. This implies that Taylor expansions of a function of Grassmann variables terminates after a finite number of terms.

One defines differentiations with respect to θ like $\partial_A \equiv \partial/\partial\theta^A$, $\partial^A \equiv \partial/\partial\theta_A$, $\bar{\partial}^{\dot{A}} \equiv \partial/\partial\bar{\theta}_{\dot{A}}$, and $\bar{\partial}_{\dot{A}} \equiv \partial/\partial\bar{\theta}^{\dot{A}}$ as

$$\partial_A\theta^B = \delta_A^B, \quad (\text{A.22a})$$

$$\partial^A\theta_B = \delta_B^A, \quad (\text{A.22b})$$

$$\bar{\partial}_{\dot{A}}\bar{\theta}^{\dot{B}} = \delta_{\dot{A}}^{\dot{B}}, \quad (\text{A.22c})$$

$$\bar{\partial}^{\dot{A}}\bar{\theta}_{\dot{B}} = \delta_{\dot{B}}^{\dot{A}}, \quad (\text{A.22d})$$

$$\partial_A\theta_B = -\epsilon_{AB}, \quad (\text{A.22e})$$

$$\partial^A\theta^B = -\epsilon^{AB}, \quad (\text{A.22f})$$

$$\bar{\partial}_{\dot{A}}\bar{\theta}_{\dot{B}} = -\epsilon_{\dot{A}\dot{B}}, \quad (\text{A.22g})$$

$$\bar{\partial}^{\dot{A}}\bar{\theta}^{\dot{B}} = -\epsilon^{\dot{A}\dot{B}}. \quad (\text{A.22h})$$

The rules for integration over θ that are of interest for us are

$$\int d^2\theta(a + \xi\theta + c\theta\theta) = [a + \xi\theta + c\theta\theta]_{\theta\theta} = c, \quad (\text{A.23a})$$

$$\int d^2\bar{\theta}(a + \bar{\xi}\bar{\theta} + c\bar{\theta}\bar{\theta}) = [a + \bar{\xi}\bar{\theta} + c\bar{\theta}\bar{\theta}]_{\bar{\theta}\bar{\theta}} = c, \quad (\text{A.23b})$$

$$\int d^2\theta d^2\bar{\theta}(a + \xi\theta + c\theta\theta + d\bar{\theta}\bar{\theta} + e\theta\theta\bar{\theta}\bar{\theta}) = [\dots]_{\theta\theta\bar{\theta}\bar{\theta}} = e, \quad (\text{A.23c})$$

where a , b , c , d , and e are complex numbers and ξ is a two-component spinor.

Appendix B

Derivation of the Effective PQ Lagrangian

In this Appendix we present some of the details of the derivation of the effective PQ interaction Lagrangian. We begin with the effective Lagrangian given by (2.58) as an integral over the fermionic superspace coordinate θ . It reads

$$\mathcal{L}_{\text{PQ}}^{\text{int}} = -\frac{\sqrt{2}\alpha_s}{8\pi f_{\text{PQ}}} \int d^2\theta A W^b W^b + \text{h.c.} \quad (\text{B.1})$$

where

$$A = \frac{\sigma + ia}{\sqrt{2}} + \sqrt{2}\theta\tilde{a} + F_A\theta\theta \quad (\text{B.2})$$

is the PQ superfield. It has the usual structure explained in Sect. 2.3, first a scalar part consisting of the saxion σ and the axion a . The second term is the fermionic partner, the axino \tilde{a} , multiplied by the superspace coordinate θ . The last part is an auxiliary field F_A that can be eliminated from the Lagrangian via its equations of motion.

The other factors in (B.1) are the color-field-strength superfields W . We drop the color index for the moment. The starting point of its derivation is a vector superfield that has been simplified using the Wess–Zumino gauge as given by (2.24). After a Taylor-expansion in the superspace coordinates

$$y^\mu = x^\mu - i\theta\sigma^\mu\bar{\theta}, \quad (\text{B.3a})$$

$$\bar{y}^\mu = x^\mu + i\theta\sigma^\mu\bar{\theta}, \quad (\text{B.3b})$$

it reads

$$V_{\text{WZ}}(y, \theta, \bar{\theta}) = \theta\sigma^\mu\bar{\theta}A_\mu(y) + \theta\theta\bar{\theta}\bar{\lambda}(y) + \bar{\theta}\bar{\theta}\theta\lambda(y) + \frac{1}{2}\theta\theta\bar{\theta}\bar{\theta}[D(y) + i\partial_\mu A^\mu(y)], \quad (\text{B.4a})$$

$$V_{\text{WZ}}(\bar{y}, \theta, \bar{\theta}) = \theta\sigma^\mu\bar{\theta}A_\mu(\bar{y}) + \theta\theta\bar{\theta}\bar{\lambda}(\bar{y}) + \bar{\theta}\bar{\theta}\theta\lambda(\bar{y}) + \frac{1}{2}\theta\theta\bar{\theta}\bar{\theta}[D(\bar{y}) - i\partial_\mu A^\mu(\bar{y})], \quad (\text{B.4b})$$

where A_μ is the gauge field strength tensor, λ the gaugino field, and D is an auxiliary D -term field, similar to the F -term of the chiral field. In order to arrive at the color-field-strength superfield, we apply the chiral covariant derivatives given in (2.12) to the vector superfield (B.4a) to get

$$W_A = -\frac{1}{4}\bar{\mathcal{D}}\bar{\mathcal{D}}\mathcal{D}_A V_{\text{WZ}}(y, \theta, \bar{\theta}). \quad (\text{B.5})$$

The first two derivatives act like a projector. The rightmost one requires some algebra. After computing the derivatives with respect to both x and θ we get

$$\begin{aligned} \mathcal{D}_A V_{\text{WZ}} = & \sigma_{A\dot{B}}^\mu \bar{\theta}^{\dot{B}} A_\mu + 2\theta_A \bar{\theta} \bar{\lambda} + \bar{\theta} \bar{\theta} \lambda_A + \bar{\theta} \bar{\theta} \theta_A (D + i\partial_\mu A^\mu) \\ & + \theta \sigma_{A\dot{B}}^\mu \bar{\theta} \partial_\nu A_\mu \left(-i\sigma_{A\dot{B}}^\nu \bar{\theta}^{\dot{B}} \right) + \theta \bar{\theta} \bar{\theta} \partial_\mu \bar{\lambda} \left(-i\sigma_{A\dot{B}}^\mu \bar{\theta}^{\dot{B}} \right) \\ & - i\sigma_{A\dot{B}}^\nu \bar{\theta}^{\dot{B}} \theta \sigma^\mu \bar{\theta} \partial_\nu A_\mu - i\sigma_{A\dot{B}}^\mu \bar{\theta}^{\dot{B}} \theta \bar{\theta} \partial_\mu \bar{\lambda}, \end{aligned} \quad (\text{B.6})$$

where all terms containing more than two θ or $\bar{\theta}$ disappear because of the Grassmann nature of θ . Next we use the identity

$$\left(\sigma_{A\dot{B}}^\mu \bar{\theta}^{\dot{B}} \right) \theta \sigma^\nu \bar{\theta} = \bar{\theta} \bar{\theta} \left[\frac{1}{2} \eta^{\mu\nu} \theta_A - i \left(\sigma_A^{\mu\nu B} \theta_B \right) \right] \quad (\text{B.7})$$

to rewrite the fifth and the seventh term of the above equation as

$$\begin{aligned} \mathcal{D}_A V_{\text{WZ}} = & \sigma_{A\dot{B}}^\mu \bar{\theta}^{\dot{B}} A_\mu + 2\theta_A \bar{\theta} \bar{\lambda} + \bar{\theta} \bar{\theta} \lambda_A + \bar{\theta} \bar{\theta} \theta_A (D + i\partial_\mu A^\mu) \\ & - 2i\bar{\theta} \bar{\theta} \left[\frac{1}{2} \eta^{\mu\nu} \theta_A - i \left(\sigma_A^{\mu\nu B} \theta_B \right) \right] \partial_\mu A_\nu + 2\theta \bar{\theta} \bar{\theta} \partial_\mu \bar{\lambda} \left(-i\sigma_{A\dot{B}}^\mu \bar{\theta}^{\dot{B}} \right). \end{aligned} \quad (\text{B.8})$$

We see that the term depending on $\eta^{\mu\nu}$ cancels with the second half of the term right before that one. Moreover, we use

$$\bar{\theta}_{\dot{C}} \bar{\theta}^{\dot{B}} = -\epsilon_{\dot{C}\dot{D}} \frac{1}{2} \epsilon^{\dot{D}\dot{B}} \bar{\theta} \bar{\theta} \quad (\text{B.9})$$

and

$$\sigma^{\mu\nu} \partial_\mu A_\nu = \frac{i}{4} (\sigma^\mu \bar{\sigma}^\nu - \sigma^\nu \bar{\sigma}^\mu) \partial_\mu A_\nu = \frac{i}{4} (\sigma^\mu \bar{\sigma}^\nu \partial_\mu A_\nu - \sigma^\mu \bar{\sigma}^\nu \partial_\nu A_\mu) = \frac{i}{4} \sigma^\mu \sigma^\nu F_{\mu\nu}. \quad (\text{B.10})$$

From symmetry reasons it follows

$$\sigma^{\mu\nu} F_{\mu\nu} = \frac{i}{2} \sigma^\mu \bar{\sigma}^\nu F_{\mu\nu}, \quad (\text{B.11})$$

and therefore

$$\sigma^{\mu\nu} \partial_\mu A_\nu = \frac{1}{2} \sigma^{\mu\nu} F_{\mu\nu}. \quad (\text{B.12})$$

This allows us to write (B.8) as

$$\mathcal{D}_A V_{\text{WZ}} = \sigma_{\dot{A}\dot{B}}^\mu \bar{\theta}^{\dot{B}} A_\mu + 2\theta_A \bar{\theta} \bar{\lambda} + \bar{\theta} \bar{\theta} \lambda_A + \bar{\theta} \bar{\theta} \theta_A D - (\sigma^{\mu\nu} \theta)_A F_{\mu\nu} \bar{\theta} \bar{\theta} + i\theta \bar{\theta} \bar{\theta} \bar{\theta} (\sigma^\mu \partial_\mu \bar{\lambda})_A. \quad (\text{B.13})$$

The projection operators in (B.5) eliminate all terms but those proportional to $\bar{\theta} \bar{\theta}$. We then arrive at the final expression for the color-field-strength tensor

$$W_A = \lambda_A(y) + D(y) \theta_A - (\sigma^{\mu\nu} \theta)_A F_{\mu\nu}(y) + i\theta \bar{\theta} \sigma_{\dot{A}\dot{B}}^\mu \partial_\mu \bar{\lambda}^{\dot{B}}(y), \quad (\text{B.14})$$

where we have made the y -dependence explicit again.

Now we turn to the right chiral superfield. It is given in terms of the vector superfield (B.4b) as

$$\bar{W}_{\dot{A}} = -\frac{1}{4} \mathcal{D} \mathcal{D} \bar{\mathcal{D}}_{\dot{A}} V_{\text{WZ}}(\bar{y}, \theta, \bar{\theta}). \quad (\text{B.15})$$

Again the first two derivatives act as a projector. We find

$$\begin{aligned} \bar{\mathcal{D}}_{\dot{A}} V_{\text{WZ}} &= \theta^B \sigma_{B\dot{A}}^\mu A_\mu + 2\bar{\theta}_{\dot{A}} \theta \lambda + \theta \theta \bar{\lambda}_{\dot{A}} + \theta \theta \bar{\theta}_{\dot{A}} (D - i\partial_\mu A^\mu) \\ &\quad + \theta \sigma^\mu \bar{\theta} \partial_\mu A_\nu (i\theta^B \sigma_{B\dot{A}}^\nu) - \bar{\theta} \bar{\theta} \theta \partial_\mu \lambda (i\theta^B \sigma_{B\dot{A}}^\mu) \\ &\quad + i\theta^B \sigma_{B\dot{A}}^\nu \theta \sigma^\mu \bar{\theta} \partial_\mu A_\nu + i\theta^B \sigma_{B\dot{A}}^\mu \bar{\theta} \bar{\theta} \theta \partial_\mu \lambda. \end{aligned} \quad (\text{B.16})$$

We use identities similar to (B.7) and (B.12), namely

$$\left(\theta^B \sigma_{B\dot{A}}^\mu \right) \theta \sigma^\nu \bar{\theta} = \theta \theta \left[\frac{1}{2} \eta^{\mu\nu} \bar{\theta}_{\dot{A}} + i \left(\bar{\theta}_{\dot{B}} \bar{\sigma}^{\mu\nu \dot{B}}_{\dot{A}} \right) \right] \quad (\text{B.17})$$

and

$$\bar{\sigma}^{\mu\nu} \partial_\mu A_\nu = \frac{1}{2} \bar{\sigma}^{\mu\nu} F_{\mu\nu}, \quad (\text{B.18})$$

and arrive at

$$\begin{aligned} \bar{\mathcal{D}}_{\dot{A}} V_{\text{WZ}} &= \theta^B \sigma_{B\dot{A}}^\mu A_\mu + 2\bar{\theta}_{\dot{A}} \theta \lambda + \theta \theta \bar{\lambda}_{\dot{A}} + \theta \theta \bar{\theta}_{\dot{A}} (D - i\partial_\mu A^\mu) \\ &\quad + \theta \theta \left[\eta^{\mu\nu} \bar{\theta}_{\dot{A}} \partial_\mu A^\nu - \left(\bar{\theta}_{\dot{B}} \bar{\sigma}^{\mu\nu \dot{B}}_{\dot{A}} \right) F_{\mu\nu} \right] - i\bar{\theta} \bar{\theta} \theta \theta \left(\partial_\mu \lambda^B \sigma_{B\dot{A}}^\mu \right). \end{aligned} \quad (\text{B.19})$$

This can be simplified to

$$\begin{aligned} \bar{\mathcal{D}}_{\dot{A}} V_{\text{WZ}} &= \theta^B \sigma_{B\dot{A}}^\mu A_\mu + 2\bar{\theta}_{\dot{A}} \theta \lambda + \theta \theta \bar{\lambda}_{\dot{A}} + \theta \theta \bar{\theta}_{\dot{A}} D \\ &\quad - \theta \theta \left(\bar{\theta} \bar{\sigma}^{\mu\nu} \right)_{\dot{A}} F_{\mu\nu} - i\bar{\theta} \bar{\theta} \theta \theta \left(\partial_\mu \lambda^B \sigma_{B\dot{A}}^\mu \right). \end{aligned} \quad (\text{B.20})$$

The other two derivatives project out the parts proportional to $\theta \theta$. The final result then reads

$$\bar{W}_{\dot{A}} = \bar{\lambda}_{\dot{A}}(\bar{y}) + \bar{\theta}_{\dot{A}} D(\bar{y}) + \epsilon_{\dot{A}\dot{B}} (\bar{\sigma}^{\mu\nu} \bar{\theta})^{\dot{B}} F_{\mu\nu}(\bar{y}) - i\bar{\theta} \bar{\theta} \left(\partial_\mu \lambda^B \sigma_{B\dot{A}}^\mu \right)(\bar{y}). \quad (\text{B.21})$$

Note that this expression differs from the one in [121] by a sign of the term proportional to $F_{\mu\nu}$. The authors of [121] agree with our finding and have corrected for this mistake online.¹

In order to get to the effective PQ interaction Lagrangian, we need to calculate the combinations $W^A W_A$ and $\bar{W}_A \bar{W}^{\dot{A}}$. Again, all terms with more than two θ or $\bar{\theta}$ vanish. So the expression for the first combination reads

$$\begin{aligned} W^A W_A &= \lambda^A \lambda_A + \theta^A D \lambda_A + \lambda^A D \theta_A - \lambda^A \sigma_A^{\mu\nu B} \theta_B F_{\mu\nu} - \epsilon^{AB} \sigma_B^{\mu\nu C} \theta_C F_{\mu\nu} \lambda_A F_{\mu\nu} \\ &\quad + \theta^A \theta_A D^2 + i \lambda^A \theta \theta \sigma_{AB}^\mu \partial_\mu \bar{\lambda}^{\dot{B}} + i \epsilon^{AB} \theta \theta \sigma_{BC}^\mu \partial_\mu \bar{\lambda}^{\dot{C}} \lambda_A \\ &\quad + \epsilon^{AB} \sigma_B^{\rho\sigma C} \theta_C \sigma_A^{\mu\nu D} \theta_D F_{\rho\sigma} F_{\mu\nu}. \end{aligned} \quad (\text{B.22})$$

We make use of

$$i \epsilon^{AB} \theta \theta \sigma_{BC}^\mu \partial_\mu \bar{\lambda}^{\dot{C}} \lambda_A = -i \theta \theta \epsilon^{AB} \lambda_A \sigma_{BC}^\mu \partial_\mu \bar{\lambda}^{\dot{C}} = i \theta \theta \lambda^B \sigma_{BC}^\mu \partial_\mu \bar{\lambda}^{\dot{C}}, \quad (\text{B.23})$$

where the first sign comes from the interchange of λ and $\bar{\lambda}$ and the second one from the commutation of the indices in ϵ . This allows us to collect the θ terms in (B.22):

$$\begin{aligned} W^A W_A &= \lambda \lambda + 2\theta (D \lambda + \sigma^{\mu\nu} \lambda F_{\mu\nu}) + \theta \theta (D^2 + 2i \lambda \sigma^\mu \partial_\mu \bar{\lambda}) \\ &\quad + \epsilon^{AB} \sigma_B^{\rho\sigma C} \theta_C \sigma_A^{\mu\nu D} \theta_D F_{\rho\sigma} F_{\mu\nu}. \end{aligned} \quad (\text{B.24})$$

The last term can be simplified using

$$\begin{aligned} \epsilon^{AB} \sigma_B^{\rho\sigma C} \theta_C \sigma_A^{\mu\nu D} \theta_D F_{\rho\sigma} F_{\mu\nu} &= \frac{1}{2} \theta \theta \epsilon_{CD} \epsilon^{AB} \sigma_B^{\rho\sigma C} \sigma_A^{\mu\nu D} F_{\rho\sigma} F_{\mu\nu} \\ &= -\frac{1}{2} \theta \theta (\delta_C^A \delta_D^B - \delta_D^A \delta_C^B) \sigma_B^{\rho\sigma C} \sigma_A^{\mu\nu D} F_{\rho\sigma} F_{\mu\nu} \\ &= -\frac{1}{2} \theta \theta (\sigma_B^{\rho\sigma A} \sigma_A^{\mu\nu B} - \sigma_A^{\rho\sigma A} \sigma_B^{\mu\nu B}) F_{\rho\sigma} F_{\mu\nu} \\ &= -\frac{1}{2} \theta \theta \text{Tr}(\sigma^{\rho\sigma} \sigma^{\mu\nu}) F_{\rho\sigma} F_{\mu\nu} \\ &= -\frac{1}{2} \theta \theta \left[\frac{1}{2} (\eta^{\rho\mu} \eta^{\sigma\nu} - \eta^{\rho\nu} \eta^{\sigma\mu}) - \frac{i}{2} \epsilon^{\rho\sigma\mu\nu} \right] F_{\rho\sigma} F_{\mu\nu} \\ &= -\frac{1}{2} \theta \theta (F^{\mu\nu} F_{\mu\nu} - i F^{\mu\nu} \tilde{F}_{\mu\nu}). \end{aligned}$$

This allows us to write (B.24) as

$$W^A W_A = \lambda \lambda + 2\theta (D \lambda + \sigma^{\mu\nu} \lambda F_{\mu\nu}) + \theta \theta \left(D^2 + 2i \lambda \sigma^\mu \partial_\mu \bar{\lambda} - \frac{1}{2} F^{\mu\nu} F_{\mu\nu} + \frac{i}{2} F^{\mu\nu} \tilde{F}_{\mu\nu} \right). \quad (\text{B.25})$$

¹The list of errors and updates can be found at
<http://www.th.physik.uni-bonn.de/groups/drees/book.html>.

Next we turn to the Hermitian conjugate

$$\begin{aligned}\overline{W}_A \overline{W}^{\dot{A}} &= \bar{\lambda}_{\dot{A}} \bar{\lambda}^{\dot{A}} + \bar{\theta}_{\dot{A}} D \bar{\lambda}^{\dot{A}} + \bar{\lambda}_{\dot{A}} D \bar{\theta}^{\dot{A}} + \bar{\lambda}_{\dot{A}} \bar{\sigma}^{\mu\nu\dot{A}}_{\dot{B}} \bar{\theta}^{\dot{B}} F_{\mu\nu} + \epsilon_{\dot{A}\dot{B}} \bar{\sigma}^{\mu\nu\dot{B}}_{\dot{C}} \bar{\theta}^{\dot{C}} F_{\mu\nu} \bar{\lambda}^{\dot{A}} F_{\mu\nu} \\ &\quad + \bar{\theta}_{\dot{A}} \bar{\theta}^{\dot{A}} D^2 - i \bar{\theta} \bar{\theta} \partial_\mu \lambda^B \sigma^\mu_{B\dot{A}} \bar{\lambda}^{\dot{A}} - i \bar{\lambda}_{\dot{A}} \epsilon^{\dot{A}\dot{B}} \bar{\theta} \bar{\theta} \partial_\mu \lambda^C \sigma^\mu_{C\dot{B}} \\ &\quad + \epsilon_{\dot{A}\dot{B}} \bar{\sigma}^{\mu\nu\dot{B}}_{\dot{C}} \bar{\theta}^{\dot{C}} \bar{\sigma}^{\mu\nu\dot{A}}_{\dot{B}} \bar{\theta}^{\dot{B}} F_{\rho\sigma} F_{\mu\nu}.\end{aligned}\tag{B.26}$$

Similar manipulations as in the case of $W^A W_A$ lead to

$$\overline{W}_A \overline{W}^{\dot{A}} = \bar{\lambda} \bar{\lambda} + 2 (D \bar{\lambda} + \bar{\lambda} \bar{\sigma}^{\mu\nu} F_{\mu\nu}) \bar{\theta} + \bar{\theta} \bar{\theta} \left(D^2 - 2i \partial_\mu \lambda \sigma^\mu \bar{\lambda} - \frac{1}{2} F^{\mu\nu} F_{\mu\nu} - \frac{i}{2} F^{\mu\nu} \tilde{F}_{\mu\nu} \right).\tag{B.27}$$

Now we need to multiply these products with the PQ superfield. The integral in (B.1) acts as a projector, leaving only the terms proportional to $\theta\theta$. So we can drop all other terms. This yields

$$\begin{aligned}\int d^2\theta A W^A W_A &= \frac{\sigma + ia}{\sqrt{2}} \left(D^2 + 2i \lambda \sigma^\mu \partial_\mu \bar{\lambda} - \frac{1}{2} F^{\mu\nu} F_{\mu\nu} + \frac{i}{2} F^{\mu\nu} \tilde{F}_{\mu\nu} \right) \\ &\quad - \sqrt{2} \tilde{a} (i D \lambda + \sigma^{\mu\nu} \lambda F_{\mu\nu}) + (F\text{-terms}).\end{aligned}\tag{B.28}$$

In the part proportional to the axino we have used

$$\theta \tilde{a} \theta \lambda = -\frac{1}{2} \tilde{a} \lambda \theta \theta.\tag{B.29}$$

The Hermitian conjugate reads

$$\begin{aligned}\int d^2\bar{\theta} A^\dagger \overline{W}_A \overline{W}^{\dot{A}} &= \frac{\sigma - ia}{\sqrt{2}} \left(D^2 - 2i \partial_\mu \lambda \sigma^\mu \bar{\lambda} - \frac{1}{2} F^{\mu\nu} F_{\mu\nu} + \frac{i}{2} F^{\mu\nu} \tilde{F}_{\mu\nu} \right) \\ &\quad + \sqrt{2} (i D \bar{\lambda} - \bar{\lambda} \bar{\sigma}^{\mu\nu} F_{\mu\nu}) \bar{\tilde{a}} + (F\text{-terms}).\end{aligned}\tag{B.30}$$

After adding both terms, multiplying with the prefactor of (B.1), and sorting according to the PQ fields, we get

$$\begin{aligned}\mathcal{L}_{\text{PQ}}^{\text{int}} &= \frac{\alpha_s}{8\pi f_{\text{PQ}}} \left[\sigma (F^{\mu\nu} F_{\mu\nu} - 2D^2 - 2i \lambda \sigma^\mu \partial_\mu \bar{\lambda} + 2i \partial_\mu \lambda \sigma^\mu \bar{\lambda}) \right. \\ &\quad + a (F^{\mu\nu} \tilde{F}_{\mu\nu} + 2\lambda \sigma^\mu \partial_\mu \bar{\lambda} + 2\partial_\mu \lambda \sigma^\mu \bar{\lambda}) \\ &\quad \left. + 2i \tilde{a} \lambda D + 2i \bar{\tilde{a}} \bar{\lambda} D - 2\tilde{a} \sigma^{\mu\nu} \lambda F_{\mu\nu} - 2\bar{\tilde{a}} \bar{\sigma}^{\mu\nu} \bar{\lambda} F_{\mu\nu} \right].\end{aligned}\tag{B.31}$$

In the axion and saxion terms, we use

$$\partial_\mu \lambda \sigma^\mu \bar{\lambda} = -\bar{\lambda} \bar{\sigma}^\mu \partial_\mu \lambda.\tag{B.32}$$

and in the axino term

$$\bar{\lambda}\bar{\sigma}^{\mu\nu}\tilde{a} = -\tilde{a}\bar{\sigma}^{\mu\nu}\bar{\lambda}. \quad (\text{B.33})$$

All of the above calculation has been done with two-component Weyl spinors. To convert this into the usual four-component Majorana notation, we make use of the identities given in Appendix A.

Now we are ready to identify the fields in this expression with the supermultiplet of the strong interaction. In fact, this transfer from the abelian U(1) case to the non-abelian SU(3)_c case can be done via the replacements (for details, see, e.g., Chap. 5.4 of Ref. [121])

$$F^{\mu\nu} \rightarrow G^{b\mu\nu}, \quad (\text{B.34a})$$

$$D \rightarrow D^b, \quad (\text{B.34b})$$

$$\partial_\mu \rightarrow D_\mu^{bd}, \quad (\text{B.34c})$$

$$\lambda_M = \begin{pmatrix} \lambda \\ \bar{\lambda}^T \end{pmatrix} \rightarrow g_M^b = \begin{pmatrix} g \\ \bar{g}^T \end{pmatrix}, \quad (\text{B.34d})$$

$$\tilde{a} \rightarrow \tilde{a}_M. \quad (\text{B.34e})$$

With these identifications we arrive at the final result for the PQ interaction Lagrangian given by Eq. (2.59).

Appendix C

Feynman Rules

Here we present the Feynman rules necessary to calculate the matrix elements in Chap. 3. We use the convention

$$F_{\mu\nu}^a = \partial_\mu A_\nu^a - \partial_\nu A_\mu^a - g_s f^{abc} A_\mu^b A_\nu^c.$$

In Feynman diagrams, all momenta are understood to run from left to right in case of the external lines and propagators and to run into the vertices in case of interactions. As we have to deal with Majorana fermions, we adopt the concept of fermion flow from Ref. [241] indicated by arrows over the respective fermion lines. Dirac traces are then constructed by moving against the fermion flow.

C.1 External Lines and Propagators

External lines

- Gluons

$$\underbrace{\text{-----}}_{\mu, a} \bullet = \epsilon_\mu^a(P) \qquad \bullet \underbrace{\text{-----}}_{\mu, a} = \epsilon_\mu^{*a}(P)$$

- Gluinos, fermions and their antiparticles

$$\begin{array}{c} \xrightarrow{\hspace{1cm}} \\ \text{oooooooooooo} \bullet \end{array} = \begin{array}{c} \xrightarrow{\hspace{1cm}} \\ \text{-----} \bullet \end{array} = \begin{array}{c} \xrightarrow{\hspace{1cm}} \\ \text{-----} \bullet \end{array} = u^s(P)$$

$$\begin{array}{c} \xrightarrow{\hspace{1cm}} \\ \bullet \text{oooooooooooo} \end{array} = \begin{array}{c} \xrightarrow{\hspace{1cm}} \\ \bullet \text{-----} \end{array} = \begin{array}{c} \xrightarrow{\hspace{1cm}} \\ \bullet \text{-----} \end{array} = \bar{u}^s(P)$$

$$\begin{array}{c} \xleftarrow{\hspace{1cm}} \\ \bullet \text{oooooooooooo} \end{array} = \begin{array}{c} \xleftarrow{\hspace{1cm}} \\ \bullet \text{-----} \end{array} = \begin{array}{c} \xleftarrow{\hspace{1cm}} \\ \bullet \text{-----} \end{array} = v^s(P)$$

$$\begin{array}{c} \xleftarrow{\hspace{1cm}} \\ \text{oooooooooooo} \bullet \end{array} = \begin{array}{c} \xleftarrow{\hspace{1cm}} \\ \text{-----} \bullet \end{array} = \begin{array}{c} \xleftarrow{\hspace{1cm}} \\ \text{-----} \bullet \end{array} = \bar{v}^s(P)$$

- Scalars

$$\text{-----} \bullet = \bullet \text{-----} = 1$$

Propagators

- Gluons

$$\begin{array}{c} \bullet \text{oooooooooooo} \bullet \\ \mu, a \qquad \nu, b \end{array} = i\delta^{ab} \left[\frac{-\eta^{\mu\nu}}{P^2} + (1 - \xi) \frac{P^\mu P^\nu}{(P^2)^2} \right]$$

- Gluinos

$$\begin{array}{c} \xrightarrow{\hspace{1cm}} \\ \bullet \text{oooooooooooo} \bullet \\ a \qquad b \end{array} = \delta_{ab} \frac{i}{\not{P} - m}$$

- Quarks

$$\begin{array}{c} \xrightarrow{\hspace{1cm}} \\ \bullet \text{-----} \bullet \\ i \qquad j \end{array} = \delta_{ij} \frac{i}{\not{P} - m_q}$$

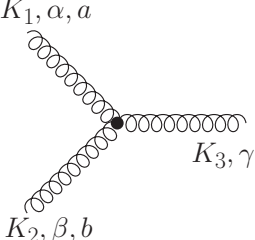
$$\begin{array}{c} \xleftarrow{\hspace{1cm}} \\ \bullet \text{-----} \bullet \\ i \qquad j \end{array} = \delta_{ij} \frac{i}{-\not{P} - m_q}$$

- Squarks

$$\begin{array}{c} \bullet \text{---} \bullet \\ i \qquad j \end{array} = \delta_{ij} \frac{i}{P^2 - m_q^2}$$

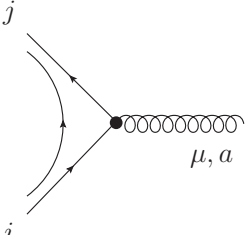
C.2 SUSY QCD Vertices

- Gluon-gluon-gluon

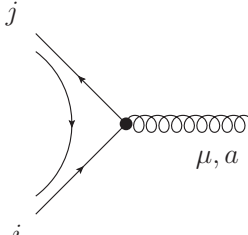


$$= -g_s f^{abc} \left[(K_1 - K_2)^\gamma \eta^{\alpha\beta} + (K_2 - K_3)^\alpha \eta^{\beta\gamma} + (K_3 - K_1)^\beta \eta^{\alpha\gamma} \right]$$

- Quark-quark-gluon

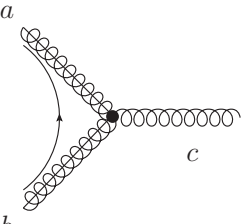


$$= -ig_s \gamma^\mu T_{ij}^a P_L$$

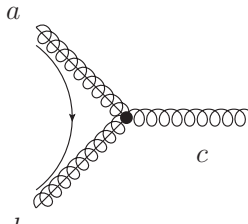


$$= ig_s \gamma^\mu T_{ij}^a P_R$$

- Gluon-gluino-gluino

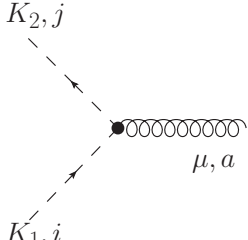


$$= -g_s f^{abc} \gamma^\mu$$



$$= g_s f^{abc} \gamma^\mu$$

- Squark-squark-gluon



$$= -ig_s T_{ij}^a (K_1 - K_2)^\mu$$

- Gluino-quark-squark

$$= -i\sqrt{2}g_s T_{ij}^a P_L \quad = -i\sqrt{2}g_s T_{ij}^a P_R$$

C.3 PQ Vertices

- Effective coupling axion-gluon-gluon

$$= i\frac{\alpha_s}{2\pi} \frac{1}{f_{\text{PQ}}} \epsilon^{\mu\nu\alpha\beta} (K_1)_\alpha (K_2)_\beta \delta^{ab}$$

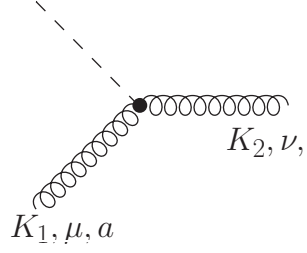
- Effective coupling axion-gluon-gluon-gluon

$$= \frac{\alpha_s}{2\pi} \frac{1}{f_{\text{PQ}}} g_s \epsilon^{\mu\nu\rho\alpha} (K_1 + K_2 + K_3)_\alpha f^{abc}$$

- Effective coupling axion-gluino-gluino

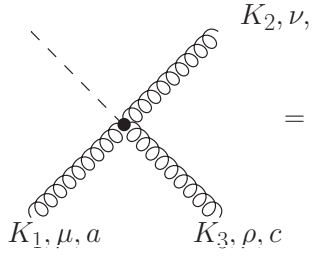
$$= \frac{\alpha_s}{4\pi} \frac{1}{f_{\text{PQ}}} (K_1 + K_2) \gamma^5 \delta^{ab}$$

- Effective coupling saxion-gluon-gluon



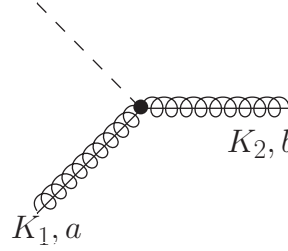
$$= i \frac{\alpha_s}{2\pi} \frac{1}{f_{PQ}} (K_1^\nu K_2^\mu - K_1 \cdot K_2 \eta^{\mu\nu}) \delta^{ab}$$

- Effective coupling saxion-gluon-gluon-gluon



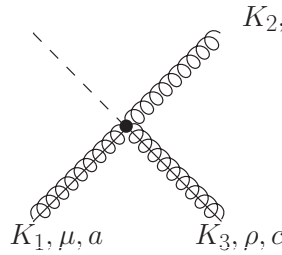
$$= -\frac{\alpha_s}{2\pi} \frac{1}{f_{PQ}} g_s [(K_2 - K_1)^\rho \eta^{\mu\nu} + (K_3 - K_2)^\mu \eta^{\nu\rho} + (K_1 - K_3)^\nu \eta^{\mu\rho}] f^{abc}$$

- Effective coupling saxion-gluino-gluino



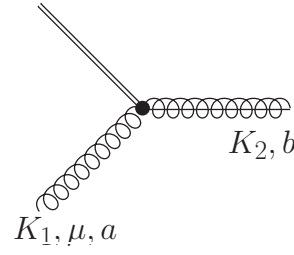
$$= -i \frac{\alpha_s}{4\pi} \frac{1}{f_{PQ}} (K_1 - K_2) \delta^{ab}$$

- Effective coupling saxion-gluon-gluino-gluino



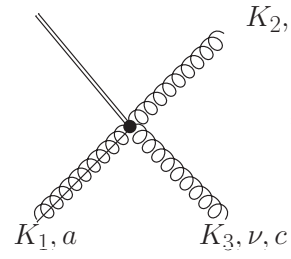
$$= -\frac{\alpha_s}{2\pi} \frac{1}{f_{PQ}} g_s \gamma^\mu f^{abc}$$

- Effective coupling axino-gluon-gluino



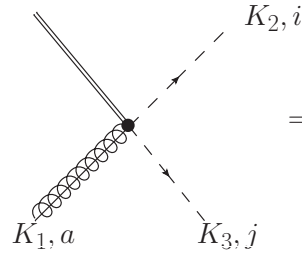
$$= i \frac{\alpha_s}{4\pi} \frac{1}{f_{\text{PQ}}} \gamma^5 [K_1 \gamma^\mu - (K_1)^\mu] \delta^{ab}$$

- Effective coupling axino-gluino-gluon-gluon



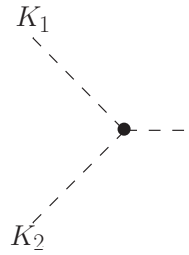
$$= \frac{\alpha_s}{4\pi} \frac{1}{f_{\text{PQ}}} g_s \gamma^5 (\gamma^\mu \gamma^\nu - \eta^{\mu\nu}) f^{abc}$$

- Effective coupling axino-gluino-squark-squark



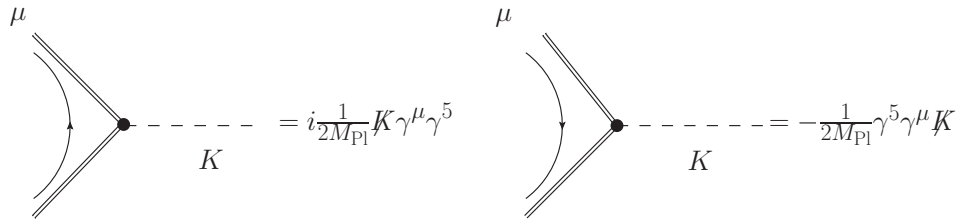
$$= i \frac{\alpha_s}{4\pi} \frac{1}{f_{\text{PQ}}} g_s T_{ij}^a$$

- Axion-axion-saxion



$$= i \frac{\sqrt{2}x}{f_{\text{PQ}}} K_1 \cdot K_2$$

- Gravitino-axino-axion



$$\begin{aligned}
 & \text{Left diagram: } \mu \text{ (gravitino)} \rightarrow \text{axino} + \text{axion} \quad = i \frac{1}{2M_{\text{Pl}}} K \gamma^\mu \gamma^5 \\
 & \text{Right diagram: } \mu \text{ (axino)} \rightarrow \text{axino} + \text{axion} \quad = -\frac{1}{2M_{\text{Pl}}} \gamma^5 \gamma^\mu K
 \end{aligned}$$

Appendix D

Hard Production Rate

In this section, we present some of the details of the phase space integration required in the calculation of the hard part of thermal saxion production. The integral we need to solve is (3.9) and reads

$$E \frac{dW_\sigma}{d^3p} \Big|_{\text{hard}} = \frac{1}{2(2\pi)^3} \int \frac{d\Omega_p}{4\pi} \int \left[\prod_{j=1}^3 \frac{d^3p_j}{(2\pi)^3 2E_j} \right] (2\pi)^4 \delta^4(P_1 + P_2 - P_3 - P) \\ \times \{f_{\text{BBB}}|M_{\text{BBB}}|^2 + f_{\text{FFB}}|M_{\text{FFB}}|^2 + f_{\text{FBF}}|M_{\text{FBF}}|^2\} \Theta(|p_1 - p_3| - k_{\text{cut}}). \quad (\text{D.1})$$

As presented in the main part, we can rewrite the matrix elements in terms of three generic ones given by (3.6), resulting in six different integrals. Only the two integrals over $|M_1|^2$ require $k_{\text{cut}} > 0$ and result in a logarithmic dependence on the cut-off parameter. These integrals have been calculated and are shown in detail in Appendix C of Ref. [155]. After extracting the k_{cut} dependence analytically, we arrive at (3.10), which reads

$$E \frac{dW_\sigma}{d^3p} \Big|_{\text{hard}} = E \frac{g_s^6(N_c^2 - 1)(N_c + n_f)}{512\pi^7 f_{\text{PQ}}^2} \\ \left\{ \frac{f_{\text{B}}(E)T^3}{32\pi} \left[\ln \left(\frac{T^2}{k_{\text{cut}}^2} \right) + \frac{17}{3} - 2\gamma + \frac{2\zeta'(2)}{\zeta(2)} + \frac{2}{3} \ln(2) \right] \right. \\ \left. + \left(I_{\text{BBB}}^{(1)} + I_{\text{FBF}}^{(1)} - I_{\text{BBB}}^{(3)} + I_{\text{FFB}}^{(3)} \right) - 2 \frac{n_f (I_{\text{FBF}}^{(2)} + I_{\text{FFB}}^{(2)})}{N_c + n_f} \right\}, \quad (\text{D.2})$$

with the remaining integrals defined in (3.11).

The four integrals in the first term of the last line of (D.2) have been computed in Ref. [155] and we are left with the evaluation of the two phase space integrals

$$I_{\text{FBF}}^{(2)} = \frac{1}{2E} \int \frac{d\Omega_p}{4\pi} \int \left[\prod_{j=1}^3 \frac{d^3p_j}{(2\pi)^3 2E_j} \right] (2\pi)^4 \delta^4(P_1 + P_2 - P_3 - P) f_{\text{FBF}} |M_2|^2 \Theta(|p_1 - p_3| - k_{\text{cut}}), \quad (\text{D.3})$$

and

$$I_{\text{FFB}}^{(2)} = \frac{1}{2E} \int \frac{d\Omega_p}{4\pi} \int \left[\prod_{j=1}^3 \frac{d^3 p_j}{(2\pi)^3 2E_j} \right] (2\pi)^4 \delta^4(P_1 + P_2 - P_3 - P) f_{\text{FFB}} |M_2|^2 \Theta(|p_1 - p_3| - k_{\text{cut}}). \quad (\text{D.4})$$

The evaluation follows similar calculations in [148, 154, 155].

D.1 Calculation of FBF Processes

We have to compute the integral (D.3). Since we do not have a possibly divergent part, we set $k_{\text{cut}} = 0$. It proves useful to define

$$\vec{q} = \vec{p} + \vec{p}_3 \quad (\text{D.5})$$

as a reference momentum. This allows us to write the integral measures as

$$\begin{aligned} \frac{d^3 p_3}{2E_3} &= \delta(P_3^2) \Theta(E_3) dE_3 d^3 p_3 \\ &= \int d^3 q \delta^3(\vec{q} - \vec{p} - \vec{p}_3) \delta(P_3^2) \Theta(E_3) dE_3 d^3 p_3 \\ &= \delta(E_3^2 - |\vec{q} - \vec{p}|^2) \Theta(E_3) dE_3 d^3 q, \end{aligned}$$

and

$$\begin{aligned} \frac{d^3 p_1}{2E_1} \delta^4(P_1 + P_2 - P_3 - P) &= \frac{\delta(E_1 - |\vec{p}_1|)}{2|\vec{p}_1|} \Theta(E_1) dE_1 d^3 p_1 \\ &\quad \times \delta(E_1 + E_2 - E_3 - E) \delta(\vec{p}_1 + \vec{p}_2 - \vec{p}_3 - \vec{p}) \\ &= \frac{\delta(E + E_3 - E_2 - |\vec{p} + \vec{p}_3 - \vec{p}_2|)}{2|\vec{p} + \vec{p}_3 - \vec{p}_2|} \Theta(E + E_3 - E_2) \\ &= \delta[(E + E_3 - E_2)^2 - |\vec{q} - \vec{p}_2|^2] \Theta(E + E_3 - E_2). \end{aligned}$$

Since the whole system is rotational invariant, we can choose for the angular variables

$$\vec{q} = q(0, 0, 1), \quad (\text{D.6a})$$

$$\vec{p} = E(0, \sin \tilde{\theta}, \cos \tilde{\theta}), \quad (\text{D.6b})$$

$$\vec{p}_2 = E_2(\cos \phi \sin \theta, \sin \phi \sin \theta, \cos \theta), \quad (\text{D.6c})$$

where the masses of the particles are assumed to be small compared to their total energy.

With this choice, the matrix element reads

$$t = (P_1 - P_3)^2 = -2EE_2(1 - \sin \tilde{\theta} \sin \phi \sin \theta - \cos \tilde{\theta} \cos \theta). \quad (\text{D.7})$$

The δ -function in (D.6) becomes

$$\delta(E_3^2 - |\vec{q} - \vec{p}|^2) = \frac{1}{2qE} \delta\left(\cos\tilde{\theta} - \frac{E^2 - E_3^2 + q^2}{2qE}\right), \quad (\text{D.8})$$

and (D.6) reads

$$\delta[(E + E_3 - E_2)^2 - |\vec{q} - \vec{p}_2|^2] = \frac{1}{2qE_2} \delta\left[\cos\theta - \frac{q^2 + E_2^2 - (E + E_3 - E_2)^2}{2qE_2}\right]. \quad (\text{D.9})$$

We are then left with the integral

$$\begin{aligned} I_{\text{FBF}}^{(2)} &= \frac{1}{2^{11}\pi^6 E^2} \int (-d\cos\tilde{\theta}) d\tilde{\phi} (-d\cos\theta) d\phi dE_2 dE_3 dq d\Omega_q \\ &\quad \delta\left[\cos\theta - \frac{q^2 + E_2^2 - (E + E_3 - E_2)^2}{2qE_2}\right] \delta\left(\cos\tilde{\theta} - \frac{E^2 - E_3^2 + q^2}{2qE}\right) \\ &\quad f_{\text{FBF}} t \Theta(E_2) \Theta(E_3) \Theta(E + E_3 - E_2). \end{aligned} \quad (\text{D.10})$$

The δ -functions can be combined with the Θ -functions to constrain the integration region to

$$\begin{aligned} \cos\theta < 1 &\rightarrow 2E_2 - E - E_3 < q < E + E_3, \\ \cos\theta > -1 &\rightarrow E + E_3 - 2E_2 < q, \\ \cos\tilde{\theta} < 1 &\rightarrow E - E_3 < q < E + E_3, \\ \cos\tilde{\theta} > -1 &\rightarrow E_3 - E < q. \end{aligned}$$

These inequalities can be written as two step functions

$$\Theta(q - |2E_2 - E - E_3|) \Theta(E + E_3 - q), \quad (\text{D.11a})$$

$$\Theta(q - |E - E_3|). \quad (\text{D.11b})$$

Next we perform the angular integration. We note that (D.10) is independent of $\tilde{\phi}$ and only depends on q , so $\int d\tilde{\phi} d\Omega_q \rightarrow 8\pi^2$. The remaining angular integrals yield

$$I_{\text{FBF}}^{(2)} = \frac{1}{2^8 \pi^3 E^2} \int dE_2 dE_3 dq f_{\text{FBF}} g_{\text{FBF}}^{|M_2|^2} \Omega, \quad (\text{D.12})$$

with

$$g_{\text{FBF}}^{|M_2|^2} = [(E + E_3)^2 - q^2] \left[-1 + \frac{E_3^2 - 2E_2 E_3 - E^2 + 2E_2 E}{q^2} \right], \quad (\text{D.13})$$

and

$$\Omega = \Theta(E_2) \Theta(E_3) \Theta(E + E_3 - E_2) \Theta(q - |2E_2 - E - E_3|) \Theta(E + E_3 - q) \Theta(q - |E - E_3|). \quad (\text{D.14})$$

The fourth step function in Ω can be written as

$$\Theta(q - |2E_2 - E - E_3|) = 1 - \Theta(|2E_2 - E - E_3| - q),$$

and the last term of this can be combined with the next to last one in Ω to yield

$$\Theta(|2E_2 - E - E_3| - q)\Theta(E + E_3 - q) = \Theta(|2E_2 - E - E_3| - q).$$

As a result, the integral gets split into the two parts

$$g_{\text{FBF},1}^{|M_2|^2} = \frac{1}{2^8 \pi^3 E^2} \int dE_2 dE_3 dq f_{\text{FBF}} g_{\text{FBF}}^{|M_2|^2} \Theta(E_2) \Theta(E_3) \Theta(E + E_3 - E_2) \Theta(E + E_3 - q) \Theta(q - |E - E_3|), \quad (\text{D.15a})$$

$$g_{\text{FBF},2}^{|M_2|^2} = \frac{1}{2^8 \pi^3 E^2} \int dE_2 dE_3 dq f_{\text{FBF}} g_{\text{FBF}}^{|M_2|^2} \Theta(E_2) \Theta(E_3) \Theta(E + E_3 - E_2) \Theta(|2E_2 - E - E_3| - q) \Theta(q - |E - E_3|). \quad (\text{D.15b})$$

Calculation of $g_{\text{FBF},1}^{|M_2|^2}$

We insert a factor of one into (D.15a), namely

$$1 = \Theta(E - E_3) + \Theta(E_3 - E),$$

to split the integral again in two parts. The first one reads

$$g_{\text{FBF},11}^{|M_2|^2} = \frac{1}{2^5 \pi^3 E^2} \int_0^\infty dE_3 \int_0^{E+E_3} dE_2 f_{\text{FBF}} \int_{E-E_3}^{E+E_3} dq g_{\text{FBF}}^{|M_2|^2} \Theta(E - E_3). \quad (\text{D.16})$$

After performing the integration over q we get

$$g_{\text{FBF},11}^{|M_2|^2} = \frac{1}{2^5 \pi^3 E^2} \int_0^\infty dE_3 \int_0^{E+E_3} dE_2 f_{\text{FBF}} \Theta(E - E_3) E_3^2 \left(\frac{E_3}{3} - E_1 \right). \quad (\text{D.17})$$

The second part of (D.15a) reads after the above insertion

$$g_{\text{FBF},12}^{|M_2|^2} = \frac{1}{2^5 \pi^3 E^2} \int_0^\infty dE_3 \int_0^{E+E_3} dE_2 f_{\text{FBF}} \int_{E-E_3}^{E+E_3} dq g_{\text{FBF}}^{|M_2|^2} \Theta(E_3 - E), \quad (\text{D.18})$$

and after integration over q

$$g_{\text{FBF},12}^{|M_2|^2} = \frac{1}{2^5 \pi^3 E^2} \int_0^\infty dE_3 \int_0^{E+E_3} dE_2 f_{\text{FBF}} \Theta(E_3 - E) E^2 \left(\frac{E}{3} - E_2 \right). \quad (\text{D.19})$$

Calculation of $g_{\text{FBF},2}^{|M_2|^2}$

We insert

$$1 = \Theta(E - E_3) + \Theta(E_3 - E)$$

also in (D.15b) to split it up as in the case of $g_{\text{FBF},1}^{|M_2|^2}$. Moreover, we insert

$$1 = \Theta(E_3 + E - 2E_2 - q) + \Theta(2E_2 - E - E_3 - q)$$

in each of the two parts and find four resulting integrals. We can simplify the step functions as

$$\begin{aligned} \Theta(q - E + E_3)\Theta(E + E_3 - 2E_2 - q) &\rightarrow E_2 < E_3, \\ \Theta(q - E + E_3)\Theta(2E_2 - E - E_3 - q) &\rightarrow E < E_2, \\ \Theta(q - E_3 + E)\Theta(E + E_3 - 2E_2 - q) &\rightarrow E_2 < E, \\ \Theta(q - E_3 + E)\Theta(2E_2 - E - E_3 - q) &\rightarrow E_3 < E_2. \end{aligned}$$

With this simplification, the four integrals read

$$\begin{aligned} g_{\text{FBF},211}^{|M_2|^2} &= -\frac{1}{2^8\pi^3 E^2} \int_0^\infty dE_3 \int_0^{E+E_3} dE_2 f_{\text{FBF}} \int_{E-E_3}^{E_3+E-2E_2} dq g_{\text{FBF}}^{|M_2|^2} \\ &\quad \Theta(E - E_3)\Theta(E_3 - E_2) \\ &= \frac{1}{2^5 3\pi^3 E^2} \int_0^\infty dE_3 \int_0^{E+E_3} dE_2 f_{\text{FBF}} \Theta(E - E_3)\Theta(E_3 - E_2) \\ &\quad (E_2 - E_3)[(E_2 - E_3)(E_2 + 2E_3) - 3(E_2 + E_3)E], \quad (\text{D.20}) \end{aligned}$$

$$\begin{aligned} g_{\text{FBF},212}^{|M_2|^2} &= -\frac{1}{2^8\pi^3 E^2} \int_0^\infty dE_3 \int_0^{E+E_3} dE_2 f_{\text{FBF}} \int_{E-E_3}^{2E_2-E-E_3} dq g_{\text{FBF}}^{|M_2|^2} \\ &\quad \Theta(E - E_3)\Theta(E_2 - E) \\ &= \frac{1}{2^5 3\pi^3 E^2} \int_0^\infty dE_3 \int_0^{E+E_3} dE_2 f_{\text{FBF}} \Theta(E - E_3)\Theta(E_2 - E) \\ &\quad (E - E_2)^2, \quad (\text{D.21}) \end{aligned}$$

$$\begin{aligned} g_{\text{FBF},221}^{|M_2|^2} &= -\frac{1}{2^8\pi^3 E^2} \int_0^\infty dE_3 \int_0^{E+E_3} dE_2 f_{\text{FBF}} \int_{E_3-E}^{E_3+E-2E_2} dq g_{\text{FBF}}^{|M_2|^2} \\ &\quad \Theta(E_3 - E)\Theta(E - E_2) \\ &= -\frac{1}{2^5 3\pi^3 E^2} \int_0^\infty dE_3 \int_0^{E+E_3} dE_2 f_{\text{FBF}} \Theta(E_3 - E)\Theta(E - E_2) \\ &\quad (E - E_2)^2, \quad (\text{D.22}) \end{aligned}$$

$$\begin{aligned}
g_{\text{FBF},222}^{[M_2]^2} &= -\frac{1}{2^8\pi^3 E^2} \int_0^\infty dE_3 \int_0^{E+E_3} dE_2 f_{\text{FBF}} \int_{E_3-E}^{2E_2-E-E_3} dq g_{\text{FBF}}^{[M_2]^2} \\
&\quad \Theta(E_3 - E)\Theta(E_2 - E_3) \\
&= -\frac{1}{2^5 3\pi^3 E^2} \int_0^\infty dE_3 \int_0^{E+E_3} dE_2 f_{\text{FBF}} \Theta(E_3 - E)\Theta(E_2 - E_3) \\
&\quad (E_2 - E_3)[(E_2 - E_3)(E_2 + 2E_3) - 3(E_2 + E_3)E], \quad (\text{D.23})
\end{aligned}$$

where we have computed the q integration for each part.

The final result is given by the sum of all six parts and reads

$$\begin{aligned}
I_{\text{FBF}}^{(2)} &= \frac{1}{96\pi^3 E^2} \int_0^\infty dE_3 \int_0^{E+E_3} dE_2 f_{\text{FBF}} \\
&\quad \times \left\{ \Theta(E - E_3) \frac{E_3^2}{E^2} \left(\frac{E_3}{3} - E_1 \right) \right. \\
&\quad + \Theta(E_3 - E) \left(\frac{E}{3} - E_2 \right) \\
&\quad + \Theta(E_3 - E_2) \Theta(E - E_3) \frac{E_2 - E_3}{3E^2} \\
&\quad \times [(E_2 - E_3)(E_2 + 2E_3) - 3(E_2 + E_3)E] \\
&\quad - \Theta(E - E_3) \Theta(E_2 - E) \frac{(E_2 - E)^3}{3E^2} \\
&\quad + \Theta(E_3 - E) \Theta(E - E_2) \frac{(E_2 - E)^3}{3E^2} \\
&\quad - \Theta(E_3 - E) \Theta(E_2 - E_3) \frac{E_2 - E_3}{3E^2} \\
&\quad \left. \times [(E_2 - E_3)(E_2 + 2E_3) - 3(E_2 + E_3)E] \right\}. \quad (\text{D.24})
\end{aligned}$$

This concludes the calculation of the FBF part.

D.2 Calculation of FFB Processes

The calculation of the integral given in Eq. (D.4) is in fact completely analog to the previous one, except for the different phase space distributions. This does not affect the computation, so we can write both integrals in the compact form given in (3.12b) in the main text.

Appendix E

Phase Space Distribution of Thermally Produced Saxions

In this chapter we estimate the phase space distribution of thermally produced saxions. In light of Sect. 3.2 the result is the same for axions and saxions. First we note that the Boltzmann equation in (3.47) reads in its differential form

$$\frac{\partial f(p, t)}{\partial t} - Hp \frac{\partial f(p, t)}{\partial p} = C[E(p)], \quad (\text{E.1})$$

with the phase space density $f(p, t)$ as a function of time t and the modulus of the momentum p , the Hubble constant H , and the differential collision term C . The integrated version of the Boltzmann equation can be inferred with the help of (3.40b) and one arrives at (3.47).

The differential collision term equals

$$C = \frac{(2\pi)^3}{g_\sigma} \frac{dW_\sigma}{d^3p}, \quad (\text{E.2})$$

where g_σ denotes the internal degrees of freedom of the saxion. Compared to (3.1), the only difference apart from E is an overall normalization factor, where $g_\sigma = 1$. The result for the differential thermal production rate is the sum of (3.10) and (3.26) multiplied by $(2\pi)^3/E$.

Since saxion production happens during the radiation dominated phase, we use (3.46) to switch from time to temperature T as the dependent variable

$$-\frac{\partial f(p, T)}{\partial T} H(T)T - H(T)p \frac{\partial f(p, T)}{\partial p} = C[E(p)]. \quad (\text{E.3})$$

Since $H \propto T^2$ for $g_* = \text{const.}$, and $C \propto T^3$, we rewrite (E.3) as

$$-\frac{\partial f(p, T)}{\partial T} - \frac{p}{T} \frac{\partial f(p, T)}{\partial p} = f_B(E) \sqrt{\frac{45m_{\text{Pl}}^2 g_s^6 (N_c^2 - 1)(N_c + n_f)}{4\pi^3 g_*}} \frac{1}{2048\pi^5 f_{\text{PQ}}^2} \times \left[\ln\left(\frac{2}{3g_s^2}\right) + 2.455 + \left(I_{\text{BBB}}^{(1)} + I_{\text{FBF}}^{(1)} - I_{\text{BBB}}^{(3)} + I_{\text{FFB}}^{(3)}\right) - 2 \frac{n_f(I_{\text{FBF}}^{(2)} + I_{\text{FFB}}^{(2)})}{N_c + n_f} \right] \quad (\text{E.4})$$

where the non-analytic integrals I depend on E and are defined in (3.11).

To solve this differential equation, we make the ansatz

$$f(p, T) = [1 + \phi(p, T)] \frac{1}{e^{p/T} - 1} \quad (\text{E.5})$$

where ϕ describes a deviation of the saxion phase space distribution from the equilibrium distribution. Plugging (E.5) into (E.4), neglecting the small temperature dependence of g_s and as a first approximation also all non-analytic integrals, we get

$$-\frac{\partial \phi(p, T)}{\partial T} - \frac{p}{T} \frac{\partial \phi(p, T)}{\partial p} = \sqrt{\frac{45m_{\text{Pl}}^2 g_s^6 (N_c^2 - 1)(N_c + n_f)}{4\pi^3 g_*}} \frac{1}{2048\pi^5 f_{\text{PQ}}^2} \left[\ln\left(\frac{2}{3g_s^2}\right) + 2.455 \right] \quad (\text{E.6})$$

so the rhs is a constant. The solution for $1 + \phi$ is

$$1 + \phi(p, T) = \sqrt{\frac{45m_{\text{Pl}}^2 g_s^6 (N_c^2 - 1)(N_c + n_f)}{4\pi^3 g_*}} \frac{1}{2048\pi^5 f_{\text{PQ}}^2} \left[\ln\left(\frac{2}{3g_s^2}\right) + 2.455 \right] (T_{\text{R}} - T) \quad (\text{E.7})$$

where we set the integration constant such that $1 + \phi(T_{\text{R}}) = 0$. Then, for $T \ll T_{\text{R}}$, the saxion phase space distribution approaches the equilibrium distribution, because the solution above approaches a constant.

The inclusion of the non-analytic integrals makes an analytic solution impossible. Numerical solutions are complicated, but they indicate that the phase space distributions of thermally produced saxions are close to the equilibrium distribution. A detailed numerical solution is postponed for future work. In our calculations, the only point where the phase-space distribution of the saxion occurs is in the estimate of the average momentum of thermal particles, i.e. at $\langle p_i^{\text{th}} \rangle = 2.7 T_i$. We do not expect a serious deviation from this result if one includes also the non-analytic integrals. Therefore, the phase space distribution of all saxions of thermal origin can be taken to be the equilibrium distribution to a good approximation.

Bibliography

- [1] P. Graf and F. D. Steffen, *Thermal axion production in the primordial quark-gluon plasma*, Phys.Rev. **D83** (2011) 075011 [[arXiv:1008.4528](#)].
- [2] P. Graf and F. D. Steffen, *Axions and saxions from the primordial supersymmetric plasma and extra radiation signatures*, JCAP **1302** (2013) 018 [[arXiv:1208.2951](#)].
- [3] P. Graf and F. D. Steffen, *Dark radiation and dark matter in supersymmetric axion models with high reheating temperature*, [[arXiv:1302.2143](#)].
- [4] S. Glashow, *Partial Symmetries of Weak Interactions*, Nucl.Phys. **22** (1961) 579–588.
- [5] S. Weinberg, *A Model of Leptons*, Phys.Rev.Lett. **19** (1967) 1264–1266.
- [6] A. Salam, *Weak and Electromagnetic Interactions*, Conf.Proc. **C680519** (1968) 367–377.
- [7] S. Glashow, J. Iliopoulos and L. Maiani, *Weak Interactions with Lepton-Hadron Symmetry*, Phys.Rev. **D2** (1970) 1285–1292.
- [8] H. Fritzsch, M. Gell-Mann and H. Leutwyler, *Advantages of the Color Octet Gluon Picture*, Phys.Lett. **B47** (1973) 365–368.
- [9] D. Gross and F. Wilczek, *Asymptotically Free Gauge Theories. 1*, Phys.Rev. **D8** (1973) 3633–3652.
- [10] D. Gross and F. Wilczek, *Asymptotically Free Gauge Theories. 2*, Phys.Rev. **D9** (1974) 980–993.
- [11] H. D. Politzer, *Reliable Perturbative Results for Strong Interactions?*, Phys.Rev.Lett. **30** (1973) 1346–1349.
- [12] **Particle Data Group** Collaboration, J. Beringer *et. al.*, *Review of Particle Physics (RPP)*, Phys.Rev. **D86** (2012) 010001.

- [13] P. W. Higgs, *Broken symmetries, massless particles and gauge fields*, Phys.Lett. **12** (1964) 132–133.
- [14] P. W. Higgs, *Broken Symmetries and the Masses of Gauge Bosons*, Phys.Rev.Lett. **13** (1964) 508–509.
- [15] F. Englert and R. Brout, *Broken Symmetry and the Mass of Gauge Vector Mesons*, Phys.Rev.Lett. **13** (1964) 321–323.
- [16] G. Guralnik, C. Hagen and T. Kibble, *Global Conservation Laws and Massless Particles*, Phys.Rev.Lett. **13** (1964) 585–587.
- [17] P. W. Higgs, *Spontaneous Symmetry Breakdown without Massless Bosons*, Phys.Rev. **145** (1966) 1156–1163.
- [18] T. Kibble, *Symmetry breaking in non-Abelian gauge theories*, Phys.Rev. **155** (1967) 1554–1561.
- [19] **ATLAS Collaboration** Collaboration, G. Aad *et. al.*, *Observation of a new particle in the search for the Standard Model Higgs boson with the ATLAS detector at the LHC*, Phys.Lett. **B716** (2012) 1–29 [[arXiv:1207.7214](#)].
- [20] **CMS Collaboration** Collaboration, S. Chatrchyan *et. al.*, *Observation of a new boson at a mass of 125 GeV with the CMS experiment at the LHC*, Phys.Lett. **B716** (2012) 30–61 [[arXiv:1207.7235](#)].
- [21] L. Anderson, E. Aubourg, S. Bailey, D. Bizyaev, M. Blanton *et. al.*, *The clustering of galaxies in the SDSS-III Baryon Oscillation Spectroscopic Survey: Baryon Acoustic Oscillations in the Data Release 9 Spectroscopic Galaxy Sample*, Mon.Not.Roy.Astron.Soc. **428** (2013) 1036–1054 [[arXiv:1203.6594](#)].
- [22] A. G. Riess, L. Macri, S. Casertano, M. Sosey, H. Lampeitl *et. al.*, *A Redetermination of the Hubble Constant with the Hubble Space Telescope from a Differential Distance Ladder*, Astrophys.J. **699** (2009) 539–563 [[arXiv:0905.0695](#)].
- [23] **WMAP Collaboration**, E. Komatsu *et. al.*, *Seven-Year Wilkinson Microwave Anisotropy Probe (WMAP) Observations: Cosmological Interpretation*, Astrophys. J. Suppl. **192** (2011) 18 [[arXiv:1001.4538](#)].
- [24] R. D. Peccei and H. R. Quinn, *CP Conservation in the Presence of Instantons*, Phys. Rev. Lett. **38** (1977) 1440–1443.
- [25] R. D. Peccei and H. R. Quinn, *Constraints Imposed by CP Conservation in the Presence of Instantons*, Phys. Rev. **D16** (1977) 1791–1797.

- [26] J. E. Kim, *Weak Interaction Singlet and Strong CP Invariance*, Phys. Rev. Lett. **43** (1979) 103.
- [27] M. A. Shifman, A. I. Vainshtein and V. I. Zakharov, *Can Confinement Ensure Natural CP Invariance of Strong Interactions?*, Nucl. Phys. **B166** (1980) 493.
- [28] P. Ramond, *Dual Theory for Free Fermions*, Phys.Rev. **D3** (1971) 2415–2418.
- [29] J.-L. Gervais and B. Sakita, *Field theory interpretation of supergauges in dual models*, Nucl.Phys. **B34** (1971) 632–639.
- [30] A. Neveu and J. Schwarz, *Factorizable dual model of pions*, Nucl.Phys. **B31** (1971) 86–112.
- [31] Y. Golfand and E. Likhtman, *Extension of the Algebra of Poincare Group Generators and Violation of P Invariance*, JETP Lett. **13** (1971) 323–326.
- [32] D. Volkov and V. Akulov, *Is the Neutrino a Goldstone Particle?*, Phys.Lett. **B46** (1973) 109–110.
- [33] J. Wess and B. Zumino, *Supergauge Transformations in Four-Dimensions*, Nucl.Phys. **B70** (1974) 39–50.
- [34] S. Weinberg, *A New Light Boson?*, Phys. Rev. Lett. **40** (1978) 223–226.
- [35] F. Wilczek, *Problem of Strong P and T Invariance in the Presence of Instantons*, Phys. Rev. Lett. **40** (1978) 279–282.
- [36] G. G. Raffelt, *Astrophysical axion bounds*, Lect. Notes Phys. **741** (2008) 51–71 [[hep-ph/0611350](#)].
- [37] M. Dine and W. Fischler, *The Not So Harmless Axion*, Phys.Lett. **B120** (1983) 137–141.
- [38] L. Abbott and P. Sikivie, *A Cosmological Bound on the Invisible Axion*, Phys.Lett. **B120** (1983) 133–136.
- [39] J. Preskill, M. B. Wise and F. Wilczek, *Cosmology of the Invisible Axion*, Phys.Lett. **B120** (1983) 127–132.
- [40] M. Beltran, J. Garcia-Bellido and J. Lesgourgues, *Isocurvature bounds on axions revisited*, Phys. Rev. **D75** (2007) 103507 [[hep-ph/0606107](#)].
- [41] P. Sikivie, *Axion cosmology*, Lect. Notes Phys. **741** (2008) 19–50 [[astro-ph/0610440](#)].

- [42] J. E. Kim and G. Carosi, *Axions and the Strong CP Problem*, Rev.Mod.Phys. **82** (2010) 557–602 [arXiv:0807.3125].
- [43] H. Goldberg, *Constraint on the Photino Mass from Cosmology*, Phys.Rev.Lett. **50** (1983) 1419.
- [44] J. R. Ellis, J. Hagelin, D. V. Nanopoulos, K. A. Olive and M. Srednicki, *Supersymmetric Relics from the Big Bang*, Nucl.Phys. **B238** (1984) 453–476.
- [45] K. Rajagopal, M. S. Turner and F. Wilczek, *Cosmological implications of axinos*, Nucl. Phys. **B358** (1991) 447–470.
- [46] S. A. Bonometto, F. Gabbiani and A. Masiero, *Mixed dark matter from axino distribution*, Phys. Rev. **D49** (1994) 3918–3922 [hep-ph/9305237].
- [47] E. J. Chun and A. Lukas, *Axino mass in supergravity models*, Phys. Lett. **B357** (1995) 43–50 [hep-ph/9503233].
- [48] T. Asaka and T. Yanagida, *Solving the gravitino problem by axino*, Phys.Lett. **B494** (2000) 297–301 [hep-ph/0006211].
- [49] L. Covi, H.-B. Kim, J. E. Kim and L. Roszkowski, *Axinos as dark matter*, JHEP **05** (2001) 033 [hep-ph/0101009].
- [50] A. Brandenburg and F. D. Steffen, *Axino dark matter from thermal production*, JCAP **0408** (2004) 008 [hep-ph/0405158].
- [51] A. Strumia, *Thermal production of axino Dark Matter*, JHEP **06** (2010) 036 [arXiv:1003.5847].
- [52] E. J. Chun, *Dark matter in the Kim-Nilles mechanism*, Phys.Rev. **D84** (2011) 043509 [arXiv:1104.2219].
- [53] K. J. Bae, K. Choi and S. H. Im, *Effective interactions of axion supermultiplet and thermal production of axino dark matter*, JHEP **1108** (2011) 065 [arXiv:1106.2452].
- [54] K.-Y. Choi, L. Covi, J. E. Kim and L. Roszkowski, *Axino Cold Dark Matter Revisited*, JHEP **1204** (2012) 106 [arXiv:1108.2282].
- [55] K. J. Bae, E. J. Chun and S. H. Im, *Cosmology of the DFSZ axino*, JCAP **1203** (2012) 013 [arXiv:1111.5962].
- [56] E. J. Chun, D. Comelli and D. H. Lyth, *The Abundance of relativistic axions in a flaton model of Peccei-Quinn symmetry*, Phys.Rev. **D62** (2000) 095013 [hep-ph/0008133].

- [57] T. Kugo, I. Ojima and T. Yanagida, *Superpotential Symmetries and Pseudo-Nambu-Goldstone Supermultiplets*, Phys. Lett. **B135** (1984) 402.
- [58] J. E. Kim, *Effects of decay of scalar partner of axion on cosmological bounds of axion supermultiplet properties*, Phys. Rev. Lett. **67** (1991) 3465–3468.
- [59] D. H. Lyth, *Dilution of cosmological densities by saxino decay*, Phys. Rev. **D48** (1993) 4523–4533 [[hep-ph/9306293](#)].
- [60] M. Kawasaki and T. Yanagida, *Constraint on cosmic density of the string moduli field in gauge-mediated supersymmetry-breaking theories*, Phys. Lett. **B399** (1997) 45–48 [[hep-ph/9701346](#)].
- [61] M. Hashimoto, K. I. Izawa, M. Yamaguchi and T. Yanagida, *Axion cosmology with its scalar superpartner*, Phys. Lett. **B437** (1998) 44–50 [[hep-ph/9803263](#)].
- [62] T. Asaka and M. Yamaguchi, *Hadronic axion model in gauge-mediated supersymmetry breaking and cosmology of saxion*, Phys. Rev. **D59** (1999) 125003 [[hep-ph/9811451](#)].
- [63] X.-L. Chen and M. Kamionkowski, *Particle decays during the cosmic dark ages*, Phys. Rev. **D70** (2004) 043502 [[astro-ph/0310473](#)].
- [64] M. Kawasaki, K. Nakayama and M. Senami, *Cosmological implications of supersymmetric axion models*, JCAP **0803** (2008) 009 [[arXiv:0711.3083](#)].
- [65] J. Hasenkamp and J. Kersten, *Leptogenesis, Gravitino Dark Matter and Entropy Production*, Phys. Rev. **D82** (2010) 115029 [[arXiv:1008.1740](#)].
- [66] H. Baer, S. Kraml, A. Lessa and S. Sekmen, *Thermal leptogenesis and the gravitino problem in the Asaka-Yanagida axion/axino dark matter scenario*, JCAP **1104** (2011) 039 [[arXiv:1012.3769](#)].
- [67] J. Hamann, S. Hannestad, G. G. Raffelt and Y. Y. Y. Wong, *Observational bounds on the cosmic radiation density*, JCAP **0708** (2007) 021 [[arXiv:0705.0440](#)].
- [68] B. A. Reid, L. Verde, R. Jimenez and O. Mena, *Robust Neutrino Constraints by Combining Low Redshift Observations with the CMB*, JCAP **1001** (2010) 003 [[arXiv:0910.0008](#)].
- [69] J. Hamann, S. Hannestad, J. Lesgourgues, C. Rampf and Y. Y. Y. Wong, *Cosmological parameters from large scale structure - geometric versus shape information*, JCAP **1007** (2010) 022 [[arXiv:1003.3999](#)].

- [70] M. C. Gonzalez-Garcia, M. Maltoni and J. Salvado, *Robust Cosmological Bounds on Neutrinos and their Combination with Oscillation Results*, JHEP **08** (2010) 117 [[arXiv:1006.3795](#)].
- [71] G. Hinshaw, D. Larson, E. Komatsu, D. Spergel, C. Bennett *et al.*, *Nine-Year Wilkinson Microwave Anisotropy Probe (WMAP) Observations: Cosmological Parameter Results*, [[arXiv:1212.5226](#)].
- [72] E. Aver, K. A. Olive and E. D. Skillman, *A New Approach to Systematic Uncertainties and Self-Consistency in Helium Abundance Determinations*, JCAP **1005** (2010) 003 [[arXiv:1001.5218](#)].
- [73] Y. I. Izotov and T. X. Thuan, *The primordial abundance of ^4He : evidence for non-standard big bang nucleosynthesis*, Astrophys. J. **710** (2010) L67–L71 [[arXiv:1001.4440](#)].
- [74] J. Hamann, S. Hannestad, G. G. Raffelt, I. Tamborra and Y. Y. Wong, *Cosmology seeking friendship with sterile neutrinos*, Phys.Rev.Lett. **105** (2010) 181301 [[arXiv:1006.5276](#)].
- [75] J. Hamann, S. Hannestad, G. G. Raffelt and Y. Y. Wong, *Sterile neutrinos with eV masses in cosmology: How disfavoured exactly?*, JCAP **1109** (2011) 034 [[arXiv:1108.4136](#)].
- [76] K. Nakayama, F. Takahashi and T. T. Yanagida, *A theory of extra radiation in the Universe*, Phys.Lett. **B697** (2011) 275–279 [[arXiv:1010.5693](#)].
- [77] C. Boehm, M. J. Dolan and C. McCabe, *Increasing N_{eff} with particles in thermal equilibrium with neutrinos*, [[arXiv:1207.0497](#)].
- [78] S. Pastor, T. Pinto and G. G. Raffelt, *Relic density of neutrinos with primordial asymmetries*, Phys.Rev.Lett. **102** (2009) 241302 [[arXiv:0808.3137](#)].
- [79] G. Mangano, G. Miele, S. Pastor, O. Pisanti and S. Sarikas, *Constraining the cosmic radiation density due to lepton number with Big Bang Nucleosynthesis*, JCAP **1103** (2011) 035 [[arXiv:1011.0916](#)].
- [80] K. Ichikawa, M. Kawasaki, K. Nakayama, M. Senami and F. Takahashi, *Increasing effective number of neutrinos by decaying particles*, JCAP **0705** (2007) 008 [[hep-ph/0703034](#)].
- [81] W. Fischler and J. Meyers, *Dark Radiation Emerging After Big Bang Nucleosynthesis?*, Phys.Rev. **D83** (2011) 063520 [[arXiv:1011.3501](#)].
- [82] J. Hasenkamp, *Dark radiation from the axino solution of the gravitino problem*, Phys.Lett. **B707** (2012) 121–128 [[arXiv:1107.4319](#)].

- [83] D. Hooper, F. S. Queiroz and N. Y. Gnedin, *Non-Thermal Dark Matter Mimicking An Additional Neutrino Species In The Early Universe*, Phys.Rev. **D85** (2012) 063513 [[arXiv:1111.6599](#)].
- [84] K. Choi, K.-Y. Choi and C. S. Shin, *Dark radiation and small-scale structure problems with decaying particles*, [[arXiv:1208.2496](#)].
- [85] M. Cicoli, J. P. Conlon and F. Quevedo, *Dark Radiation in LARGE Volume Models*, [[arXiv:1208.3562](#)].
- [86] T. Higaki and F. Takahashi, *Dark Radiation and Dark Matter in Large Volume Compactifications*, [[arXiv:1208.3563](#)].
- [87] M. Gonzalez-Garcia, V. Niro and J. Salvado, *Dark Radiation and Decaying Matter*, [[arXiv:1212.1472](#)].
- [88] J. Hasenkamp and J. Kersten, *Dark radiation from particle decay: cosmological constraints and opportunities*, [[arXiv:1212.4160](#)].
- [89] K. J. Bae, H. Baer and A. Lessa, *Dark Radiation Constraints on Mixed Axion/Neutralino Dark Matter*, [[arXiv:1301.7428](#)].
- [90] K. S. Jeong and F. Takahashi, *Axionic Co-genesis of Baryon, Dark Matter and Dark Radiation*, [[arXiv:1302.1486](#)].
- [91] S. Chang and H. B. Kim, *A Dark matter solution from the supersymmetric axion model*, Phys.Rev.Lett. **77** (1996) 591–594 [[hep-ph/9604222](#)].
- [92] T. Asaka and M. Yamaguchi, *Hadronic axion model in gauge-mediated supersymmetry breaking*, Phys. Lett. **B437** (1998) 51–61 [[hep-ph/9805449](#)].
- [93] M. Kawasaki, N. Kitajima and K. Nakayama, *Revisiting the cosmological coherent oscillation*, [[arXiv:1112.2818](#)].
- [94] R. Peccei, *The Strong CP problem and axions*, Lect.Notes Phys. **741** (2008) 3–17 [[hep-ph/0607268](#)].
- [95] O. Wantz and E. Shellard, *Axion Cosmology Revisited*, Phys.Rev. **D82** (2010) 123508 [[arXiv:0910.1066](#)].
- [96] S. Weinberg, *The U(1) Problem*, Phys.Rev. **D11** (1975) 3583–3593.
- [97] G. 't Hooft, *Symmetry breaking through Bell-Jackiw anomalies*, Phys. Rev. Lett. **37** (1976) 8–11.
- [98] G. 't Hooft, *Computation of the Quantum Effects Due to a Four-Dimensional Pseudoparticle*, Phys.Rev. **D14** (1976) 3432–3450.

-
- [99] J. S. Bell and R. Jackiw, *A PCAC puzzle: $\pi_0 \rightarrow \gamma \gamma$ in the sigma model*, Nuovo Cim. **A60** (1969) 47–61.
- [100] S. L. Adler, *Axial vector vertex in spinor electrodynamics*, Phys. Rev. **177** (1969) 2426–2438.
- [101] J. E. Kim, *Light Pseudoscalars, Particle Physics and Cosmology*, Phys.Rept. **150** (1987) 1–177.
- [102] J. Callan, Curtis G., R. Dashen and D. J. Gross, *The Structure of the Gauge Theory Vacuum*, Phys.Lett. **B63** (1976) 334–340.
- [103] R. Jackiw and C. Rebbi, *Vacuum Periodicity in a Yang-Mills Quantum Theory*, Phys.Rev.Lett. **37** (1976) 172–175.
- [104] C. Baker, D. Doyle, P. Geltenbort, K. Green, M. van der Grinten *et. al.*, *An Improved experimental limit on the electric dipole moment of the neutron*, Phys.Rev.Lett. **97** (2006) 131801 [[hep-ex/0602020](#)].
- [105] H.-Y. Cheng, *The Strong CP Problem Revisited*, Phys.Rept. **158** (1988) 1.
- [106] C. Vafa and E. Witten, *Parity Conservation in QCD*, Phys.Rev.Lett. **53** (1984) 535.
- [107] W. A. Bardeen and S.-H. Tye, *Current Algebra Applied to Properties of the Light Higgs Boson*, Phys.Lett. **B74** (1978) 229.
- [108] J. R. Ellis and M. K. Gaillard, *No new light boson?*, Phys.Lett. **B74** (1978) 374.
- [109] S. Weinberg, *Implications of Dynamical Symmetry Breaking*, Phys.Rev. **D13** (1976) 974–996.
- [110] E. Gildener, *Gauge Symmetry Hierarchies*, Phys.Rev. **D14** (1976) 1667.
- [111] L. Susskind, *Dynamics of Spontaneous Symmetry Breaking in the Weinberg-Salam Theory*, Phys.Rev. **D20** (1979) 2619–2625.
- [112] S. Weinberg, *Implications of Dynamical Symmetry Breaking: An Addendum*, Phys.Rev. **D19** (1979) 1277–1280.
- [113] S. Dimopoulos and S. Raby, *Supercolor*, Nucl.Phys. **B192** (1981) 353.
- [114] E. Witten, *Dynamical Breaking of Supersymmetry*, Nucl.Phys. **B188** (1981) 513.
- [115] M. Dine, W. Fischler and M. Srednicki, *Supersymmetric Technicolor*, Nucl.Phys. **B189** (1981) 575–593.

- [116] S. Dimopoulos and H. Georgi, *Softly Broken Supersymmetry and $SU(5)$* , Nucl.Phys. **B193** (1981) 150.
- [117] N. Sakai, *Naturalness in Supersymmetric Guts*, Z.Phys. **C11** (1981) 153.
- [118] R. K. Kaul and P. Majumdar, *Cancellation of quadratically divergent mass corrections in globally supersymmetric spontaneously broken gauge theories*, Nucl.Phys. **B199** (1982) 36.
- [119] S. P. Martin, *A Supersymmetry Primer*, [hep-ph/9709356].
- [120] S. R. Coleman and J. Mandula, *All possible symmetries of the S matrix*, Phys.Rev. **159** (1967) 1251–1256.
- [121] M. Drees, R. Godbole and P. Roy, *Theory and phenomenology of sparticles: An account of four-dimensional $N=1$ supersymmetry in high energy physics*. World Scientific, USA, 2004.
- [122] R. Haag, J. T. Lopuszanski and M. Sohnius, *All Possible Generators of Supersymmetries of the s Matrix*, Nucl.Phys. **B88** (1975) 257.
- [123] J. Wess and B. Zumino, *Supergauge Invariant Extension of Quantum Electrodynamics*, Nucl.Phys. **B78** (1974) 1.
- [124] J. Wess and B. Zumino, *A Lagrangian Model Invariant Under Supergauge Transformations*, Phys.Lett. **B49** (1974) 52.
- [125] G. R. Farrar and P. Fayet, *Phenomenology of the Production, Decay, and Detection of New Hadronic States Associated with Supersymmetry*, Phys.Lett. **B76** (1978) 575–579.
- [126] L. Girardello and M. T. Grisaru, *Soft Breaking of Supersymmetry*, Nucl.Phys. **B194** (1982) 65.
- [127] P. Fayet and J. Iliopoulos, *Spontaneously Broken Supergauge Symmetries and Goldstone Spinors*, Phys.Lett. **B51** (1974) 461–464.
- [128] J. Wess and J. Bagger, *Supersymmetry and supergravity*. Princeton University Press, USA, 1992.
- [129] P. Nath and R. L. Arnowitt, *Generalized Supergauge Symmetry as a New Framework for Unified Gauge Theories*, Phys.Lett. **B56** (1975) 177.
- [130] R. L. Arnowitt, P. Nath and B. Zumino, *Superfield Densities and Action Principle in Curved Superspace*, Phys.Lett. **B56** (1975) 81.
- [131] D. Z. Freedman, P. van Nieuwenhuizen and S. Ferrara, *Progress Toward a Theory of Supergravity*, Phys.Rev. **D13** (1976) 3214–3218.

- [132] S. Deser and B. Zumino, *Consistent Supergravity*, Phys.Lett. **B62** (1976) 335.
- [133] D. Z. Freedman and P. van Nieuwenhuizen, *Properties of Supergravity Theory*, Phys.Rev. **D14** (1976) 912.
- [134] E. Cremmer, B. Julia, J. Scherk, S. Ferrara, L. Girardello *et. al.*, *Spontaneous Symmetry Breaking and Higgs Effect in Supergravity Without Cosmological Constant*, Nucl.Phys. **B147** (1979) 105.
- [135] J. A. Bagger, *Coupling the Gauge Invariant Supersymmetric Nonlinear Sigma Model to Supergravity*, Nucl.Phys. **B211** (1983) 302.
- [136] E. Cremmer, S. Ferrara, L. Girardello and A. Van Proeyen, *Yang-Mills Theories with Local Supersymmetry: Lagrangian, Transformation Laws and SuperHiggs Effect*, Nucl.Phys. **B212** (1983) 413.
- [137] M. Dine, W. Fischler and M. Srednicki, *A Simple Solution to the Strong CP Problem with a Harmless Axion*, Phys. Lett. **B104** (1981) 199.
- [138] A. R. Zhitnitsky, *On Possible Suppression of the Axion Hadron Interactions. (In Russian)*, Sov. J. Nucl. Phys. **31** (1980) 260.
- [139] P. Sikivie, *Of Axions, Domain Walls and the Early Universe*, Phys.Rev.Lett. **48** (1982) 1156–1159.
- [140] J. E. Kim, *A Common Scale for the Invisible Axion, local SUSY GUTs and Saxino Decay*, Phys.Lett. **B136** (1984) 378.
- [141] T. Moroi and M. Takimoto, *Thermal Effects on Saxion in Supersymmetric Model with Peccei-Quinn Symmetry*, [arXiv:1207.4858].
- [142] H. K. Dreiner, H. E. Haber and S. P. Martin, *Two-component spinor techniques and Feynman rules for quantum field theory and supersymmetry*, Phys.Rept. **494** (2010) 1–196 [arXiv:0812.1594].
- [143] M. Kawasaki, N. Kitajima and K. Nakayama, *Cosmological Aspects of Inflation in a Supersymmetric Axion Model*, Phys.Rev. **D83** (2011) 123521 [arXiv:1104.1262].
- [144] E. Chun, J. E. Kim and H. P. Nilles, *Axino mass*, Phys.Lett. **B287** (1992) 123–127 [hep-ph/9205229].
- [145] C. Cheung, Y. Nomura and J. Thaler, *Goldstini*, JHEP **1003** (2010) 073 [arXiv:1002.1967].
- [146] T. Higaki and R. Kitano, *On Supersymmetric Effective Theories of Axion*, [arXiv:1104.0170].

- [147] J. E. Kim and M.-S. Seo, *Mixing of axino and goldstino, and axino mass*, Nucl.Phys. **B864** (2012) 296–316 [[arXiv:1204.5495](#)].
- [148] M. Bolz, A. Brandenburg and W. Buchmüller, *Thermal Production of Gravitinos*, Nucl. Phys. **B606** (2001) 518–544 [[hep-ph/0012052](#)].
- [149] K. A. Olive, D. N. Schramm and M. Srednicki, *Gravitinos as the Cold Dark Matter in an $\Omega = 1$ Universe*, Nucl.Phys. **B255** (1985) 495.
- [150] E. Braaten and R. D. Pisarski, *Soft Amplitudes in Hot Gauge Theories: A General Analysis*, Nucl. Phys. **B337** (1990) 569.
- [151] E. Braaten and T. C. Yuan, *Calculation of screening in a hot plasma*, Phys. Rev. Lett. **66** (1991) 2183–2186.
- [152] J. Pradler and F. D. Steffen, *Thermal Gravitino Production and Collider Tests of Leptogenesis*, Phys. Rev. **D75** (2007) 023509 [[hep-ph/0608344](#)].
- [153] J. Pradler and F. D. Steffen, *Constraints on the Reheating Temperature in Gravitino Dark Matter Scenarios*, Phys.Lett. **B648** (2007) 224–235 [[hep-ph/0612291](#)].
- [154] J. Pradler, *Electroweak Contributions to Thermal Gravitino Production*, diploma thesis, Univ. of Vienna, 2006.
- [155] P. Graf, *Axions in the Early Universe*, diploma thesis, Univ. of Regensburg, 2009.
- [156] A. D. Linde, *Particle physics and inflationary cosmology*, Contemp.Concepts Phys. **5** (1990) 1–362 [[hep-th/0503203](#)].
- [157] E. W. Kolb and M. S. Turner, *The Early Universe*. Westview Press, 1990.
- [158] A. D. Linde, *Axions in inflationary cosmology*, Phys.Lett. **B259** (1991) 38–47.
- [159] M. S. Turner, *Thermal Production of Not SO Invisible Axions in the Early Universe*, Phys. Rev. Lett. **59** (1987) 2489.
- [160] T. Hahn, *Generating Feynman diagrams and amplitudes with FeynArts 3*, Comput. Phys. Commun. **140** (2001) 418–431 [[hep-ph/0012260](#)].
- [161] T. Hahn and M. Perez-Victoria, *Automatized one-loop calculations in four and D dimensions*, Comput. Phys. Commun. **118** (1999) 153–165 [[hep-ph/9807565](#)].
- [162] H. A. Weldon, *Simple Rules for Discontinuities in Finite Temperature Field Theory*, Phys. Rev. **D28** (1983) 2007.

- [163] O. K. Kalashnikov and V. V. Klimov, *Polarization Tensor in QCD for Finite Temperature and Density*, Sov. J. Nucl. Phys. **31** (1980) 699.
- [164] R. D. Pisarski, *Renormalized Gauge Propagators in Hot Gauge Theories*, Physica **A158** (1989) 146–157.
- [165] S. Chang and K. Choi, *Hadronic axion window and the big-bang nucleosynthesis*, Phys. Lett. **B316** (1993) 51–56 [[hep-ph/9306216](#)].
- [166] S. Hannestad, A. Mirizzi and G. Raffelt, *New cosmological mass limit on thermal relic axions*, JCAP **0507** (2005) 002 [[hep-ph/0504059](#)].
- [167] A. A. Starobinsky, *A New Type of Isotropic Cosmological Models Without Singularity*, Phys.Lett. **B91** (1980) 99–102.
- [168] A. H. Guth, *The Inflationary Universe: A Possible Solution to the Horizon and Flatness Problems*, Phys.Rev. **D23** (1981) 347–356.
- [169] A. D. Linde, *A New Inflationary Universe Scenario: A Possible Solution of the Horizon, Flatness, Homogeneity, Isotropy and Primordial Monopole Problems*, Phys.Lett. **B108** (1982) 389–393.
- [170] A. Albrecht and P. J. Steinhardt, *Cosmology for Grand Unified Theories with Radiatively Induced Symmetry Breaking*, Phys.Rev.Lett. **48** (1982) 1220–1223.
- [171] A. D. Linde, *Chaotic Inflation*, Phys.Lett. **B129** (1983) 177–181.
- [172] E. W. Kolb, A. Notari and A. Riotto, *On the reheating stage after inflation*, Phys.Rev. **D68** (2003) 123505 [[hep-ph/0307241](#)].
- [173] M. Kawasaki, K. Kohri and T. Moroi, *Big-Bang nucleosynthesis and hadronic decay of long-lived massive particles*, Phys.Rev. **D71** (2005) 083502 [[astro-ph/0408426](#)].
- [174] F. D. Steffen, *Dark Matter Candidates - Axions, Neutralinos, Gravitinos, and Axinos*, Eur. Phys. J. **C59** (2009) 557–588 [[arXiv:0811.3347](#)].
- [175] K. Mukaida and K. Nakayama, *Dynamics of oscillating scalar field in thermal environment*, JCAP **1301** (2013) 017 [[arXiv:1208.3399](#)].
- [176] K. Choi, E. J. Chun and J. E. Kim, *Cosmological implications of radiatively generated axion scale*, Phys. Lett. **B403** (1997) 209–217 [[hep-ph/9608222](#)].
- [177] M. Kawasaki and T. Moroi, *Electromagnetic cascade in the early universe and its application to the big bang nucleosynthesis*, Astrophys. J. **452** (1995) 506 [[astro-ph/9412055](#)].

- [178] E. Holtmann, M. Kawasaki, K. Kohri and T. Moroi, *Radiative decay of a longlived particle and big bang nucleosynthesis*, Phys.Rev. **D60** (1999) 023506 [hep-ph/9805405].
- [179] K. Jedamzik, *Lithium 6: A Probe of the early universe*, Phys.Rev.Lett. **84** (2000) 3248 [astro-ph/9909445].
- [180] M. Kawasaki, K. Kohri and T. Moroi, *Radiative decay of a massive particle and the nonthermal process in primordial nucleosynthesis*, Phys.Rev. **D63** (2001) 103502 [hep-ph/0012279].
- [181] K. Kohri, *Primordial nucleosynthesis and hadronic decay of a massive particle with a relatively short lifetime*, Phys.Rev. **D64** (2001) 043515 [astro-ph/0103411].
- [182] R. H. Cyburt, J. R. Ellis, B. D. Fields and K. A. Olive, *Updated nucleosynthesis constraints on unstable relic particles*, Phys.Rev. **D67** (2003) 103521 [astro-ph/0211258].
- [183] M. Kawasaki, K. Kohri and T. Moroi, *Hadronic decay of late - decaying particles and Big-Bang Nucleosynthesis*, Phys.Lett. **B625** (2005) 7–12 [astro-ph/0402490].
- [184] L. Zhang, X. Chen, M. Kamionkowski, Z.-g. Si and Z. Zheng, *Constraints on radiative dark-matter decay from the cosmic microwave background*, Phys.Rev. **D76** (2007) 061301 [arXiv:0704.2444].
- [185] G. Mangano *et. al.*, *Relic neutrino decoupling including flavour oscillations*, Nucl. Phys. **B729** (2005) 221–234 [hep-ph/0506164].
- [186] M. J. White, D. Scott and J. Silk, *Anisotropies in the cosmic microwave background*, Ann.Rev.Astron.Astrophys. **32** (1994) 319–370.
- [187] W. Hu and S. Dodelson, *Cosmic microwave background anisotropies*, Ann.Rev.Astron.Astrophys. **40** (2002) 171–216 [astro-ph/0110414].
- [188] G. F. Smoot, C. Bennett, A. Kogut, E. Wright, J. Aymon *et. al.*, *Structure in the COBE differential microwave radiometer first year maps*, Astrophys.J. **396** (1992) L1–L5.
- [189] R. Sachs and A. Wolfe, *Perturbations of a cosmological model and angular variations of the microwave background*, Astrophys.J. **147** (1967) 73–90.
- [190] J. Silk, *Cosmic black body radiation and galaxy formation*, Astrophys.J. **151** (1968) 459–471.
- [191] A. Challinor and A. Lewis, *The linear power spectrum of observed source number counts*, Phys.Rev. **D84** (2011) 043516 [arXiv:1105.5292].

- [192] **WMAP Collaboration** Collaboration, E. Komatsu *et. al.*, *Five-Year Wilkinson Microwave Anisotropy Probe (WMAP) Observations: Cosmological Interpretation*, *Astrophys.J.Suppl.* **180** (2009) 330–376 [arXiv:0803.0547].
- [193] W. Hu, D. Scott, N. Sugiyama and M. White, *The Effect of physical assumptions on the calculation of microwave background anisotropies*, *Phys.Rev.* **D52** (1995) 5498–5515 [astro-ph/9505043].
- [194] L. Perotto, J. Lesgourgues, S. Hannestad, H. Tu and Y. Y. Y. Wong, *Probing cosmological parameters with the CMB: Forecasts from full Monte Carlo simulations*, *JCAP* **0610** (2006) 013 [astro-ph/0606227].
- [195] J. Hamann, J. Lesgourgues and G. Mangano, *Using BBN in cosmological parameter extraction from CMB: A Forecast for PLANCK*, *JCAP* **0803** (2008) 004 [arXiv:0712.2826].
- [196] J. Hasenkamp and J. Kersten, *Dark and visible matter with broken R-parity and the axion multiplet*, *Phys.Lett.* **B701** (2011) 660–666 [arXiv:1103.6193].
- [197] R. V. Wagoner, W. A. Fowler and F. Hoyle, *On the Synthesis of elements at very high temperatures*, *Astrophys.J.* **148** (1967) 3–49.
- [198] S. Sarkar, *Big bang nucleosynthesis and physics beyond the standard model*, *Rept.Prog.Phys.* **59** (1996) 1493–1610 [hep-ph/9602260].
- [199] D. N. Schramm and M. S. Turner, *Big bang nucleosynthesis enters the precision era*, *Rev.Mod.Phys.* **70** (1998) 303–318 [astro-ph/9706069].
- [200] K. A. Olive, G. Steigman and T. P. Walker, *Primordial nucleosynthesis: Theory and observations*, *Phys.Rept.* **333** (2000) 389–407 [astro-ph/9905320].
- [201] M. Pospelov and J. Pradler, *Big Bang Nucleosynthesis as a Probe of New Physics*, *Ann.Rev.Nucl.Part.Sci.* **60** (2010) 539–568 [arXiv:1011.1054].
- [202] K. A. Olive and E. D. Skillman, *A Realistic determination of the error on the primordial helium abundance: Steps toward non-parametric nebular helium abundances*, *Astrophys.J.* **617** (2004) 29 [astro-ph/0405588].
- [203] E. Aver, K. A. Olive and E. D. Skillman, *Mapping systematic errors in helium abundance determinations using Markov Chain Monte Carlo*, *JCAP* **1103** (2011) 043 [arXiv:1012.2385].
- [204] E. Aver, K. A. Olive and E. D. Skillman, *An MCMC determination of the primordial helium abundance*, *JCAP* **1204** (2012) 004 [arXiv:1112.3713].

- [205] R. Epstein, J. Lattimer and D. Schramm, *The Origin of deuterium*, Nature **263** (1976) 198–202.
- [206] M. Pettini, B. J. Zych, M. T. Murphy, A. Lewis and C. C. Steidel, *Deuterium abundance in the most metal-poor damped lyman alpha system: converging on $\omega_{b,0}h^2$* , Monthly Notices of the Royal Astronomical Society **391** (2008), no. 4 1499–1510.
- [207] O. Pisanti *et. al.*, *PARthENoPE: Public Algorithm Evaluating the Nucleosynthesis of Primordial Elements*, Comp. Phys. Commun. **178** (2008) 956–971 [[arXiv:0705.0290](#)].
- [208] H.-S. Kang and G. Steigman, *Cosmological constraints on neutrino degeneracy*, Nucl.Phys. **B372** (1992) 494–520.
- [209] G. Mangano, G. Miele, S. Pastor, O. Pisanti and S. Sarikas, *Updated BBN bounds on the cosmological lepton asymmetry for non-zero θ_{13}* , Phys.Lett. **B708** (2012) 1–5 [[arXiv:1110.4335](#)].
- [210] **Particle Data Group** Collaboration, K. Nakamura *et. al.*, *Review of particle physics*, J. Phys. **G37** (2010) 075021.
- [211] M. S. Turner, *Cosmic and Local Mass Density of Invisible Axions*, Phys.Rev. **D33** (1986) 889–896.
- [212] D. Lyth, *Axions and inflation: Sitting in the vacuum*, Phys.Rev. **D45** (1992) 3394–3404.
- [213] L. Visinelli and P. Gondolo, *Dark Matter Axions Revisited*, Phys.Rev. **D80** (2009) 035024 [[arXiv:0903.4377](#)].
- [214] P. Sikivie and Q. Yang, *Bose-Einstein Condensation of Dark Matter Axions*, Phys.Rev.Lett. **103** (2009) 111301 [[arXiv:0901.1106](#)].
- [215] O. Erken, P. Sikivie, H. Tam and Q. Yang, *Cosmic axion thermalization*, Phys.Rev. **D85** (2012) 063520 [[arXiv:1111.1157](#)].
- [216] G. Carosi and K. van Bibber, *Cavity microwave searches for cosmological axions*, Lect.Notes Phys. **741** (2008) 135–156 [[hep-ex/0701025](#)].
- [217] T. Moroi, H. Murayama and M. Yamaguchi, *Cosmological constraints on the light stable gravitino*, Phys. Lett. **B303** (1993) 289–294.
- [218] R. J. Scherrer and M. S. Turner, *Primordial Nucleosynthesis with Decaying Particles. 2. Inert Decays*, Astrophys.J. **331** (1988) 33–37.
- [219] R. J. Scherrer and M. S. Turner, *Primordial Nucleosynthesis with Decaying Particles. 1. Entropy Producing Decays.*, Astrophys.J. **331** (1988) 19–32.

- [220] R. J. Scherrer and M. S. Turner, *Decaying Particles Do Not Heat Up the Universe*, Phys.Rev. **D31** (1985) 681.
- [221] W. Porod, *SPheno, a program for calculating supersymmetric spectra, SUSY particle decays and SUSY particle production at e^+e^- colliders*, Comput.Phys.Commun. **153** (2003) 275–315 [[hep-ph/0301101](#)].
- [222] W. Porod and F. Staub, *SPheno 3.1: Extensions including flavour, CP-phases and models beyond the MSSM*, Comput.Phys.Commun. **183** (2012) 2458–2469 [[arXiv:1104.1573](#)].
- [223] **ATLAS Collaboration** Collaboration, G. Aad *et. al.*, *Multi-channel search for squarks and gluinos in $\sqrt{s} = 7$ TeV pp collisions with the ATLAS detector*, [[arXiv:1212.6149](#)].
- [224] W. Buchmüller, R. Peccei and T. Yanagida, *Leptogenesis as the origin of matter*, Ann.Rev.Nucl.Part.Sci. **55** (2005) 311–355 [[hep-ph/0502169](#)].
- [225] W. Buchmüller, P. Di Bari and M. Plümacher, *Cosmic microwave background, matter - antimatter asymmetry and neutrino masses*, Nucl.Phys. **B643** (2002) 367–390 [[hep-ph/0205349](#)].
- [226] W. Buchmüller, P. Di Bari and M. Plümacher, *A Bound on neutrino masses from baryogenesis*, Phys.Lett. **B547** (2002) 128–132 [[hep-ph/0209301](#)].
- [227] A. Freitas, F. D. Steffen, N. Tajuddin and D. Wyler, *Axinos in Cosmology and at Colliders*, JHEP **1106** (2011) 036 [[arXiv:1105.1113](#)].
- [228] J. Pradler and F. D. Steffen, *Implications of Catalyzed BBN in the CMSSM with Gravitino Dark Matter*, Phys.Lett. **B666** (2008) 181–184 [[arXiv:0710.2213](#)].
- [229] J. Pradler and F. D. Steffen, *CBBN in the CMSSM*, Eur.Phys.J. **C56** (2008) 287–291 [[arXiv:0710.4548](#)].
- [230] M. Pospelov, J. Pradler and F. D. Steffen, *Constraints on Supersymmetric Models from Catalytic Primordial Nucleosynthesis of Beryllium*, JCAP **0811** (2008) 020 [[arXiv:0807.4287](#)].
- [231] M. Kawasaki, K. Kohri, T. Moroi and A. Yotsuyanagi, *Big-Bang Nucleosynthesis and Gravitino*, Phys.Rev. **D78** (2008) 065011 [[arXiv:0804.3745](#)].
- [232] J. L. Feng, S. Su and F. Takayama, *Supergravity with a gravitino LSP*, Phys.Rev. **D70** (2004) 075019 [[hep-ph/0404231](#)].

- [233] J. R. Ellis, K. A. Olive and Y. Santoso, *Sneutrino NLSP Scenarios in the NUHM with Gravitino Dark Matter*, JHEP **0810** (2008) 005 [arXiv:0807.3736].
- [234] L. Covi and S. Kraml, *Collider signatures of gravitino dark matter with a sneutrino NLSP*, JHEP **0708** (2007) 015 [hep-ph/0703130].
- [235] A. Katz and B. Tweedie, *Signals of a Sneutrino (N)LSP at the LHC*, Phys.Rev. **D81** (2010) 035012 [arXiv:0911.4132].
- [236] T. Figy, K. Rolbiecki and Y. Santoso, *Tau-Sneutrino NLSP and Multilepton Signatures at the LHC*, Phys.Rev. **D82** (2010) 075016 [arXiv:1005.5136].
- [237] G. Bertone, ed., *Particle dark matter: Observations, models and searches*. Cambridge University Press, UK, 2010.
- [238] A. Freitas, F. D. Steffen, N. Tajuddin and D. Wyler, *Upper Limits on the Peccei-Quinn Scale and on the Reheating Temperature in Axino Dark Matter Scenarios*, Phys.Lett. **B679** (2009) 270–277 [arXiv:0904.3218].
- [239] A. Freitas, F. D. Steffen, N. Tajuddin and D. Wyler, *Late Energy Injection and Cosmological Constraints in Axino Dark Matter Scenarios*, Phys.Lett. **B682** (2009) 193–199 [arXiv:0909.3293].
- [240] N. Tajuddin, *Axions in the Sky and on Earth*. PhD thesis, Univ. of Zürich, 2010.
- [241] A. Denner, H. Eck, O. Hahn and J. Kublbeck, *Feynman rules for fermion number violating interactions*, Nucl.Phys. **B387** (1992) 467–484.

Acknowledgments

First of all, I would like to thank my supervisor Dr. Frank Daniel Steffen for the opportunity to work on this topic. His support lead to my acceptance in the IMPRS program and his trust and patience enabled the success of my Ph.D. project.

I want to thank Dr. habil. Georg Raffelt and Prof. Dr. Gerhard Buchalla for acting as first and second referee.

Then, I thank my office mates and colleagues at the institute, Jochen Baumann, Phillip Kostka, Clemens Kießig, Max Huber, Sebastian Halter, Davide Cadamuro, Silke Zollinger, Srđan Sarikas, Jonas Lindert and Hendrik Vogel for the nice time we had together and the discussions in and out of physics. Especially the trips to Florida/New Orleans, Mexico and Porto as well as the weeks at Castle Ringberg (and Wildbad Kreuth) are times to remember. Thanks to Jonas, Srđan, Hendrik, and of course Frank for proof-reading parts of this thesis.

Finally, I am thankful to my family and my girlfriend Carole for their support during these last three years.